Titre: Title:	N-Butane Partial Oxidation to Maleic Anhydride : Experimental and Kinetic Studies Under Transient Conditions
Auteur: Author:	Ali Shekari
Date:	2011
Type:	Mémoire ou thèse / Dissertation or Thesis
Référence: Citation:	Shekari, A. (2011). N-Butane Partial Oxidation to Maleic Anhydride : Experimental and Kinetic Studies Under Transient Conditions [Ph.D. thesis, École Polytechnique de Montréal]. PolyPublie. https://publications.polymtl.ca/653/

UNIVERSITÉ DE MONTRÉAL

N-BUTANE PARTIAL OXIDATION TO MALEIC ANHYDRIDE: EXPERIMENTAL AND KINETIC STUDIES UNDER TRANSIENT CONDITIONS

ALI SHEKARI

DÉPARTEMENT DE GÉNIE CHIMIQUE

ÉCOLE POLYTECHNIQUE DE MONTRÉAL

THÈSE PRÉSENTÉE EN VUE DE L'OBTENTION

DU DIPLÔME DE PHILOSOPHIAE DOCTOR (Ph.D.)

(GÉNIE CHIMIQUE)

AOÛT 2011

UNIVERSITÉ DE MONTRÉAL

ÉCOLE POLYTECHNIQUE DE MONTRÉAL

Cette thèse intitulée:

N-BUTANE PARTIAL OXIDATION TO MALEIC ANHYDRIDE: EXPERIMENTAL AND KINETIC STUDIES UNDER TRANSIENT CONDITIONS

présentée par : SHEKARI Ali

en vue de l'obtention du diplôme de : Philosophiae Doctor

a été dûment accepté par le jury d'examen constitué de :

M. BUSCHMANN Michael D., Ph. D., président

M. PATIENCE Gregory S., Ph. D., membre et directeur de recherche

M. HENRY Olivier, Ph. D., membre

M. BERK Dimitrios, Ph. D., membre

DEDICATION

To my family, for their endless care.

ACKNOWLEDGEMENTS

I would like to express my sincere gratitude to my supervisor, Professor Gregory S. Patience for his continual support, encouragement and friendship. His scientific knowledge and industrial experience helped me choose the right path during my research. Out of the academia, I enjoy being a friend of him and I appreciate his supportive attitude.

I would also like to thank the Génie Chimique department staff, our chemists Martine Lamarche and Gino Robin and the technical assistance of Carol Painchaud, Jean Huard and Robert Delisle. Their support helped me pass through the experimental hurdles in the lab.

During my studies, I had the opportunity of friendship with Jean-Philippe Laviolette, Mads Kristian Kaarsholm, François-Xavier Chiron, Milad Aghabararnejad, Patrice Perreault, Laurent Spreutels, Sherif Farag, Babak Esmaeili, Omid Ebrahimpour, and many more. Their friendship and interesting discussions on research topics made my PhD studies more prosperous.

My appreciation goes to my family for their invaluable support, care and encouragement during my studies and my life. Without having them on my side, I could not have been where I am now.

Finally, I would like to thank Nadi, my companion during these years. I appreciate her collaboration, care and support and being with me throughout the path to success.

RÉSUMÉ

Cette thèse de doctorat présente l'activité transitoire du pyrophosphate de vanadyle (PPV), catalyseur utilisé par la compagnie Dupont pour la synthèse de l'anhydride maléique (AM) par oxydation partielle du n-butane. Les principaux objectifs de ce travail ont été de caractériser l'influence des paramètres ayant attrait à la nature redox du catalyseur afin d'optimiser la productivité d'AM et de proposer un modèle cinétique transitoire, applicable sur une large plage de conditions opératoires. Les principaux facteurs étudiés ont été : la composition des gaz réactifs, le temps d'oxydation du catalyseur, la température et la pression d'opération.

La première partie de cette thèse se focalise sur le comportement du PPV en oxydoréduction, qui a été étudié en régime permanent dans un réacteur lit fluidisé de laboratoire. Des données issues du réacteur type lit fluidisé circulant (LFC) de l'entreprise Dupont ont également été analysées quant à la production d'AM. L'objectif était d'étudier l'influence des configurations d'alimentation ainsi que l'injection d'oxygène supplémentaire (i.e. en excès) pour améliorer les taux de production d'AM, dans des réacteurs de diverses échelles. Le réacteur de laboratoire a été équipé d'un injecteur réglable à différentes hauteurs du lit. Le réacteur commercial avait lui aussi la possibilité d'injecter de l'oxygène supplémentaire dans la zone réactionnelle à l'aide de buses d'injections installées à différentes hauteurs du réacteur.

Les expériences à l'échelle du laboratoire ont montré que la sélectivité en AM ainsi que la conversion du n-butane augmentaient lorsque l'on diminuait la distance entre le point d'alimentation du n-butane et celui de l'oxygène. Les rendements en AM les plus élevés ont été observés alors qu'on co-alimentait de l'oxygène avec du n-butane à concentration élevée. La même observation a été réalisée dans le réacteur commercial. Le taux de production d'AM pourrait être augmenté de 15 % en alimentant seulement de l'oxygène supplémentaire dans la section inferieure du réacteur (*fast bed*). Ces résultats suggèrent que le PPV est extrêmement sensible à la configuration du système d'alimentation des gaz réactifs ainsi qu'à la présence d'oxygène en excès lorsque la concentration en n-butane est élevée. L'augmentation du

rendement d'AM a été attribuée au maintient d'un état d'oxydation supérieur tout en alimentant suffisamment d'oxygène dans la zone réactionnelle.

La majeure partie de cette thèse traite de la caractérisation et de l'optimisation de l'activité transitoire du PPV de Dupont, testées dans un microréacteur (lit fixe). Ces expériences ont eu aussi pour but de proposer un modèle cinétique transitoire. L'opération en LFC a été simulée en alternant les phases d'oxydation et de réduction sur environ 500 mg de catalyseur. Les expériences redox ont été conduites entre 360 et 400 °C et a une pression maximale de 4,1 bar. L'effet de la pression sur la cinétique de cette réaction n'a été que très peu discutée dans la littérature. Un large panel de composition de gaz réactifs et de temps d'oxydation du catalyseur a été étudié dans ce projet, afin de couvrir l'ensemble de la plage opérationnelle communément observée dans les lits fixes industriels, les lits fluidisés ou les réacteurs LFC.

Les données transitoires recueillies quant à la production d'AM ont montré que, indépendamment de la composition de l'alimentation, il existe une relation linéaire entre la production d'AM et le temps d'oxydation du catalyseur. Le taux de production d'AM a été amélioré de 50 % en augmentant le temps d'oxydation de 0,3 à 10 minutes, même en condition oxydantes (O_2/C_4H_{10} > 3,7). L'amélioration dans les taux d'AM est supposée venir d'une meilleure disponibilité de l'oxygène de surface lorsque le temps d'oxydation est supérieur. Cet effet était même plus prononcé lorsque la concentration de n-butane dans l'alimentation approchait la réduction pure (10 vol. % n-butane dilué dans l'argon). Cependant, en réduction pure, une désactivation majeure du catalyseur a été observée (baisse dans la production d'AM) même après 10 minutes de pré-oxydation. Une faible désactivation a aussi été observée à faible concentration d'oxygène dans l'alimentation. Dans ces conditions, l'oxydation du catalyseur joue un rôle important pour retrouver une activité catalytique. Ces observations, une fois encore, soulèvent l'importance d'une co-alimentation d'oxygène dans le gaz réducteur de façon à conserver une bonne activité catalytique et pour régénérer la surface en permanence.

Concernant la composition de l'alimentation, une composition équimolaire de n-butane et d'oxygène (~ 6 vol. %) a été identifiée comme étant la meilleure pour maximiser le taux d'AM.

Conformément aux tendances observées dans l'installation commerciale, les données recueillies ont reconfirmé que la performance du LFC pourrait être améliorée par une régénération efficace du catalyseur et une composition optimisée des gaz réactifs. La méthodologie présentée dans cette thèse a été développée de façon à être utile pour la conception et l'optimisation de technologies émergentes similaires, telles que la combustion en boucle chimique (CBC) ou d'autres procédés basés sur une technologie à lits transportés.

Une analyse approfondie des données expérimentales a montré que dans des conditions oxydantes (alimentation), l'augmentation de la conversion du n-butane était le principal facteur pour l'amélioration du rendement en AM. Par opposition, pendant une opération en conditions réductrices ($O_2/C_4H_{10} \leq 1{,}1$), la sélectivité en AM et la conversion du n-butane ont contribué conjointement à l'amélioration des performances du catalyseur. Une forte dépendance de la conversion du n-butane et de la sélectivité en AM sur la composition de l'alimentation ou sur le temps d'oxydation du catalyseur a alors été observée. Une baisse de la conversion du n-butane à de faibles concentrations d'oxygène peut indiquer que la contribution de l'oxygène de structure est très limitée dans la réaction. Par conséquent, l'oxygène de surface (i.e. disponible) absorbé depuis la phase gazeuse pourrait être considéré comme le facteur principal pour l'activation du n-butane.

À la fois la température et la pression ont montré un effet améliorant sur le rendement en AM. Ces effets ont été encore plus significatifs lorsque la concentration en oxygène dans l'alimentation était plus grande. La sélectivité en AM a chuté d'environ 20 % lorsque la pression du réacteur a été augmentée à 4,1 bar. Cependant, jusqu'à 60 % d'augmentation dans la conversion du n-butane a entrainé une amélioration du rendement global d'AM d'environ 30 %. Une hausse de température a également un effet positif sur la conversion du n-butane. Cependant, la sélectivité en AM était plus ou moins constante lorsqu'assez d'oxygène était alimenté. Ces observations se sont révélées encore plus vraies à plus haute pression. L'effet négatif de la température sur la sélectivité en AM doit cependant être minimisé.

La dernière partie de cette thèse présente le modèle cinétique transitoire développé. Malgré la simplicité de son mécanisme, le modèle a pu adéquatement prédire les résultats sur une large gamme de conditions, applicables aux lits fixes, fluidisés et/ou circulants. De plus, l'effet de la pression sur l'activité transitoire du PPV a été inclue dans le modèle, ce qui constitue une avancée majeure, puisque les études précédentes n'en tenaient pas compte. Ce point peut être considéré comme une contribution majeure de cette thèse. Les intervalles de confiance déterminés pour ce modèle, indiquent que ce seul modèle est applicable à pression ambiante ainsi qu'à plus hautes pressions.

Le modèle prédit les tendances pour un recouvrement transitoire d'oxygène de surface, ce qui explique le comportement observé durant les essais redox sur le PPV. D'après les donnes récoltées, une plus haute pression aide à obtenir une surface active du catalyseur plus oxydée (en conditions oxydante), alors que, en conditions réductrices, la surface devenait plus réduite. Sous de telles conditions, de plus hautes énergies d'activation ont été observées, ce qui est expliqué par l'accumulation de sites réduits de basse énergie sur la surface. De plus, la chute de la sélectivité en AM est attribuable à l'augmentation de l'énergie d'activation, ce qui implique une diminution du taux sélectif de réaction par la pression.

ABSTRACT

In this research thesis, the transient redox activity of the DuPont's vanadyl pyrophosphate (VPP) catalyst has been studied for partial oxidation of n-butane to maleic anhydride (MA). The main objectives have been to characterize the influence of redox parameters on the catalyst activity with an aim to optimize the MA productivity as well as to propose a transient kinetic model, which could be applied to the relatively wide range of the studied conditions. The major redox parameters include: redox feed composition, catalyst oxidation time, temperature and pressure.

In the first part of the thesis, the steady state redox behaviour of the VPP catalyst was analyzed in a lab scale fluidized bed. The industrial reactor data collected in DuPont's commercial circulating fluidized bed (CFB) for MA production were also studied. The objective was to study the effect of different feeding configurations and extra oxygen injection on the observed improvement in the MA production rates at different reactor scales. The lab scale reactor was equipped with a feed sparger adjustable at different bed heights. The commercial scale reactor had also the provisions of feeding extra oxygen to the reaction zone through multiple pre-installed nozzles at different reactor heights.

The lab scale sparger experiments showed that both MA selectivity and n-butane conversion increase by decreasing the distance between n-butane and oxygen feeds. The highest MA yields were achievable by co-feeding oxygen at relatively high n-butane concentrations. The same observation was confirmed in the commercial scale reactor. The MA production rate could be improved by about 15 % only by feeding extra oxygen into the lower section of the fast bed reactor. These findings suggested that the VPP catalyst is extremely sensitive to the reactor feed configuration and the presence of adequate amounts of oxygen is essential for optimal catalytic performance especially at relatively high n-butane concentrations. The improvement in the MA yield was attributed to maintaining higher catalyst oxidation state while providing adequate oxygen to the reaction zone.

The major part of this thesis dealt with characterizing and optimizing the transient activity of the DuPont's VPP catalyst in a lab scale micro-fixed bed reactor and proposing a transient kinetic model. The operation of a CFB reactor was simulated by switching between oxidizing and reducing feed compositions over about 500 mg of calcined VPP catalyst. The redox experiments were conducted in the temperature range of 360 to 400 °C and the reactor pressure of up to 4.1 bar. The effect of pressure on VPP kinetics has rarely been considered in the literature. A wide range of redox feed compositions and catalyst oxidation times were studied. The redox conditions essentially covered the entire range of operation, which is typically practiced in the industrial fixed bed, fluidized bed and CFB reactors.

The maleic anhydride transient rate studies revealed that irrespective of the feed composition, there is a linear correlation between the MA productivity and the catalyst oxidation time. The MA production rate was improved by up to 50 % by increasing the catalyst oxidation time from 0.3 to 10 minute even at oxidizing feed conditions ($O_2/C_4H_{10} > 3.7$). The improvement in MA rates was believed to be related to the higher availability of the catalyst's surface oxygen when the oxidation time was longer. This effect was more pronounced as n-butane concentration in the feed approached to pure redox mode (10 vol. % n-butane in argon). However, under the pure redox operation, a major catalyst deactivation (drop in MA rate) was detected even after excessive catalyst pre-oxidation (10 minute). Slight catalyst deactivation was also observed at very low oxygen concentrations in the feed. Under these conditions, the catalyst oxidation step played an important role in recovering the catalyst activity. These observations again highlighted the critical importance of co-feeding oxygen in the reduction feed as well as the adequate catalyst regeneration to preserve the catalytic activity.

With regard to the feed composition, a near equimolar concentration of n-butane and oxygen in the feed (~ 6 vol. %) was found to maximize the MA production rate. In accordance with the previously observed trends in the commercial reactor, the experimental data reconfirmed that the performance of the CFB reactor could be improved by efficient catalyst regeneration and by optimizing feed compositions. The experimental methodology presented in this thesis is believed

to be useful in design and optimization of similar emerging technologies such as chemical looping combustion (CLC) as well as other transport bed technologies.

Further analysis of the experimental data showed that under oxidizing feed conditions, the increase in n-butane conversion was the major contributor to MA yield improvement. While, during operation at reducing feed conditions ($O_2/C_4H_{10} \leq 1.1$), both MA selectivity and n-butane conversion contributed to the observed improvement in catalytic performance. Under these conditions, a strong dependency of n-butane conversion and MA selectivity on feed composition or catalyst oxidation time was observed. The drop in n-butane conversion at low oxygen concentrations might indicate that the contribution of the catalyst's structural oxygen in surface reactions is limited. Therefore, the surface adsorbed oxygen from gas phase could be considered as the main responsible for n-butane activation.

Both temperature and pressure showed an improving effect on MA yield. These effects were more significant when the concentration of oxygen in the feed was higher. MA selectivity dropped by about 20 % when the reactor pressure increased to 4.1 bar. However, up to 60 % increase in n-butane conversion resulted in an overall MA yield improvement of up to 30 %. Higher temperature increased n-butane conversion. However, MA selectivity was more or less constant provided that adequate oxygen was present in the feed. These effects were more noticeable at higher pressure. Data showed that maximum catalytic performance should be achievable at a higher pressure. However, the negative effect of temperature on MA selectivity had to be minimized.

In the last part of this thesis, a transient kinetic model was proposed. Despite its simple mechanism, the kinetic model could successfully predict the data for a wide range of redox conditions, which made it applicable to fixed bed, fluidized bed and CFB reactor operations. Moreover, the effect of pressure on VPP transient activity was considered in the model, which has been rarely studied in the literature. This achievement could be considered as one of the main contribution of this thesis. The estimated confidence intervals for the model parameters suggested that a single model could be applied to both ambient and higher pressures.

The model predicted trends for transient surface oxygen coverage helped explain the observed redox behaviour of the VPP catalyst. According to these data, higher pressure improved the catalyst surface oxidation state under oxidizing feed conditions; while at relatively higher n-butane concentration in the feed, increase in the pressure caused the surface to become more reduced. Under these conditions, the activation energies were estimated to increase for the redox reactions. This increase was attributed to the accumulation of low energy surface reduced sites while operating at reducing feed conditions. Moreover, the drop in the MA selectivity was explained by the increase observed in the activation energy of the selective reaction as well as the decrease in the corresponding reaction rate constant.

CONDENSÉ EN FRANÇAIS

Cette thèse traite de l'activité redox du, polyphosphate de vanadyle (PPV), catalyseur utilisé pour l'oxydation partielle du n-butane en anhydride maléique (AM), en régime transitoire. Malgré les efforts de caractérisation du comportement du catalyseur et de la cinétique en condition redox, il subsiste des controverses quant à la nature des phases actives du catalyseur et du rôle des espèces oxygénées, surtout en conditions transitoires. Il est communément accepté que le PPV (V^{4+}) est la phase active du catalyseur ; cependant, certaines études ont rapporté la possible participation de la phase V^{5+} comme étant essentielle à l'activité catalytique. L'objectif principal de cette thèse a été de caractériser l'activité redox du PPV en conditions transitoires, dans le but d'optimiser les performances catalytiques, ainsi que de proposer un modèle cinétique applicable à une plage étendue de conditions expérimentales et surtout à la pression. Les paramètres étudiés les plus importants ont été : la composition d'alimentation oxygène/n-butane, le temps d'oxydation du catalyseur, la température et la pression. Afin d'atteindre ces objectifs, le travail de recherche s'est focalisé sur ces quatre points :

1- Analyse du PPV en terme de performance dans un lit fluidisé de laboratoire et dans une unité commerciale type lit fluidisé circulant (LFC) de l'entreprise Dupont
2- Optimisation de la production d'AM dans un microréacteur en jouant sur la composition de l'alimentation et sur le temps d'oxydation du catalyseur
3- Étude de l'effet de la pression sur l'activité redox transitoire du PPV
4- Développement d'un modèle cinétique transitoire

La première partie de cette thèse présente les données relatives à l'activité du PPV, récoltées dans un réacteur lit fluidisé de 9 cm de diamètre externe ; ainsi que les taux de production d'AM étudiés dans l'installation de Dupont. L'objectif était d'étudier l'effet de la configuration de l'alimentation dans le lit fluidisé et de fournir de l'oxygène en excès dans un réacteur industriel pour analyser les répercussions sur l'activité catalytique. Il est généralement admis dans la

littérature que le taux de transfert d'oxygène du PPV est naturellement limité. En opérant en conditions réductrices ($O_2/C_4H_{10} \leq 1,1$), les performances catalytiques sont hautement dépendantes de la présence suffisante ou non d'oxygène afin de maintenir la productivité. Dans l'objectif de vérifier ces effets, les expériences conduites chez Dupont ont été réalisées à trois échelles différentes. L'analyse seule de ces données est cependant présentée dans cette thèse (et non la partie expérimentale).

Le lit fluidisé a été équipé d'un *sparger* de 6,4 mm qui a pu être ajusté à diverses hauteurs dans le lit de catalyseur. Les compositions d'alimentation suivantes ont été testées : n-butane/azote, air, n-butane/air et n-butane/azote/air. Les flux d'alimentation ont pu entrer soit par le distributeur ou par le *sparger* de façon indépendante. La hauteur du catalyseur était d'environ 20 cm sous des conditions normales de vitesses linéaires de gaz. Le *sparger* pouvait être ajusté à 2,5, 8 ou 18 cm au dessus du distributeur. Avant de mettre en marche l'unité commerciale, des essais en pilote (6,1 m de hauteur) ont permis de vérifier l'effet de la distribution de l'oxygène sur les performances du réacteur. Il a été trouvé qu'injecter de l'oxygène par des buses à 0,9, 2,1 et 3,7 m de hauteur a eu un impact positif sur les performances, par opposition à une injection seule à 0,9 m. dans le réacteur industriel. De l'oxygène additionnel dans la région de « *fast bed* » (4,2 m de diamètre) à également pu être injecté par 3 buses latérales. Initialement, il y avait 2 buses d'injection à 1,9 m et 5,5 m de hauteur. Cependant, une troisième buse a été installée à 0,5 m afin d'ajouter davantage d'oxygène.

Lors des expériences réalisées sur le lit fluidisé, les différentes configurations d'alimentation ont été testées : 1) n-butane/azote au *sparger* et air au distributeur, 2) n-butane/azote au distributeur et air au *sparger*, 3) air/n-butane au *sparger* et azote au distributeur et 4) 20 % de l'air avec n-butane/azote au distributeur et 80 % de l'air restant au *sparger*. Dans les expériences où le n-butane et l'oxygène ont été alimentés séparément (tests 1 et 2), la conversion du n-butane et la sélectivité en AM ont chuté ensemble au fur et à mesure que la distance entre le *sparger* et le distributeur augmentait. Le taux de production d'AM était au plus haut lorsqu'à la fois le n-butane et l'oxygène ont été co-alimentés (test 4). Des tendances similaires ont été observées pour la conversion de n-butane et la sélectivité en AM dans le réacteur industriel. La sélectivité en AM

était hautement dépendante des concentrations en oxygène lors de conditions réductrices. Dans les expériences relatives au *sparger*, le catalyseur était soumis a des conditions réductrices (~ 6 % volumique). Par conséquent, au fur et à mesure que le *sparger* était élevé dans le lit, le catalyseur lui-même n'était pas adéquatement exposé aux concentrations optimales en oxygène. Ceci a abouti à un degré d'oxydation inférieur du catalyseur et a induit une chute dans la sélectivité en AM. Le test 3 a donné les plus faibles rendements et sélectivités en AM. Ceci peut être attribué au court temps de contact entre le catalyseur et l'oxygène et le butane, alimentés par le *sparger*. Les bulles émises par le *sparger* ont probablement excité le lit sans optimiser le mélange dans la phase d'émulsion. Au test 4, les hauts taux observés en AM ont été attribués à l'effet de la co-alimentation d'oxygène à travers le distributeur. En conditions réductrices, la sélectivité en AM n'a pas chuté alors que la hauteur du *sparger* augmentait. Ces observations démontrent l'importance d'une alimentation suffisante d'oxygène dans la zone réactionnelle ainsi qu'une distribution optimale du gaz le long du lit, pour assurer de hauts rendements en AM.

Deux séries d'expériences sur l'injection d'oxygène ont été conduites dans le réacteur industriel. Dans la première expérience, les taux d'alimentation d'oxygène ont été changés entre le milieu (1,9 m) et la buse supérieure (5,5 m). Quatre conditions ont alors été testées : 1) fort taux d'oxygène au *sparger* du milieu, 2) faible taux d'oxygène au *sparger* du milieu, 3) faible taux d'oxygène au *sparger* du haut et 4) fort taux d'oxygène au *sparger* du haut. Indépendamment de la position de la buse, la production d'AM a été améliorée du fait que l'oxygène a été plus alimenté. Néanmoins, les fortes hausses de températures observées en sortie de réacteur ont limité l'injection de davantage d'oxygène (condition 4). La sélectivité en AM était plus élevée en conditions 2 qu'en condition 3. Ces données sont en parfait accord avec les expériences focalisées sur le *sparger*. Le taux en AM le plus haut a été observé en condition 4 ; cependant, une productivité encore supérieure aurait pu être obtenue en condition 1 dans des conditions similaires d'alimentation à la condition 4.

Dans la deuxième série d'expériences conduites sur l'unité commerciale, l'effet du changement de l'alimentation en oxygène depuis la buse médiane (1,9 m) à celle la plus basse (0,5 m) a été étudié. La production est passée de 3500 à 3800 kg/h alors que le passage de la buse du milieu a

celle du bas était encore incomplet. Il a même être possible d'atteindre 4000 kg/h en alimentant d'avantage d'oxygène pas la buse du milieu (15 % d'augmentation de capacité). Ces observations sont en accord avec celles réalisées lors des tests sur le *sparger* ou le taux d'AM avait été augmenté en diminuant la distance entre le *sparger* et le distributeur. Une fois encore, on démontre ici l'importance de l'alimentation optimale en oxygène en conditions réductrices.

En conclusion, les données du lit fluidisé et de l'unité commerciale montrent que le PPV est extrêmement sensible à l'oxygène durant des conditions où la concentration en n-butane est élevée. L'apport en oxygène et sa distribution adéquate dans le lit sont cruciaux afin d'optimiser les performances catalytiques (amélioration du taux de production d'AM). En outre, le maintien d'un taux élevé d'oxydation du catalyseur tout en évitant une réduction trop poussée, semblent être les facteurs déterminants.

La partie principale de cette thèse est consacrée à l'étude des paramètres redox sur l'activité du PPV, en microréacteur. Ce réacteur est en fait en tube de quartz ou d'acier inoxydable de 8 mm de diamètre externe, placé dans un four électrique. Les produits ont été analysés en ligne grâce à un spectromètre de masse, à une fréquence de 3 à 5 Hz. L'évolution de la concentration de l'acide produit (l'acide maléique surtout) a été suivie pas conductimètre dans un absorbeur placé après le réacteur. Un dosage quantitatif de l'acide produit a été réalisé par HPLC. Les conditions transitoires d'opération du LFC ont été simulées en alternant les phases d'oxydation et de réduction sur environ 500 mg de catalyseur PPV fourni par Dupont, et préalablement calciné. Les débits gazeux ont été ajustés à 40 mL/min, par 4 contrôleurs de débit massique. Une grande variété de composition d'alimentation et d'oxydation du catalyseur a pu être testée. Les conditions redox ont essentiellement couvert l'ensemble des compositions réelles d'opération typiquement conduites en lit fixe, lit fluidisé et lit fluidisé circulant industriels. Le temps d'oxydation du catalyseur a été varié entre 0,3 et 10 minutes alors que le temps de réduction a été maintenu à 2 minutes. La température a été variée entre 360 et 400 °C, en accord avec les conditions classiques d'opération. Afin d'étudier l'effet de la pression sur l'activité catalytique, un nombre défini d'expériences a été conduit à 4,1 bar. Ce type d'expérience a été peu développé dans la littérature.

Dans la seconde partie de cette thèse, l'effet de la composition de l'alimentation et de l'état d'oxydation du catalyseur sur la production d'AM a été étudié en régime transitoire. Les données recueillies montrent que, indépendamment de la composition de l'alimentation, il existe une relation linéaire entre les taux de production d'AM et le temps d'oxydation du catalyseur. En fait, les taux d'AM ont été améliorés même sous des conditions très oxydantes (1,4 vol. % n-butane/18,1 vol. % oxygène, bal. argon). Dans ces expériences, où de l'oxygène était présent dans l'alimentation, le taux d'AM enregistré a été supérieur de 50 % lorsque le temps d'oxydation est passé de 0,3 à 10 minutes. Cet effet était encore plus significatif alors que l'alimentation s'approchait de conditions extrêmes de réduction (i.e. pas d'oxygène). Sous de telles conditions, la production d'AM a été améliorée d'un facteur 3,5 après avoir étendu la durée d'oxydation préalable du catalyseur à 10 minutes. L'amélioration de la production d'AM est reliée à une meilleure disponibilité de l'oxygène de surface du catalyseur (pour un temps d'oxydation plus long). Ces résultats mettent en lumière l'importance de la régénération du catalyseur en conditions industrielles (conditions réductrices). De plus, les données montrent que, même en conditions d'alimentation plus oxydantes, une régénération efficace du catalyseur contribue à une meilleure production d'AM.

Les données de redox montrent que le taux de production d'AM peut-être maximisée pour un ratio d'alimentation équimolaire en n-butane et oxygène à environ 6 vol. %. Le taux de production d'AM a augmenté alors que l'oxygène a été augmenté de 0 à 6 vol. %. A ce point, le taux à commencer à décroitre de 15 % en conditions lit fluidisé et encore de 30 % alors que l'on approchait des conditions lit fixe. On peut attribuer cette observation au double effet de l'augmentation du n-butane dans l'alimentation. L'effet positif peut être attribué à l'augmentation du débit alors que l'effet négatif peut être l'état d'oxydation inférieur du catalyseur (perte de sélectivité).

Le taux de production d'AM sous réduction pure montre une désactivation du catalyseur après quelques cycles redox (pure réduction i.e. pas d'oxygène puis régénération avec oxygène). Même une régénération poussée pendent 10 minutes n'a pas pu compenser pour ce manque d'activité. Cependant, aucun oxyde de carbone n'a été détecté durant la phase de régénération. Ceci peut

indiquer que la désactivation est uniquement due a une exposition excessive au n-butane qui a trop réduit le catalyseur. Dans les conditions $O_2/C_4H_{10} \leq 0,6$, le catalyseur se désactivait aussi après quelques cycles. Ces observations démontrent l'importance énorme de la présence d'oxygène en quantités suffisantes durant la phase de réduction et l'importance de la régénération du catalyseur de façon à préserver l'activité du catalyseur, surtout lors d'opérations en conditions riches en n-butane.

La troisième partie de cette thèse présente l'analyse détaillée de l'effet de la pression sur l'activité du PPV, étudiée sur une large gamme de conditions redox. Pour les tests réalisés a haute pression, le réacteur en quartz a été remplacé par un tube en acier inoxydable et des vannes ont été installées pour tenir la pression dans le système. Même si l'effet de la pression a été rarement mentionné dans la littérature, ce travail consiste en une contribution majeure.

Les données recueillies à pression ambiante ont montrée que travailler en conditions oxydantes ($O_2/C_4H_{10} \geq 3,7$), améliorait le rendement en AM, surtout grâce a l'augmentation de la conversion du n-butane. Cependant, en conditions réductrices, la sélectivité en AM a montré une forte dépendance sur le temps d'oxydation du catalyseur et de la composition de l'alimentation. Sous ces conditions, la conversion du n-butane et la sélectivité en AM ont contribuées à l'amélioration observée en rendement en AM. En l'absence d'oxygène dans l'alimentation, la conversion en n-butane a chuté de 10 % à 2 %. Ceci peut indiquer que l'activation du n-butane se fait principalement à travers l'oxygène de surface. Sous des conditions redox pures, même une régénération poussée du catalyseur ne suffit pas pour contrebalancer les effets de l'alimentation seule du n-butane, entrainant une trop forte réduction du catalyseur. Il apparaît que, sous des conditions riches en combustible (*fuel rich*), l'oxygène de la structure du catalyseur ne participe donc que très peu dans les réactions de surface. C'est donc l'oxygène adsorbé directement de la phase gazeuse qui est important afin de maintenir une haute conversion en n-butane et un haut rendement envers l'AM.

Les expériences réalisées en microréacteur montrent que la pression et la température ont un effet positif sur l'activité catalytique. Jusqu'à 60 % d'augmentation dans la conversion du n-butane a

été relevée, en augmentant la pression à 4,1 bar. Parallèlement, la sélectivité en AM a diminuée de 20 %. Globalement cependant, le rendement en AM a été augmenté de 30 %. Une plus haute température augmente également la conversion en n-butane. Cet effet est encore plus net lorsque la concentration en oxygène est augmentée dans l'alimentation. Sous ces conditions, la sélectivité en AM était plus ou moins constante. L'effet de la température était plus important à plus haute pression. Ces observations démontrent que le rendement en AM peut être amélioré en jouant sur la température et sur la pression. Cependant, l'effet négatif de la température sur la sélectivité de l'AM doit être minimisé en conditions réductrices. L'effet de la pression sur l'activité catalytique peut être expliqué plus en détail en regardant les prédictions du modèle.

La dernière partie de cette thèse expose le modèle cinétique proposée. L'écoulement à travers le réacteur a été modélisé par un modèle type n-réacteurs en série, et a été trouvé très proche d'un écoulement piston. Le modèle cinétique est quant à lui, basé sur un mécanisme type Mars-van Krevelen (MvK) à un site redox :

$$O_2 + S \longrightarrow O_2 \cdot S \tag{1}$$

$$C_4H_{10} + 3.5\ O_2 \cdot S \longrightarrow C_4H_2O_3 + 4\ H_2O + 3.5\ S \tag{2}$$

$$C_4H_{10} + 5.5\ O_2 \cdot S \longrightarrow 4\ CO_x + 5\ H_2O + 5.5\ S \tag{3}$$

$$CO_x = \frac{(CO+CO_2)}{2} \tag{4}$$

Dans ce mécanisme, les sites réduits (S) sont premièrement oxydés par de l'oxygène moléculaire (réaction 1). Les sites oxydés participent soit à la réaction sélective (réaction 2) ou à la non sélective (réaction 3). Le cycle redox est terminé par la réoxydation des sites réduits par réaction (1). À cause des incertitudes autour des états d'équilibre entre les gaz et les espèces de surface ou entre les espèces adsorbées elles-mêmes, seulement les interactions entre la phase gazeuse et les espèces de surface ont été considérées dans le mécanisme. L'application de ce modèle

relativement simple, suggère que, malgré la complexité du système catalytique, le comportement redox du PPV peut être représenté de façon adéquate pas la paire de sites actifs V^{4+}/V^{5+}.

Le modèle a prédit les tendances pour l'oxydation du catalyseur, fournissant plus de connaissances sur l'effet de la pression sur l'activité catalytique. Les données prédites ont montré que, au fur et à mesure que la pression augmente, l'état d'oxydation du catalyseur change en fonction de la composition de l'alimentation. En opérant en conditions oxydantes, la surface du catalyseur était oxydée à plus haute pression. Cependant, sous des conditions réductrices, typiques des conditions du réacteur en LFC, la surface du catalyseur était réduite au fur et à mesure que la pression augmentait. De plus, le modèle a pu prévoir que les énergies d'activation augmentaient avec la pression. Des variations similaires dans l'énergie d'activation ont été reportées par Schuurman et Gleaves (1997). L'augmentation dans l'énergie d'activation avec la pression peut être attribuée à l'état d'oxydation inférieur observé lorsque les conditions étaient réductrices. En accord avec ceci, la chute de la sélectivité de l'AM avec la pression peut-être expliquée par la hausse de l'énergie d'activation de la réaction sélective (réaction 3). Le modèle prévoit également que la constante de production pour la réaction sélective est considérablement diminuée par la pression. Ceci peut être une raison supplémentaire à la chute de la sélectivité en AM. Ces résultats confirment encore l'importance de maintenir la surface du catalyseur oxydée, surtout en conditions très réductrices.

En conclusion, le modèle cinétique proposé a démontré une habilité particulière à prévoir adéquatement les observations quant au comportement redox du catalyseur, pour un large éventail de conditions (composition, température, pression), typiques des opérations en lit fixe, fluidisé ou LFC. De plus, les prédictions du modèle sur les variations du degré d'oxydation du PPV à plus hautes pressions ont aidé à une meilleure compréhension de l'activité transitoire de ce catalyseur.

TABLE OF CONTENTS

DEDICATION III

ACKNOWLEDGEMENTS IV

RÉSUMÉ V

ABSTRACT IX

CONDENSÉ EN FRANÇAIS XIII

TABLE OF CONTENTS XXI

LIST OF TABLES XXV

LIST OF FIGURES XXVI

LIST OF SYMBOLS AND ABBREVIATIONS XXIX

LIST OF APPENDICES XXXIII

INTRODUCTION 1

CHAPTER 1 LITERATURE STUDY 6

1.1 Introduction 6

1.2 Circulating fluidized bed concept 7

1.3 Redox parameters 9

1.3.1 Oxygen capacity 9

1.3.2 Redox duration 10

1.3.3 Temperature 11

1.3.4 Feed composition 12

1.3.5 Pressure 12

1.4 Transient kinetic modeling 14

1.4.1 Oxidation kinetics 16

1.4.2 Reduction kinetics 18

1.5 Carbon deposition 24
1.6 Active sites 25
1.6.1 Vanadium states 26
1.6.2 Oxygen species 27
1.7 Redox operations 27
CHAPTER 2 RESEARCH METHODOLOGY 29
2.1 Problem statement 29
2.2 Objectives 29
2.3 Thesis organization 31
2.4 Catalyst preparation 32
2.5 Ambient pressure experiments 33
2.6 High pressure experiments 34
2.7 Kinetic model development 36
CHAPTER 3 MALEIC ANHYDRIDE YIELD DURING CYCLIC N-BUTANE/OXYGEN OPERATION 37
3.1 Presentation of the article 37
3.2 Abstract 38
3.3 Introduction 38
3.4 Experimental 42
3.4.1 VPO catalyst preparation 42
3.4.2 Experimental setup 42
3.4.3 Redox experiments 43
3.5 Results and discussion 45
3.5.1 Effect of redox parameters 45
3.5.2 Transient maleic anhydride rates 48

3.6 Conclusions 51
3.7 Acknowledgements 52
3.8 References 52
CHAPTER 4 TRANSIENT REDOX ACTIVITY OF VANADYL PYROPHOSPHATE AT AMBIENT AND ELEVATED PRESSURE 54
4.1 Presentation of the article 54
4.2 Abstract 55
4.3 Introduction 56
4.4 Experimental 60
4.4.1 Micro-reactor setup 60
4.4.2 Transient redox experiments 61
4.5 Results and discussion 64
4.5.1 Data analysis 64
4.5.2 Transient catalytic activity 64
4.5.3 Effect of temperature 74
4.5.4 Effect of pressure 75
4.6 Conclusions 81
4.7 Acknowledgements 82
4.8 References 83
CHAPTER 5 TRANSIENT KINETICS OF N-BUTANE PARTIAL OXIDATION AT ELEVATED PRESSURE 91
5.1 Presentation of the article 91
5.2 Abstract 92
5.3 Introduction 92
5.4 Experimental 96

5.4.1 Experimental setup 96
5.4.2 Redox experiments 97
5.5 Model development 98
5.5.1 Hydrodynamic model 98
5.5.2 Kinetic model 99
5.5.3 Transient mass balance equations 101
5.5.4 Parameter estimation 103
5.6 Results and discussion 105
5.6.1 RTD model 105
5.6.2 Kinetic model 106
5.6.3 Model validation 111
5.7 Conclusions 116
5.8 Acknowledgements 117
5.9 Nomenclature 117
5.10 References 120
GENERAL DISCUSSION 125
CONCLUSIONS AND RECOMMENDATIONS 130
BIBLIOGRAPHY 135
APPENDICES 148

LIST OF TABLES

Table 1.1: Kinetic models for n-butane oxidation to maleic anhydride 20

Table 2.1: Technical specification of VPP samples 32

Table 2.2: Experimental conditions at P = 1 bar 34

Table 2.3: Experimental conditions at P = 4.1 bar 35

Table 3.1: Technical specifications of DuPont's calcined VPO catalyst 42

Table 3.2: Experimental conditions of transient redox runs 45

Table 4.1: Transient experimental conditions: ambient pressure 62

Table 4.2: Transient experimental conditions at 4.1 bar 63

Table 5.1: Transient redox experimental conditions (100 and 410 kPa) 98

Table 5.2: RTD model parameters 106

Table 5.3: Activation energies, kJ/mol 110

Table A.1: Air to distributor and n-butane/N_2 to sparger (5.0 /0.1/1.6 l/min (STP)) 158

Table A.2: Air to sparger and n-butane/N_2 to distributor (5.0 /0.1/1.6 l/min (STP)) 161

Table A.3: Air/n-butane to sparger and N_2 to distributor (5.0/0.1/1.6 l/min (STP)) 162

Table A.4: Air to sparger air/n-butane/N_2 to distributor (4.1 and 0.9/0.1/1.6 l/min (STP)) 164

Table A.5: Initial reactor conditions before switching the oxygen feed (Temperature ≈ 380 °C) 169

Table A.6: Switching oxygen to the upper oxygen sparger (Temperature ≈ 380 °C) 170

LIST OF FIGURES

Figure 1-1: CFB reactor configuration 8

Figure 1-2: VPP oxygen storage capacity 10

Figure 1-3: Outlet oxygen partial pressure in oxidation 13

Figure 1-4: Effect of oxygen concentration on MA yield 13

Figure 1-5: Redox mechanism for n-butane oxidation over VPP 14

Figure 1-6: Effect of oxygen concentration on re-oxidation rate 19

Figure 1-7: Effect of inert purging on n-butane conversion 22

Figure 1-8: Carbon deposition during redox cycles 26

Figure 1-9: Simulation of cyclic redox operation 28

Figure 2-1: Micro-reactor setup 33

Figure 2-2: High pressure reactor 35

Figure 3-1: Micro-reactor experimental setup 44

Figure 3-2: Effect of oxidation time on maleic anhydride production rate 47

Figure 3-3: Effect of feed composition on maleic anhydride production rate 48

Figure 3-4: Effect of temperature on maleic anhydride production rate 49

Figure 3-5: Maleic anhydride transient production rates 50

Figure 3-6: VPO catalyst deactivation during redox operations at fuel rich conditions 51

Figure 4-1: Micro-reactor setup at elevated pressure 60

Figure 4-2: n-Butane conversion vs. feed composition 65

Figure 4-3: Maleic anhydride selectivity vs. feed composition 67

Figure 4-4: Maleic anhydride selectivity vs. n-butane conversion 69

Figure 4-5: CO selectivity vs. catalyst oxidation time 70

Figure 4-6: CO_2 selectivity vs. catalyst oxidation time....71
Figure 4-7: CO selectivity vs. n-butane conversion....72
Figure 4-8: CO_2 selectivity vs. n-butane conversion....73
Figure 4-9: Effect of temperature on n-butane conversion....75
Figure 4-10: Effect of temperature on maleic anhydride selectivity....76
Figure 4-11: Effect of pressure on n-butane conversion....77
Figure 4-12: Effect of pressure on oxygen conversion....78
Figure 4-13: Effect of pressure on maleic anhydride selectivity....79
Figure 4-14: Effect of pressure on maleic anhydride yield....80
Figure 4-15: Effect of temperature/pressure on n-butane conversion....81
Figure 5-1: Experimental micro-reactor setup....97
Figure 5-2: Reactor model scheme....98
Figure 5-3: Reactor RTD versus model predictions....105
Figure 5-4: Transient rate constants....107
Figure 5-5: Estimated initial VPP oxygen coverage....109
Figure 5-6: Transient VPP oxidation during reaction....110
Figure 5-7: n-Butane conversion vs. model....111
Figure 5-8: Oxygen conversion vs. model....112
Figure 5-9: MA selectivity vs. model....113
Figure 5-10: CO_x selectivity vs. model....114
Figure 5-11: Model predictions vs. experimental data....115
Figure 5-12: Residuals versus predicted values....115
Figure 5-13: Normal probability plot of the residuals....116
Figure A-1: 89 mm OD fluidized bed reactor....153

Figure A-2: Pilot plant reactor 155

Figure A-3: Commercial CFB reactor 156

Figure A-4: Fixed bed experiments: selectivity vs. conversion 160

Figure A-5: Sparger experimental data compared to operation when all gases are co-fed through the distributor 165

Figure A-6: n-Butane conversion and maleic acid selectivity versus freeboard temperature 167

Figure A-7: Effect of sparger height on maleic acid selectivity 168

Figure A-8: Maleic acid productivity versus feed rates to the oxygen spargers 171

LIST OF SYMBOLS AND ABBREVIATIONS

CFB	Circulating fluidized bed
CLC	Chemical looping combustion
CO_x	Averaged property between CO and CO_2
C_{SO_2}	Surface oxygen concentration, mol/mg
C_{ST}	Total concentration of surface sites, mol/mg
CSTR	Continuously stirred tank reactor
C_T	Total gas concentration, mol/mL
d_P	Average particle size, µm
E_i	i^{th} reaction activation energy, kJ/mol
ΔE_i	i^{th} activation energy difference, %
$E(t)$	Residence time distribution, s^{-1}
$E(\theta)$	Normalized residence time distribution = $\bar{t}E(t)$
F_{0Ar}	Initial molar flow rate of argon, mol/s
F_j	Molar flow rate of component *j* in general form, mol/s
$F_{j1}(t)$	Inlet molar flow rate function for component *j*, mol/s
$F_{j,n}(t)$	Molar flow rate of component *j* entering n^{th} sub-section, mol/s
$F_j(t,n)$	Molar flow rate of component *j* at time *t* entering sub-section *n*, mol/s
$F_7(0,n)$	Molar flow rate of argon at time zero entering sub-section *n*, mol/s
F_T	Total molar flow rate, mol/s
$F_{T1}(t)$	Inlet total molar flow rate function, mol/s
$F_T(t,n)$	Total molar flow at time *t* entering sub-section *n*, mol/s
HPLC	High performance liquid chromatography

k_i	i^{th} reaction rate constant, s^{-1}
k_{r_i}	i^{th} reference reaction rate constant, s^{-1}
LH	Langmuir-Hinshelwood mechanism
LOC	Lattice oxygen contribution
LSQ	Least square method
MA	Maleic anhydride
MFC	Mass flow controller
MvK	Mars-van Krevelen mechanism
n	Index representing the n^{th} catalyst bed or blank sub-section
N	Total number of tanks in series
N_r	Number of tanks in series for catalyst bed
OD	Outside diameter, various units
$O_2 \cdot S$	Catalyst's oxidized site
O_2/C_4H_{10}	Oxygen to n-butane molar ratio
Pe	Peclet number = 2(*N*-1)
P/V	Phosphorous to vanadium ratio, molar
r_i	i^{th} transient reaction rate, mol/mg.s
R	Universal gas constant = 8.314 J/mol.K
R_l^2	R-square of fit for data point *l*
$R_j(t,n)$	Global reaction rate of component *j* at time *t* and sub-section *n*, mol/mg.s
RTD	Residence time distribution
S	Catalyst's reduced site
S_{CO_x}	CO_x selectivity, %
S_{MA}	Maleic anhydride selectivity, %

STP	Standard Temperature and Pressure
t	Time, s
$\bar{t}$	Gas residence time, s
T	Reaction temperature, K
T_r	Reference reaction temperature = 653.15 K
u_g	Superficial gas velocity, cm/s
vol.	Volumetric percentage, %
VPO	Vanadium phosphorous oxide
VPP	Vanadyl pyrophosphate
V^{4+}, V^{5+}	Vanadium oxidation states
V(n)	Gas phase volume at n^{th} sub-section, mL
wt.	Weight percentage, %
W(n)	Catalyst weight at n^{th} bed sub-section, mg
$X_{C_4H_{10}}$	n-Butane conversion, %
X_{O_2}	Oxygen conversion, %
y_l	Experimental value for data point *l*, %
y_l^p	Predicted value for data point *l*, %
$\bar{y}_l$	Average value of all experimental values for data point *l*, %

Greek letters

θ	Normalized time, $t/\bar{t}$
θ_{O_2}	Oxygen surface coverage, %
θ_{0O_2}	Initial catalyst surface oxygen coverage, %
$\theta_{O_2}(t,n)$	Oxygen surface coverage at time *t* and bed sub-section *n*, %

v_{ij}	Stoichiometric coefficient for component j in i^{th} reaction
ρ_P	Catalyst's particle density, kg/m^3
σ^2	Variance of $E(t)$ curve, s^2
σ_θ^2	Variance of $E(\theta)$ curve
Φ_{fmin}	Objective function for minimization method
Φ_{lsq}	Objective function for least square method

Subscripts and superscripts

i	Number of reactions
j	Components: C_4H_{10}, O_2, MA, H_2O, CO, CO_2 and Ar
l	$X_{C_4H_{10}}$, X_{O_2}, S_{MA} and S_{CO_x}
m	Number of experiments
p	Predicted values

LIST OF APPENDICES

APPENDIX A – EFFECT OF FEED NOZZLE CONFIGURATION ON N-BUTANE TO MALEIC ANHYDRIDE YIELD: FROM LAB SCALE TO COMMERCIAL 148

APPENDIX B – DATA ANALYSIS..... 175

APPENDIX C – KINETIC MODELING PROGRAM 187

INTRODUCTION

Catalytic partial oxidation of light alkanes to value added chemicals is by far one of the most studied topics in heterogeneous catalysis. The major incentive for research in this field has been probably the economical interest to produce higher value petrochemical products from inexpensive and non-toxic feedstock. Among the highly studied topics, n-butane partial oxidation to maleic anhydride (MA) has received a special attention due to its commercial viability and relatively complex catalyst system as well as the huge global demand for maleic anhydride as an intermediate chemical product. World production and consumption of maleic anhydride in 2010 were reported to be approximately 1.7 million metric tons. The demand was expected to grow on an average of 3-6 % by 2020. Maleic anhydride (or acid) is an important multifunctional chemical intermediate that is mainly used in the manufacture of phthalic-type alkyd and polyester resins (39 %) followed by the production of 1,4-butanediol (SRI, 2011). Some of the other applications include: surface coatings, lubricant additives, plasticizers, copolymers, and agricultural chemicals (Kirk-Othmer, 2001).

Partial oxidation of n-butane to maleic anhydride has been commercialized for decades. The reaction occurs by contacting a mixture of n-butane and oxygen well below the flammability limits with a vanadium-phosphorous-oxide (VPO) catalyst at a typical temperature range of 350-420 °C. The active phase of the catalyst is known to be mainly the vanadyl pyrophosphate (VPP) phase – $(VO)_2P_2O_7$ – representing the V^{4+} vanadium oxidation state. Several other crystalline phases have been known to exist on the surface in conjunction with the catalyst active phase. These phases have been usually referred to by the general form of $VOPO_4$, which is representing the V^{5+} oxidation state. Although the VPO system is regarded as a complex catalytic system, it is generally understood that a selective n-butane oxidation proceeds through the contribution of both V^{4+} and V^{5+} sites. An average surface P/V ratio slightly above 1.0 was also found to be essential for optimum catalyst activity. While catalyst lattice oxygen located at uppermost surface layers is known to be highly selective to maleic anhydride, its contribution to the surface reactions has been reported to be very limited. On

the contrary, the surface adsorbed oxygen or loosely bound oxygen species on the surface were reported to play an important role in n-butane activation.

The following set of reactions represents the main pathways for n-butane conversion to maleic anhydride. In these reactions, n-butane is either selectively converted into maleic anhydride (Reaction (1)) or it undergoes non-selective conversion into total combustion products (Reactions (2) and (3)). Apart from maleic anhydride, minor production of several other carboxylic acid products has been reported in the literature. Some of the common products include: acetic, acrylic, methacrylic, fumaric and phthalic acid (Lorences et al., 2003).

$$C_4H_{10} + 3.5\ O_2 \rightarrow C_4H_2O_3 + 4\ H_2O \quad (1)$$

$$C_4H_{10} + 4.5\ O_2 \rightarrow 4\ CO + 5\ H_2O \quad (2)$$

$$C_4H_{10} + 6.5\ O_2 \rightarrow 4\ CO_2 + 5\ H_2O \quad (3)$$

In the process of selective oxidation of n-butane to maleic anhydride, it has always been desirable to achieve higher maleic anhydride productivity by increasing the n-butane throughput to the reactor. However, this has normally been accompanied by a loss in MA selectivity and declining catalytic activity as well as the explosion risk. The catalytic activity loss could be due to the accumulation of surface reduced sites or in extreme cases the catalyst over-reduction at relatively high n-butane concentrations. Industrial fixed bed reactors for MA production are normally operated at a maximum of 1.8 vol. % n-butane in the inlet feed. However, the fluidized bed reactors could operate at up to 4 vol. %. Higher n-butane concentrations of up to 10-20 vol. % are possible in industrial circulating fluidized bed (CFB) reactors. Practically, maintaining an optimized catalytic activity at relatively high n-butane feed compositions requires the presence of sufficient amounts of oxygen in the feed. Oxygen function is to re-oxidize the catalyst’s surface during reaction and to prevent the catalyst from being excessively or in some cases irreversibly reduced.

Several reactor configurations have been developed for commercial maleic anhydride production. Fixed bed reactors have been conventionally in practice since several decades. However, limited inlet concentrations of n-butane due to explosion hazards, heat transfer (creation of hotspot) and catalyst instability have been among the major concerns facing this technology. Fluidized bed reactors offer more flexibility in terms of inlet n-butane concentrations with low risk of explosion due to quenching effects of particles on free radicals in the bed. Heat of reaction is effectively managed and the MA productivity is improved. Membrane reactors could operate at relatively high feed concentrations as the oxygen and hydrocarbon are fed separately. Oxygen is available to the reaction through diffusion along a permeable membrane wall. Hot spot formation is minimized and the runaway combustion risk is suppressed. However, this technology has not shown a great impact on catalyst performance compared to fixed bed reactors. Latest reactor developments include the circulating fluidized bed reactors in which the oxidizing and reducing zones are separated by using two different reaction vessels (Contractor et al., 1994). The main objective has been to maximize the utilization of selective catalyst lattice oxygen. Since n-butane and oxygen are fed separately, much higher n-butane concentrations (up to 20 vol. %) could be fed to the reactor resulting in a lower catalyst inventory. Major technological concerns include mechanical stability of the circulating catalyst, catalyst attrition or agglomeration, management of fines, complexity of operation due to several interconnected vessels and inherently low catalyst oxygen transfer capability.

DuPont Company developed a circulating fluidized bed reactor technology for maleic anhydride production in which the VPP catalyst was circulated between regeneration and reaction vessels. The oxidized catalyst was transferred from the regenerator through a standpipe to the bottom section of the reaction vessel (fast bed) which was in turbulent fluidization regime. The solids and gas mixture were then transferred in an upward flow through a riser reactor and they entered a cyclone/stripper assembly. After product separation, the reduced solids were returned to the regenerator through another standpipe. In this configuration, MA productivity could be enhanced by using relatively high concentrations of n-butane in the feed and effective utilization of catalyst lattice oxygen. Moreover, by separating the redox zones, the operating conditions of each vessel could be

optimized independently. However, in practice, due to insufficient catalyst oxygen transfer from the regeneration zone, molecular oxygen had to be fed along with the reduction feed to achieve the designed MA production rates and to prevent catalyst over-reduction.

The redox kinetics of n-butane partial oxidation over VPP catalyst could be considered among the most challenged kinetic studies. Despite the large volume of research on this topic, the actual redox mechanism of the reaction and the transient behaviour of the catalyst under redox conditions are still not fully understood. Most of the existing kinetic models are either proposed for catalyst re-oxidation or reduction reactions. In addition, these models are only valid for a narrow range of redox operating conditions. The major challenges against developing a kinetic model applicable to a wide range of redox conditions might have been the insufficient knowledge on the catalyst active phases and the variation of catalyst oxidation state during reaction. Moreover, the exact role of surface oxygen species during reaction has not been clearly identified (Wang and Barteau, 2002, 2003).

Research objectives

In this doctoral thesis, the catalytic behaviour of an industrial VPP catalyst has been studied. The main objectives have been:

1- To characterize and optimize the transient catalytic activity of DuPont's VPP catalyst in a wide range of redox operating conditions

2- To propose a transient kinetic model which could be applicable to the range of studied conditions and specifically valid for higher pressures

The effect of pressure on VPP kinetics has rarely been studied in the open literature. Since the industrial reactors normally operate at higher than atmospheric pressures, the redox experiments in this thesis were conducted at a pressure of 4.1 bar to study the effect of pressure on catalytic activity and redox kinetics.

In the first part of the thesis, the redox behaviour of the VPP catalyst was analysed in a laboratory fluidized bed as well as in the DuPont's commercial CFB reactor under different feeding configurations. This study revealed the importance of providing adequate oxygen to the reaction zone while operating at high n-butane concentrations.

In the second part of the research, the transient redox behaviour of the same catalyst was characterized in a micro-fixed bed laboratory scale reactor. A linear correlation was found between the catalyst oxidation time and MA production rates. The MA productivity was maximized at an equimolar feed composition. Some catalyst deactivation was observed at highly reducing conditions.

In the third part of the studies, a large collection of transient redox data were analysed and discussed in full detail for the whole range of operating conditions including higher reactor pressure (4.1 bar). Pressure was found to significantly influence the catalytic performance.

Finally, based on a single site redox mechanism, a transient kinetic model was proposed. The model was applicable to the wide range of redox conditions typically practiced in fixed and fluidized bed as well as CFB reactors. The specific feature of the model was that it was applicable to higher reactor pressure.

The scientific contributions of this research thesis could be summarized as:

1- To characterize the transient activity of VPP catalyst over a wide range of redox conditions including higher pressure

2- To define a correlation between MA production rates and catalyst oxidation time

3- To optimize the catalytic performance with regard to redox feed composition

4- To propose a transient kinetic model which is applicable to a wide range of feed compositions and higher pressure

CHAPTER 1 LITERATURE STUDY

In this Chapter, a detailed review of the pertinent scientific literature available on n-butane partial oxidation over VPP catalyst is presented.

1.1 Introduction

For over four decades, numerous research studies have been conducted to gain a better insight on the ambiguous behaviour of VPP catalyst for n-butane partial oxidation to maleic anhydride. In a research review, Ballarini et al. (2006) studied 156 articles and presented the past and current challenges in VPP catalysis for maleic anhydride production. According to this review, the production of maleic anhydride from n-butane and the physico-chemical properties of the catalyst's active phase have been among the most studied catalysis topics during recent decades. Despite these efforts, there are still considerable uncertainties on the catalyst active phases and the role of oxygen species during reaction.

Two catalyst phases have been identified to play the major role in catalytic activity: the vanadyl pyrophosphate – $(VO)_2P_2O_7$ – and its oxidized forms generally known as $VOPO_4$. Latest developments indicated that the catalyst's surface lattice oxygen is selective to maleic anhydride. However, it was shown that the participation of this oxygen species in the surface reactions is limited. Instead, the surface adsorbed oxygen or the loosely bound oxygen was reported to largely contribute to the catalytic activity.

Several reactor configurations have been studied in an attempt to improve the MA productivity. Fixed bed, fluidized bed and circulating fluidized bed reactors are among the most studied reactor types. Membrane reactors are among the less studied reactor types. Fixed bed reactors typically operate at below flammability limits (1.8 vol. % n-butane in air). Fluidized bed reactors have the advantage of operation at higher n-butane concentrations (up to 4 vol. %) by avoiding the flammability ranges due to the quenching effect of fluidized

particles. More complex reactor types are the CFB reactors having separate reduction and oxidation zones enabling high n-butane throughputs. A higher MA selectivity is achievable due to utilizing the catalyst's selective oxygen (Contractor et al., 1994).

The proposed kinetic models for n-butane partial oxidation over VPP catalyst are generally limited to narrow ranges of operating conditions. Usually, these models are developed for either catalyst oxidation or reduction steps. Moreover, the effect of pressure on VPP catalytic activity has rarely been considered in the kinetic studies. A comprehensive kinetic model applicable to an adequately wide range of transient redox conditions, including reactor pressure, has not been available in the open literature.

1.2 Circulating fluidized bed concept

The CFB reactor concept was first proposed by the DuPont Company (Contractor et al., 1986; Contractor, 1987, 1999). This technology was a significant breakthrough for improving maleic anhydride selectivity. In the CFB reactor, the catalyst was circulated between two reaction and regeneration zones. The extremely high rate of catalyst recirculation was required to ensure economic MA production rates by supplying enough catalyst oxygen to the reaction zone. For example, a recirculation rate of 650 kg/s of catalyst was required to for a MA production rate of 20,000 tons/year. This corresponds approximately to the production of one gram of maleic anhydride per kilogram of the catalyst (Emig, 1994).

Figure 1-1 illustrates the DuPont's CFB reactor configuration. The reaction section consisted of a turbulent fluidized bed (fast bed) and a riser. The catalyst was transferred through the riser reactor to the regeneration section after being separated from the product gas in a stripper/cyclone assembly. The reduced catalyst then entered the regeneration section where it was re-oxidized by air in a fluidized bed. Finally, the oxidized catalyst returned to the bottom section of the fast bed reactor through a standpipe. Product acids (mostly maleic acid) were subsequently recovered from the product gas stream by absorption in the scrubbers.

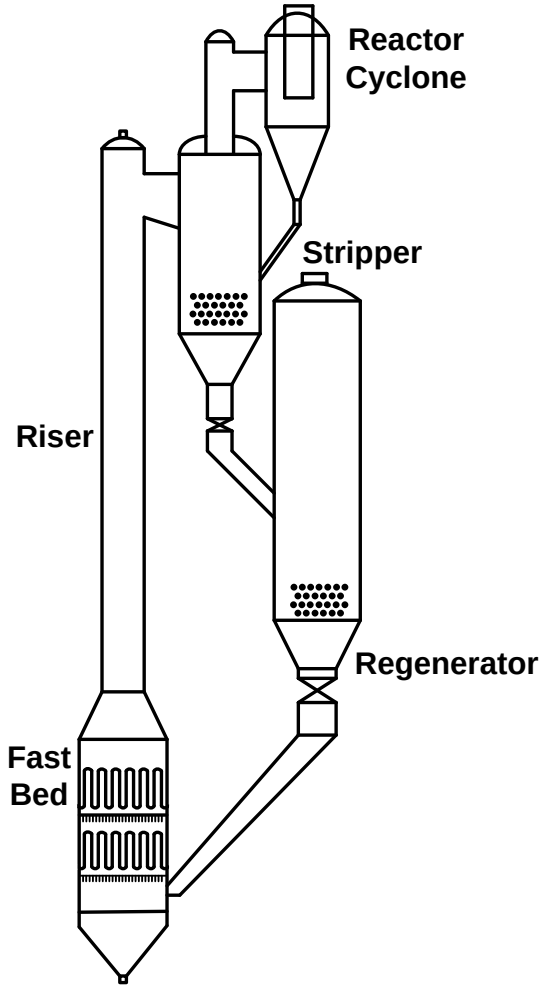

Figure 1-1: CFB reactor configuration

(Hutchenson et al., 2010)

The most significant feature of the CFB reactor was the separate reduction and oxidation sections; this allowed feeding higher concentrations of n-butane and higher MA selectivity while avoiding flammability ranges. Up to 90 % maleic anhydride selectivity was reported to be achievable by this reactor configuration (Contractor, 1994). Moreover, higher yields in the order of four times the steady state operation values were reported for cyclic operations in circulating bed reactors (Emig, 1994; Patience and Lorences, 2006). The other advantage of CFB reactor was that the operating conditions in each reaction zone could be optimized independently. However, the major limitation was the intrinsically low oxygen transfer

capacity of the VPP catalyst. This required extremely high solid recirculation rates to provide adequate oxygen to the reaction.

1.3 Redox parameters

The major redox parameters are: catalyst's oxygen transfer capacity, duration of redox steps, temperature, feed composition and pressure. In the following sections, a research review on the effect of these parameters on the redox activity of the VPP catalyst is presented.

1.3.1 Oxygen capacity

The circulating bed technology relied on the catalyst lattice oxygen as a source of selective oxygen for reaction. The key factor for industrial success of this technology was the sufficient ability of the catalyst to supply oxygen to the reaction zone. The lattice oxygen has been reported as a highly active and selective source for transformation of n-butane to maleic anhydride (Schuurman and Gleaves, 1997; Patience and Lorences, 2006). During the regeneration period, the catalyst surface is exposed to molecular oxygen, which is adsorbed and incorporated into the surface lattice of the catalyst. Therefore, higher capability of catalyst for oxygen transfer to reaction zone will ensure higher productivity and lower energy costs by reducing the catalyst recirculation rates.

Wang and Barteau (2001) predicted the oxygen transfer capacity of the VPP catalyst during reduction as a function of n-butane gas phase concentration (Figure 1-2). Based on their reduction kinetic model, the maximum possible oxygen storage capacity of the catalyst was 990 μg/mg. However, in practice, the oxygen transfer capacity of the catalyst during redox operations is limited by kinetics and depends on operating conditions. Figure 1-2 specially shows that by increasing n-butane concentrations in the feed to reduction (especially for lower concentrations of n-butane (0-20 vol. %), the oxygen available for reduction reaction could be increased. However, there is a limitation for regeneration of the catalyst as the

extent of reduction increases; there is also the risk of catalyst over reduction and formation of excessive amounts of carbon deposits by severe reduction conditions.

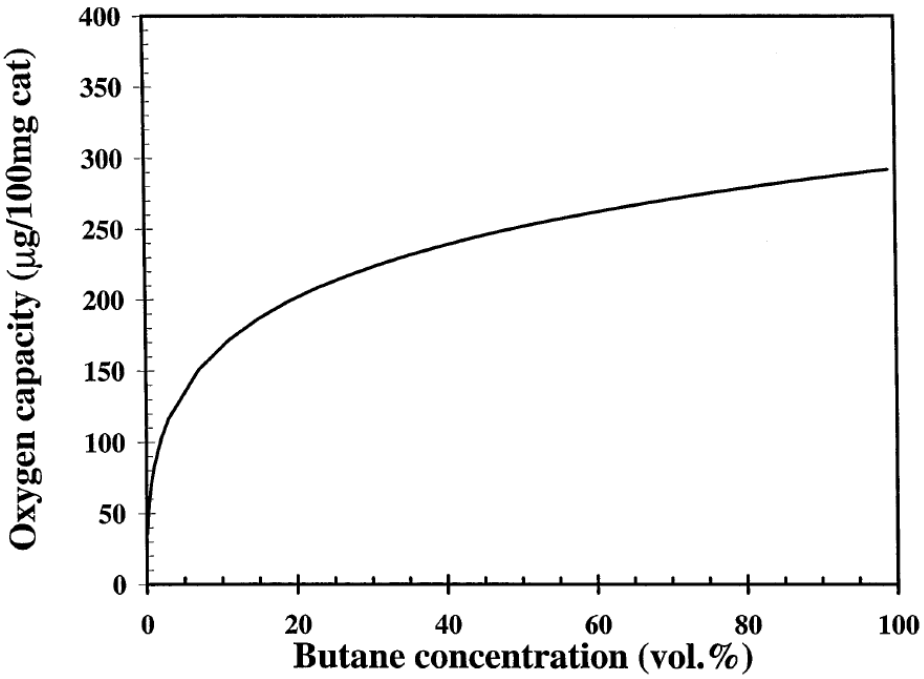

Figure 1-2: VPP oxygen storage capacity

(Wang and Barteau, 2001)

1.3.2 Redox duration

Since the incorporation of oxygen in the catalyst lattice is basically a slow process, the catalyst oxidation could be improved by optimizing the regeneration time. An optimum residence time is required for solids to allow for sufficient oxygen uptake for maximum productivity. Emig (1994) reported that under cyclic operating conditions, MA production rates increased by a factor of three when the regeneration period was increased from 30 to 18 hours. During their transient kinetics experiments, Patience and Lorences (2006) observed a high level of n-butane conversion and maleic anhydride selectivity during the first few minutes of exposing the catalyst to reducing conditions; they attributed this to the high activity and selectivity of the stored lattice oxygen during the pre-oxidation period. There

was a 40 minute pre-oxidation step prior to reduction period which is obviously long for industrial operations; also, they observed that the high MA yields last only for a few minutes after starting the reduction period and gradually drops to a steady state values after 10 minute. Contrary to these findings, Huang et al. (2002a) reported that the catalyst may become inactive due to over oxidation or sintering after relatively longer periods of oxidation. These findings show that maintaining high yields during redox periodic operations is strongly dependent on the duration of each reaction step. Therefore, it would be very important to define an appropriate time schedule for oxidation and reduction periods to achieve optimum yields.

1.3.3 Temperature

An influencing factor on catalyst re-oxidation rate is the reactor temperature; higher temperatures are proven to enhance the re-oxidation rate and thereby increase the oxygen storage capacity of the catalyst (Huang et al., 2002a; Gascón et al., 2006). Gascón et al. (2006) observed that the highest initial oxygen conversion in the re-oxidation step never exceeds 50 % and the completion of oxidation depends on the oxidation temperature. They concluded that the maximum oxidation state of the catalyst will not go to completion at temperatures lower than 420 °C and higher temperatures are needed for completion of the catalyst oxidation. In addition, Huang et al. (2002a) reported a significant improvement in MA yield when using higher than normal temperatures in the oxidation step (500-620 °C). They further observed that even under pure oxygen gas the oxidation of the catalyst is not complete at a temperature of 580 °C. A temperature of at least 620 °C was needed for complete oxidation of the catalyst under normal oxidation environments. Higher temperatures increase the rate of re-oxidation but it will be probably accompanied by sintering of the catalyst surface and loss of the phosphorous (P/V ratio) from the surface.

The effect of temperature on reduction reaction has not been usually a subject of research in the literature. The temperatures used in the literature were essentially the same temperatures as the steady state n-butane oxidation (~ 350-400 °C). The higher temperature during

reduction is not recommended due to adverse effect in accelerating gas phase non-selective combustion.

1.3.4 Feed composition

Gascón et al. (2006) observed that oxygen partial pressure has a strong effect on the re-oxidation rate and the rate decreased exponentially with time as the catalyst took up oxygen,

Figure 1-3. Lorences et al. (2004) have also shown that overexposure of the catalyst to oxygen during 48 hour of oxidation provides twice as more surface oxygen for reaction as one hour oxygen treatment. Oxygen soaking may also increase the maleic anhydride yields of up to four times the steady state value. Patience and Lorences (2006) also found that higher oxygen concentration in the reduction step will result in higher initial values for MA yield. They also observed the positive effect of oxygen on the steady state MA yield during reduction (Figure 1-4). However, they did not define an optimum oxygen concentration. These data show that oxygen concentration is a determining factor during the reduction period. Moreover, as it can be seen in Figure 1-4 that n-butane concentration in the reduction feed has less effect on MA yields. This may be showing that the oxygen insertion is the limiting step during reaction.

1.3.5 Pressure

Normal operating pressures of industrial reactors are in the order of 2-4 bar. However, pressure has been rarely considered as an affecting parameter during redox experiments. Higher reactor pressure in believed to affect the partial pressures of the reactive species and the corresponding redox rates. A higher carbon build up over the catalyst surface during reduction was reported by Patience and Lorences (2006).

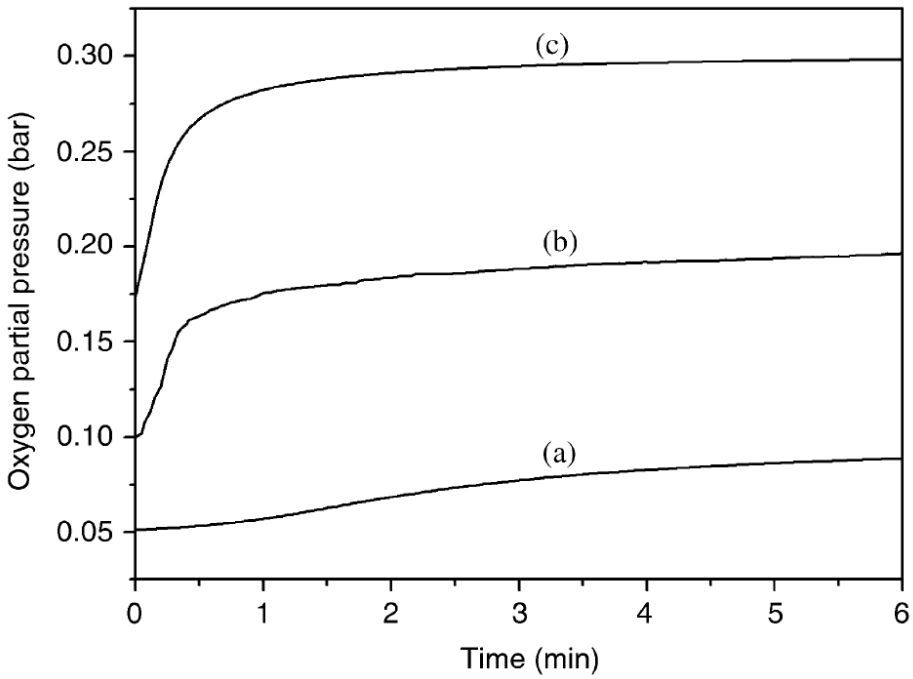

Figure 1-3: Outlet oxygen partial pressure in oxidation

P_{oxygen} = 10 kPa (a), 20 kPa (b), and 30 kPa (c) (Gascón et al., 2006)

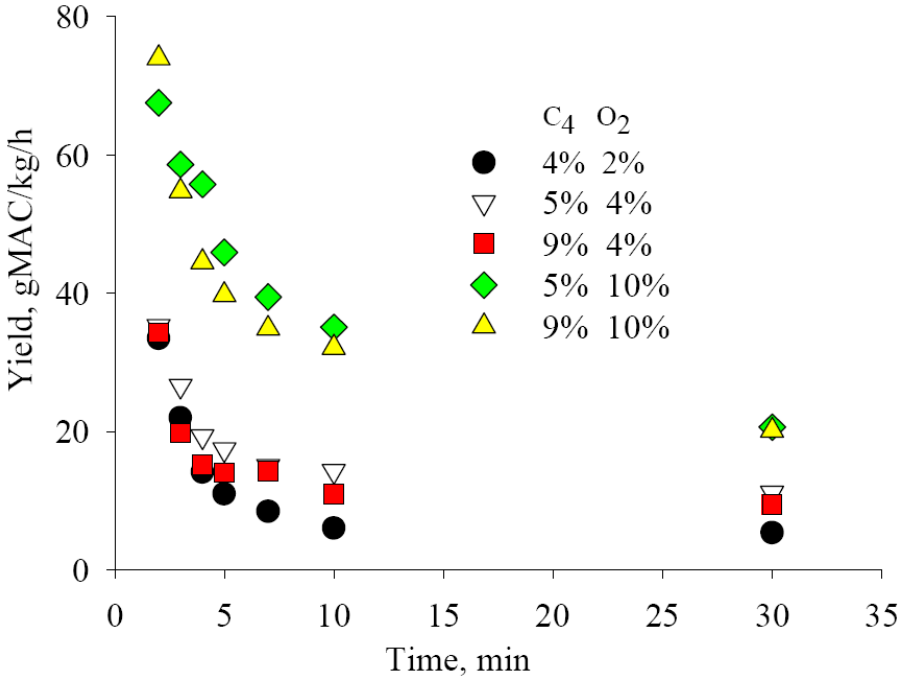

Figure 1-4: Effect of oxygen concentration on MA yield

(Patience and Lorences, 2006)

1.4 Transient kinetic modeling

A steady state kinetic model is not usually capable of fitting transient kinetic data because of special considerations during transient regimes. In the transient regime, the behaviour of the catalyst depends not only on the reaction environment, but also on the oxidation or reduction history of the catalyst (Gascón et al., 2006). This suggests that a basic knowledge on both n-butane oxidation (catalyst reduction) and catalyst oxidation kinetics need to be combined together to predict the catalyst's transient behaviour during redox operations.

Several kinetic models have been proposed for transient conditions. Generally, these models can be divided into two main categories: catalyst re-oxidation and catalyst reduction kinetics. However, despite the large extent of research on re-oxidation kinetics there has been relatively fewer studies regarding reduction kinetics (Wang and Barteau, 2001; Lorences et al., 2003, Patience and Lorences, 2006). There is also still a lack of generality in proposed transient kinetic models to adequately cover the wide range of feed concentrations i.e. from fuel rich to fuel lean conditions. Gascón et al. (2006) proposed a generalized kinetic model based on a relatively detailed redox mechanism (Figure 1-5 and Table 1.1) which predicted the transient behaviour of the VPP catalyst during transient regimes.

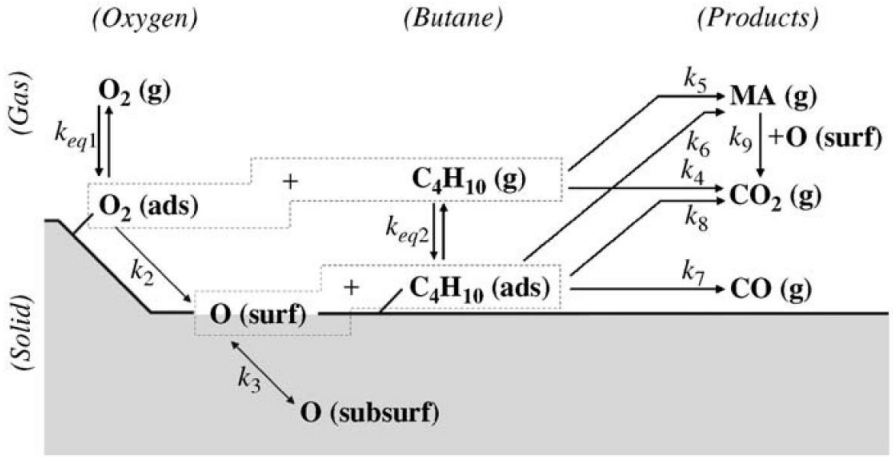

Figure 1-5: Redox mechanism for n-butane oxidation over VPP

(Gascón et al., 2006)

In general, transient kinetic modeling of n-butane oxidation to maleic anhydride has been hindered due to the lack of data regarding the detailed reaction mechanism and the identification of active sites under transient conditions. For example, information on the mechanism of carbon formation on catalyst surface under fuel rich conditions is still lacking as well as the quantification of the mass of carbon adsorbed on the surface (Patience and Lorences et al., 2006).

Regarding the catalyst surface species, the role of the oxygen has been the subject of research for many years and it is still hotly debated (Lorences et al., 2006). The role of lattice oxygen, as a source of selective oxygen, has not bee fully determined. More complexity arises with regard to the role of other surface adsorbed oxygen species (Wang and Barteau, 2003). Regarding vanadium oxidation states, although three states – V^{3+}, V^{4+} and V^{5+} – have been identified as the main oxidation states of VPP catalyst during reaction, the mechanism and contribution of each phase during reaction is not very well understood. Moreover, due to the sensitivity of the VPP catalyst surface to the reaction environment, the catalyst redox behaviour and variation of the catalyst oxidation state with time would add to the complexity of kinetic modeling under transient conditions (Wang and Barteau, 2002).

Transient kinetic models can be categorized according to the active sites responsible for selective and non-selective reactions during n-butane oxidation to maleic anhydride. Single site models like the one proposed by Buchanan and Sundaresan (1986), considered that both the n-butane activation and reaction MA takes place on the same active site. However, it poorly fits MA selectivity. Various two site models have been proposed in the literature (Bej and Rao, 1991; Lorences et al., 2003). The advantage of these models is that they differentiate between active sites for selective and non-selective reactions. Therefore, they are superior to single site models in predicting MA selectivity and n-butane conversion. For example, Lorences et al. (2003) characterized a wide range of transient kinetic data by examining different kinetic models available in the literature and proposed a pseudo-two site model which accounts also for irreversible adsorption of n-butane on reduced vanadium sites

(V^{4+}). Table 1.1 presents a summary of transient kinetic models in the literature for n-butane oxidation to maleic anhydride.

As presented in Table 1.1, nearly none of the kinetic models proposed for n-butane transient oxidation are generalized. Even, some models have been proposed for a very narrow range of concentrations. Therefore, they might not be able to account for other events that can happen at higher hydrocarbon concentrations. For example, the reduction model that was proposed by Wang and Barteau (2001) did not take into account the effect of carbon deposition during reduction at high n-butane concentrations. However, those models which account for these events (Patience and Lorences, 2006) are usually unable to characterize the fuel lean conditions.

In the following sections the details of the research work on two main categories of transient models i.e. oxidation and reduction kinetics are presented.

1.4.1 Oxidation kinetics

Several authors studied the oxidation kinetics of VPP catalyst (Mills et al., 1999; Huang et al., 2002a; Lorences et al., 2004; Patience and Lorences, 2006). The objective in catalyst oxidation is the insertion of oxygen from gas phase into the catalyst surface or bulk lattice. Many adsorbed species can be present during this transformation: molecular oxygen species, O_2 and O or charged species such as: O_2^-, O^- and O^{2-}, etc. However, the role of these species during reaction and the details of transformations between these species are not clearly understood. A simple approach has been to consider the lumped behaviour of oxygen during oxidation step.

Wang and Barteau (2002) proposed a simple mechanism for insertion of the oxygen into the catalyst lattice Table 1.1. They showed that the insertion of the surface adsorbed oxygen into the lattice of the catalyst is the rate determining step in the overall oxidation process and the

reversible adsorption of oxygen on the surface plays a minor role in weight gain of the catalyst. They did not consider the effect of n-butane on the consumption of surface adsorbed species during catalyst oxidation while n-butane was present at small amounts. Their kinetic model is valid only for initial moments where the oxidation rates are high and does not cover the whole re-oxidation period until reaching to steady state rates. A similar simple re-oxidation mechanism was adopted by Huang et al. (2002a) which considered a two step insertion of the gaseous oxygen into the catalyst lattice. They assumed a first order oxidation reaction rate with regard to gas phase oxygen and a second order one with regard to the concentration of surface active sites (Table 1.1).

1.4.1.1 Adsorbed carbon

An important factor, which has been of less attention in the oxidation kinetic modeling, is combustion of adsorbed carbon during regeneration of the catalyst. Lorences et al. (2004) and Patience and Lorences (2006) studied the effect of carbon deposition on re-oxidation kinetics. According to their results, a significant part of the oxygen required to re-oxidize the catalyst was primarily consumed for removal of the carbon species from the surface, which was formed during reduction. To account for carbon combustion during oxidation, they considered the formation of a relatively strong vanadium-carbon complex (V^{C4}) during reduction period, which undergoes the following oxidation reaction:

$$O_2 + V^{4+} \xrightarrow{k_1} V^{5+} \tag{1-1}$$

$$5.5\ O_2 + V^{C4} \xrightarrow{k_2} 4\ CO_x + 5\ V^{4+} + 4\ H_2O \tag{1-2}$$

The kinetic model for re-oxidation of reduced catalyst (Reaction 1-1) was assumed to be first order with respect to both oxygen and reduced sites (V^{4+}) and the re-oxidation rate of the adsorbed carbon (Reaction 1-2) was first order regarding to adsorbed carbon sites (V^{C4}) and half order in oxygen. However, in a prior work (Lorences et al., 2004), the authors tried to derive a general kinetic model to fit a range of operating conditions (fuel lean to fuel rich)

and considered a re-oxidation rate of adsorbed carbon as first order for both carbon species and oxygen. A summary of the corresponding kinetic expressions is presented in Table 1.1.

1.4.1.2 Oxidation rate

Figure 1-6 demonstrates the effect of oxygen concentration on the re-oxidation rate after reduction in anaerobic conditions. It is clearly shown that the re-oxidation rate is improved by increasing oxygen concentration in the feed. It is also shown that the predicted first order model for re-oxidation satisfies well the experimental data.

The initial catalyst oxidation state and relative concentration of catalyst active sites are important factors that affect the oxidation rate. Typically, while operating at fixed and fluidized bed feed conditions, the surface concentration of V^{5+} is relatively high. Patience and Lorences (2006) assumed a total oxidation of all active sites to final state of V^{5+} after relatively long time of oxidation periods and guessed the catalyst's initial oxidation state values accordingly. Regarding to these uncertainties, further work has been suggested by authors to investigate the effect of pre-oxidation conditions (duration, temperature etc.) on the initial oxidation state and oxygen conversions.

1.4.2 Reduction kinetics

Wang and Barteau (2003) and Lorences et al. (2004) studied the transient VPP kinetics at moderate to high concentrations of n-butane in the feed. These models were not adequately general to cover the range of conditions from presence to the absence of oxygen. Lorences et al. (2004) used the same kinetic model to fit both transient and steady state data and concluded that this was only possible by changing the model parameters. Gascón et al. (2006) developed a general kinetic model based on a detailed mechanism. The model was applicable to reduction, oxidation and co-feed conditions as well as steady state conditions. The formation of carbon on the surface due to high n-butane to oxygen ratios was not

considered in the proposed mechanism. Moreover, the effect of pressure on kinetics was not included in the model.

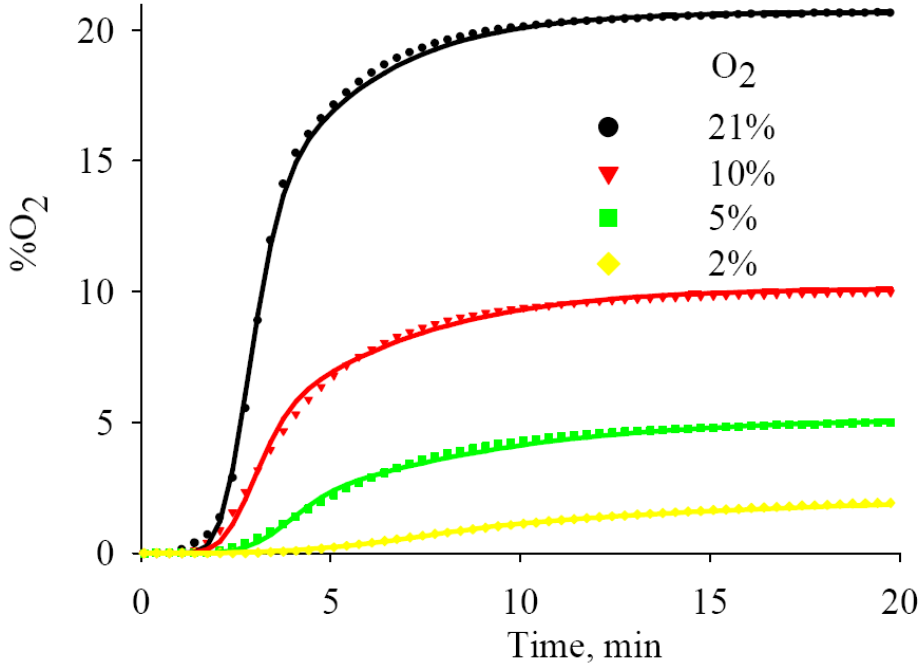

Figure 1-6: Effect of oxygen concentration on re-oxidation rate

(Patience and Lorences, 2006)

Wang and Barteau (2001) studied the reduction kinetics of VPP and proposed a kinetic expression for the rate of catalyst reduction, which was 0.4 order in n-butane partial pressure and 4 with regards to lattice oxygen concentration (Table 1.1). However, the model was based on a single site mechanism and in the mechanism, they only considered the presence of catalyst oxidized sites (lattice oxygen) without any consideration of the participation of surface chemisorbed oxygen species in n-butane conversion. The kinetic model was capable of predicting the entire reduction period (15 min). They showed that under conditions of reduction, the activation energy for reduction reaction was similar to the corresponding value for reaction under steady state operations (~ 85-88 kJ/mol). This means that the determining step under reduction condition could be the same as steady state conditions in which the n-butane activation is taking place on four surface oxidized sites.

Table 1.1: Kinetic models for n-butane oxidation to maleic anhydride

Reference	Model type	Conditions	Kinetic expression	Mechanism	Comments
Wang and Barteau (2001)	Reduction	C_4 in He vol. % = 0.4-2.4 T = 340-400 °C	$r_{red} = -\frac{dm}{dt} = k_1 P_{C_4H_{10}}^{0.4}[O]^4$	C_4H_{10} + a [O] $\xrightarrow{k_1}$ b MA + c CO_x + d H_2O + a [*] MA + e [O] → f CO_x + e [*] CO + g [O] → CO_2 + g [*] [O] = lattice oxygen [*] = lattice oxygen vacancy	Valid for entire reduction period E_a = 85 kJ/mol
Golbig and Werther (1997), Emig (1994)	Re-oxidation	Oxygen up to 50 vol. %	$r_{12} = k_{12}\frac{p_B p_{O_2}^{1/2}}{1 + K_1 p_{H_2O} + K_2 p_B}$	n-butane $\xrightarrow{k_{12}}$ MA MA ⟶ CO_x n-butane ⟶ CO_x	-
Wang and Barteau (2002)	Re-oxidation	C_4/O_2/He = 1.7/21/bal. T = 400 °C	$r_{ox} = \frac{dm}{dt} = k_2 K_1^{½} P_{O_2}^{½}\theta$ θ = oxygen vacancy concentration	O_2 + 2 [*] $\xleftrightarrow{K_1}$ 2 O^* O^* $\xrightarrow{k_2}$ [O] (slow) [*] = reduced site [O] = oxidized site (lattice)	Valid for initial moments of oxidation E_a = 70 kJ/mol
Huang et al. (2002a)	Re-oxidation	Oxidation: O_2/He = 21/79 Reduction: C_4/O_2/He = 4/20/bal. T = up to 650 °C	$r_1 = k_1 y_{O_2}(1-\theta_S)^2$ $r_2 = k_2(1-\theta_L)\theta_S - k_2'\theta_L(1-\theta_S)$ θ_S = surface oxygen sites θ_L = lattice oxygen sites	(1) O_2 + 2(S) $\xrightarrow{k_1}$ 2O(S) (2) O(S) + (L) $\xleftrightarrow{k_2,\ k_2'}$ O(L) + S S = surface site L = oxygen vacancy in lattice	Oxygen uptake by catalyst without reduction E_1 = 157.4 kJ/mol E_2 = 199.4 kJ/mol

Table 1.1: Kinetic models for n-butane oxidation to maleic anhydride (continued)

Reference	Model type	Conditions	Kinetic expression	Mechanism	Comments
Gascón et al. (2006)	Generalized	Oxidizing: P_{O_2} = 10-30 kPa Anaerobic: $P_{C_4H_{10}}$ = 0.8-5 kPa Aerobic: P_{O_2} = 2.5-10 kPa $P_{C_4H_{10}}$ = 1.5-2.5 kPa Temperature = 400-435 °C	$-r_{MA} = \frac{k_6 P_{C_4H_{10}} \theta^2_{surface}}{1 + K_{eq2} P_{C_4H_{10}} + K_{eq1} P_{O_2}}$ $-r_{CO} = \frac{k_7 P_{C_4H_{10}} \theta_{surface}}{1 + K_{eq2} P_{C_4H_{10}} + K_{eq1} P_{O_2}}$ $-r_{CO_2} = \frac{k_8 P_{C_4H_{10}} \theta_{surface}}{1 + K_{eq2} P_{C_4H_{10}} + K_{eq1} P_{O_2}}$ θ = surface lattice oxygen	See Figure 1-5	Not considering carbon formation or pressure
Lorences et al. (2004)	Generalized	Fuel lean to fuel rich conditions	$r_1 = k_1 [C_4H_{10}] [V^{5+}]$ $r_2 = k_2 [MA] [V^{5+}]$ $r_3 = k_3 [C_4H_{10}] [V^{4+}]$ $r_4 = k_4 [O_2] [V^{4+}]$ $r_5 = k_5 [O_2] [V^{C4}]$	$C_4H_{10} + \alpha\ V^{5+} \xrightarrow{k_1} MA + \alpha\ V^{4+} + 4\ H_2O$ $MA + \beta\ V^{5+} \xrightarrow{k_2} 4\ CO_x + \beta\ V^{4+} + H_2O$ $C_4H_{10} + 4\ V^{4+} \xrightarrow{k_3} 4\ V^{C4}$ $O_2 + V^{4+} \xrightarrow{k_4} V^{5+}$ $\gamma\ O_2 + 4\ V^{C4} \xrightarrow{k_5} 4\ CO_x + 4\ V^{4+} + 5\ H_2O$	Considering the carbon formation, not pressure

1.4.2.1 Fuel rich operation

Wang and Barteau (2003), compared the catalyst oxidation rates under steady state conditions with catalyst reduction (or oxidation) rates under mild reducing conditions (n-butane to oxygen ratio = 0.83). Due to the very low oxidation rate in the absence of gas phase and surface adsorbed oxygen, they concluded that the participation of lattice oxygen in reaction rate is very low and it might be less than 5 % of the total steady state oxidation rate. They suggested that the surface adsorbed oxygen species are the main source of selective n-butane oxidation during reaction. Gascón et al. (2006) also confirmed the effect of weakly adsorbed surface oxygen on conversion of n-butane under fuel rich conditions by varying inert purging durations between oxidation and reduction periods. They noticed a decrease in n-butane conversion during reduction period due to elimination of physically adsorbed surface oxygen by helium purge (Figure 1-7)

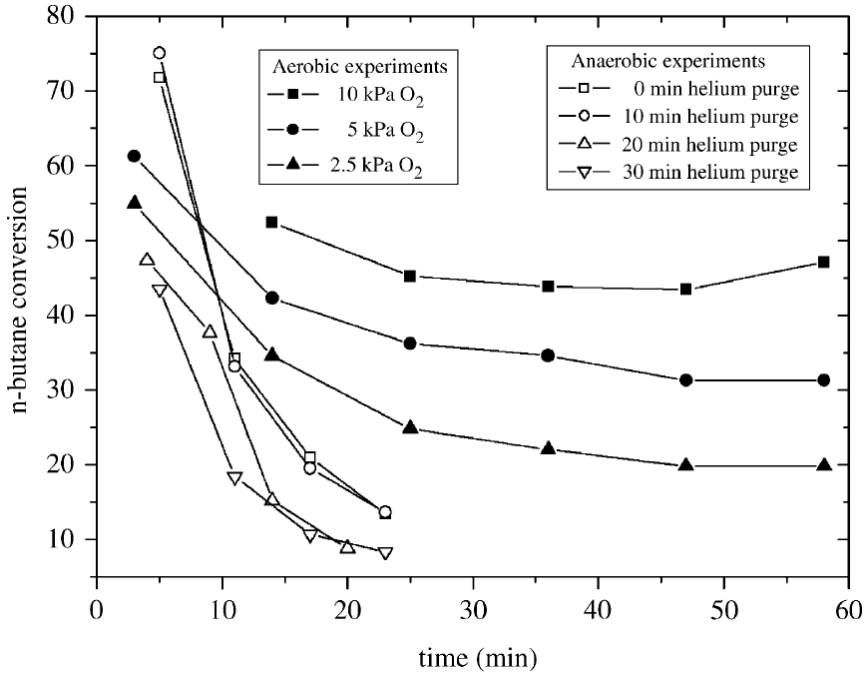

Figure 1-7: Effect of inert purging on n-butane conversion

(Gascón et al., 2006)

These findings suggest that the participation of lattice oxygen might not be enough to maintain a high rate of reaction during catalyst reduction. The presence of gas phase oxygen during reduction seems essential to supply oxygen to reaction through adsorption on the surface. However, there is still controversy regarding the role of these adsorbed surface species during reduction kinetics.

Wang and Barteau (2003) proposed an elementary kinetic expression for the reduction rate of surface adsorbed species during aerobic conditions:

$$r_{[O^*]} = k[O^*]^a[\text{reductant}]^b \qquad (1\text{-}3)$$

In Equation 1-3, [O*] and [reductant] are the surface concentration of adsorbed oxygen species and adsorbed n-butane (or hydrocarbon intermediates), respectively. They also defined the total rate of reduction (oxygen consumption rate) in aerobic conditions as the sum of lattice oxygen [O] and adsorbed oxygen [O*] consumption rates (Equation 1-4). The applicability of this rate equation under fuel rich (slightly aerobic) conditions was not proven.

$$r_O = r_{[O]} + r_{[O^*]} \qquad (1\text{-}4)$$

Ballarini et al. (2005) observed unusual effects during reduction at total oxygen conversions; they observed a considerably lower MA selectivity at higher temperatures which was partly due to the formation of higher molecular weight compounds (C_8) at total oxygen conversions (i.e. when oxygen was depleted). They attributed these substances as products of side reaction between C_4 intermediates and maleic anhydride in the absence of oxidation sites. They also observed non-negligible effect of gas phase non-oxidative reactions to olefins during reduction when oxygen was not limiting reactant. Consequently, an unusual increase in MA selectivity was observed at temperatures higher than 400 °C, which was due to heterogeneous reactions of olefins to maleic anhydride on the surface. According to these findings, the effect of gas phase oxygen

concentration on byproduct profile and the effect of homogeneously initiated heterogeneous reactions would be interesting for further studies. Moreover, a general conclusion of these findings may suggest that the VPP catalyst is not suitable for reactions under high n-butane to oxygen ratio (fuel rich). To prevent the side reactions under fuel rich conditions, the presence of co-fed oxygen during reduction is always necessary to prevent excessive reduction of V^{5+} and V^{4+} active sites (Ballarini et al., 2006).

The effect of oxygen partial pressure during reduction period was also examined by Gascón et al. (2006). They observed a steady n-butane conversion during reduction, which was dependent on oxygen partial pressure. These results show that catalyst oxidizing sites are preserved as long as oxygen is present in the gas phase. Patience and Lorences (2006) also confirmed that the key factor to achieve high MA selectivity during fuel rich conditions is to keep the catalyst in an oxidized state during reduction.

1.5 Carbon deposition

Carbon deposition during reduction under fuel rich conditions affects the catalyst performance by occupation of active sites. It is reported that, for each C_4 species which is irreversibly adsorbed on the surface of the catalyst, four adjacent V^{4+} sites are occupied (Patience and Lorences, 2006). There are some implications in the literature about the formation of such deactivated sites during fuel rich operations. However, there is still controversy regarding the extent of carbon deposition and parameters affecting this phenomenon during reduction of catalyst. For example, Lorences et al. (2003) considered this phenomenon as a part of their kinetic modeling. However, Mota et al. (2000) argued that since the activation of n-butane is placed on a limited fraction of surface V^{4+} sites, the formation of carbonaceous species might not affect the catalytic performance.

Wang and Barteau (2001) observed that carbon oxides (CO and CO_2) evolution during initial moments of oxidation of reduced catalyst is not significant and the weight change of the catalyst due to deposition of carbonaceous species during several hours of n-butane reduction was only in the order of less than 5 wt. % of originally oxidized catalyst. This might be due to that they only

used lean mixtures (0.4-2.4 vol. %) of n-butane in helium as reducing stream. On the other hand, Lorences et al. (2003, 2004) and Mallada et al. (2000) reported a considerable amount of carbon deposition during reduction in n-butane rich conditions. They reported that the quantity of adsorbed carbon is dependent on n-butane to oxygen ratio and temperature during reduction.

Patience and Lorences (2006) indicted that the initiation of carbon deposition takes place as n-butane to oxygen ratio rose above one or two. This phenomenon resulted in a lower catalyst activity and MA selectivity. Figure 1-8 presents the concentration profiles during cyclic feed operations on VPP catalyst. The presence of adsorbed carbon species on the surface is confirmed by evolution of carbon monoxide during the first oxidation period (circled peak).

In an earlier study, Lorences et al. (2004) proposed a general transient kinetic model in which the formation of a carbon-vanadium complex (V^{C4}) during reduction (Reaction 1-5) was accounted for by considering a reaction rate which was first order with respect to both carbon (n-butane) and reduced catalyst sites (V^{4+}) (Table 1.1).

$$C_4H_{10} + 4\,V^{4+} \xrightarrow{k_5} 4\,V^{C4} \qquad (1\text{-}5)$$

1.6 Active sites

Identification of the catalyst active surface sites and their role during n-butane oxidation is essential in defining the reaction mechanism and kinetic modeling. The reaction initiates by activation of n-butane on the catalyst surface sites and proceeds by transformation of intermediates species through selective or non-selective pathways. Different vanadium oxidation states have been identified as the catalyst active phases. Moreover, different oxygen species have been identified to participate in the surface reactions. In the following, a brief literature review on catalyst active species is presented.

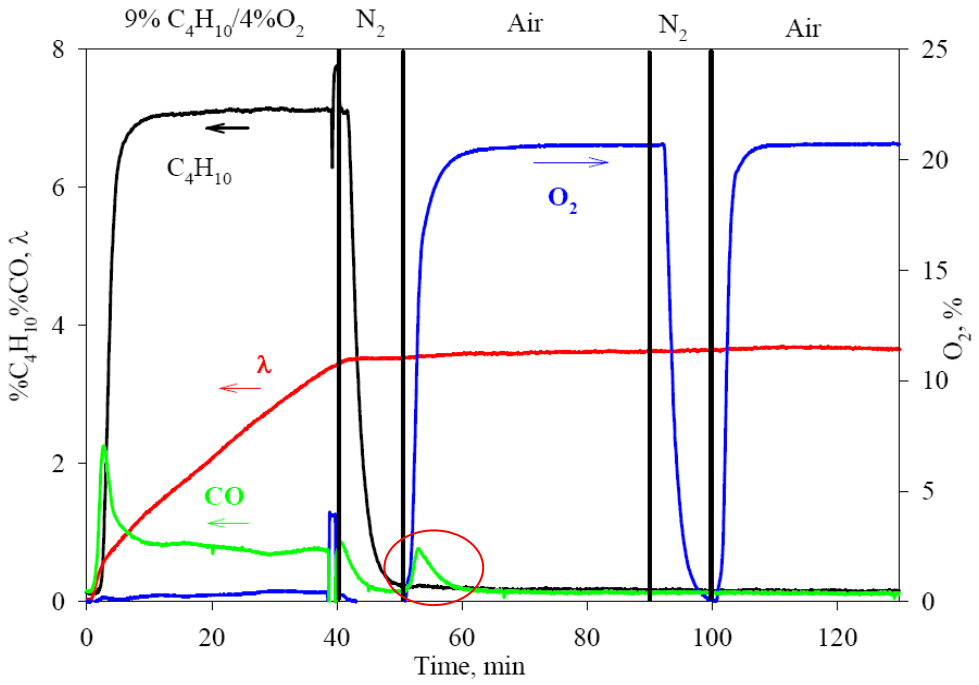

Figure 1-8: Carbon deposition during redox cycles

(Patience and Lorences, 2006)

1.6.1 Vanadium states

The vanadium oxidation state depends on the reaction conditions as well as the gas phase composition. It has been well confirmed that vanadyl pyrophosphate – $(VO)_2P_2O_7$ (V^{4+}) – is the main catalyst active phase during n-butane oxidation to maleic anhydride. Other vanadium oxidation states such as V^{5+} and V^{3+} have also been identified to participate in the catalytic activity. A proper combination of V^{4+} and V^{5+} phases have been reported to be essential for an optimal catalytic activity. There is however some controversy on the positive effect of V^{5+} species as the catalyst is highly oxidized (Huang et al., 2002a)

The effect of reducing (and oxidizing) conditions on vanadium oxidation state during reaction has been investigated by Mallada et al. (2000). Their results showed that under fuel rich conditions, the formation of V^{3+} species strongly reduces the MA selectivity. These results were also

confirmed by Mota et al. (2000), which stated that reduction of V^{5+} species is responsible for decrease in MA selectivity. Rodemerck et al. (1997b) also concluded that all the steps of oxidation to maleic anhydride in anaerobic conditions, is proceeded over V^{5+} and V^{4+} sites and the selective sites are those who have the higher oxidation potential. They also mentioned that the contribution of the V^{4+}/V^{3+} redox couple could not be overlooked during reaction.

1.6.2 Oxygen species

The oxygen of the catalyst is assumed the main source of activity and selectivity during circulating fluidized bed operations. However, the exact role of lattice oxygen or other oxygen species (adsorbed and gas phase) during the reaction is not fully identified. It is also believed that the surface oxygen and chemisorbed oxygen on the surface of the catalyst are the main source for n-butane conversion to maleic anhydride and carbon oxides under fuel rich conditions (Gascón et al., 2006). The presence of gas phase oxygen adds to the complexity of the kinetics by considering its transformations into surface adsorbed oxygen species. To simplify the role of several different oxygen species, a general approach in kinetic modeling has been to consider a lumped behaviour for oxygen species on the surface as well as the lattice oxygen (Wang and Barteau, 2002, 2003).

1.7 Redox operations

To simulate the operating conditions of a CFB reactor in the laboratory and to examine the applicability of the transient kinetic models under redox conditions, sequential redox experiments including consecutive reduction and oxidation of the catalyst sample could be an efficient approach. The sequential redox operation would also be beneficial to optimize the redox parameters for each redox half-cycle.

Wang and Barteau (2002) demonstrated the applicability of their proposed oxidation kinetic model by simulating the redox conditions of a CFB reactor in a microbalance reactor. Figure 1-9 shows the catalyst's mass change during consecutive oxidation/reduction cycles at different

temperatures. The results showed that the redox rates decreased as the temperature decreased; no redox activity was seen below 280 °C. There was also a continuous decrease in the net catalyst mass due to the redox activities. The drop in catalyst mass was attributed to a lower oxidation rate with regard to the reduction rate at each half cycle. They showed that this effect was more noticeable at higher temperatures.

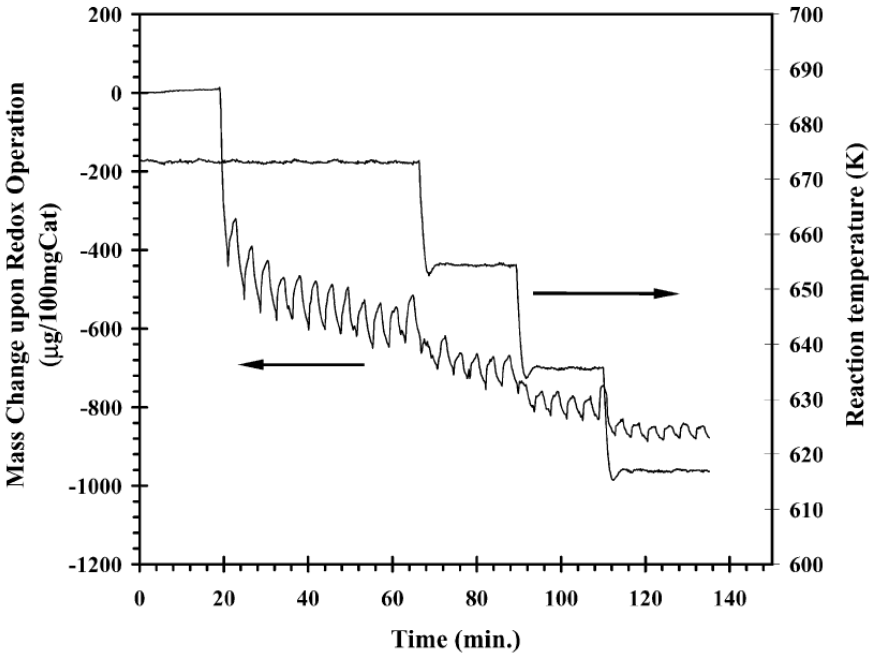

Figure 1-9: Simulation of cyclic redox operation

(Wang and Barteau, 2002)

Huang et al. (2002) applied a similar approach to study the effect of temperature on the catalyst performance during redox cycles. They observed a significant improvement in MA yield at very high oxidation temperatures (> 580 °C). However, they did not show the validity of the model for redox experiments and did not study the long term effect of higher temperatures on catalyst activity during consecutive redox operations. These findings suggest that by conducting redox simulations, there is an opportunity to optimize operating parameters of each section.

CHAPTER 2 RESEARCH METHODOLOGY

In this Chapter, the principal research objectives as well as the experimental and modeling methodology to achieve these objectives are described. The general thesis organization with respect to the consistency of published/submitted articles is also presented.

2.1 Problem statement

As discussed in the literature study, during the past few decades, a significant amount of research has been conducted on different aspects of n-butane to maleic anhydride reaction over VPP catalyst. The majority of the research has been devoted to characterize the ambiguous catalytic behaviour of VPP under various redox conditions. The major impediments against the kinetic developments have been the unclear role of surface or lattice oxygen species and the dynamic transformation of catalyst surface active phases during reaction. These issues prevented the proposal of a comprehensive redox kinetics, which could be applicable to a wide range of redox conditions. Other issues have been around the naturally insufficient oxygen transfer capacity of the VPP catalyst for CFB reactors. Additional oxygen injection to the reaction zone while avoiding flammability limits at the freeboard region has been among the solutions to maintain high MA productivities in the commercial reactor.

In the following section, the principal objectives of this research are presented based on the described problems.

2.2 Objectives

Providing a clear picture on complex behaviour of VPP catalyst during redox operations has been an enormous challenge. These data are of significant importance in proposing the correct mechanism and kinetics for the reaction. For this purpose, in the major part of this thesis, the

transient catalytic behaviour of VPP was characterized in a micro-reactor for a wide range of redox conditions including higher reactor pressure.

To better understand the improving effect of catalyst oxidation state and availability of molecular oxygen on MA productivity, the performance data collected in a 9 cm OD fluidized bed reactor as well as the industrial data from DuPont's commercial CFB reactor were also analysed and discussed.

The other objective was to propose a transient kinetic model, which could be valid for the entire range of studied conditions. This model had to be applicable to higher pressure as a new contribution in this field.

The specific objectives of this research thesis could be summarized as the following:

1- To study the effect of injecting gas phase oxygen, feeding configuration on catalytic activity and reactor performance at different scales

2- To optimize the MA productivity with respect to redox operating conditions, specifically catalyst oxidation time and feed composition

3- To characterize the VPP catalyst behaviour under transient regimes particularly at higher reactor pressure

4- To propose a transient kinetic model applicable to a wide range of feed compositions as well as higher reactor pressure

2.3 Thesis organization

To achieve the described objectives, this thesis was conducted under the following four principal sections. The scientific articles resulting from these studies are presented in Appendix A and Chapters 3 to 5.

I - Catalytic performance analysis (Appendix A: Article 1)

To better understand the effect of catalyst oxidation on reactor performance, the experimental data in a lab scale fluidized bed and the industrial data from DuPont's commercial CFB reactor were studied. A significant dependency of MA rates on reactor feed configuration was observed at both scales. Keeping the catalyst in an oxidized state was believed to be the key for higher MA productivities. The results of these analyses are presented in Appendix A as the first article.

II - Optimizing MA productivity (Chapter 3: Article 2)

The MA rates were studied at a wide range of redox conditions at ambient pressure. The objective was to find a correlation between MA production rate and feed composition as well as the catalyst oxidation time. A linear correlation was observed for MA rates with respect to catalyst oxidation time. The MA production rate could be maximized at an equimolar concentration of n-butane and oxygen. These results were published as the second article and the paper is presented in Chapter 3.

III - Catalytic activity at higher pressure (Chapter 4: Article 3)

A wide range of redox parameters including feed composition, temperature, pressure and catalyst oxidation time was studied. The objective was to observe the effect of pressure along with other redox parameters on VPP catalytic activity. The pressure had a significant effect on MA yield improvement. These data provided the grounds to study transient kinetics at higher pressure. The results were submitted as the third article and they are presented in Chapter 4.

IV - Transient kinetic modeling (Chapter 5: Article 4)

Based on a redox mechanism, a kinetic model was proposed that could predict the ambient and higher pressure data. The model predictions helped further analyse the pressure effect on catalytic activity. Despite its simple mechanism, the model was able to predict a wide range of feed composition. The major contribution was the generality of kinetic model and characterizing the effect of pressure. This study was submitted as the fourth article and the paper is presented in Chapter 5.

2.4 Catalyst preparation

The catalyst samples in this study were provided by the DuPont Company. The catalyst was composed of a vanadyl pyrophosphate phase, which was encapsulated in a silica shell for attrition resistance. This catalyst was calcined and activated according to the industrial protocols in DuPont's facilities (Patience et al., 2007). Some of the technical specifications are presented in Table 2.1.

Table 2.1: Technical specification of VPP samples

Composition	**Color**	**ρ_p, kg/m^3**	**Area, m^2/g**	**d_p, µm**
$(VO)_2P_2O_7$ + 10 wt. % SiO_2	Gray/green	1700	34.9	70

The catalyst precursor – vanadyl hydrogen phosphate hemihydrate, $VOHPO_4 \cdot ½H2O$ – was synthesized in an organic solvent; the dried powder was micronized to less than 2 µm. The micronized powder was slurried with polysilicic acid and then it was spray dried. The catalyst samples were sieved to a particle size of between 106-180 µm. Due to the porosity and small particle size as well as the relatively low reaction rates, the intra-particle mass transfer resistance was neglected. To stabilize the catalytic activity, the catalyst samples were treated for 24 h at 380 °C under fixed bed operating conditions (1.4 C_4H_{10} in 18.1 vol. % O_2 in argon).

2.5 Ambient pressure experiments

The ambient pressure experiments were conducted over about 500 mg of the calcined and activated VPP catalyst. The experimental setup comprised of a 7.7 mm OD quartz tube reactor, which was located in an electrical furnace (Figure 2-1). The feed gases were mixed and their flow rates were adjusted using the mass flow controllers (MFCs). An automatic six-way valve was used to switch between reducing, purge and oxidizing streams. The catalyst powder was supported over quartz wool in the middle of the reactor tube. The whole system was controlled by Catlab reactor control system (from Hiden Analytical). The product gases were analysed using an online mass spectrometer (MS) with a data collection frequency of about 3-5 points per second. Maleic anhydride was collected in a quench absorber and its evolution was monitored by online conductivity measurements. All the outlet tubing was heat traced at 150 °C. High-performance liquid chromatography (HPLC) was used as an offline method to analyse the accumulated acid concentrations in the absorber for each redox cycle.

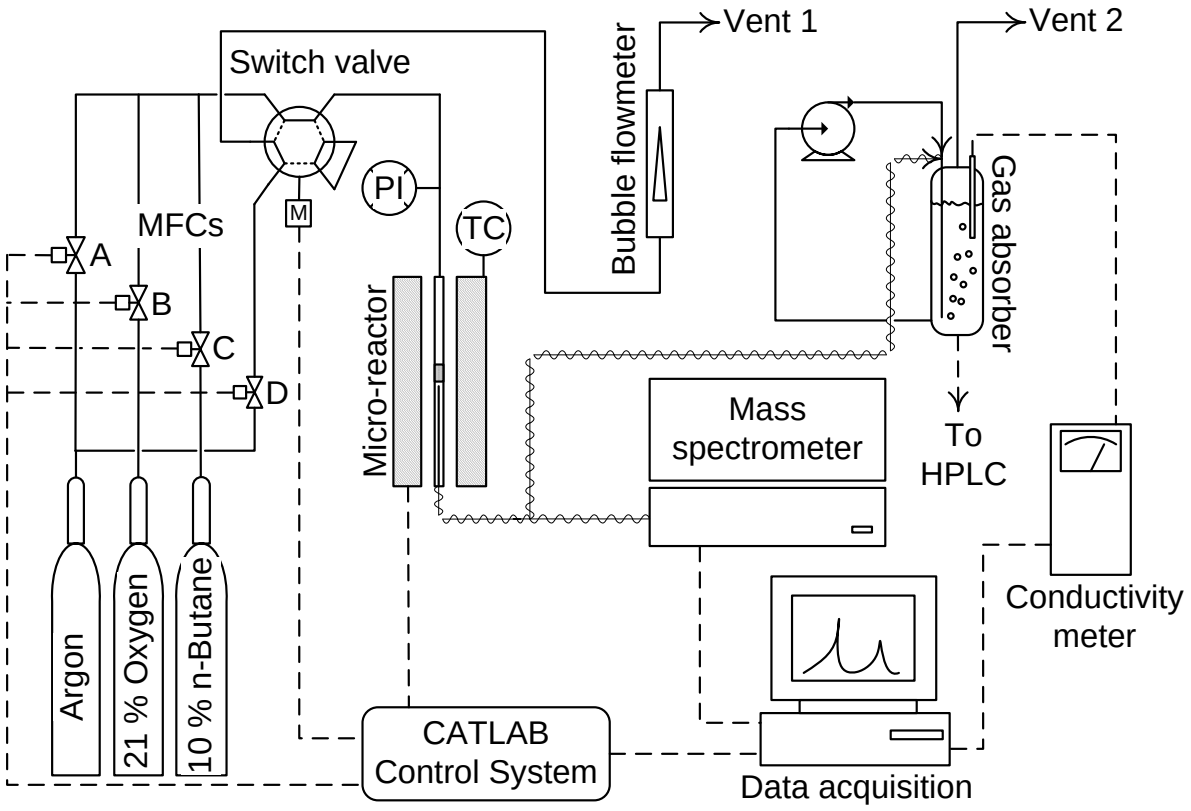

Figure 2-1: Micro-reactor setup

The redox experiments were conducted under a wide range of operating conditions (Table 2.2). These ranges covered the operating conditions of fixed bed, fluidized bed and CFB reactors. To verify the repeatability of the data and to stabilize the catalytic activity, each redox experiment was repeated for 3-5 times at a given set of conditions. The details of analysis methods on MS, conductivity and HPLC data as well as the calibration correlations are presented in Appendix B. These calculations are in a Matlab® programming code format.

Table 2.2: Experimental conditions at P = 1 bar

Simulated condition	**Feed composition, vol. %**		**O_2/C_4H_{10}**	**Oxidation time, min**	**Temperature, °C**
	C_4H_{10}	**O_2**			
Fixed bed	1.4	18.2	13.4	0.3, 1, 3, 10	380
Fluidized bed	3.6	13.4	3.7	0.3, 1, 3, 10	380
CFB	6.5	7.3	1.1	0.3, 1, 3, 10	360, 380, 400
	7.7	4.7	0.6	0.3, 1, 3, 10	380
	8.7	2.6	0.3	0.3, 1, 3, 10	360, 380, 400
Redox	9.9	0.0	0.0	0.3, 1, 3, 10	380

Reduction time = 2.0 min; Feed flow rate = 40 mL/min (STP)

2.6 High pressure experiments

To characterize the effect of pressure on redox kinetics, a selected number of experiments were conducted at a pressure of 4.1 bar. The micro-reactor setup was modified to accommodate higher pressures. Moreover, the quartz reactor was replaced by a stainless steel tube of the same dimensions. The pressure setup comprised of three additional needle valves to adjust and maintain the pressure and to provide a stable flow to the analysis system (Figure 2-2).

High pressure experiments covered the operating ranges of fixed bed, fluidized bed and CFB reactors (Table 2.3). A base case temperature of 380 °C was selected. According to the ambient

pressure results, the catalyst oxidation time was mainly fixed at 10 minute to maximize the MA production rate. The corresponding Matlab® programming code for analysis of redox data are presented in Appendix B.

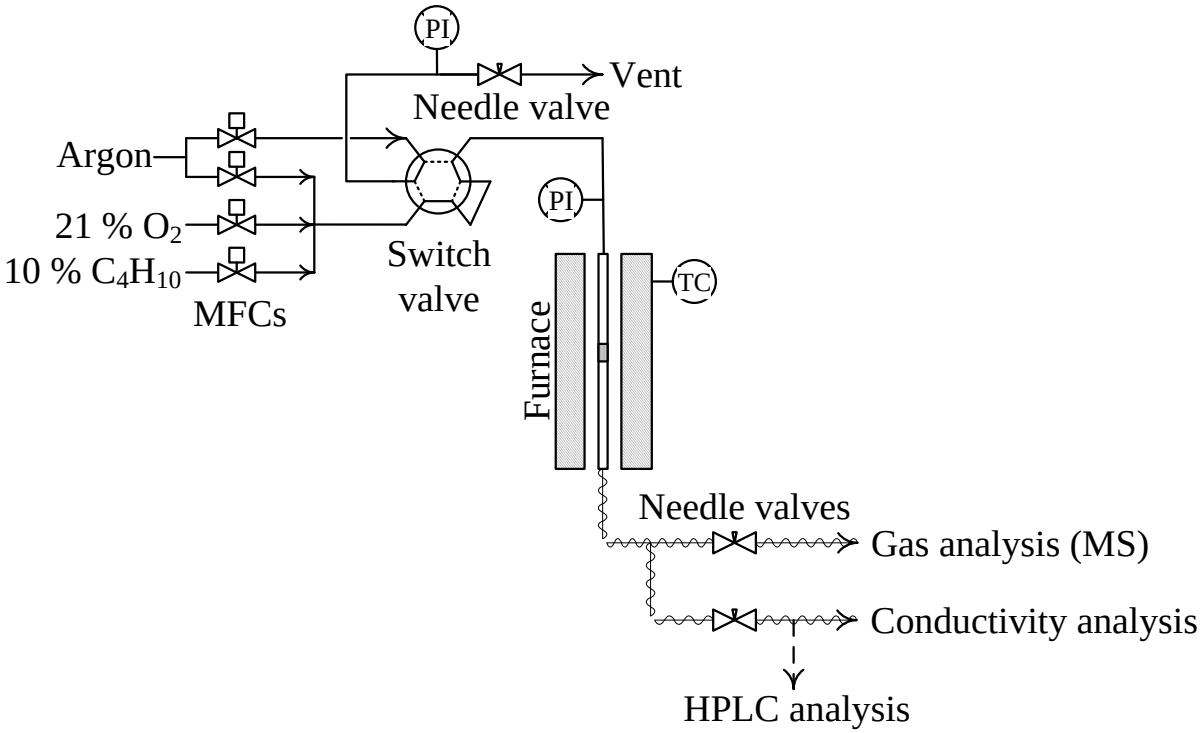

Figure 2-2: High pressure reactor

Table 2.3: Experimental conditions at P = 4.1 bar

Simulated condition	**Feed composition, vol. %**		**O_2/C_4H_{10}**	**Oxidation time, min**	**Temperature, °C**
	C_4H_{10}	**O_2**			
Fixed bed	1.4	18.2	13.4	10	380
Fluidized bed	3.6	13.4	3.7	10	380
CFB	6.5	7.3	1.1	1, 10	380, 400

2.7 Kinetic model development

The kinetic modeling study mainly consisted of characterizing the reactor flow behaviour and developing a transient kinetic model based on the proposed redox mechanism. The reactor flow behaviour was found to be well represented by a series of perfectly mixed reactors (n-CSTR); an almost plug flow behaviour was observed. A Mars-van Krevelen (MvK) type redox mechanism was found to adequately represent the catalyst redox behaviour (Reactions 2-1 to 2-4). According to this mechanism, the catalytic activity was represented by interaction of gaseous species with catalyst reduced (S) or oxidized ($O_2 \cdot$ S) sites through selective or non-selective pathways.

$$O_2 + S \longrightarrow O_2 \cdot S \tag{2-1}$$

$$C_4H_{10} + 3.5\ O_2 \cdot S \longrightarrow C_4H_2O_3 + 4\ H_2O + 3.5\ S \tag{2-2}$$

$$C_4H_{10} + 5.5\ O_2 \cdot S \longrightarrow 4\ CO_x + 5\ H_2O + 5.5\ S \tag{2-3}$$

$$CO_x = \frac{(CO+CO_2)}{2} \tag{2-4}$$

The transient kinetic model was constructed by embedding the kinetic expressions in the transient flow model equations. The transient mass balance equations for the model were derived for all the components presented in the reaction system. This resulted in a set of ordinary differential equations (ODE) which were simultaneously solved by Matlab® program. A fitting program was developed to optimize the model parameters (reaction rate constants and activation energies) as well as the catalyst initial oxidation states. A least square (LSQ) method algorithm was adopted to minimize the error between experimental and predicted data. The corresponding Matlab® programming codes are presented in Appendix C.

CHAPTER 3 MALEIC ANHYDRIDE YIELD DURING CYCLIC N-BUTANE/OXYGEN OPERATION

This article was published in Catalysis Today, Volume: 157, Year: 2010, Pages: 334-338, Special volume dedicated to "6th World Congress on Oxidation Catalysis", Lille, France, 2009.

3.1 Presentation of the article

In this article, transient MA production rates were studied in a wide range of operating conditions. These conditions represented the typical operation of fixed and fluidized bed as well as CFB reactors. The objective was to optimize the catalytic performance with respect to most influencing redox parameters. The results showed that the VPP catalyst performance depends primarily on feed composition and catalyst oxidation time. A linear correlation was observed between MA production rate and catalyst oxidation time. Moreover, it was found that the productivity to MA could be maximized at equimolar concentrations of n-butane and oxygen in the feed. At the end, the catalyst deactivation trends under purely reducing conditions were presented and discussed.

The improvement in catalytic activity by oxidation time or feed oxygen content reconfirmed that by preserving the catalyst surface at oxidized state, a high MA productivity would be ensured. This effect was more critical while operating at higher n-butane concentrations. Under these conditions, providing co-fed oxygen was essential to prevent catalyst surface from being excessively reduced.

Maleic Anhydride Yield during Cyclic n-Butane/Oxygen Operation

Ali Shekari, Gregory S. Patience

3.2 Abstract

Cycling catalyst between a net oxidizing and reducing gaseous environment has been practiced commercially to produce maleic anhydride from n-butane over vanadium pyrophosphate. Typically, the oxidation period is less than one minute to minimize catalyst inventory. In this study, the effect of the oxidation period on maleic anhydride productivity was assessed in the range of 0.3 to 10 minutes. Irrespective of the feed gas composition during the reduction period, the productivity increased linearly with the oxidation soak time in air. A full range of reducing conditions was examined from the pure redox mode (10 % n-butane in argon) to highly oxidizing conditions typical of fixed bed operation (1.4 % n-butane and 18.1 % oxygen). On average, maleic anhydride yield increased by up to 50 % when the oxidation time was extended from 0.3 to 10 minutes. The maleic anhydride yield was lowest under redox mode and it was highest when the feed composition was close to equimolar in n-butane (~ 6 %) and oxygen. Our results show that industrial CFB reactor performance may be improved considerably by efficient regeneration of the catalyst and optimization of the reducing feed gas composition.

Keywords: Maleic Anhydride, VPO, Vanadium Pyrophosphate, n-Butane Partial Oxidation, Redox, Forced Concentration Cycling, CFB

3.3 Introduction

For almost three decades, maleic anhydride (MA) has been commercially produced by partial oxidation of n-butane over vanadium phosphorous oxide (VPO) catalysts in fixed beds, fluidized beds and other reactor types [1]. In one of the most recent developments, DuPont commercialized circulating fluidized bed (CFB) reactor technology in which the reduction and oxidation zones were conducted in separated vessels [2]. The reactor consisted of a high gas velocity riser

coupled to a turbulent fluidized bed (fast bed), a counter current flow fluidized bed regenerator and a stripper (gas up – solids down). The gas in the fast bed riser contained a high concentration of n-butane that carried the catalyst upwards. The reduced catalyst was transferred to a stripping vessel in which the product gas was separated from the catalyst; the catalyst was then transferred to a fluidized bed regenerator where it was oxidized by air. The freshly oxidized catalyst was circulated back to the fast bed of the riser through a stand pipe and subsequently to the riser where n-butane reacted with catalyst oxygen to produce maleic anhydride, CO, CO_2 and water. This configuration was designed to achieve high maleic anhydride productivity and selectivity due to the utilization of selective catalyst surface lattice oxygen. One of the original concepts involved operating in the pure redox mode in which the reducing zone contained n-butane (+recycle gas) and air was fed to the regenerator. However, to maximize reaction rates and, thereby, minimize catalyst inventory, molecular oxygen was introduced into the reducing zone. Minimizing non-selective gas phase combustion of n-butane by the molecular oxygen was achieved by carefully distributing the oxygen across the fast bed at three levels.

Maintaining the VPO surface highly oxidized is a major challenge for fluidized bed processes that operate with high n-butane concentrations. In CFB reactors, there is an economic trade-off between solids residence time in the regenerator, solids circulation rate and selectivity/conversion: increasing catalyst inventory in the regenerator will increase n-butane conversion and maleic anhydride selectivity in the fast bed/riser but catalyst inventory increases total investment costs. Moreover, yield is sensitive to flow patterns in each of the vessels: gas and solids bypassing and solids gulfstreaming must be minimized to ensure an efficient contact between the two phases. Mal-distribution or short circuiting of the solids in the regenerator results in an overly reduced catalyst and potentially lower maleic anhydride yields. Understanding and accounting for the solids residence time distribution in the vessels becomes critically important in the design stage when translating laboratory scale and pilot scale experimental data to the commercial scale.

There has been some controversy on the role of lattice oxygen versus surface oxygen on maleic anhydride selectivity and n-butane conversion. There is a general agreement in the literature that

the surface lattice oxygen is more selective to n-butane conversion to maleic anhydride [3-7]. However, the exact role of this oxygen species or other species – adsorbed and molecular oxygen – during the reaction has not been fully identified. The "loosely bound" surface oxygen and chemisorbed (adsorbed) oxygen on the surface of the catalyst were believed to be the main source of non-selective conversion of n-butane [8]. Creaser et al. [9] also showed that surface oxygen was less selective compared to lattice oxygen in the oxy-dehydrogenation of propane. Early in the development stages of DuPont's n-butane partial oxidation program, we installed a regenerator stripper in the pilot plant to eliminate "loosely bound" surface lattice oxygen to achieve higher maleic anhydride selectivity. This vessel was removed in the commercial design, since its efficacy remained unproven during the trials.

Wang et al. [10] conducted forced concentration cycling tests in a microbalance reactor and proposed that both lattice oxygen and adsorbed oxygen were selective to maleic anhydride. However, the contribution of the lattice oxygen was lower than the adsorbed oxygen species. Gascon et al. [11] and Centi et al. [12] also confirmed the active role of adsorbed surface oxygen on conversion of n-butane. Under fuel rich conditions, Gascon et al. [11] observed a decrease in n-butane conversion during reduction by increasing purge time between oxidation and reduction periods due to elimination of physically adsorbed surface oxygen. These findings suggest that contrary to the common belief on the selective role of lattice oxygen in the reaction, the participation of lattice oxygen is not enough to maintain a high rate of reaction and therefore the presence of gas phase oxygen is essential to supply oxygen to the reaction through adsorption on the surface. A general conclusion of these findings may suggest that the VPO catalyst is not naturally suitable for redox reactions under high n-butane to oxygen ratio. To prevent the side reactions under fuel rich conditions (higher selectivity) and to maintain a higher reaction rate, Ballarini et al. [1] suggested that the presence of co-feed oxygen during the reaction is always required to prevent excessive reduction of V^{5+} and V^{4+} as the catalyst active sites.

Many researchers have reported maleic anhydride yield improvement as a result of increasing VPO catalyst regeneration time. Emig et al. [13] showed that under cyclic redox operating conditions, maleic anhydride production rates increased by a factor of three when the catalyst

regeneration time was increased from 30 minutes to 18 hours. During their forced concentration cycling experiments, Patience et al. [4] observed a higher level of n-butane conversion and maleic anhydride selectivity during the first few minutes after switching the feed from oxidizing to reducing conditions; they attributed the high initial reaction yields to the accumulation of selective oxygen species (most likely surface lattice oxygen) during a 40 minute oxidation period. Lorences et al. [14] also showed that exposure of the catalyst to an oxidizing environment for 48 hours provided twice as much surface oxygen compared to a one hour oxygen treatment. They showed that soaking the catalyst with oxygen could increase the maleic anhydride yield by up to four times the steady state value. Contrary to these findings Huang et al. [15] reported that the catalyst may become inactive due to over oxidation for a long time. Catalyst deactivation could be probably due to accumulation of highly oxidized vanadium sites (V^{5+}) or sintering of the catalyst surface during relatively long oxidation periods. When the catalyst is exposed to air with even low amounts of water vapour (< 3 %), the oxidation state can rise above 4.5 and thereby deactivate the catalyst [16]. Irreversible oxidation was only possible when water vapour was co-fed. In general, as long as the water vapour partial pressure is low, longer regeneration times enhance catalyst performance.

In experimental facilities, oxidation times of up to 10 minutes are commonly tested. However, in commercial operation, the mean residence time of the solids in the regenerator may be as low as one minute [17]. The economic incentive for low residence times translates to lower catalyst inventory and thus lower operating costs but the penalty in reduced maleic anhydride yield must also be considered. In this study, we have systematically varied catalyst oxidation time, reduction feed composition and temperature to assess their impact on maleic anhydride production rates. The catalyst oxidation times corresponded to the values tested in DuPont's laboratory scale equipment, pilot plant and commercial reactor. Several feed compositions were tested that represented typical operating conditions of fixed bed and fluidized bed reactors as well as the CFB technology. The experimental methodology proposed in this study should be helpful in assessing emerging CFB technologies including: Chemical Looping Combustion (CLC) [18], Chemical Looping Reforming (CLR) for hydrogen and CO production [19], propane oxidation to acrylic acid [20], propane oxy-dehydrogenation [9], hot gas desulphurization (ZnS-ZnO) [21], Methanol to Olefins (MTO) [22] and Methanol to Gasoline (MTG) [23].

3.4 Experimental

3.4.1 VPO catalyst preparation

The transient redox experiments were conducted on DuPont catalyst that was calcined in the industrial CFB reactor [16]. The precursor was synthesized in an organic solvent, dried and then micronized to less than 2 μm. The micronized powder was slurried with polysilicic acid and spray dried. The average particle diameter was approximately 70 μm with 10 % silica and the BET surface area of the calcined catalyst was about 35 m^2/g – Table 3.1. The predominate phase was vanadium pyrophosphate – $(VO)_2P_2O_7$ (VPP).

Table 3.1: Technical specifications of DuPont's calcined VPO catalyst

Composition	**Color**	**ρ_p, kg/m^3**	**BET m^2/g**	**d_p μm**
$(VO)_2P_2O_7$ + 10 % SiO_2	Gray/green	1700	34.9	70

The catalyst powder was sieved to a particle size between 125 to 180 μm prior to experimentation. This range of particle size is commonly used in the literature [11]. Due to the high porosity and relatively low reaction rates, the intra-particle mass transfer resistance was neglected. Approximately 500 mg of calcined catalyst was used for all transient redox experiments. Before beginning an experiment, the fresh catalyst was activated by a mixture of 1.4 % n-butane in 18.1 % oxygen (balance argon) for 24 hours. The base case temperature was 380 °C and the total feed flow rate was 40 mL/min (STP). Catalyst activity was reasonably stable after this time period.

3.4.2 Experimental setup

The transient redox experiments were conducted in a 7 mm ID quartz tube micro-reactor that was placed in an electrical furnace. The process flow diagram of the micro-reactor experimental setup is shown in Figure 3-1. Four mass flow controllers (MFC) maintained the feed flow rates to the reactor. The first three MFCs (A to C) were used to mix the feed streams for the reaction and also

to feed oxygen during catalyst oxidation. The feed streams were taken from three gas bottles: 10 vol. % n-butane in argon, 21 vol. % oxygen in argon and 99.9 vol. % argon. The fourth mass flow controller (D) was used to purge the reactor with argon between the reduction and oxidation half-cycles and also between two redox cycles. An electrically controlled 6-way valve was used to switch between the feed streams at a specified time sequence. There was also a possibility for manual flow rate measurements by directing different gases to a bubble flow meter using proper valve positions. The CATLAB software developed for the micro-reactor system (from Hiden Analytical) controlled the operation of the MFCs and the reactor furnace as well as the automated switching valve. Downstream of the reactor, a small fraction of the exit stream (~ 1 %) was sent to an online mass spectrometer (Quadrupole type QIC-20 from Hiden Analytical) for real time measurement of gaseous products (CO, CO_2 and water) as well as un-reacted n-butane and oxygen. The frequency of the measurements in the mass spectrometer was in the order of 2-5 data point per second. The main part of the effluent stream was sent to an aqueous quench to absorb product acids, in which the electrical conductivity was monitored in real time to estimate the evolution of the product acids. To cross check the validity of the conductivity measurements and also to identify the acid product distribution, a liquid sample from quench was taken at the end of each redox cycle and analyzed by HPLC (Modular ProStar unit from Varian).

3.4.3 Redox experiments

To study the effect of catalyst oxidation time and reduction feed composition on reactor performance, experiments at four oxidation times and six feed compositions were conducted. A list of experimental conditions is presented in Table 3.2. The reduction feed compositions were selected to cover the full range of industrial operation: from fuel rich conditions typical of CFB reactors, with as much as 10 % n-butane, to fuel lean conditions, characteristic of fixed bed reactors with as little as 1.4 % n-butane in the feed. The lower bound concentration of n-butane in the feed to the reactor was selected such that to avoid the explosion limits (1.8 % n-butane in air). The catalyst oxidation times were varied from 10 minutes (standard for bench top laboratory experiments) to as low as 0.3 minute that represents conditions in an industrial CFB reactor. Finally, to observe the effect of temperature on the reaction yield, two selected feed compositions

were run at 360 and 400 °C with a 10 minute re-oxidation period. The selected runs corresponded to the actual industrial fuel rich conditions (i.e. O_2/n-butane = 0.3 and 1.2).

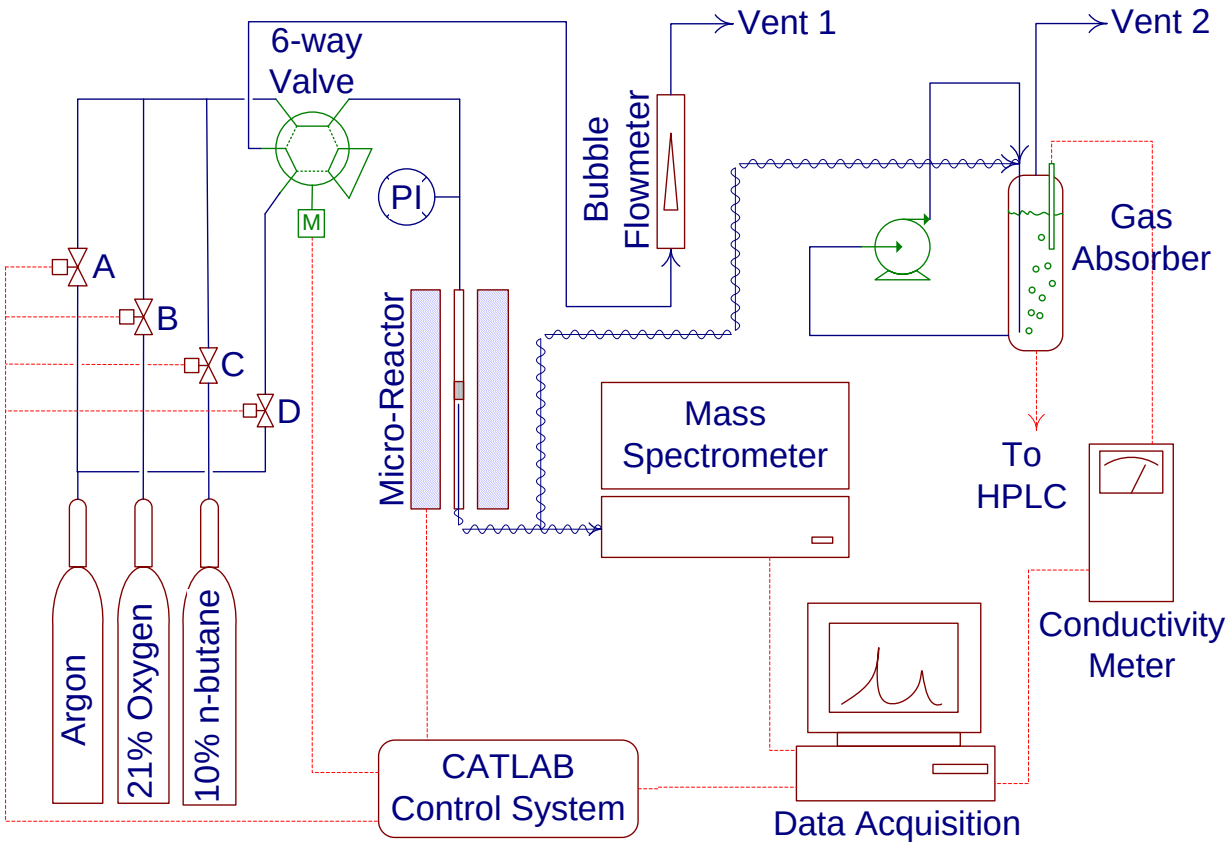

Figure 3-1: Micro-reactor experimental setup

The micro-reactor setup was designed so that the operation of a circulating fluidized bed reactor could be simulated by switching between reduction and oxidation feed streams over the fixed catalyst bed. In this way, data interpretation was simplified in that the gas phase hydrodynamics were much less complicated compared to fluidized bed reactors. For each redox condition described in Table 3.2, a series of at least 5 identical redox cycles were conducted. The catalyst activity was then calculated by averaging the results obtained for each repeated run. Adequately long purging between the redox half-cycles and between repeated full cycles ensured the removal

of gas phase oxygen and reaction products from the reactor and the connecting lines and provided identical conditions for each redox cycle.

For each redox experiment, a time sequence of events was programmed in the CATLAB software including: flow rate of each MFC, valve switch moments, and temperature. The catalyst was first heated under an inert argon stream until the desired temperature was achieved and then exposed to a series of 5-8 cycles. Each oxidation half-cycle was followed by a 10 minute purge. The reduction half-cycle lasted for 2 minutes while there was 30 minutes of purging between redox cycles.

Table 3.2: Experimental conditions of transient redox runs

Reduction[1] composition, vol. %		**O_2/n-butane ratio**	**Oxidation time, minute**	**Temperature, °C**
n-butane	**Oxygen**			
9.9	0.0	0.0	0.3-10	380
8.8	2.5	0.3	0.3-10	360, 380, 400
7.7	4.8	0.6	0.3-10	380
6.4	7.5	1.2	0.3-10	360, 380, 400
3.6	13.4	3.7	0.3-10	380
1.4	18.2	13.6	0.3-10	380

[1]Reduction time: 2.0 minutes; average feed flow rate: 40 mL/min (STP)

3.5 Results and discussion

3.5.1 Effect of redox parameters

3.5.1.1 Oxidation time

The oxidation step has a significant effect on maleic anhydride yield, even under fuel lean conditions. Based on the extensive literature data, we expected that the oxidation time would

improve maleic anhydride yield for fuel rich conditions but there would be little to no effect for fuel lean conditions. Figure 3-2 shows that the average maleic anhydride production rates increase linearly with an increase in the catalyst oxidation time irrespective of the reduction feed composition (O_2/n-butane ratio). In most of the experiments, where there was some oxygen co-fed with n-butane, the maleic anhydride yield improved by up to 50 % by increasing the catalyst oxidation time from 0.3 to 10 minutes. The increase in maleic anhydride production was much more noticeable in the pure redox mode (O_2/n-butane = 0.0). In this case, the maleic anhydride production increased by a factor of 3.5 times after extending the catalyst oxidation time from 0.3 to 10 minutes. These results are similar to the findings of Emig et al. [13] where they reported an increase in the maleic anhydride production rate by a factor of three when the catalyst regeneration time was increased from 30 minutes to 18 hours. The time allowed for catalyst oxidation in the lab scale micro-reactor could be actually correlated to the solids residence time in the regeneration section of an industrial CFB reactor. These results show how important it could be to optimize the solids residence time in the regenerator and the ability to supply oxygen. The higher observed rates are believed to be due to the higher availability of the selective surface lattice oxygen.

3.5.1.2 Feed composition

Figure 3-2 shows the relationship between oxidation time and maleic anhydride production rate. The same data is re-plotted in Figure 3-3 to demonstrate the effect of feed composition on productivity: maleic anhydride production rate increases with increasing n-butane concentration up to a 1:1 feed composition. The maximum maleic anhydride production rate exceeds 160 gMA/h/kg VPO when the feed concentrations of n-butane and oxygen are equimolar. MA production drops by about 15 % at conditions typical of turbulent fluidized beds and then by another 30 % in fuel lean conditions characteristic of fixed bed operation. The lowest production rates are under purely redox conditions. Clearly, maintaining sufficient oxygen together with n-butane is critical to maintaining high maleic anhydride productivity. This observation could be attributed to the opposing positive and negative effects of elevated n-butane concentration in the feed to the reactor. The positive effect is related to the increased reaction rate with high n-butane concentrations. However, high n-butane concentrations negatively affect the catalyst performance

by decreasing the catalyst oxidation state and by accelerating catalyst deactivation (loss of surface oxygen) or probably due to higher rate of surface carbon formation.

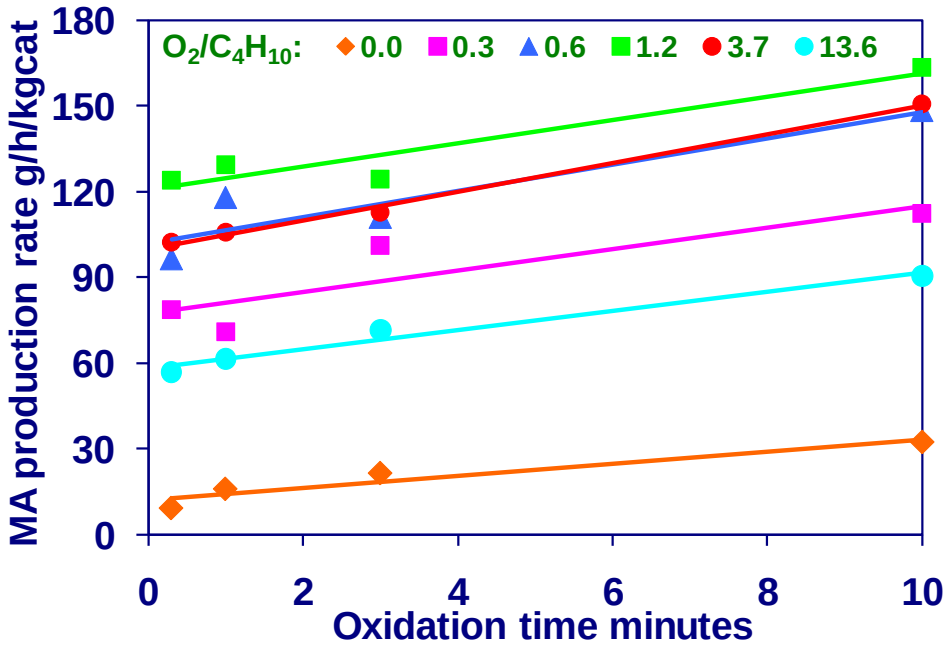

Figure 3-2: Effect of oxidation time on maleic anhydride production rate

(Feed flow rate: 40 mL/min (STP), temperature: 380 °C)

3.5.1.3 Temperature

We studied the effect of temperature on maleic anhydride production rate at two feed compositions: O_2/n-butane = 0.3 and 1.2. The latter condition represents typical feed composition of a CFB plant while the former corresponds to the exit conditions when the plant is run at high inlet n-butane concentrations. The latter ratio is close to the optimum feed ratio that resulted in the highest maleic anhydride productivity. As is shown in Figure 3-4, temperature has little effect on productivity when the n-butane feed rate is high compared to the oxygen feed rate even though the catalyst was soaked in air for 10 minutes. On the other hand, temperature has a measurable effect on yield with a close to an equimolar feed composition of oxygen and n-butane: the productivity increased approximately 10 % when the temperature was increased by 20

°C from 380 °C and it dropped by 40 %, when the temperature was decreased by 20 °C. This data is consistent with previous studies that showed increasing the temperature during re-oxidation enhanced the oxidation rate of the VPO catalyst during reduction [11, 15]. More oxygen is incorporated into the surface lattice resulting in increased maleic anhydride productivity.

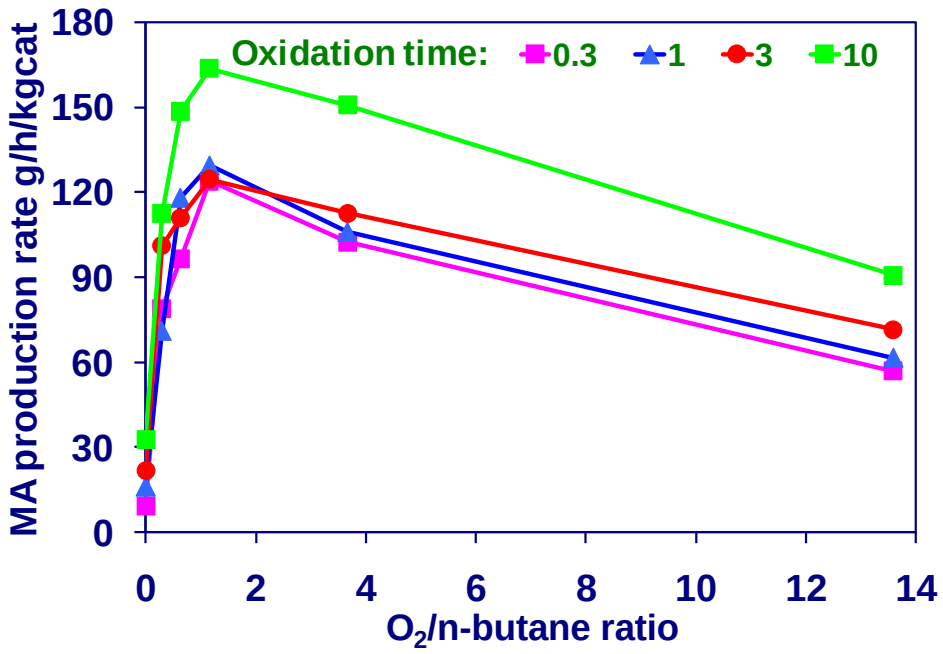

Figure 3-3: Effect of feed composition on maleic anhydride production rate

(Feed flow rate: 40 mL/min (STP), temperature: 380 °C)

3.5.2 Transient maleic anhydride rates

We measured the transient maleic anhydride production rates by monitoring the electrical conductivity of the acid solution accumulated in the liquid quench that was located downstream of the micro-reactor (Figure 3-1). The results were in agreement with our observations: the transient production rates increased with increasing the oxidation time. The transient rates presented in Figure 3-5 show that the initial rates of maleic anhydride (at initial moments of the curves) increase by increasing the oxidation time before each reduction cycle. This could be due to the higher accumulation of selective oxygen species on the catalyst surface when the catalyst is

exposed to the oxidation environment for a longer period of time. Similar high initial catalyst activities were reported by Patience et al. [4] and Lorences et al. [14], at the first few minutes of reduction period after an extensive catalyst oxidation.

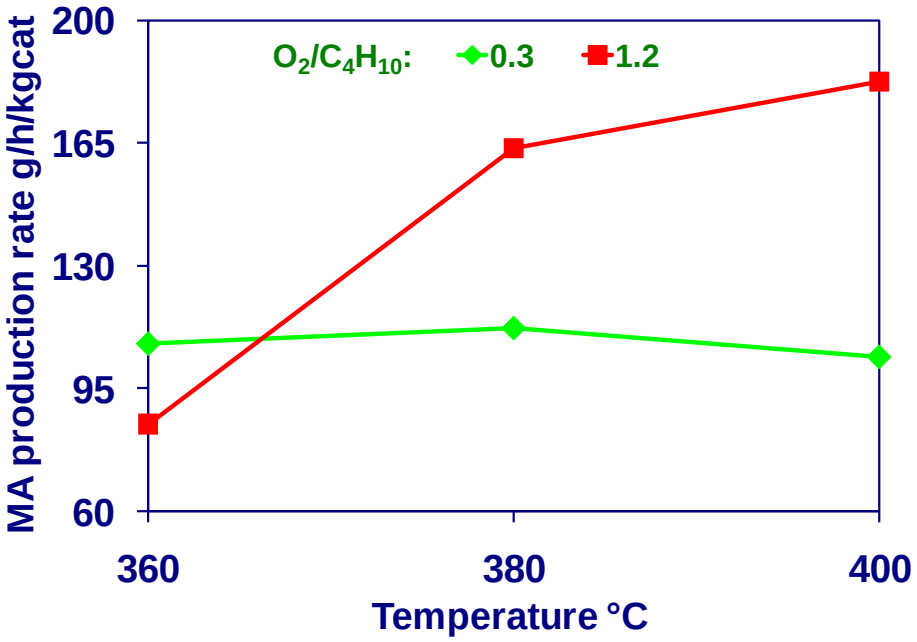

Figure 3-4: Effect of temperature on maleic anhydride production rate

(Oxidation time: 10 minutes, feed flow rate: 40 mL/min (STP))

3.5.2.1 Catalyst deactivation

During the transient redox experiments, we observed that at relatively high n-butane concentrations in the feed (O_2/n-butane ≤ 0.3), the catalyst undergoes a considerable deactivation during the reduction period even with a relatively long oxygen pre-treatment before each reduction cycle (10 minutes). The catalyst deactivation was characterized by a stepwise decrease in the maleic anhydride transient rates during 5-8 consecutive redox cycles under the same operating conditions. Figure 3-6 demonstrates the transient maleic anhydride rates selected from eight consecutive redox cycles at the conditions where there was no oxygen in the reduction feed. A significant decrease in the maleic anhydride transient rate could be observed by exposing the

catalyst to these consecutive redox cycles. These data show that the deactivation of catalyst could not be compensated even by 10 minutes of catalyst oxidation before each reduction cycle.

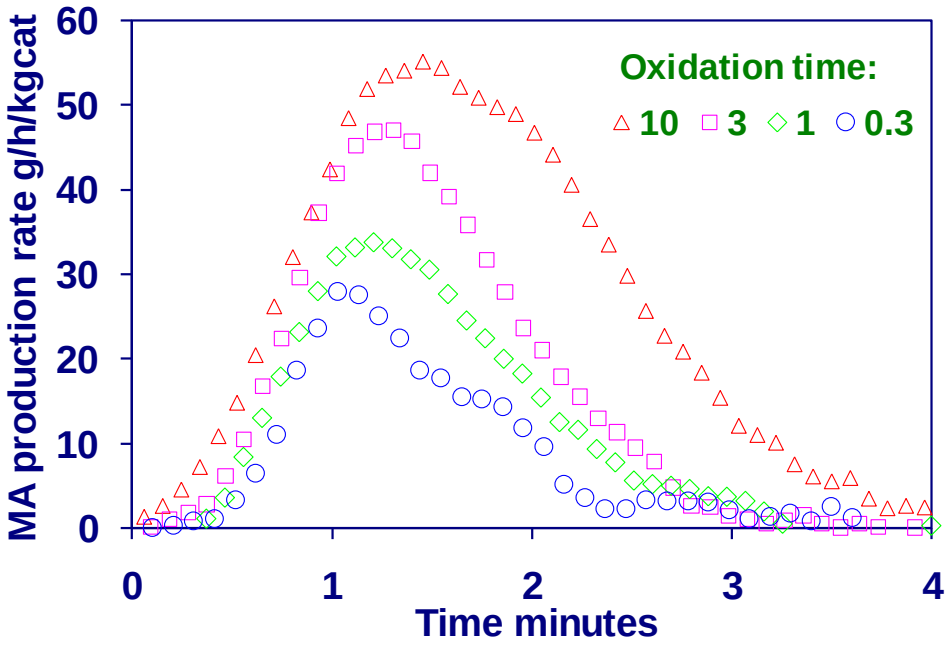

Figure 3-5: Maleic anhydride transient production rates

(Feed flow rate: 40 mL/min (STP), temperature: 380 °C, O_2/n-butane: 0.0)

When the catalyst oxidation time is relatively short, even in the presence of some oxygen in the reduction feed (O_2/n-butane $\leq$ 0.6), the catalyst still suffers a slight deactivation during consecutive redox cycles. Generally, this effect is more noticeable when the oxygen to n-butane molar ratio in the feed falls below 0.3. Under these conditions, the catalyst deactivation occurs irrespective of the duration of oxidation period prior to each reduction cycle (Figure 3-6). These results suggest that to maintain a relatively high production rate at fuel rich conditions, the feed to the reactor must have an appreciable amount of oxygen to prevent catalyst over reduction. Also, even in the presence of oxygen in the reduction feed, efficient catalyst oxidation would still be required to compensate for the catalyst deactivation during reduction under fuel rich conditions.

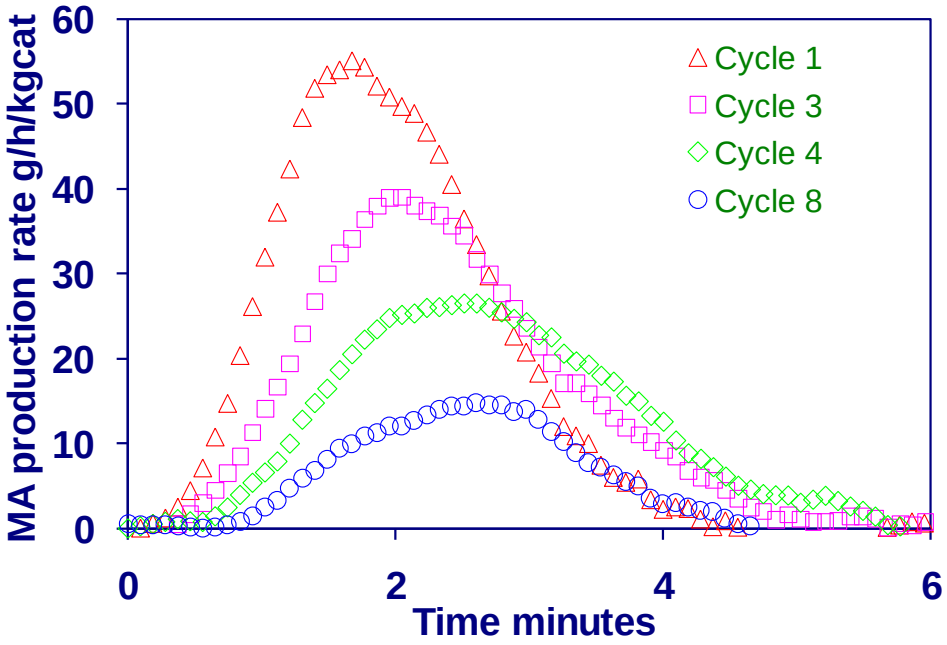

Figure 3-6: VPO catalyst deactivation during redox operations at fuel rich conditions

(Feed flow rate: 40 mL/min (STP), temperature: 380 °C, oxidation time: 10 minutes, O_2/n-butane: 0.0)

3.6 Conclusions

Maleic anhydride production rate is sensitive to catalyst oxidation time and reduction feed composition. Irrespective of the reduction feed composition, the average maleic anhydride production rate in a redox cycle could be increased by up to almost 50 % by extending the catalyst oxidation time from 0.3 to 10 minutes. Maleic anhydride production rates increase even with a feed composition containing 1.4 vol. % n-butane in air. The effect of catalyst oxidation on maleic anhydride production becomes more important when operating under fuel rich conditions. Under such conditions, an improvement of the order of 3.5 times in maleic anhydride production rate could be expected by extending the catalyst oxidation time to 10 minutes. A near equimolar feed of 6 % n-butane and oxygen resulted in the highest maleic anhydride production rate. The transient maleic anhydride rate data showed that to prevent the catalyst deactivation and to maintain a high production rate at fuel rich conditions, the feed to the reactor must have an appreciable amount of oxygen. These data also suggested that efficient catalyst regeneration

would still be required to compensate for catalyst deactivation even at the presence of relatively large amounts of oxygen in the reduction feed.

3.7 Acknowledgements

We would like to thank the Natural Sciences and Engineering Research Council of Canada (NSERC), Ministre du Développement Economique, de l'Innovation et de l'Exportation (MDEIE) of Quebec and Canadian Foundation for Innovation (CFI) for their financial support of this project. We wish to thank also the DuPont Company for providing the catalyst samples for this research.

3.8 References

[1] N. Ballarini, F. Cavani, C. Cortelli, S. Ligi, F. Pierelli, F. Trifiro, C. Fumagalli, G. Mazzoni, T. Monti, Top. Catal. 38 (2006) 147-156.

[2] R.M. Contractor, Chem. Eng. Sci. 54 (1999) 5627-5632.

[3] Y. Schuurman, J.T. Gleaves, Catal. Today 33 (1997) 25-37.

[4] G.S. Patience, M.J. Lorences, Int. J. Chem. Reactor Eng. 4 (2006) 1-18.

[5] Y.H. Taufiq-Yap, B.H. Sakakini, K.C. Waugh, Catal. Lett. 48 (1997) 105.

[6] B.H. Sakakini, Y.H. Taugiq-Yap, K.C. Waugh, J. Catal. 189 (2000) 253.

[7] S.K. Bej, M.S. Rao, Ind. Eng. Chem. Res. 30 (1991) 1819.

[8] U. Rodemerck, B. Kubias, H.-W. Zanthoff, M. Baerns, Appl. Catal., A: Gen. 153 (1997) 203.

[9] D. Creaser, B. Andersson, R.R. Hudgins, P.L. Silveston, J. Catal. 182 (1999) 264-269.

[10] D.X. Wang, M.A. Barteau, Catal. Lett. 90 (2003) 7-11.

[11] J. Gascón, R. Valenciano, C. Téllez, J. Herguido, M. Menéndez, Chem. Eng. Sci. 61 (2006) 6385-6394.

[12] G. Centi, F. Trifiro, J.R. Ebner, V.M. Franchetti, Chem. Rev. 88 (1988) 55.

[13] G. Emig, K. Uihlein, C.-J. Hacker, in: V.C. Corberan, S.V. Bellon (Eds.), New Developments in Selective Oxidation, Elsevier, Amsterdam, 1994, pp. 243-251.

[14] M.J. Lorences, G.S. Patience, F.V. Diez, J. Coca, Appl. Catal. A: Gen. 263 (2004) 193-202.

[15] X.-F. Huang, C.-Y. Li, and B.-H. Chen, P.L. Silveston, AIChE J. 48 (2002) 846-855.

[16] G.S. Patience, R.E. Bockrath, J.D. Sullivan, H.S. Horowitz, Ind. Eng. Chem. Res. 46 (2007) 4374-4381.

[17] G.S. Patience, R.E. Bockrath, Appl. Catal. A: Gen., accepted October (2009).

[18] E. Johansson, A. Lyngfelt, T. Mattisson, F. Johnsson, Powder Technol. 134 (2003) 210-217.

[19] M. Ryden, A. Lyngfelt, T. Mattisson, Fuel 85 (2006) 1631-1641.

[20] J.L. Dubois, D. Garrait, A. Legall, G. Bazin, S. Serreau, J. Dubois, Arkema France, WO 2006/072682 A1 (2006).

[21] B. Turk, J. Schlather, Gasification Technologies Conference, (2006). http://www.gasification.org/Docs/2006_Papers/53SCHL.pdf

[22] L.W. Miller, UOP LLC, U.S. Patent 6,166,282 (2000).

[23] F.J. Keil, Microporous Mesoporous Mater. 29 (1999) 49-66.

CHAPTER 4 TRANSIENT REDOX ACTIVITY OF VANADYL PYROPHOSPHATE AT AMBIENT AND ELEVATED PRESSURE

This article was submitted to International Journal of Chemical Reactor Engineering on February 2011. The article was reviewed on August 2011.

4.1 Presentation of the article

In this article, the VPP catalytic activity was studied in a wide range of redox conditions at ambient and higher reactor pressure (4.1 bar). The main objective was to characterize the effect of pressure on transient catalytic activity. This effect was rarely reported in the open literature. Higher pressure significantly improved the catalytic performance: MA yield improved by up to 30 %. Ambient pressure data showed the importance of efficient catalyst regeneration while operating at fuel rich conditions. However, in the absence of gas phase oxygen, even extensive catalyst regeneration could not compensate for the catalyst's loss of activity.

This article presented an extensive literature review (53 references) including the most recent developments in the field of VPP transient catalysis. The results provided a better insight on the catalyst redox behaviour as well as the experimental background for development of a transient kinetic model at higher reactor pressure.

Transient Redox Activity of Vanadyl Pyrophosphate at Ambient and Elevated Pressure

Ali Shekari, Gregory S. Patience

4.2 Abstract

The transient catalytic activity of vanadyl pyrophosphate (VPP) catalyst was studied at ambient and elevated pressure (up to 4.1 bar) and a wide range of operating conditions. The range included the commercial operating conditions typical of fixed bed, fluidized bed and circulating fluidized beds (CFB) for the partial oxidation of n-butane to maleic anhydride (MA). The maleic anhydride yield improved by increasing the feed oxygen molar fraction, temperature and pressure. When the catalyst was cycled between an oxidizing (synthetic air) and a reducing environment; yield increased with an increase in the catalyst residence time in the oxidizing environment. This effect was more pronounced at higher pressure. At ambient pressure, MA selectivity varied between 50-73 % while it decreased to about 48-54 % at a pressure of 4.1 bar. A strong MA selectivity dependency on feed composition was observed when the oxidation time was in the range of actual industrial reactors (< 1 minute). Selectivity data suggested that different oxygen species might be responsible for CO formation compared to other products such as CO_2 and MA.

Under oxidizing feed conditions ($O_2/C_4H_{10} \geq 3.7$), an increase in n-butane conversion was the main contributor to improved MA yield: n-butane conversion increased by about 70 % when the catalyst oxidation time extended from 0.3 to 10 minutes. While, under fuel rich feed conditions, typical of industrial CFB operations, both MA selectivity and n-butane conversion contributed to enhancement in MA yield. Depending on the feed composition, MA selectivity increases by about 16-30 % and n-butane conversion increases by about 32-55 % by extending the catalyst oxidation time. These results show the critical importance of catalyst oxidation time on reaction yield improvement especially when operating at fuel rich feed conditions. The surface adsorbed or surface lattice oxygen species were suggested to be the main responsible for n-butane activation. While, the contribution of catalyst's sub-surface lattice oxygen was believed to be

very limited at fuel rich feed conditions. Under these conditions, catalyst over-reduction cannot be effectively compensated even after excessive catalyst regeneration and presence of gas phase oxygen is critical to maintain a high catalytic activity.

As the reactor pressure increased to 4.1 bar, up to 60 % increase in n-butane conversion accompanied by 100 % increase in oxygen conversion was observed. MA selectivity decreased by about 20 % on average but the increase in n-butane conversion resulted in an overall yield improvement of up to 30 %. Data show that the catalytic performance could be enhanced at certain combination of reactor pressure and temperature.

Keywords: n-butane, vanadyl pyrophosphate, pressure, temperature, transient, redox, activity, yield, maleic anhydride, oxidation time, oxygen

4.3 Introduction

During the past few decades, numerous studies have been undertaken to elucidate different aspects of the n-butane partial oxidation to maleic anhydride over vanadyl pyrophosphate catalyst (Ballarini et al., 2006a). The research on this subject is still being actively pursued (Cavani et al., 2010a,b; Shekari and Patience, 2010; Fernandez et al., 2010; Patience and Bockrath, 2010; Shekari et al., 2010; Dummer et al., 2010; Hutchenson et al., 2010; Zhang and Liu, 2010). In general, the maximum maleic anhydride yield in the lab or commercial scale reactors still remains in the range of 50-65 % (Ballarini et al., 2006a). The reason for such extensive research could be partly due to the complexity of the catalyst structural system and also the dynamic dependency of its active phases under different reaction conditions (Ballarini et al., 2006a; Cavani et al., 2010a; Hävecker et al., 2003, 2004; Mallada et al., 2000; Kleimenov et al., 2005).

The VPP catalyst reactivity has been extensively examined under transient redox conditions (Cavani et al., 2010a,b; Shekari and Patience, 2010; Fernandez et al., 2010; Wang et al., 2000; Wang and Barteau, 2001, 2002, 2003; Huang et al., 2001, 2002a,b; Schuurman and Gleaves,

1994, 1997; Kamiya et al., 2001; Lorences et al., 2003, 2004, 2006; Chen and Munson, 2002; Gascón et al., 2006; Ballarini et al., 2006b; Pérez-Moreno et al., 2009; Song et al., 2006). Some of the experimental techniques employed includes: thermogravimetric analysis (TGA) (Wang et al., 2000; Wang and Barteau, 2001, 2002, 2003; Huang et al., 2001, 2002a; Chen et al., 2007), in-situ characterization techniques such as FTIR (Cavani et al., 2010a; Xue and Schrader, 1999) and Temporal Analysis of Products (TAP) (Schuurman and Gleaves, 1994, 1997; Kamiya et al., 2001; Kubias et al., 1996; Mills et al., 1999; Rodemerck et al., 1997a,b). The main focus of these studies have been generally to investigate the transient kinetics and reaction mechanism by identifying the reaction intermediates (Wang et al., 2000; Wang and Barteau, 2001, 2002; Huang et al., 2001, 2002a,b; Lorences et al., 2003, 2004, 2006; Chen and Munson, 2002; Gascón et al., 2006; Xue and Schrader, 1999; Kubias et al., 1996) and to characterize the catalyst active phases during reaction (Cavani et al., 2010a; Hävecker et al., 2003; Wang et al., 2000; Wang and Barteau, 2003; Ballarini et al., 2006b). However, depending on the pursued research objective, only limited ranges of redox conditions have been explored. Moreover, due to proprietary reaction feeding modes or the specific experimental configurations, the results of some of these studies might not be directly correlated with operational modes exercised in industrial reactors.

The redox operating conditions have a significant effect on the performance of VPP catalyst under transient conditions. Some of the redox conditions studied in the literature are reduction or oxidation composition, catalyst residence time, temperature and pressure (Lorences et al., 2006; Patience and Lorences, 2006; Liang et al., 2003; Patience et al., 2007). The operating ranges could be widely distributed: typically, the fixed bed or fluidized bed reactors operate at 1.8-4 vol. % n-butane while an industrial circulating fluidized bed reactor may operate up to 20 vol. % n-butane in the feed (Patience and Bockrath, 2010; Contractor et al., 1994). Oxidation times may vary from 40 seconds to one minute in CFB regenerators to up to several minutes in the lab scale reactors. Recently, we showed that irrespective of the feed composition in a lab scale micro-reactor, maleic anhydride yield could be improved by 50 % when increasing the catalyst oxidation time from 0.3 to 10 minute (Shekari and Patience, 2010). Similar yield improvements were reported elsewhere by extending catalyst oxygen treatment time (Schuurman and Gleaves, 1994, 1997; Lorences et al., 2006; Patience and Lorences, 2006; Emig et al., 1994; Aït Lachgar et al., 1997). We have also shown that the maleic anhydride production rate was improved in

DuPont's commercial CFB reactor by supplying adequate oxygen along with increasing n-butane throughput to the reactor (Patience and Bockrath, 2010; Shekari et al., 2010). Higher n-butane concentration in the feed has been reported to be favourable for maleic anhydride yield (Ballarini et al., 2006a; Mallada et al., 2000; Kamiya et al., 2001; Hutchings, 1991; Centi and Trifirò, 1984). Reversible catalyst deactivation could occur under higher n-butane concentrations. Catalyst deactivation could be due to carbon formation, catalyst over-reduction or yield loss due to side reactions (Mallada et al., 2000; Wang et al., 2000; Lorences et al., 2003, 2004; Mota et al., 2000; Ballarini et al., 2005). In our earlier study (Shekari and Patience, 2010), we showed that an optimum ratio for oxygen/n-butane in the feed exists which is about unity (~ 6 vol. % n-butane and oxygen in the feed). These studies show that the key for a selective catalyst at higher n-butane concentrations might be to keep the catalyst surface at an optimized oxidation state by feeding molecular oxygen at specific concentrations. Among other operating conditions, temperature has been reported to improve either the catalyst re-oxidation rate (Huang et al., 2002a; Wang and Barteau, 2002; Liang et al., 2003) or the catalyst active phase transformations (V^{4+} to V^{5+}) (Cavani et al., 2010a). However, despite the extensive research on the effects of several redox parameters, few studies are reported on the effect of pressure on VPP transient reactivity (Lorences et al., 2006; Patience et al., 2007).

There is considerable controversy on the nature of catalyst's active phases and the role of oxygen and vanadium sites during reaction (Hutchings, 2004; Volta, 2000). Vanadyl pyrophosphate – $(VO)_2P_2O_7$ (V^{4+}) – has been identified as the predominant catalyst active phase (Ballarini et al., 2006a; Hutchings, 2004; Volta, 2000). However, the presence of various $VOPO_4$ (V^{5+}) crystalline phases and even limited presence of V^{3+} on the catalyst surface has been described as favourable for catalytic performance (Ballarini et al., 2006a; Schuurman and Gleaves, 1997; Rodemerck et al., 1997b; Mota et al., 2000; Hutchings, 2004; Volta, 2000; Taufiq-Yap et al., 2009; Cavani et al., 2000). Two vanadium oxidation states (V^{4+} and V^{5+}) are considered as the main redox couple during reaction (Ballarini et al., 2006a; Schuurman and Gleaves, 1994, 1997; Lorences et al., 2003, 2004, 2006; Mota et al., 2000; Taufiq-Yap et al., 2009). The role of the oxidized state of the catalyst (V^{5+}) has been attributed to lower n-butane activation energy and thus a higher catalytic activity (Schuurman and Gleaves, 1994, 1997). It was also shown that the presence of V^{5+} oxidation sites is detrimental to n-butane selective oxidation under both n-butane lean and

rich conditions (Ballarini et al., 2006a; Patience and Lorences, 2006; Mota et al., 2000). Despite these findings, an excessive amount of V^{5+} was reported to decrease n-butane conversion (Taufiq-Yap et al., 2009). An optimal ratio of V^{5+}/V^{4+} equal to 0.25 was suggested for the best catalyst performance (Aït-Lachgar et al., 1998). In general, the active and selective catalyst has been described to have slightly higher than +4 vanadium oxidation state which involves the simultaneous presence of V^{4+} and V^{5+} phases on the surface.

Regarding the role of active oxygen species, there is a general agreement that the surface lattice oxygen (O^{2-}) is the main active and selective species (Wang et al., 2000; Wang and Barteau, 2001, 2002, 2003; Huang et al., 2002a; Schuurman and Gleaves, 1997; Lorences et al., 2004; Chen and Munson, 2002; Rodemerck et al., 1997a). The presence of gas phase or adsorbed oxygen was found to promote non-selective oxidation (Huang et al., 2002a,b; Chen and Munson, 2002; Rodemerck et al., 1997a; Emig et al., 1994). However, some authors reported a considerable contribution of surface adsorbed or loosely bound oxygen during the reaction (Wang and Barteau, 2001, 2002, 2003; Gascón et al., 2006). The participation of bulk lattice oxygen in the surface reactions through diffusion has rarely been reported (Gascón et al., 2006; Mills et al., 1999).

Although a significant volume of research was devoted to n-butane partial oxidation, a comprehensive assessment of the effects of the redox parameters on VPP transient reactivity seems to be still lacking. In this study, we have systematically analysed the effect of a wide range of feed compositions and catalyst oxidation times and temperature on the transient reactivity of DuPont's VPP catalyst. The operating conditions were selected so as to adequately cover the existing conditions in commercial reactors. None of the industrial reactors operate at ambient pressure, so we have also performed additional experiments by increasing the reactor pressure (up to 4.1 bar). Studying the effect of pressure on catalytic performance could be beneficial in providing more reliable experimental data that correspond better to the actual operating conditions in industrial reactors. The methodology presented in this paper is expected to be helpful in the process design and scale up of novel circulating bed reactor technologies such as

Chemical Looping Combustion (CLC), Chemical Looping Reforming (CLR) of methane and Methanol to Olefins or Gasoline (MTO/MTG).

4.4 Experimental

4.4.1 Micro-reactor setup

Transient redox experiments were performed over DuPont's calcined commercial VPP catalyst (Shekari and Patience, 2010) in a micro-reactor at ambient and elevated pressures as presented in Figure 4-1.

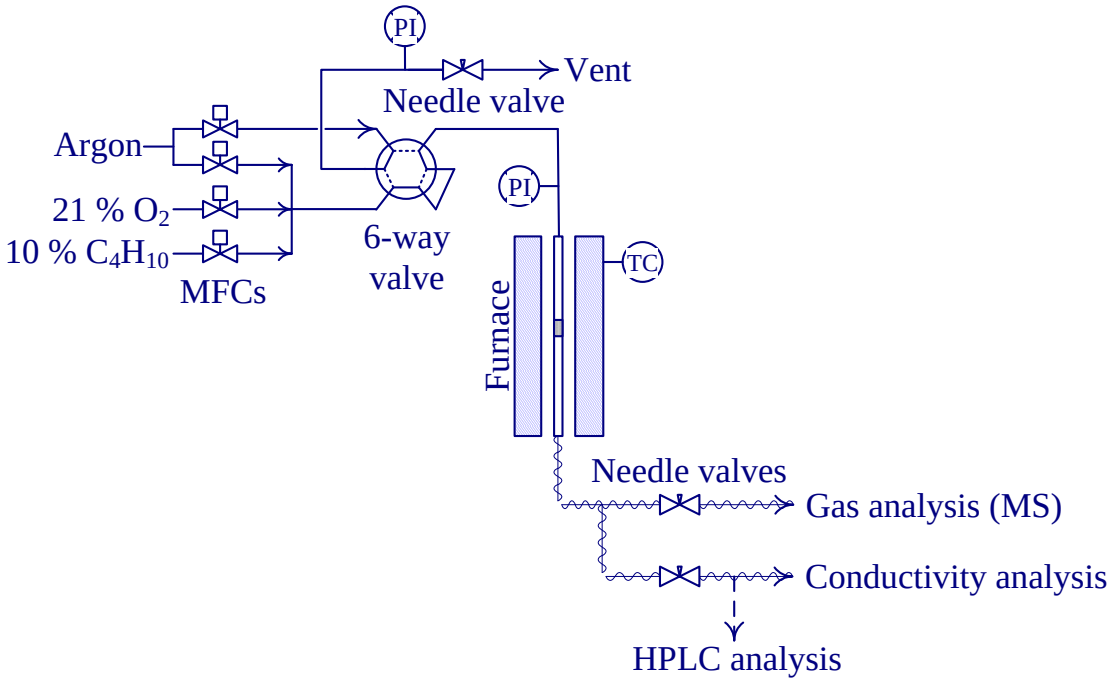

Figure 4-1: Micro-reactor setup at elevated pressure

A 7.7 mm ID quartz tube was used as a reactor for experiments at ambient pressure. For experiments at elevated pressure (up to 4.1 bar), the quartz tube was replaced by a stainless steel tube with the same internal diameter. The reactors were placed in an electrical furnace and the feed stream flow rates were controlled by Brooks mass flow controllers (from Hiden Analytical). In the metal reactor, the catalyst powder was placed on quartz wool while in the quartz reactor a

60 μm sintered quartz frit was installed in the center of reactor to support the catalyst bed. An electrically controlled six-way switching valve (Valco Instruments) was used to alternate between the reaction mixture and the inert purging stream at designated time intervals. In this way, the transient conditions existing in an industrial circulating fluidized bed reactor were simulated. The product gas stream from the reactor was sent to a liquid quench (not shown) and the maleic acid production was monitored in real time by measuring electrical conductivity of the acid solution. Liquid samples of the acid solution were taken periodically for offline HPLC analysis (Modular ProStar unit from Varian). A conductivity probe (Accumet 4-Cell from Fisher Scientific) and an HPLC column (MetaCarb 87H from Varian) were used for liquid acids analyses. A small portion (< 1 %) of the exit gas stream entered a mass spectrometer (Quadrupole type QIC-20 from Hiden Analytical) for online scanning of the reaction products such as CO, CO_2 and water as well as to detect un-reacted n-butane and oxygen from the feed.

To perform the redox experiments at a higher pressure, two needle valves (from Swagelok®) were installed at the two reactor exit streams. The purpose of these valves was to finely adjust the necessary back pressure inside the reactor and to ensure an atmospheric outlet pressure stream to the mass spectrometer and to provide a stable flow to the downstream acid gas absorber. To avoid a sudden drop in the reactor pressure when switching to an atmospheric stream, the vent line was maintained at a high pressure using a third needle valve.

4.4.2 Transient redox experiments

About 500 mg of DuPont's calcined and activated VPP catalyst with a particle size ranging between 106 and 180 μm and the BET surface area of 34.5 m^2/g was used for all experiments. For ambient pressure experiments, 24 runs were conducted covering six different feed compositions (O_2/C_4H_{10} = 0-13.6 molar ratio) and four different catalyst oxidation times (0.3-10 minute). The experimental conditions are summarized in Table 4.1. The base case temperature for the reaction was selected to be 380 °C, commonly practiced in industry. A wide range of catalyst oxidation times was selected to adequately cover the conditions from lab scale reactors (up to 10 minutes) to the industrial regeneration times (generally less than one minute). The

catalyst reduction time for all tests was selected to be 2 minutes. To achieve adequate n-butane conversion and gas residence time across the reactor, the total feed rate was kept at 40 ml/min (STP). To observe the effect of temperature, four additional experiments were conducted at 360 °C and 400 °C and at two feed compositions (O_2/C_4H_{10} = 0.3 and 1.1). These compositions were selected among the fuel rich conditions typically used in the industrial operation (O_2/C_4H_{10} > 1.0). The temperatures were also in the operating range of industrial maleic anhydride reactors. At the end of the experimental program, the catalyst deactivation was verified by repeating some of the tests at identical conditions (R tests in Table 4.1); the catalyst activity was satisfactorily stable during the entire period.

To observe the effect of pressure on the reaction kinetics and catalytic activity, six additional experiments were performed after the reactor pressure was increased to 4.1 bar. The experimental conditions of high pressure runs are presented in Table 4.2. The feed compositions were selected to cover the range of operation for fixed bed, fluidized bed and industrial CFB reactors. The fuel rich conditions: O_2/C_4H_{10} = 1.2, temperature = 380 °C and the catalyst oxidation time = 10 minutes was selected as the base case condition. This condition resulted in the highest maleic anhydride production rate reported in a previous study (Shekari and Patience, 2010).

Table 4.1: Transient experimental conditions: ambient pressure

Feed composition (vol. %)		**O_2/C_4H_{10}**	**Oxidation time (min)**	**Temperature (°C)**
n-Butane	**Oxygen**			
1.4	18.2	13.4	0.3, 1, 3, 10	380
3.6	13.4	3.7	0.3, 1, 3, 10	380
6.5	7.3	1.1	0.3, 1, 3, 10	360, 380(R), 400
7.7	4.7	0.6	0.3, 1, 3, 10	380
8.7	2.6	0.3	0.3, 1, 3, 10	360, 380(R), 400
9.9	0.0	0.0	0.3, 1, 3, 10	380

R: replicate run at 10 minute oxidation time

To observe the effect of temperature on catalytic activity at elevated pressure, an experiment was conducted at 400 °C (all other conditions remaining constant). Also, to observe the effect of catalyst oxidation time, an experiment was repeated at a catalyst oxidation time of 1 minute.

Table 4.2: Transient experimental conditions at 4.1 bar

Simulated conditions	**Feed composition (vol. %)**		**O_2/ C_4H_{10}**	**Oxidation time (min)**	**Temperature (°C)**
	n-Butane	**Oxygen**			
Fixed bed	1.4	18.2	13.4	10	380
Fluid bed	3.6	13.4	3.7	10	380
CFB	6.5	7.3	1.1	1, 10	380, 400

All redox experiments at ambient and elevated pressure were conducted according to a sequence of timed event. Initially, the catalyst was heated under an inert atmosphere (argon) up to the specified reaction temperature. Time zero corresponds to the first valve switch from argon to synthetic air (21 % O_2, balance Ar). The reactor was returned to an inert atmosphere at the second valve switch for as long as 10 minutes. At the third valve switch, argon was replaced by the reducing gas stream for two minutes. The reactor was then purged again with argon for 30 minutes (to ensure that all maleic anhydride was desorbed). The sequence was completed with a fifth valve switch that reintroduced synthetic air for the specified regeneration time. This sequence was repeated at least five times for each condition tested to ensure catalyst stability and to verify the repeatability of the results and acid analysis. All the catalyst samples were treated for 24 hours at 380 °C and under typical fixed bed reactor feed composition: 1.4 vol. % n-butane and 18.1 % oxygen in argon. The catalyst was previously activated under commercial conditions according to DuPont's calcination/activation protocol (Patience et al., 2007). Before each experiment, actual feed flow rates were measured while bypassing the feed stream to a bubble flow meter. The mass spectrometer and the conductivity probe as well as the HPLC instrument were regularly calibrated and cross checked using standard gas and liquid mixtures.

4.5 Results and discussion

4.5.1 Data analysis

Over several months of transient experiments, a wide range of transient activity data were collected for n-butane partial oxidation over VPP catalyst at different feed compositions, catalyst oxidation times, temperatures and pressures. These data included the real time concentrations of feeds and products and maleic acid conductivity trends as well as the total acid productions measured offline by HPLC. Several experiments were also conducted to calibrate the MS, the conductivity probe and HPLC. The MS calibration was done by measuring the fractional mass overlaps for each component and by considering the effect of product composition matrix and concentration effects on MS relative sensitivity toward each mass fraction. The transient acid concentration data recorded by the conductivity probe were integrated, cross checked and adjusted based on the total acid production values measured by HPLC for each redox cycle. In every case, the maleic acid values measured by HPLC were regarded as the reference to calculate the reaction parameters and the mass balances. To calculate the total values of feed consumption and product generation, the transient concentrations of all components were integrated over time for each reduction cycle and the results were averaged for several repetitive cycles. The average overall carbon balance was better than 99 % for all tests and the total average elemental balances for C, H, O and Ar was greater than 98 %. Reactor feed volumetric flow expansion due to generation of moles during reaction was assumed to be negligible. The maximum volume expansion based on the stoichiometry was 3 %.

4.5.2 Transient catalytic activity

4.5.2.1 n-Butane conversion

n-Butane conversion strongly depends on the reduction feed composition and catalyst oxidation time. At every oxygen to n-butane feed ratio (O_2/C_4H_{10}), n-butane conversion increases with increasing catalyst regeneration time: it approaches 45 % after 10 minutes in an oxidizing environment and a feed concentration of 1.4 vol. % n-butane and 18.2 vol. % O_2 in the reducing environment, Figure 4-2. There is a considerable drop in the n-butane conversion as oxygen

concentration in the feed decreases (lower O_2/C_4H_{10} ratio). The drop in conversion is more noticeable when the O_2/C_4H_{10} ratio in the feed is below 1.1 (fuel rich conditions). It is especially significant when switching from 2.6 vol. % oxygen in the feed to the pure redox mode (zero oxygen in the feed). In this case, the n-butane conversion drops from a range of 6-10 % to below 2 %. The drop in n-butane conversion may be related to the fact that the n-butane activation might proceed through reaction with surface lattice or adsorbed oxygen. The role of surface lattice or adsorbed oxygen in n-butane activation has already been reported to be significant (Wang and Barteau, 2003; Schuurman and Gleaves, 1997; Lorences et al., 2004; Gascón et al., 2006; Rodemerck et al., 1997a). As the oxygen partial pressure in the feed decreases, the available surface oxygen which is supplied through incorporation of gas phase oxygen into the catalyst surface layers is reduced. Therefore, the oxygen available for n-butane activation on the surface and hence n-butane conversion is decreased. These results may also show that the contribution of lattice oxygen in the surface reactions is very limited as it cannot compensate for the loss of surface lattice oxygen when the oxygen in the gas phase is limiting.

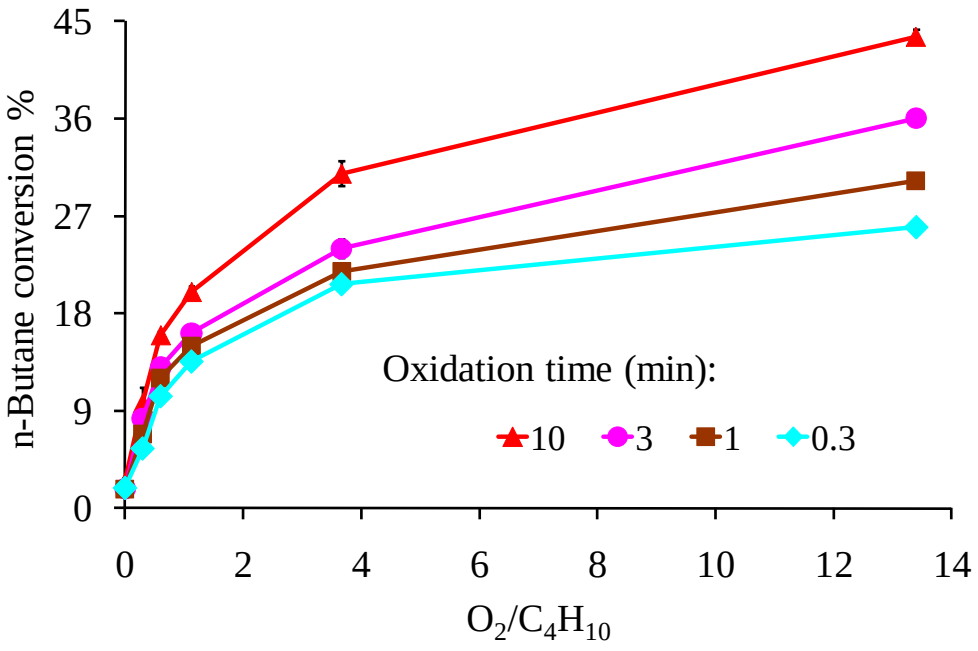

Figure 4-2: n-Butane conversion vs. feed composition

(T = 380 °C, Flowrate = 40 mL/min (STP), P = 1 bar, 500 mg calcined/activated VPP, confidence intervals at 95 %)

4.5.2.2 Maleic anhydride selectivity

Figure 4-3 shows that the MA selectivity is highly dependent on the reduction feed composition. As the n-butane concentration in the feed increases (lower O_2/C_4H_{10} ratio), MA selectivity drops from a steady value of about 65 % at oxidation time of 10 minutes to a value of 50 % at a catalyst oxidation time of 0.3 minute. Except for experiments with a 10 minute re-oxidation time, as the n-butane concentration in the feed increases or the oxygen concentration decreases, MA selectivity tends to decrease. However, the selectivity shows a steady behaviour when the catalyst oxidation time is 10 minutes. This indicates the important role of catalyst regeneration stage in a redox operation. When the catalyst is adequately oxidized, MA selectivity tends to stay constant even at the highest concentration of n-butane (9.9 vol. %) in the feed which corresponds to a pure redox mode with no oxygen. The selectivity drop by changes in the feed composition is more noticeable when the catalyst oxidation time is shorter. The drop in selectivity when the feed composition is changed from the most oxidizing (O_2/C_4H_{10} = 13.4) to the most reducing (O_2/C_4H_{10} = 0.0) conditions is around 6 % (from 63 to 59 %) when the catalyst oxidation time is 3 minutes compared to a drop of about 18 % (from 62 to 50 %) when the oxidation time is 0.3 minute. This drop in MA selectivity obviously shows the favourable effect of catalyst oxidation time on reaction yield especially at industrial range of catalyst regeneration times which could be in the order of less than a minute.

The data presented in Figure 4-3 show that when the feed composition approaches the oxygen rich conditions (O_2/C_4H_{10} = 13.4), the MA selectivity tends to converge to a narrow range of between 62-65 %. This indicates that the effect of catalyst oxidation time on selectivity might be less critical at more oxidizing feed conditions. Under such conditions (typically when $O_2/C_4H_{10} \geq$ 3.7), the improvement observed in the reaction yield by increasing the catalyst oxidation time could be mainly attributed to the increase in n-butane conversion (see Figure 4-2) rather than to the increase in MA selectivity.

In our previous study (Shekari and Patience, 2010), we showed that even when the reduction feed is highly oxidizing (O_2/C_4H_{10} = 13.4), the reaction yield could be still improved by increasing the catalyst oxidation time. For example, our data showed that at 18.2 vol. % oxygen in the feed,

extending the catalyst oxidation time from 0.3 to 10 minute resulted in considerable n-butane conversion improvement of about 68 % (from 26 to 44 %), see Figure 4-2. It is interesting to note that under these conditions, the MA selectivity increases only from 62 to 65 % (Figure 4-3). On the other hand, when operating under typical fuel rich conditions of a CFB reactor ($O_2/C_4H_{10} \leq$ 1.1), the effect of oxidation time becomes critically important in both improving the MA selectivity and n-butane conversion (Figures 4-2 and 4-3). Under such conditions, by extending the oxidation time from 0.3 to 10 minute, MA selectivity increases by about 16-30 % and n-butane conversion increases by about 32-55 % depending on the feed composition. These results show the critical importance of catalyst oxidation time on yield improvement especially when operating at fuel rich feed conditions. Also, it could be concluded that the reaction yield improvement only depends on the n-butane conversion while operating at highly oxidizing feed conditions.

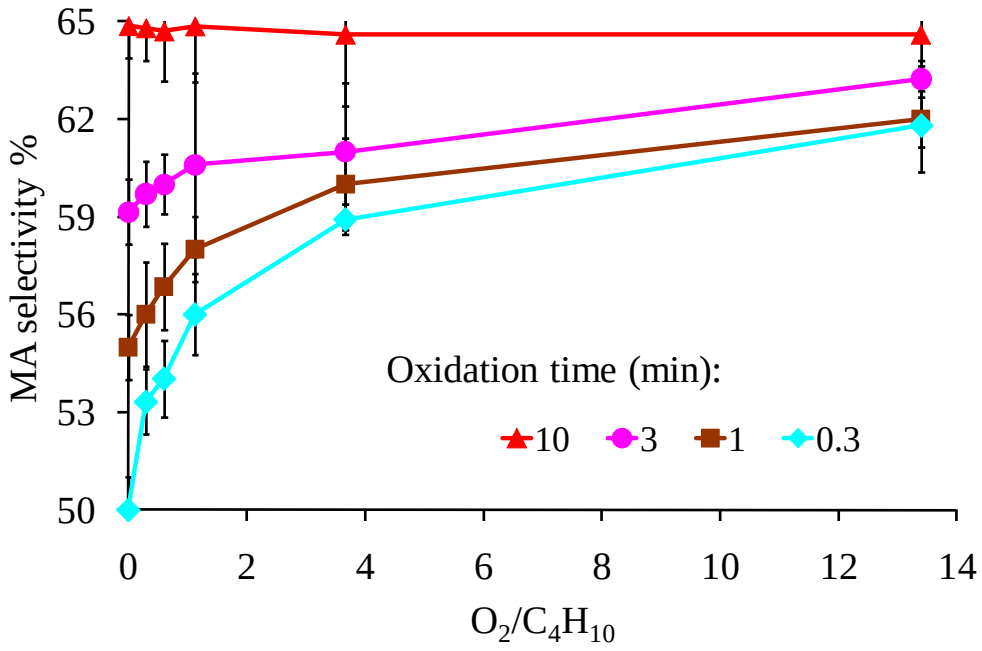

Figure 4-3: Maleic anhydride selectivity vs. feed composition

(T = 380 °C, Flowrate = 40 mL/min (STP), P = 1 bar, 500 mg calcined/activated VPP, confidence intervals at 95 %)

4.5.2.3 MA selectivity vs. n-butane conversion

Figure 4-4 demonstrates the maleic anhydride selectivity data versus the corresponding n-butane conversion over the whole range of feed composition. Irrespective of n-butane conversion values, the highest MA selectivity (about 65 %) is achievable only at longest catalyst oxidation time which is 10 minutes. At these conditions, MA selectivity is stable even at relatively high n-butane conversions (as high as about 45 %). However, as the catalyst oxidation time is reduced to 3 minutes or less, both MA selectivity and n-butane conversion decrease together. This observation is contrary to the commonly observed behaviour for steady state catalyst performance for n-butane partial oxidation in which the MA selectivity normally decreases as n-butane conversion increases. However, the observed behaviour could be attributed to typical transient redox operations in which the reduction and the oxidation stages are separated. According to the data presented in Figure 4-4, there is always a possibility to improve both n-butane conversion and MA selectivity even when the catalyst oxidation time is as low as 0.3 minute. This could be achieved by increasing the oxygen concentration in the feed. However, these data show that the maximum achievable n-butane conversion decreases as the catalyst oxidation time is decreased. The maximum n-butane conversion value is 36 % for 3 minute oxidation time while the maximum achievable conversion is 30 % for 1 minute oxidation time and it is 26 % when the catalyst oxidation time is 0.3 minute. Data in Figure 4-4 also show that at any value of n-butane conversion, the MA selectivity increases with catalyst oxidation time. The improvement in MA selectivity is less noticeable when the catalyst oxidation time is longer. This indicates that as the feed conditions become more reducing (left side of the graph); the effect of gas phase oxygen in increasing selectivity and conversion becomes more critical which results in a higher slope for the trend lines.

4.5.2.4 CO_x selectivity

Figures 4-5 and 4-6 demonstrate the CO and CO_2 selectivities during redox experiments. According to Figure 4-5, at a certain catalyst oxidation time, no significant correlation between CO selectivity with respect to feed composition was observed (CO selectivity ranges only between 18-21 %). However, the CO selectivity slightly decreased as the catalyst oxidation time dropped below 3 minutes. The general trend of the data shows that as the oxygen concentration in

the feed increases (higher O_2/C_4H_{10} ratio), the CO formation is also slightly decreased. These results might indicate that the surface adsorbed oxygen originating from gas/surface equilibriums could not be responsible for CO formation. However, the mechanism for CO generation might proceed through the surface lattice oxygen formed during catalyst regeneration step.

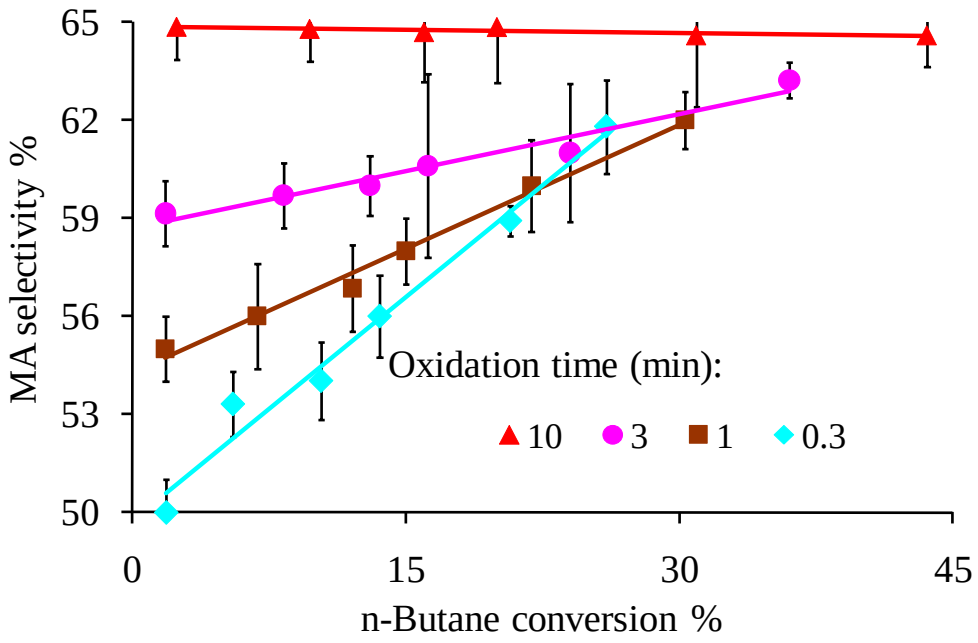

Figure 4-4: Maleic anhydride selectivity vs. n-butane conversion

(T = 380 °C, O_2/C_4H_{10} = 0-13.6, Flowrate = 40 mL/min (STP), P = 1 bar, 500 mg calcined/activated VPP, confidence intervals at 95 %)

Figure 4-6 shows that CO_2 selectivity is decreased as the feed composition becomes more reducing or the catalyst oxidation time is shorter. Contrary to the CO selectivity, the CO_2 selectivity shows a stronger dependency on feed composition. This could be due to the fact that different catalyst active sites are probably involved in the formation of CO and CO_2. The results show a decrease in CO_2 selectivity as the feed to the reactor becomes more reducing (O_2/C_4H_{10} toward 0.0). This decrease is even more significant when the catalyst oxidation time falls below 3 minutes. These data also show that CO_2 selectivity becomes a stronger function of catalyst oxidation time as the feed composition falls in the range of fuel rich compositions ($O_2/C_4H_{10} \geq$

1.1). However, as the feed composition is enriched with oxygen or the catalyst oxidation time is higher than 3 minutes, a steady value for CO_2 selectivity was observed. The similarity in selectivity behaviour for MA and CO_2 might indicate that the same catalyst active site is responsible for formation of these two species when the feed is reducing while the active site for CO formation might be of a different type. Moreover, the almost steady behaviour observed for MA, CO and CO_2 selectivity under oxidizing feed conditions ($O_2/C_4H_{10} \geq 3.7$) at whole range of catalyst oxidation times might indicate that any product yield improvement under oxidizing feed conditions could be attributed solely to the improvement in n-butane conversion. According to these results, n-butane activation might be considered as the critical step for yield improvement under highly oxidizing feed conditions.

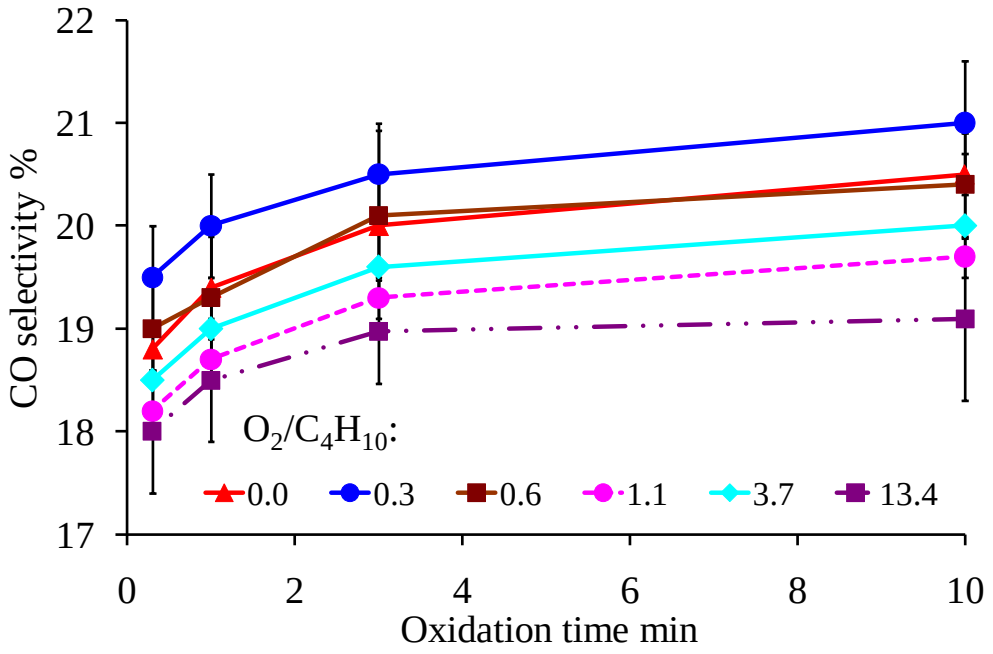

Figure 4-5: CO selectivity vs. catalyst oxidation time

(T = 380 °C, O_2/C_4H_{10} = 0-13.6, Flowrate = 40 mL/min (STP), P = 1 bar, 500 mg calcined/activated VPP, confidence intervals at 95 %)

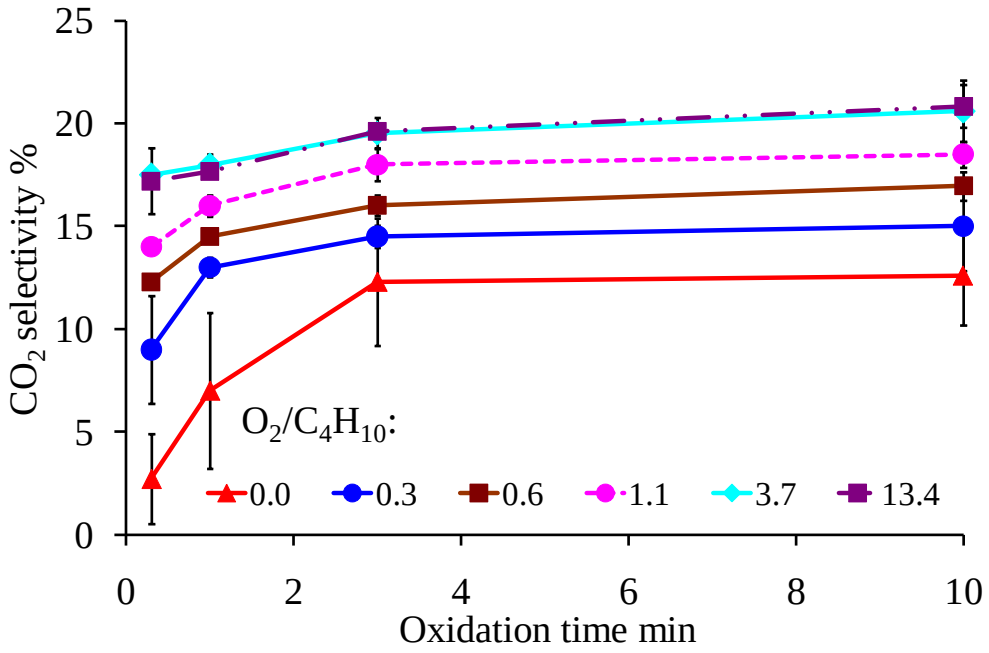

Figure 4-6: CO_2 selectivity vs. catalyst oxidation time

(T = 380 °C, O_2/C_4H_{10} = 0-13.6, Flowrate = 40 mL/min (STP), P = 1 bar, 500 mg calcined/activated VPP, confidence intervals at 95 %)

4.5.2.5 By-product selectivities vs. n-butane conversion

Figures 4-7 and 4-8 present the relationship between by-product CO and CO_2 selectivities and n-butane conversion. Figure 4-7 shows that there is an almost linear relationship between CO selectivity and n-butane conversion. Similar to MA selectivity, at any feed composition, longer catalyst oxidation time results in a higher CO selectivity. Moreover, the CO selectivity becomes less sensitive to n-butane conversion as feed composition becomes more oxidizing (moving to the right side of the graph). The data also show that at each level of catalyst oxidation, CO selectivity is declining with n-butane conversion. This behaviour is opposite to what we have seen for MA selectivity in Figure 4-4. In Figure 4-2, we showed that the n-butane conversion increases as the catalyst is exposed to a higher concentration of oxygen in the feed. Therefore, it could be concluded that oxidizing environment is not favourable for CO formation. However, these data show that even at highest oxygen concentration in the feed (O_2/C_4H_{10} = 13.4), there is a possibility to increase CO formation by increasing the catalyst oxidation time. Based on these

two different behaviours for MA and CO selectivities, we could conclude that there are at least two different types of oxygen or surface oxidized sites involved in the formation of these products. The formation of these active sites is affected by the presence of oxygen in the reduction feed or the duration of catalyst regeneration step.

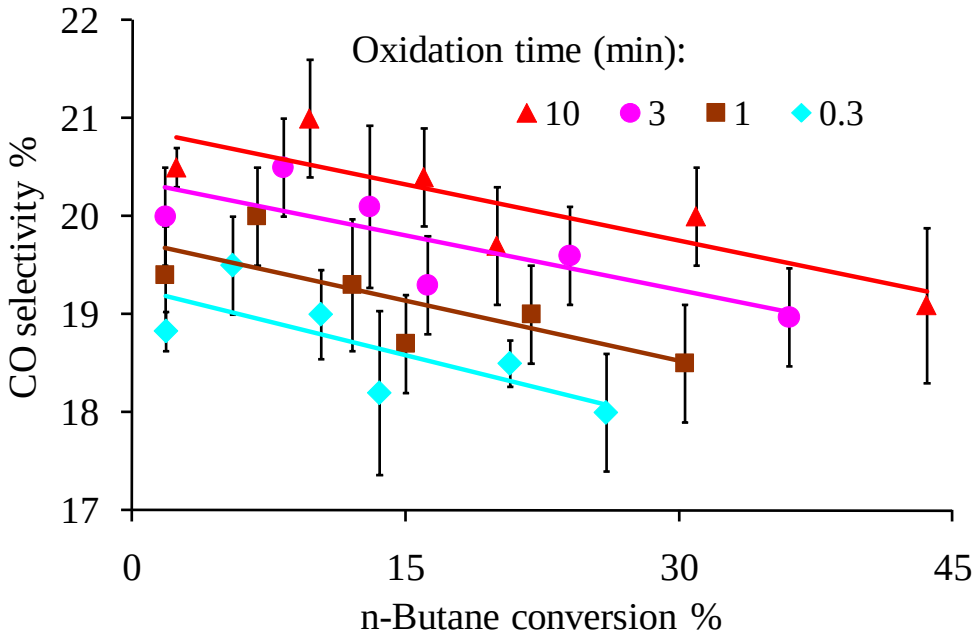

Figure 4-7: CO selectivity vs. n-butane conversion

(T = 380 °C, O_2/C_4H_{10} = 0-13.6, Flowrate = 40 mL/min (STP), P = 1 bar, 500 mg calcined/activated VPP, confidence intervals at 95 %)

Despite the CO selectivity trend observed in Figure 4-7, data presented in Figure 4-8 show that the CO_2 selectivity increases with n-butane conversion. These results are similar to those observed for MA selectivity versus n-butane conversion. Likewise MA selectivity, the CO_2 selectivity is more sensitive to n-butane conversion at lower n-butane conversion values corresponding to more reducing feed compositions. The CO_2 selectivity increases as the feed becomes more oxidizing (higher n-butane conversions). Also, the results show only a little improvement on CO_2 selectivity as long as the catalyst oxidation time is adequately high (> 1

min). Considering the similarity of these results, there should be similar surface oxygen species that are probably responsible for CO_2 and MA formation.

The opposite behaviour of CO_2 selectivity compared to CO selectivity versus n-butane conversion shows that the catalyst active sites responsible for formation of these two by-products might be different. As the gas phase oxygen is increased in the feed, the CO_2 selectivity increases. It appears that surface adsorbed oxygen resulted from gas phase oxygen interaction with surface during reaction has a stronger role in CO_2 formation. Moreover, as the catalyst oxidation time has generally little or no significant effect on CO_2 selectivity the catalyst surface lattice oxygen should have a minor role in CO_2 formation.

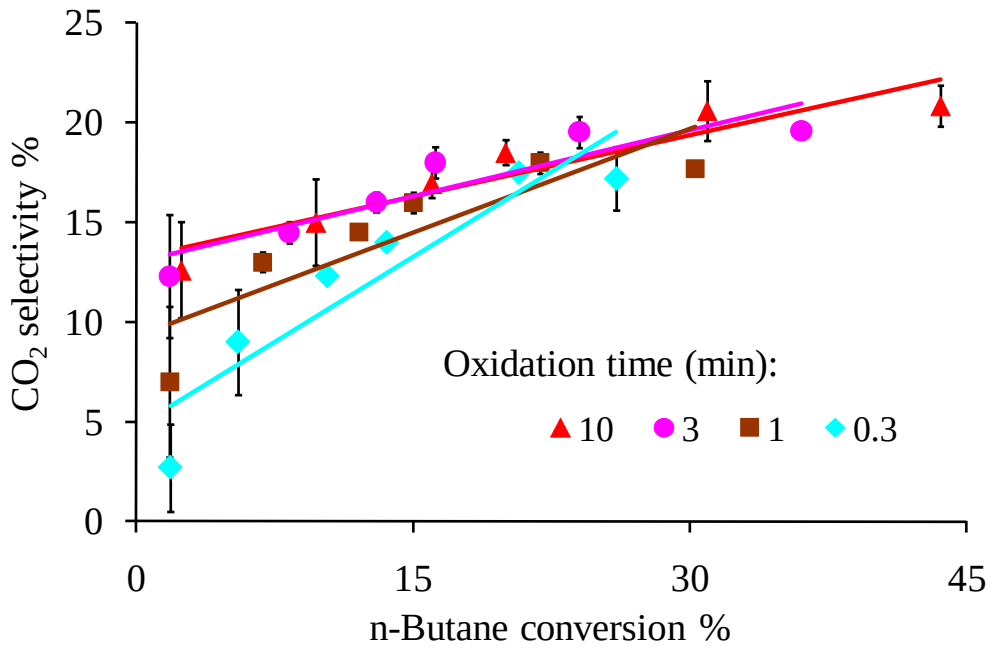

Figure 4-8: CO_2 selectivity vs. n-butane conversion

(T = 380 °C, O_2/C_4H_{10} = 0-13.6, Flowrate = 40 mL/min (STP), P = 1 bar, 500 mg calcined/activated VPP, confidence intervals at 95 %)

4.5.3 Effect of temperature

4.5.3.1 n-Butane conversion

Figure 4-9, shows the effect of temperature on n-butane conversion at feed compositions corresponding to fuel rich operation. Temperature causes an increase in n-butane conversion at both feed compositions. However, this effect is more pronounced when the feed composition is richer in oxygen. The reason could be attributed to the higher rate of catalyst surface oxidation while oxygen is more available in the feed. Therefore, more surface oxygen species would be available for n-butane activation and the conversion would increase to a higher extent. There is a relatively large jump in n-butane conversion when passing from 360 °C to 380 °C compared to when the temperature is increased from 380 °C to 400 °C at both feed compositions. This jump in n-butane conversion is larger when the feed has more oxygen (O_2/C_4H_{10} = 1.1). This suggests that irrespective of feed composition, the minimum activation temperature for n-butane over the VPP catalyst surface should lie somewhere between 360-380 °C. Also, availability of gas phase oxygen makes n-butane activation much easier at similar temperatures.

4.5.3.2 Maleic anhydride selectivity

Figure 4-10 demonstrates the effect of temperature on MA selectivity at two fuel rich feed compositions. Depending on the feed composition, MA selectivity shows a different behaviour versus reaction temperature. When there is relatively less concentration of oxygen in the feed (O_2/C_4H_{10} = 0.3), MA selectivity drops by increasing reaction temperature. This could be due to the fact that the catalyst oxidation state could not be compensated at higher temperatures where there is a high rate of catalyst reduction by n-butane and limited oxygen partial pressure in the gas phase for an effective catalyst re-oxidation. Moreover, gas phase combustion of n-butane at higher temperatures should also be taken into account. On the other hand, when there are relatively higher concentrations of oxygen in the feed, the MA selectivity tends to be constant and interestingly it is independent of the temperature. In this case, higher rate of catalyst reduction at 400 °C should be effectively compensated due to higher availability of oxygen in the gas phase. Similar to the results observed previously, in this case also any improvement in the MA yield could be attributed solely to the increase in n-butane conversion rather than MA

selectivity provided that adequate amounts of oxygen exists to compensate for excessive catalyst reduction at higher temperatures.

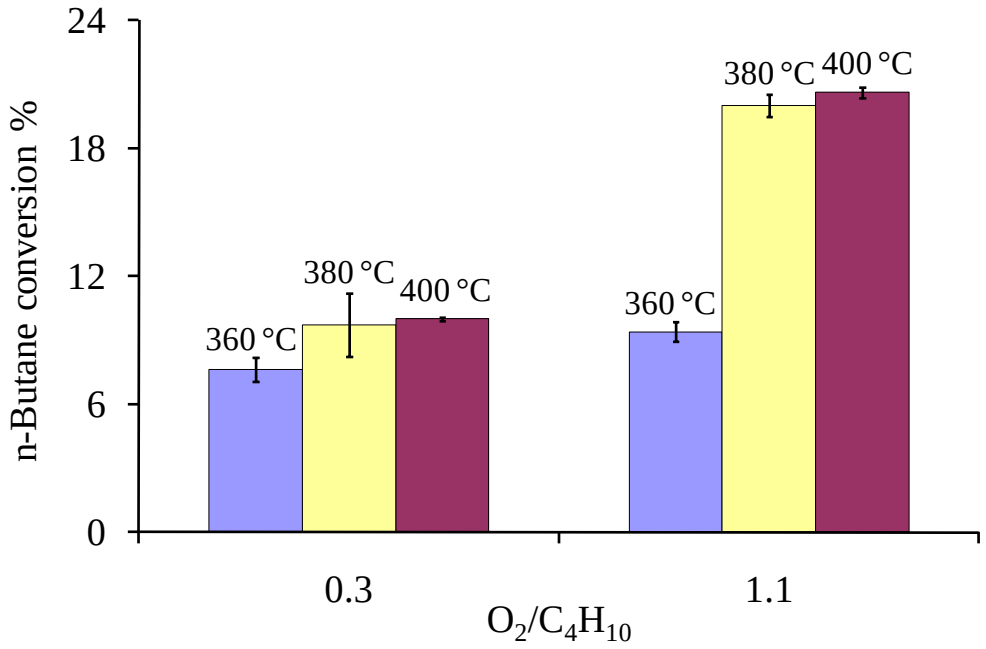

Figure 4-9: Effect of temperature on n-butane conversion

(Oxidation time = 10 minute, Flowrate = 40 mL/min (STP), P = 1 bar, 500 mg calcined/activated VPP, confidence intervals at 95 %)

4.5.4 Effect of pressure

To study the effect of pressure on catalytic activity, we performed selected redox experiments at a pressure of 4.1 bar, which is rarely reported in the literature (Lorences et al., 2006; Patience et al., 2007). Since the industrial reactors normally operate at above atmospheric pressures, the data presented here should be helpful in understanding the real behaviour of the VPP catalyst in industrial operations.

4.5.4.1 n-Butane/oxygen conversion

Our data show that the reactor pressure has a significant effect on n-butane conversion (Figure 4-11). The effect of pressure on n-butane conversion is even more noticeable when the oxygen concentration in the feed is increased. Actually, n-butane conversion increased by about 37 %

(from 20 to 27 %) for a feed containing 7.3 vol. % oxygen while this increase was about 54-56 % (from 31 to 48 % and from 44 to 68 %) when the feed oxygen concentrations were 13.4 and 18.2 vol. % respectively. The partial pressure of oxygen plays an important role in improvement of n-butane conversion. When the pressure is higher, the kinetics of catalyst oxidation moves forward to generate more surface oxygen species due to the higher oxygen partial pressure and therefore there is more oxygen species on the catalyst surface to react with n-butane, this causes n-butane to be more easily converted to intermediate surface species.

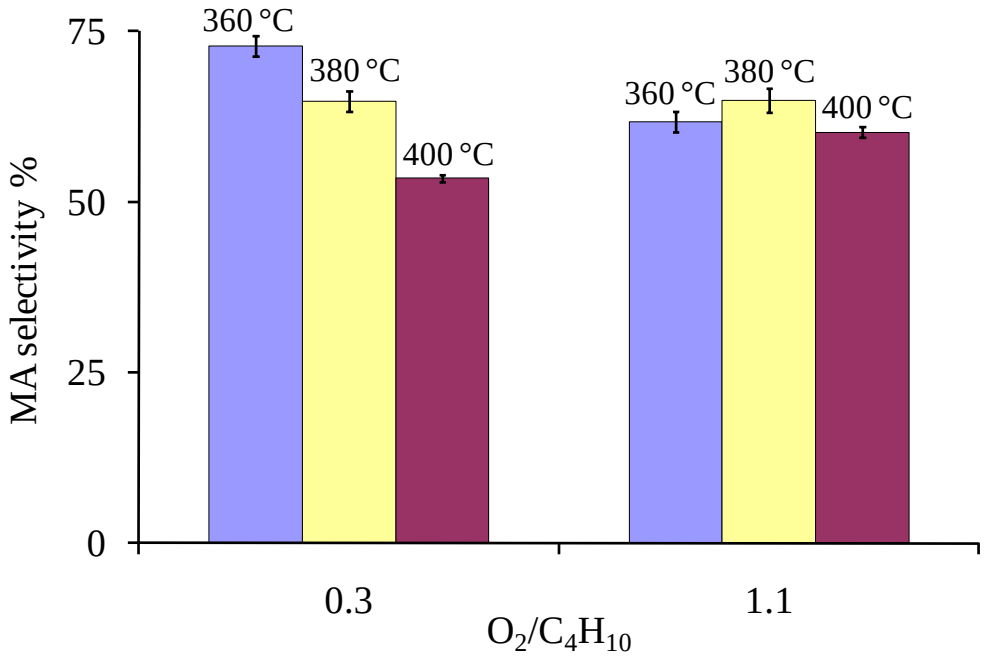

Figure 4-10: Effect of temperature on maleic anhydride selectivity

(Oxidation time = 10 minute, Flowrate = 40 mL/min (STP), P = 1 bar, 500 mg calcined/activated VPP, confidence intervals at 95 %)

Looking at similar data for oxygen conversion presented in Figure 4-12, we realize that the pressure also has a tremendous effect on oxygen conversion. Similar to the n-butane conversion, the oxygen conversion increased more when there was more oxygen available in the feed. In fact, oxygen conversion was increased by about 53 % (from 56 to 85 %) when the feed had 7.3 vol. % oxygen while this increase was about 97-98 % (from 26 to 51 % and from 12 to 23 %) when the

feed oxygen content was 13.4 and 18.2 vol. % respectively. From the data presented in Figures 4-11 and 4-12, it appears that when the oxygen level in the feed reaches a certain minimum concentration (at least 7.3 vol. %), the effect of pressure on n-butane or oxygen conversions remains constant irrespective of the feed composition. This could suggest that an equilibrium or saturation concentration point might exist for oxygen species on the catalyst surface that above which increasing the pressure does not further increase the catalytic activity.

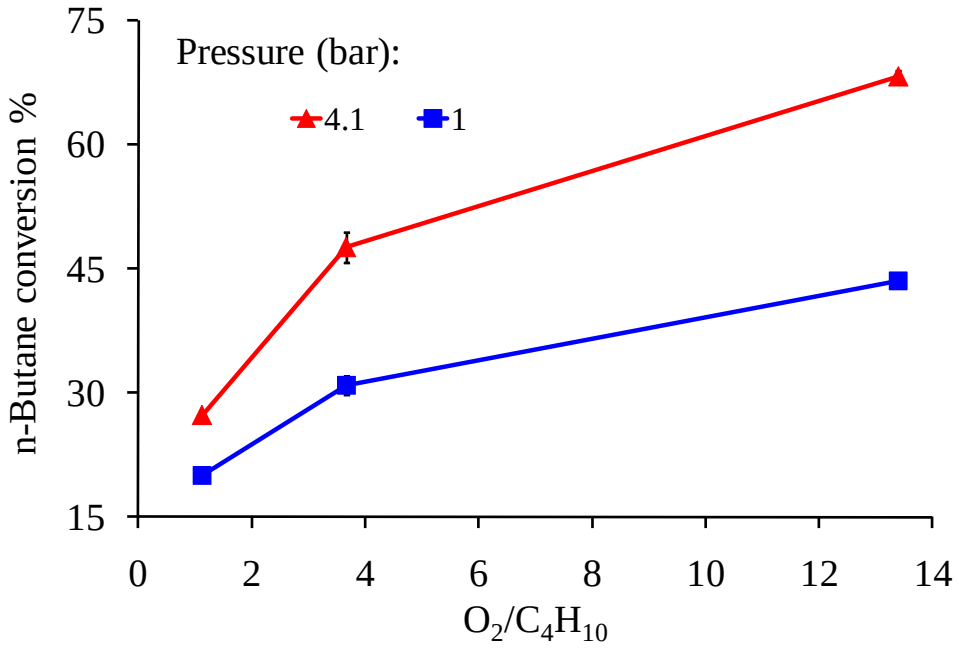

Figure 4-11: Effect of pressure on n-butane conversion

(T = 380 °C, Oxidation time = 10 minute, Flowrate = 40 mL/min (STP), 500 mg calcined/activated VPP, confidence intervals at 95 %)

4.5.4.2 Maleic anhydride selectivity and yield

Contrary to n-butane or oxygen conversion, the MA selectivity showed an opposite behaviour versus the reactor pressure. The MA selectivity dropped by an average value of about 18 % (from about 65 to 53 %) when the reactor pressure increased from atmospheric pressure to 4.1 bar, Figure 4-13. The drop in MA selectivity could be attributed to higher concentrations of non-

selective surface oxygen species as a result of increased oxygen partial pressure. In other words, when the pressure increases, the surface population of oxygen species responsible for n-butane activation increases but these species are not necessarily responsible for a selective MA formation. Other reasons for MA selectivity drop could be the promotion of gas phase combustion of n-butane which results in a lower maleic anhydride concentration at the reactor outlet. Generally speaking, despite the drop in MA selectivity with increased pressure, as the pressure increases, the increase in n-butane conversion (37-56 %) results in an overall increase in MA productivity and yield. Actually, the MA yield was increased from 10 to 30 % when O_2/C_4H_{10} ratio in the feed changed from 1.1 to 13.4 and the pressure increased from ambient to 4.1 bar, Figure 4-14.

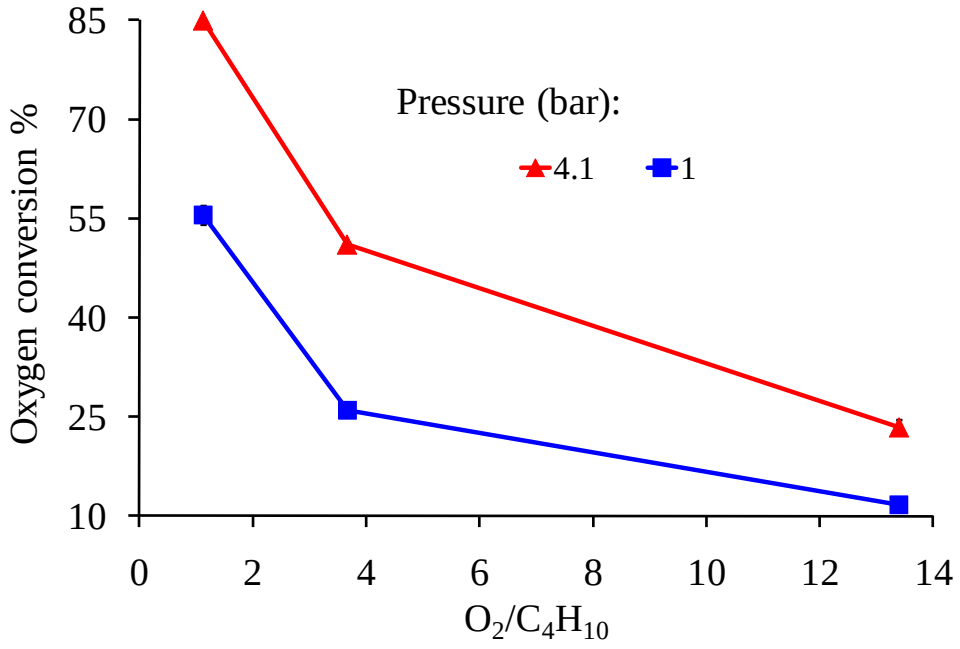

Figure 4-12: Effect of pressure on oxygen conversion

(T = 380 °C, Oxidation time = 10 minute, Flowrate = 40 mL/min (STP), 500 mg calcined/activated VPP, confidence intervals at 95 %)

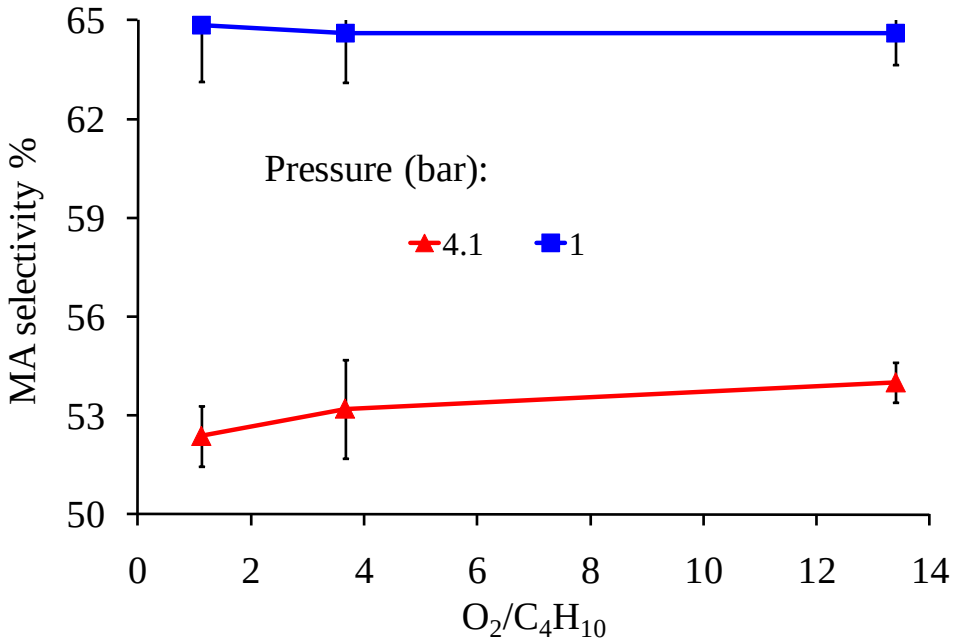

Figure 4-13: Effect of pressure on maleic anhydride selectivity

(T = 380 °C, Oxidation time = 10 minute, Flowrate = 40 mL/min (STP), 500 mg calcined/activated VPP, confidence intervals at 95 %)

4.5.4.3 Effect of temperature at higher pressure

In an effort to maximize the catalytic activity, we studied the combined effect of pressure and temperature on the reactor performance. Our data showed that as the pressure increased, the effect of temperature on n-butane conversion became more pronounced (Figure 4-15). At ambient pressure, a temperature increase from 380 to 400 °C only caused a 3 % increase in n-butane conversion (from 20 to 20.6 %), while the same change in temperature at higher pressure of 4.1 bar caused about 21 % increase in n-butane conversion (from 27 to 33 %). These data show that there should be a certain combination of operating temperature and pressure at which the catalyst activity could be enhanced. For this purpose, we should also consider the combined effect of temperature and pressure on MA selectivity.

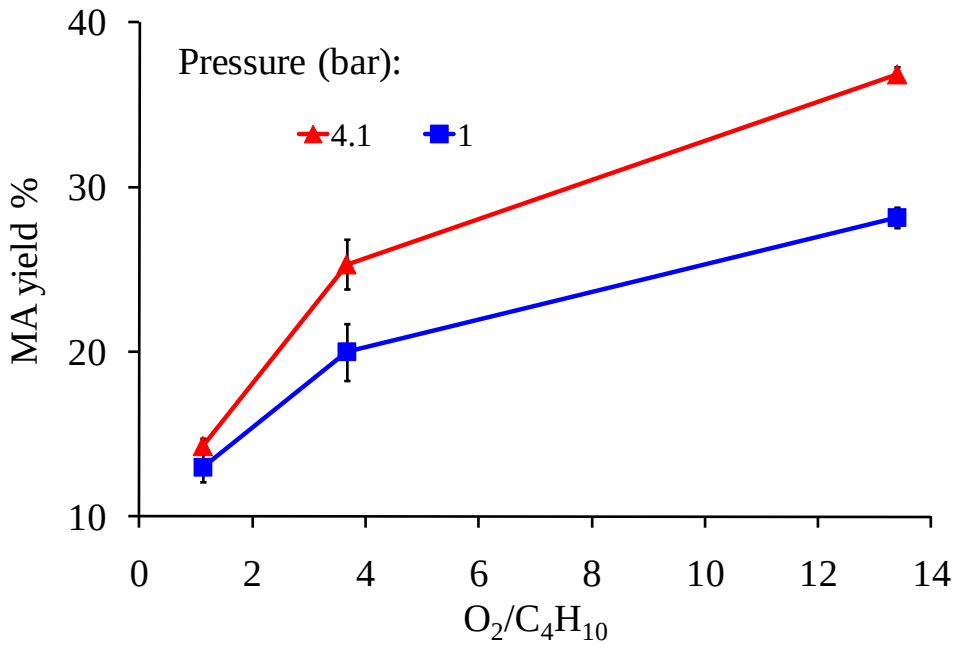

Figure 4-14: Effect of pressure on maleic anhydride yield

(T = 380 °C, Oxidation time = 10 minute, Flowrate = 40 mL/min (STP), 500 mg calcined/activated VPP, confidence intervals at 95 %)

Irrespective of the operating pressure, the maleic anhydride selectivity decreased by only about 6-7 % as the temperature increased from 380 to 400 °C. Accordingly, at atmospheric pressure the MA yield slightly decreased by about 5 % (from 13 to 12.4 %) when the temperature increased by 20 °C. While surprisingly, the MA yield showed an increase of about 13 % (from 14.3 to 16.1 %) by the same increase in temperature but at a pressure of 4.1 bar. These data show that the increase in pressure not only enhances the n-butane conversion, but it also causes the MA yield to increase at a higher temperature contrary to the yield decrease observed for ambient pressure. Therefore, to maximize the catalytic performance, it would be preferable to work at a higher pressure while keeping the temperature limited to some optimized values to avoid excessive MA selectivity loss.

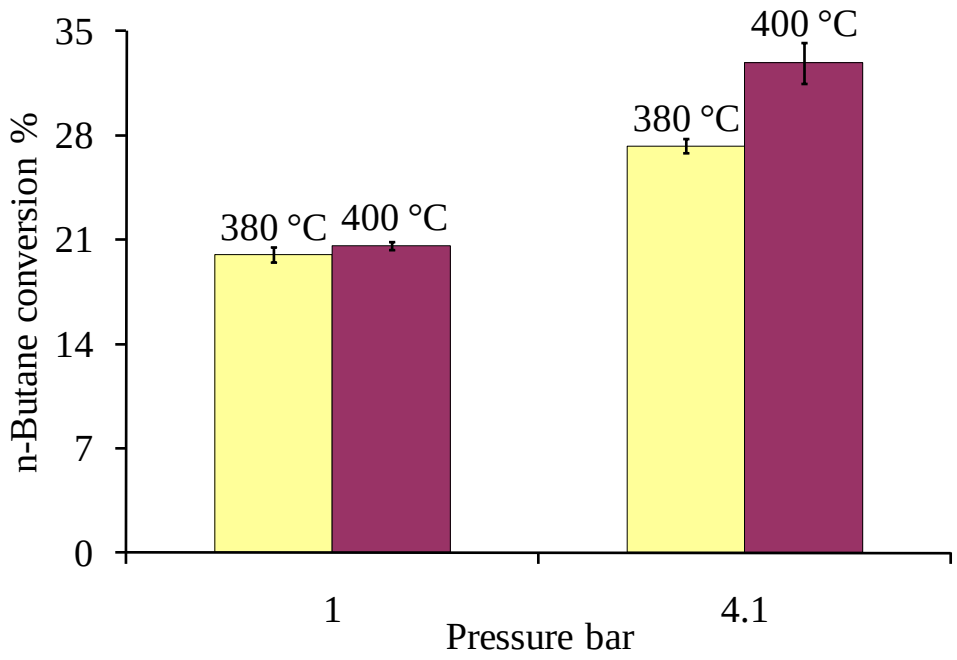

Figure 4-15: Effect of temperature/pressure on n-butane conversion

(O_2/C_4H_{10} = 1.1, Oxidation time = 10 minute, Flowrate = 40 mL/min (STP), 500 mg calcined/activated VPP, confidence intervals at 95 %)

4.6 Conclusions

The transient redox data showed that there is a strong relationship between VPP catalyst reactivity with reduction feed composition and catalyst oxidation time as well as the pressure and the temperature of the reaction. The MA yield could be improved by increasing the catalyst oxidation time and also by feeding more oxygen in the feed. Both temperature and pressure improved reactor performance. These effects were more important when the concentration of oxygen in the feed was higher. A strong dependency of maleic anhydride selectivity was observed on feed composition at relatively short catalyst oxidation times (< 1 min) corresponding to operations in industrial reactors.

According to the different behaviour observed for CO selectivity versus n-butane conversion in comparison with other by-products, probably a different oxygen species are involved in the CO formation with respect to the rest of products including MA. The CO formation probably

proceeds through the surface lattice oxygen species generated during the catalyst regeneration, while surface adsorbed oxygen species available during reaction might have a stronger role in CO_2 and MA formation.

Generally, while the concentration ratio of the feed to the reactor is oxidizing ($O_2/C_4H_{10} \geq 3.7$) any improvement in the reaction yield could be attributed to the increase in n-butane conversion with catalyst oxidation time. Surface adsorbed or lattice oxygen species were suggested as the main source for n-butane activation. However, when operating under fuel rich feed conditions and short oxidation times, both n-butane conversion and MA selectivity contribute to MA yield improvement. Under these conditions, the effect of catalyst oxidation time on catalytic performance is critical. The contribution of catalyst's sub-surface lattice oxygen was believed to be very limited under fuel rich feed conditions. Data show that at fuel rich conditions, catalyst over-reduction cannot be effectively compensated even after excessive catalyst regeneration and the presence of gas phase oxygen is critical to maintain a high catalytic activity.

Both n-butane and oxygen conversions increased by increasing reactor pressure. The MA selectivity dropped, but the increase in n-butane conversion resulted in an overall MA yield improvement of up to 30 %. Data show that there should be a certain combination of operating temperature and pressure at which the catalyst activity could be enhanced. The maximum catalytic performance should be achievable at a higher pressure. However, the negative effect of temperature on MA selectivity has to be minimized.

4.7 Acknowledgements

The financial support of the Natural Sciences and Engineering Research Council of Canada (NSERC), Ministère du Développement Economique, de l'Innovation et de l'Exportation (MDEIE) of Quebec and the Canadian Foundation for Innovation (CFI) is greatly appreciated. We wish to thank also the DuPont Company for providing the catalyst samples for this research.

4.8 References

Aït-Lachgar K., Abon M. and Volta J. C., "Selective Oxidation of n-Butane to Maleic Anhydride on Vanadyl Pyrophosphate, I. Influence of Oxidation Pretreatments on the Catalytic Performances", Journal of Catalysis, 1997, 171, 383-390.

Aït-Lachgar K., Tuel A., Brun M., Herrmann J. M., Krafft J. M., Martin J. R., Volta J. C. and Abon M., "Selective Oxidation of n-Butane to Maleic Anhydride on Vanadyl Pyrophosphate, II. Characterization of the Oxygen-Treated Catalyst by Electrical Conductivity, Raman, XPS, and NMR Spectroscopic Techniques", Journal of Catalysis, 1998, 177, 224-230.

Ballarini N., Cavani F., Cortelli C., Ligi S., Pierelli F., Trifirò F., Fumagalli C., Mazzoni G. and Monti T., "VPO catalyst for n-butane oxidation to maleic anhydride: A goal achieved, or a still open challenge?", Topics in Catalysis, 2006a, 38, 1-3, 147-156.

Ballarini N., Cavani F., Cortelli C., Ricotta M., Rodeghiero F., Trifirò F., Fumagalli C. and Mazzoni G., "Non-steady catalytic performance as a tool for the identification of the active surface in VPO, catalyst for n-butane oxidation to maleic anhydride", Catalysis Today, 2006b, 117, 174-179.

Ballarini N., Cavani F., Cortelli C., Gasparini F., Mignani A., Pierelli F., Trifirò F., Fumagalli C. and Mazzoni G., "The contribution of homogeneous and non-oxidative side reactions in the performance of vanadyl pyrophosphate, catalyst for the oxidation of n-butane to maleic anhydride, under hydrocarbon-rich conditions", Catalysis Today, 2005, 99, 115-122.

Cavani F., Luciani S., Esposti E. D., Cortelli C. and Leanza R., "Surface Dynamics of AVanadyl Pyrophosphate Catalyst for n-Butane Oxidation to Maleic Anhydride: An In Situ Raman and Reactivity Study of the Effect of the P/V Atomic Ratio", Chem. Eur. J., 2010a, 16, 1646-1655.

Cavani F., De Santi D., Luciani S., Löfberg A., Bordes-Richard E., Cortelli C. and Leanza R., "Transient reactivity of vanadyl pyrophosphate, the catalyst for n-butane oxidation to maleic anhydride, in response to in-situ treatments", Applied Catalysis A: General, 2010b, 376, 66-75.

Cavani F., Ligi S., Monti T., Pierelli F., Trifirò F., Albonetti S. and Mazzoni G., "Relationship between structural/surface characteristics and reactivity in n-butane oxidation to maleic anhydride The role of V^{3+} species", Catalysis Today, 2000, 61, 203-210.

Centi G. and Trifirò F., "Some aspects of the control of selectivity in catalytic oxidation on mixed oxides: a review", Applied Catalysis, 1984, 12, 1, 1-21.

Chen B. and Munson E. J., "Investigation of the Mechanism of n-Butane Oxidation on Vanadium Phosphorus Oxide Catalysts: Evidence from Isotopic Labeling Studies", J. Am. Chem. Soc., 2002, 124, 8, 1638-1652.

Chen D., Bjorgum E., Christensen K. O., Holmen A. and Lodeng R., "Characterization of Catalysts under Working Conditions with an Oscillating Microbalance Reactor", Advances in Catalysis, 2007, 51, 351-382.

Contractor R. M., Garnett D. I., Horowitz H. S., Bergna H. E., Patience G. S., Schwartz J. T. and Sisler G. M., "A New Commercial Scale Process for n-Butane Oxidation to Maleic Anhydride Using a Circulating Fluidized Bed Reactor", in "New Developments in Selective Oxidation II", V. Cortés-Corberan and S. Vic Bellon Eds., Elsevier, Amsterdam, 1994, 233-242.

Dummer N. F., Weng W., Kiely C., Carley A. F., Bartley J. K., Kiely C. J. and Hutchings G. J., "Structural evolution and catalytic performance of DuPont V-P-O/SiO_2 materials designed for fluidized bed applications", Applied Catalysis A: General, 2010, 376, 47-55.

Emig G., Uihlein K. and Hacker C.-J., “Separation of Catalyst Oxidation and Reduction - An Alternative to the Conventional Oxidation of n-Butane to Maleic Anhydride?” in “New Developments in Selective Oxidation II”, V. Cortés-Corberan and S. Vic Bellon Eds., Elsevier, Amsterdam, 1994, 243-251.

Fernández J. R., Vega A. and Díez F. V., “Partial oxidation of n-butane to maleic anhydride over VPO in a simulated circulating fluidized bed reactor”, Applied Catalysis A: General, 2010, 376, 76-82.

Gascón J., Valenciano R., Téllez C., Herguido J. and Menéndez M., “A generalized kinetic model for the partial oxidation of n-butane to maleic anhydride under aerobic and anaerobic conditions”, Chemical Engineering Science, 2006, 61, 6385-6394.

Hävecker M., Mayer R. W., Knop-Gericke A., Bluhm H., Kleimenov E., Liskowski A., Su D., Follath R., Requejo F. G., Ogletree D. F., Salmeron M., Lopez-Sanchez J. A., Bartley J. K., Hutchings G. J. and Schlägl R., “In Situ Investigation of the Nature of the Active Surface of a Vanadyl Pyrophosphate Catalyst during n-Butane Oxidation to Maleic Anhydride”, J. Phys. Chem. B, 2003, 107, 4587-4596.

Hävecker M., Knop-Gericke A., Bluhm H., Kleimenov E., Mayer R. W., Fait M. and Schlägl R., “Dynamic surface behaviour of VPO catalysts under reactive and non-reactive gas compositions: an in situ XAS study”, Applied Surface Science, 2004, 230, 272-282.

Huang X.-F., Chen B.-H., Liu B.-J., Silveston P. L. and Li C.-Y., “Re-oxidation kinetics of a VPO catalyst”, Catalysis Today, 2002a, 74, 121-130.

Huang X.-F., Li C.-Y., Chen B.-H. and Silveston P. L., “Transient Kinetics of n-Butane Oxidation to Maleic Anhydride over a VPO Catalyst”, AIChE Journal, 2002b, 48, 4, 846-855.

Huang X.-F., Li C.-Y., Chen B.-H., Qiao C.-Z. and Yang D.-H., "Investigation of the Unsteady-State Oxidation of n-Butane to Maleic Anhydride in Fixed-Bed Reactors", Ind. Eng. Chem. Res., 2001, 40, 768-773.

Hutchenson K. W., La Marca C., Patience G. S., Laviolette J.-P. and Bockrath R. E., "Parametric study of n-butane oxidation in a circulating fluidized bed reactor", Applied Catalysis A: General, 2010, 376, 91-103.

Hutchings G. J., "Effect of promoters and reactant concentration on the selective oxidation of n-butane to maleic anhydride using vanadium phosphorus oxide catalysts", Applied Catalysis, 1991, 72, 1, 1-32.

Hutchings G. J., "Vanadium phosphate: a new look at the active components of catalysts for the oxidation of butane to maleic anhydride", J. Mater. Chem., 2004, 14, 3385-3395.

Kamiya Y., Nishikawa E., Okuhara T. and Hattori T., "Catalytic property of vanadyl pyrophosphates for selective oxidation of n-butane at high n-butane concentrations", Applied Catalysis A: General, 2001, 206, 103-112.

Kleimenov E., Bluhm H., Hävecker M., Knop-Gericke A., Pestryakov A., Teschner D., Lopez-Sanchez J. A., Bartley J. K., Hutchings G. J. and Schlögl R., "XPS investigations of VPO catalysts under reaction conditions", Surface Science, 2005, 575, 181-188.

Kubias B., Rodemerck U., Zanthoff H.-W. and Meisel M., "The reaction network of the selective oxidation of n-butane on $(VO)_2P_2O_7$ catalysts: Nature of oxygen containing intermediates", Catalysis Today, 1996, 32, 243-253.

Liang R. Z., Li Y. X., Li C. Y., Chen B. H. and Hu S. Y., "On-line mass spectroscopic transient measurement of vanadium-phosphorous oxide re-oxidation", Chinese Journal of Catalysis, 2003, 24, 11, 881-884.

Lorences M. J., Patience G. S., Cenni R., Díez F. and Coca J., "VPO transient lattice oxygen contribution", Catalysis Today, 2006, 112, 45-48.

Lorences M. J., Patience G. S., Díez F. V. and Coca J., "Butane Oxidation to Maleic Anhydride: Kinetic Modeling and Byproducts", Ind. Eng. Chem. Res., 2003, 42, 6730-6742.

Lorences M. J., Patience G. S., Díez F. V. and Coca J., "Transient n-butane partial oxidation kinetics over VPO", Applied Catalysis A: General, 2004, 263, 193-202.

Mallada R., Sajip S., Kiely C. J., Menéndez M. and Santamaría J., "Influence of the Reaction Atmosphere on the Characteristics and Performance of VPO Catalysts", Journal of Catalysis, 2000, 196, 1-7.

Mills P. L., Randall H. T. and McCracken J. S., "Redox kinetics of $VOPO_4$ with butane and oxygen using the TAP reactor system", Chemical Engineering Science, 1999, 54, 3709-3721.

Mota S., Abon M., Volta J. C. and Dalmon J. A., "Selective Oxidation of n-Butane on a V-P-O Catalyst: Study under Fuel-Rich Conditions", Journal of Catalysis, 2000, 193, 308-318.

Patience G. S. and Bockrath R. E., "Butane oxidation process development in a circulating fluidized bed", Applied Catalysis A: General, 2010, 376, 4-12.

Patience G. S. and Lorences M. J., “VPO Transient Oxidation Kinetics”, Int. J. Chem. Reactor Eng., 2006, 4, Article A22, 1-16.

Patience G. S., Bockrath R. E., Sullivan J. D. and Horowitz H. S., “Pressure Calcination of VPO Catalyst”, Ind. Eng. Chem. Res., 2007, 46, 4374-4381.

Pérez-Moreno L., Irusta S., Soler J., Herguido J. and Menéndez M., “Effect of the use in circulating fluidized bed on the performance of a VPO catalyst: Characterization and transient studies”, Chemical Engineering Journal, 2009, 147, 330-335.

Rodemerck U., Kubias B., Zanthoff H.-W. and Baerns M., “The reaction mechanism of the selective oxidation of butane on $(VO)_2P_2O_7$ catalysts: The role of oxygen in the reaction chain to maleic anhydride”, Applied Catalysis A: General, 1997a, 153, 203-216.

Rodemerck U., Kubias B., Zanthoff H.-W., Wolf G.-U. and Baerns M., “The reaction mechanism of the selective oxidation of butane on $(VO)_2P_2O_7$ catalysts: The influence of the valence state of vanadium”, Applied Catalysis A: General, 1997b, 153, 217-231.

Schuurman Y. and Gleaves J. T., “Activation of Vanadium Phosphorus Oxide Catalysts for Alkane Oxidation. The Influence of the Oxidation State on Catalyst Selectivity”, Ind. Eng. Chem. Res., 1994, 33, 2935-2941.

Schuurman Y. and Gleaves J. T., “A comparison of steady-state and unsteady-state reaction kinetics of n-butane oxidation over VPO catalysts using a TAP-2 reactor system”, Catalysis Today, 1997, 33, 25-37.

Shekari A. and Patience G. S., “Maleic anhydride yield during cyclic n-butane/oxygen operation”, Catalysis Today, 2010, 157, 334-338.

Shekari A., Patience G. S. and Bockrath R. E., “Effect of feed nozzle configuration on n-butane to maleic anhydride yield: From lab scale to commercial”, Applied Catalysis A: General, 2010, 376, 83-90.

Song N., Xuan Z., Bartley J. K., Taylor S. H., Chadwick D. and Hutchings G. J., “Oxidation of butane to maleic anhydride using vanadium phosphate catalysts: comparison of operation in aerobic and anaerobic conditions using a gas-gas periodic flow reactor”, Catalysis Letters, 2006, 106, 3-4, 127-131.

Taufiq-Yap Y. H., Goh C. K., Hutchings G. J., Dummer N. and Bartley J., “Dependence of n-Butane Activation on Active Site of Vanadium Phosphate Catalysts”, Catal. Lett., 2009, 130, 327-334.

Volta J.-C., “Vanadium phosphorus oxides, a reference catalyst for mild oxidation of light alkanes: a review”, C. R. Acad. Sci. Paris, Série IIc, Chimie / Chemistry, 2000, 3, 717-723.

Wang D., Kung H. H. and Barteau M. A., “Identification of vanadium species involved in sequential redox operation of VPO catalysts”, Applied Catalysis A: General, 2000, 201, 203-213.

Wang D. and Barteau M. A., “Oxidation kinetics of partially reduced vanadyl pyrophosphate catalyst”, Applied Catalysis A: General, 2002, 223, 205-214.

Wang D. and Barteau M. A., “Kinetics of Butane Oxidation by a Vanadyl Pyrophosphate Catalyst”, Journal of Catalysis, 2001, 197, 17-25.

Wang D. and Barteau M. A., “Differentiation of active oxygen species for butane oxidation on vanadyl pyrophosphate”, Catalysis Letters, 2003, 90, 1-2, 7-11.

Xue Z.-Y. and Schrader G. L., “Transient FTIR Studies of the Reaction Pathway for n-Butane Selective Oxidiation over Vanadyl Pyrophosphate”, Journal of Catalysis, 1999, 184, 87-104.

Zhang S. H. and Liu H. C., “Relationship between the Structures of Metal Oxide Catalysts and Their Properties in Selective Oxidation of Light Alkanes”, Acta Physico-Chimica Sinica, 2010, 26, 4, 895-907.

CHAPTER 5 TRANSIENT KINETICS OF N-BUTANE PARTIAL OXIDATION AT ELEVATED PRESSURE

This article was submitted to The Canadian Journal of Chemical Engineering on July 2011. The article was reviewed on August 2011.

5.1 Presentation of the article

In this article, the transient kinetics of n-butane partial oxidation over VPP catalyst was studied. The proposed kinetic model was applicable to a wide range of feed compositions as well as the higher reactor pressure. The effect of pressure on VPP transient kinetics was rarely considered in the literature. Therefore, this could be the main contribution of this article. Moreover, the wide range of model validity made it applicable to fixed bed, fluidized bed and CFB reactor operations.

Higher pressure considerably improved the VPP catalytic activity and MA yield. The model predictions showed that pressure promoted the catalyst oxidation state at oxidizing feed conditions. However, under fuel rich conditions, the catalyst was more reduced as the pressure increased. These observations together with reaction rate and activation energy data provided a better understanding of VPP catalyst redox behaviour at higher pressure.

Transient kinetics of n-butane partial oxidation at elevated pressure

Ali Shekari, Gregory S. Patience

5.2 Abstract

A transient Mars-van Krevelen type kinetic model was developed for n-butane partial oxidation over vanadyl pyrophosphate (VPP) catalyst. The model validity was verified over a relatively wide range of redox feed compositions as well as higher reactor pressure (410 kPa). Oxygen and n-butane conversion increased with higher pressure while maleic anhydride (MA) selectivity decreased by as much as 20 %. However, the overall MA yield was enhanced by up to 30 %. High pressure maintains the catalyst in a higher oxidation state (as long as there is sufficient oxygen in the gas phase) and as a consequence, the catalytic activity is improved together with the yield. High pressure also affects the redox reaction rates and activation energies.

Keywords: n-butane, maleic anhydride, vanadyl pyrophosphate, transient, kinetic model, pressure, activation energy, oxidation state

5.3 Introduction

Partial oxidation of n-butane to maleic anhydride over vanadyl pyrophosphate (VPP) catalyst has been widely studied for over four decades (Ballarini et al., 2006). Despite the attempts to elucidate the ambiguous nature of the VPP catalyst during reaction, the actual mechanism and the kinetics of this industrially significant reaction is still under investigation. Insufficient knowledge on the dynamic behaviour of the catalyst active phases and the variation of catalyst oxidation state during reaction as well as the role of surface oxygen species have been among the major impediments to the kinetic development of this reaction (Wang and Barteau, 2002, 2003).

Numerous kinetic studies have been conducted in an attempt to model the complex behaviour of the VPP catalyst under transient redox conditions. The majority of these studies have focused

either on the catalyst re-oxidation kinetics (Huang et al., 2002a; Wang and Barteau, 2002; Patience and Lorences, 2006), or on the catalyst reduction kinetics (Mills et al., 1999; Wang and Barteau, 2001; Lorences et al., 2003, 2004; Gascón et al., 2006; Huang et al., 2002b; Schuurman and Gleaves, 1997). Moreover, most of the proposed kinetic models are valid only for a relatively narrow range of redox conditions. A comprehensive kinetic model applicable to a wide range of industrial operating conditions, including reactor pressure, is absent in the open literature.

Among the most recent kinetic investigations, Gleaves et al. (2010) summarized the C_4 kinetic achievements by the temporal analysis of products (TAP) reactor. Other recent studies were mostly related to the analysis and simulation of different types of steady state reactors by using previously established redox kinetic models (Marín et al., 2010; Brandstädter and Kraushaar-Czarnetzki, 2007; Hakimelahi et al., 2006). Gascón et al. (2006) proposed a redox kinetic model based on a relatively detailed redox mechanism in which the activation of n-butane took place on both surface and lattice oxygen. Lorences et al. (2003, 2004, 2006) also modeled the transient VPP redox kinetics by proposing a mechanism involving V^{4+}/V^{5+} redox pairs as well as a catalyst deactivation site. They showed that the steady state kinetic models are usually incapable of predicting transient regimes. This might indicate that under transient conditions, the redox history of the catalyst becomes critically important to control catalytic performance (Gascón et al., 2006).

Wang and Barteau (2001, 2002, 2003) proposed an elementary kinetic expression for catalyst reduction rate under aerobic conditions. They considered the catalyst reduction rate to be equal to the sum of the surface and lattice oxygen consumption rates and also proposed a mechanism for oxygen insertion into the catalyst lattice during the initial moments of re-oxidation. A similar re-oxidation mechanism was proposed by (Huang et al., 2002a) by considering first and second order reaction rates for a two step lattice oxygen insertion from the gas phase. Gascón et al. (2006) and Patience and Lorences (2006) observed that the catalyst oxidation rate and the subsequent maleic anhydride yield increase by increasing oxygen partial pressure in the gas phase. A common agreement has been that the oxygen insertion from the surface to the lattice could be the rate controlling step. Regarding the fuel rich operations, few studies have examined

moderate and high n-butane concentrations (Lorences et al. (2003, 2004) and Wang and Barteau (2001, 2002)). These studies identified that the surface adsorbed oxygen species are the main source of selective n-butane oxidation. Wang and Barteau (2001) showed that the activation energy for transient reduction is comparable to its corresponding value for steady state operation (~ 85-88 kJ/mol). Probably, the rate determining step – n-butane activation over reduced catalyst site (V^{4+}) (Mota et al., 2000) – should be the same for transient and steady state operations.

The redox kinetic models for n-butane oxidation over VPP could be generally classified according to the number of active sites responsible for selective and non-selective reactions. The single site mechanisms are characterized by considering only one catalyst active site to be responsible for all redox reactions (Wang and Barteau, 2001; Buchanan and Sundaresan, 1986). These mechanisms are generally successful in predicting the n-butane conversion while they are rather poor at characterizing the maleic anhydride selectivity. Various two site or pseudo-two site mechanisms have been developed: Bej and Rao (1991) and Lorences et al. (2003, 2004, 2006). The advantage of these models is that they differentiate between selective and non-selective sites and may predict selectivity better than single site models.

Identifying the catalyst active sites and accounting for their dynamic transformations during redox reactions is critical in defining the best representative mechanism. For the vanadium-phosphorous-oxide system, the vanadyl pyrophosphate – $(VO)_2P_2O_7$ (V^{4+}) – has been identified as the predominant catalyst active phase (Ballarini et al., 2006; Hutchings, 2004; Volta, 2000). However, during the transient operations, a dynamic transformation between this phase and an its oxidized form, $VOPO_4$ (V^{5+}) has been commonly reported (Ballarini et al., 2006; Schuurman and Gleaves, 1997; Rodemerck et al., 1997; Mota et al., 2000; Hutchings, 2004; Volta, 2000; Taufiq-Yap et al., 2009; Cavani et al., 2000). The V^{5+} oxidized sites have been attributed with a lower activation energy resulting in a higher catalytic activity (Schuurman and Gleaves, 1994, 1997). It is generally agreed that maintaining a certain V^{5+}/V^{4+} ratio on the catalyst surface would be essential for optimal catalytic activity (Patience and Lorences, 2006; Ballarini et al., 2006; Schuurman and Gleaves, 1997; Lorences et al., 2003, 2004, 2006; Mota et al., 2000; Taufiq-Yap et al., 2009).

There has been a considerable debate on the role of surface oxygen species during reaction over the VPP catalyst (Lorences et al., 2006). There is a general agreement that the surface lattice oxygen is more selective than the adsorbed oxygen species (Schuurman et al., 1997; Patience and Lorences, 2006; Bej and Rao, 1991). However, studies showed that while operating under fuel rich feed conditions, both lattice and surface oxygen become responsible for maleic anhydride formation (Wang and Barteau, 2003; Gascón et al., 2006). Under these conditions, the participation of the lattice oxygen in surface reactions was reported to be very limited. Therefore, at high n-butane concentrations, the interaction of gas phase oxygen with the catalyst surface becomes critical for catalytic activity by maintaining the surface in an oxidized state (Ballarini et al., 2006; Patience and Lorences, 2006). Further mechanistic complications might arise while identifying the rate determining steps or considering the equilibrium transformations between different oxygen species (Wang and Barteau, 2002) as well as accounting for the role of physically adsorbed oxygen in n-butane activation (Gascón et al., 2006). These observations represent the challenges in proposing a unique redox mechanism which is valid for a wide range of feed compositions. A practical approach in the literature has been to consider a lumped behaviour for the complex transformations of different oxygen species.

Circulating fluidized bed (CFB) technology relies primarily on the VPP catalyst lattice oxygen as a source of selective oxygen. A key factor for industrial success of this technology is the sufficient ability of the catalyst to supply its lattice oxygen to the reaction zone. Therefore, higher capability of the catalyst for oxygen transfer to the reaction ensures higher maleic anhydride productivity and also lower compression costs by reducing the catalyst recirculation rates. There have been some research studies on the effect of redox conditions on VPP catalyst's lattice oxygen contribution (LOC) or oxygen storage during regeneration (Patience and Bockrath, 2010; Wang and Barteau, 2001; Emig et al., 1994). A common conclusion is that by feeding higher concentrations of n-butane, the catalyst oxygen contribution could be improved. However, lower catalyst oxidation state is often accompanied by a loss in selectivity. Other factors which influence the catalyst oxygen transfer capacity have been described to be the catalyst residence time and temperature (Huang et al., 2002a; Gascón et al., 2006).

In this research, we have modeled the transient kinetics of n-butane partial oxidation over DuPont's VPP catalyst for a relatively wide range of redox operating conditions including feed composition, catalyst oxidation time, temperature and pressure. Since the industrial reactors normally operate at higher than atmospheric pressures, the reactor pressure was also considered in the model and its effect on the transient redox kinetics was discussed. The range of redox parameters were selected according to the corresponding values which are typically practiced in industrial fixed bed, fluidized bed and CFB reactors. Based on a previous kinetic study (Lorences et al., 2004), a modified redox mechanism of the type Mars-van Krevelen was implemented. The proposed transient kinetic model was able to successfully predict the n-butane and oxygen conversions as well as the selectivity toward products at the studied range of redox parameters as well as the higher pressure. The predicted trends for variation of catalyst oxidation state during reaction helped gaining a better understanding on the reasons for the catalyst's redox behaviour at higher pressure.

5.4 Experimental

5.4.1 Experimental setup

The atmospheric and high pressure (410 kPa) redox experiments were conducted in a 7.7 mm ID quartz and a stainless steel tube micro-fixed bed reactor respectively, over about 500 mg of DuPont's VPP catalyst which was calcined according to an industrial protocol (Patience et al., 2007).

The transient redox operation of a CFB reactor was simulated in the laboratory scale micro-reactor by switching between the premixed reducing and oxidizing gases over the catalyst bed using a multi-port automatic electrical valve (Figure 5-1). The composition of the gaseous reactor effluents was monitored using online mass spectroscopy (MS). The evolution of the acid products was tracked by real time electrical conductivity measurements in a quench absorber and cross checked by offline HPLC analysis. More details on the high pressure and atmospheric setups, the experimental procedures and the catalyst preparation could be found in our previous publications (Shekari and Patience, 2010, 2011).

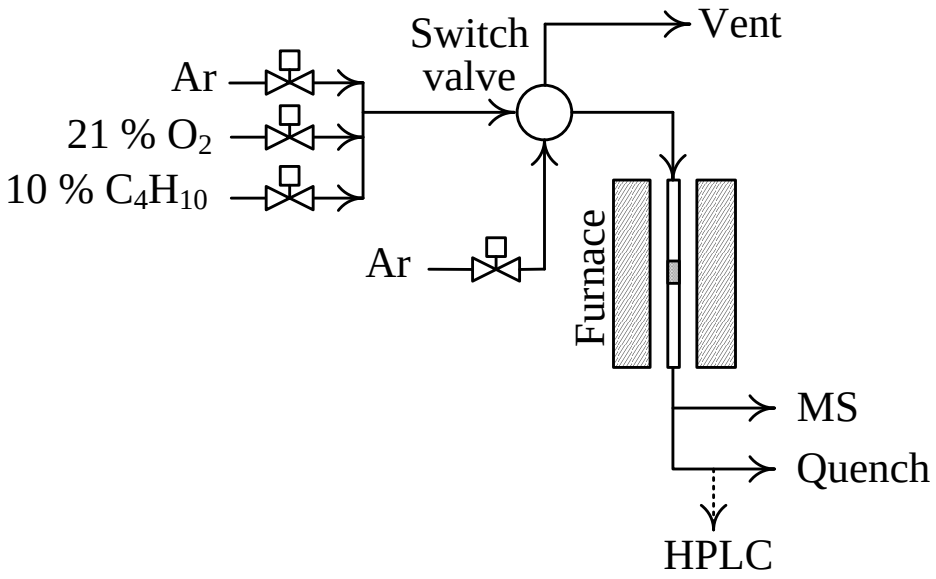

Figure 5-1: Experimental micro-reactor setup

5.4.2 Redox experiments

A wide range of experimental redox conditions were studied (Shekari and Patience, 2010 and 2011). These ranges enclosed practically all the possible combinations that normally exist from lab scale to industrial operations. To conduct a transient kinetic study at different reactor pressures, two series of the experimental data were selected (Table 5.1). These data covered a feed composition range of O_2/C_4H_{10} = 1.1 typical for a CFB operation up to the ratio of 13.1 which is typically practiced in a fixed bed reactor. The catalyst oxidation times were varied between 1 and 10 minute to represent the solid residence times from the large scale regenerators down to the lab scale experiments. A base case temperature of 380 °C was selected for all tests. To estimate the reactions activation energies, additional experiments were conducted at temperatures of 360 and 400 °C under fuel rich conditions. The total flow rate for all tests was about 40 mL/min (STP) and the catalyst reduction time was set to be 2 minutes. To ensure the repeatability of the data and also to stabilise the catalytic activity for each redox condition, all experiments were run for 3-5 consecutive redox cycles; in this way it was possible to estimate the standard errors and the confidence intervals around each experimental point.

Table 5.1: Transient redox experimental conditions (100 and 410 kPa)

Simulated conditions	Feed composition (vol. %)		O_2/ C_4H_{10}	Oxidation time (min)	Temperature (°C)
	n-Butane	Oxygen			
CFB	6.5	7.3	1.1	1, 10	360, 380, 400[1]
Fluid bed	3.6	13.4	3.6	10	380
Fixed bed	1.4	18.2	13.1	10	380

[1] No temperature variation for 1 minute oxidation test and ambient pressure

5.5 Model development

5.5.1 Hydrodynamic model

To characterize the reactor system hydrodynamics, residence time distribution (RTD) experiments were conducted at atmospheric and high pressure (410 kPa). The reactor flow model was found to be adequately represented by a tanks-in-series (n-CSTR) model (Figure 5-2). The reactor gas volume was divided into two sub-sections: reactive (1 to N_r) and non-reactive space (N_r+1 to N).

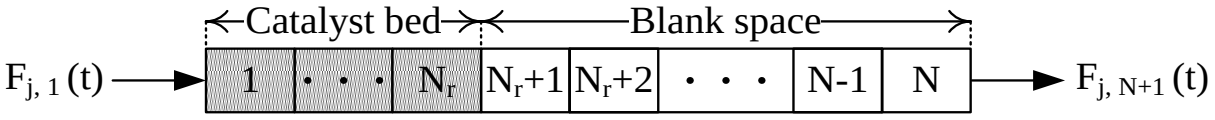

Figure 5-2: Reactor model scheme

The total number of tanks in series (N) for the whole reactor volume was found by fitting the following equation on the experimental RTD data (Fogler, 2006):

$$E(\theta) = \bar{t}E(t) = \frac{N(N\theta)^{N-1}}{(N-1)!}e^{-N\theta} \quad (5\text{-}1)$$

where:

$$\theta = {}^{t}/_{\bar{t}} \quad (5\text{-}2)$$

An oxygen tracer step function was introduced into the reactor system by switching from pure argon to 21 vol. % oxygen in argon using an automatic switching valve. The oxygen response signal was detected by the MS at a frequency of 0.2-0.3 s^{-1}. About 500 mg of the catalyst was loaded into reactor at a base case temperature of 380 °C. The whole reactor system – from the switching valve up to the mass spectrometer – was continuously purged at 40 mL/min (STP) by argon as the career gas. To minimize the effect of catalyst oxygen take up on the exit oxygen response, the samples were priorly treated by the tracer gas (21 vol. % O_2 in argon) for about one hour. The catalyst surface was assumed to be saturated by oxygen after this period.

5.5.2 Kinetic model

5.5.2.1 Redox mechanism

Several redox mechanisms in the literature were examined to verify their applicability to the transient redox data. Generally, the steady state mechanisms or the Langmuir-Hinshelwood (LH) type mechanisms which considered the equilibrium adsorption or desorption of the reactive components could not satisfactorily represent the entire range of transient data. The main reason for the failure of the LH type mechanisms could be related to the assumptions over equilibrium rates which might not be applicable to transient regimes.

To keep the simplicity and easy application of the kinetic model, a single site redox mechanism of the type Mars-van Krevelen (MvK) comprising three elementary reactions was proposed (Equations (5-3)-(5-6)). The redox mechanism was inspired from our previous kinetic study (Lorences et al., 2003, 2004). Based on the observed redox behaviour, some modifications were

made to the original mechanism. As there was virtually no observation of the carbon oxides evolution during the catalyst oxidation step, the reactions related to the catalyst deactivation were eliminated. In addition, the reaction for non-selective combustion of maleic anhydride was not considered in the mechanism as the rate constant for this reaction approached zero while fitting the model parameters.

$$O_2 + S \longrightarrow O_2 \cdot S \tag{5-3}$$

$$C_4H_{10} + 3.5\, O_2 \cdot S \longrightarrow C_4H_2O_3 + 4\, H_2O + 3.5\, S \tag{5-4}$$

$$C_4H_{10} + 5.5\, O_2 \cdot S \longrightarrow 4\, CO_x + 5\, H_2O + 5.5\, S \tag{5-5}$$

$$CO_x = \frac{(CO + CO_2)}{2} \tag{5-6}$$

In the redox mechanism, the catalyst oxidation (Reaction (5-3)) was assumed to proceed through non-dissociative adsorption of the molecular oxygen over a catalyst reduced site (S). Consequently, the oxidized catalyst site ($O_2 \cdot S$) undergoes selective (5-4) or non-selective (5-5) reactions through direct interaction with n-butane in the gas phase and thereby leaving the surface in a reduced state. No adsorption or desorption of reactants or products were considered and the products were assumed to leave the surface as soon as they are formed. Direct interactions of gaseous reactants with surface species were considered to control the overall reaction rate. Moreover, due to the relatively short reduction times (2 minute), it was assumed that the equilibrium state for the reactions or the surface concentrations could not be achieved.

5.5.2.2 Reaction rates

In the following, the reaction rate equations associated with the proposed redox mechanism are presented. The elementary reaction rates are defined as the functions of the molar reactants molar flow rates and the catalyst surface oxygen coverage (θ_{O_2}). An Arrhenius type dependency on temperature was assumed for the reaction rate constants (k_i). For the sake of simplicity and also

to achieve a more reliable value for kinetic parameters, the reaction rate constants were normalized to their reference values (k_{r_i}) calculated at the base case temperature of T_r = 653.15 K (Equation (5-10)). The reaction rate units were converted from volumetric basis to catalyst weight basis by applying a corrective factor which was cumulative gas volume divided by the catalyst weight (*V(n)/W(n)*) at each catalyst bed sub-section.

$$r_1 = - k_1 C_T \frac{F_{O_2}}{F_T}(1 - \theta_{O_2})\frac{V(n)}{W(n)}, \quad n = 1 - N_r \tag{5-7}$$

$$r_2 = - k_2 C_T \frac{F_{C_4H_{10}}}{F_T}\theta_{O_2}\frac{V(n)}{W(n)} \tag{5-8}$$

$$r_3 = - k_3 C_T \frac{F_{C_4H_{10}}}{F_T}\theta_{O_2}\frac{V(n)}{W(n)} \tag{5-9}$$

$$k_i = k_{r_i}\, exp\left[-\frac{E_i}{R}\left(\frac{1}{T} - \frac{1}{T_r}\right)\right], \quad i = 1 - 3 \tag{5-10}$$

5.5.3 Transient mass balance equations

According to the reactor flow model and the proposed kinetics, transient partial mass balances were set up for each component present in the system including the catalyst oxidized site (θ_{O_2}). The mass balances were derived for each reactor sub-volume (*V(n)*) for both reactive and non-reactive sections. In this way, two sets of ordinary differential equations (ODEs) were generated for each reactor sub-section: the catalyst bed, from 1 to N_r and the non-reactive blank space, from N_r*+1* to *N*) (Figure 5-2).

As the proposed set of reactions involved a positive change in the number of product moles with respect to the number of reactant moles, an increase in the total volumetric flow rate due to the reaction was assumed. To account for reaction volume expansion, the transient mass balance equations were converted to their components molar flow rate (F_j) forms rather than the

concentrations. In this way, the increase in the total molar flow rate (F_T) could be accounted for by considering the time derivative terms for flow rates.

5.5.3.1 Catalyst bed

The following system of ODEs was developed for the catalyst bed section of the reactor:

$$\frac{dF_j(t,n+1)}{dt} = \left(\frac{F_T(t,n+1)}{C_T V(n)}\right)\left(F_j(t,n) - F_j(t,n+1) + W(n)R_j(t,n)\right) + \left(\frac{F_j(t,n+1)}{F_T(t,n+1)}\right)\frac{dF_T(t,n+1)}{dt}, \qquad j = 1-7\,, \qquad n = 1-N_r \tag{5-11}$$

$$\frac{dF_T(t,n+1)}{dt} = \sum_{j=1}^{7}\frac{dF_j(t,n+1)}{dt}, \qquad n = 1-\ N_r \tag{5-12}$$

$$\frac{d\theta_{O_2}(t,n)}{dt} = \frac{R_j(t,n)}{C_{ST}}, \qquad j = 8\,, \qquad n = 1-N_r \tag{5-13}$$

$$R_j(t,n) = \sum_{j=1}^{8}\nu_{ij}r_i\ \ , \qquad i = 1-3 \tag{5-14}$$

5.5.3.2 Blank space

To account for the gas phase diffusion of the reaction components through the reactor empty space (including piping, dead volumes, etc.); the following ODE system was derived:

$$\frac{dF_j(t,n+1)}{dt} = \left(\frac{F_T(t,n+1)}{C_T V(n)}\right)\left(F_j(t,n) - F_j(t,n+1)\right), \qquad j = 1-7, \quad n = N_r + 1\ to\ N \tag{5-15}$$

$$\frac{dF_T(t,n+1)}{dt} = \sum_{j=1}^{7} \frac{dF_j(t,n+1)}{dt}, \qquad n = N_r + 1 \; to \; N \tag{5-16}$$

5.5.3.3 Initial and inlet conditions

The following sets of values were used to initialize the ODE systems both in the time (*t*) and in the reactor volume (*n*) axes:

Initial values (*n = 1 to N*):

$F_j(0,n) = 0$ $\quad j = 1-6$, excluding Ar (5-17)

$F_7(0,n) = F_{0Ar}$ (5-18)

$F_T(0,n) = F_{0Ar}$ (5-19)

$\theta_{O_2}(0,n) = \theta_{0O_2}$ $\quad n = 1 - N_r$ (5-20)

Inlet conditions (*n = 1*):

$F_j(t,1) = F_{j1}(t)$ for C_4H_{10}, O_2 and Ar (5-21)

$F_j(t,1) = 0$ for MA, CO, CO_2 and H_2O (5-22)

$F_T(t,1) = F_{T1}(t)$ (5-23)

5.5.4 Parameter estimation

After implementing the model expressions in a Matlab® program code, a non-linear least square regression function (*nlinfit*) was used to estimate the model parameters (k_i, θ_{O_2} and E_i, *i =1-3*) using the initial and boundary conditions presented above as well as the initially guessed parameter values. The parameter optimization was proceeded by trying to minimize the squared

differences (errors) between the model predictions (y_l^p) and the experimental values (y_l) (Equation (5-24)). The regression function used the Levenberg-Marquardt algorithm according to the program's default selection. The systems of simultaneous ODEs (Equations (5-11) to (5-16)) along with the embedded kinetic functions (Equations (5-7) to (5-10)) were simultaneously solved using Matlab®'s "*ode15s*" function recommended for solving "stiff" type problems. Alternatively, the Matlab®'s "*fminsearch*" function was utilized to minimize an R-square type objective function (Equation (5-25)) using the *Simplex* algorithm.

During the kinetic modeling study, both parameter fitting techniques were found to provide similar results. However, the "*nlinfit*" regression approach was preferred as it provided the statistical analysis tools to estimate the confidence intervals on the model parameters and also on the predicted values using "*nlparci*" and "*nlpredci*" sub-functions, respectively.

$$\Phi_{lsq} = \sum_{l}\sum_{m}\left(y_l - y_l^p\right)^2, \qquad l = \text{data points},\ m = \text{experiments} \tag{5-24}$$

$$\Phi_{fmin} = 4 - \sum_{l} R_l^2 \qquad \text{where } R_l^2 = 1 - \frac{\sum_m\left(y_l - y_l^p\right)^2}{\sum_m (y_l - \bar{y}_l)^2} \text{ and } \bar{y}_l = \frac{\sum_m y_l}{m} \tag{5-25}$$

In the above equations, y_l and y_l^p represent the experimental and predicted conversion and selectivity data, respectively.

The total n-butane and oxygen conversions ($X_{C_4H_{10}}$ and X_{O_2}) as well as the total products' selectivity (S_{MA} and S_{CO_x}) were calculated according to their conventional definitions described elsewhere. For this purpose, the total moles of the consumed or produced reactants or products were calculated by integrating the corresponding transient molar flow rates (F_j) during the two minutes of reduction time.

5.6 Results and discussion

5.6.1 RTD model

Figure 5-3 demonstrates a comparison between the residence time distribution of the reactor system at ambient and higher pressure of 410 kPa. The results show a widening effect in the RTD response peak as the pressure increases. This could be due to the lower superficial gas velocity (u_g) as the gas density increases by pressure. However, the predicted number of CSTRs in series (*N*) also increases by pressure from 53 to 72 tanks. The characteristics of the reactor flow model are presented in Table 5.2. These results clearly show that there is a strong justification to assume plug flow behaviour for the gas flow in the reactor. Accordingly, the total number of reactor sub-sections (*N*) in the kinetic modeling was considered adequately high (> 40) to represent the plug flow behaviour at both atmospheric and higher operating pressures.

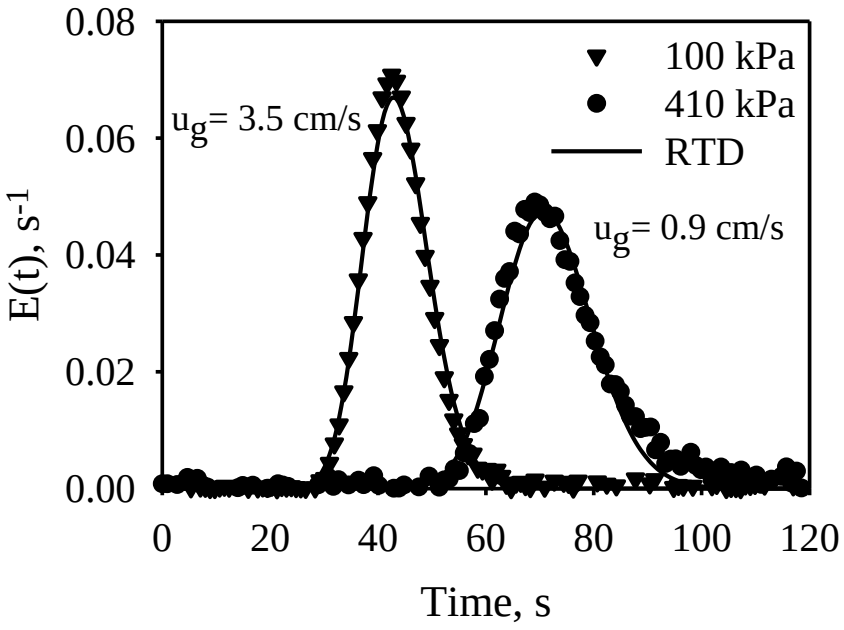

Figure 5-3: Reactor RTD versus model predictions

(Tracer = 21 vol. % O_2 in Ar, Flow rate = 40 mL/min (STP), 380 °C)

Table 5.2: RTD model parameters

Pressure, kPa	$\boldsymbol{\sigma^2}$**, s**^{2}	$\boldsymbol{\bar{t}}$**, s**	**N =** $\boldsymbol{1/\sigma_\theta^2}$	**Pe = 2(N-1)**
100	36.3	43.7	53	103.1
410	71.8	71.7	72	141.2

5.6.2 Kinetic model

5.6.2.1 Reaction rate constants

The bar graphs in Figure 5-4 represent a comparison between the kinetic rate constants at atmospheric and high pressure. Irrespective of the pressure, the catalyst oxidation rate constant (k_1) is much higher than the other two reduction rate constants (k_2 and k_3). This difference is about 3-6 times at ambient pressure while it is about eight times higher at the elevated pressure. This observation might show that higher catalyst oxidation rates would be required to compensate for a relatively low amount of catalyst reduction. Moreover, it appears that by increasing the pressure, the rate constant for oxidation (k_1) slightly increases while the catalyst reduction rate constants decrease. However, these changes are within the range of statistical confidence intervals. In general, considering the expected variability for the rate constants within the 95% confidence intervals, it appears that the proposed kinetic model is valid for both ambient and high pressure experiments.

5.6.2.2 Initial oxygen coverage

One of the fitted parameter in the kinetic modeling study was the catalyst initial surface oxygen coverage (θ_{0O_2}) introduced in Equation (5-20). Due to the uncertainty over the absolute values of the catalyst's surface oxygen concentrations (C_{SO_2}), the catalyst oxidation extent was represented by normalizing the surface oxygen concentrations over the total theoretical concentration of the oxygen adsorption sites (S) available on the catalyst surface (C_{ST}). In the catalyst oxidation mechanism, it was proposed that every single oxygen molecule is adsorbed over one catalyst active site (S), Equation (5-3). Therefore, it is logical to assume that the surface oxygen

concentration could be represented by the available catalyst surface site concentration. Moreover, it was assumed that the total oxygen amount that the catalyst could incorporate in its surface sites could be correlated with the amount of oxygen that converts the catalyst active phase – vanadyl pyrophosphate, $(VO)_2P_2O_7$ – into its oxidized form, $VOPO_4$ (Reaction (5-26)):

$$(VO)_2P_2O_7 + \frac{1}{2}O_2 \longrightarrow 2\ VOPO_4 \qquad (5\text{-}26)$$

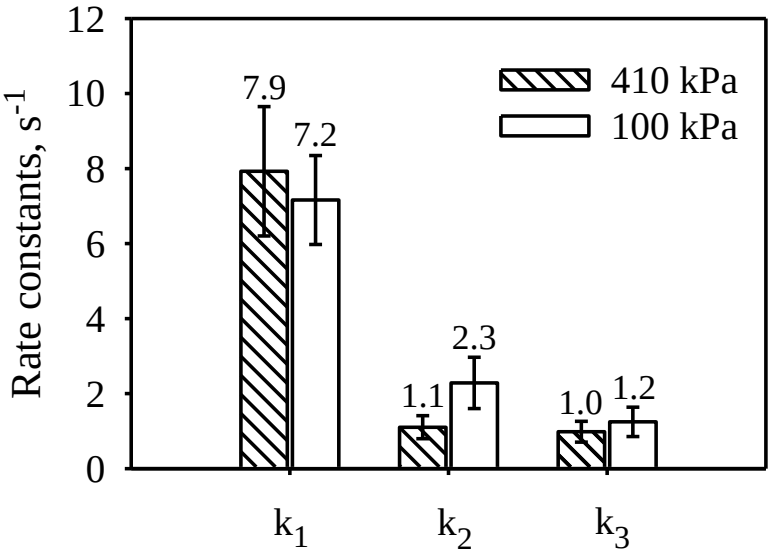

Figure 5-4: Transient rate constants

(T = 380 °C, O_2/C_4H_{10} = 1.1-13.1, Oxidation time = 1 and 10 min)

As different proportions of these phases jointly exist on the catalyst surface, only a portion of the vanadyl pyrophosphate (V^{4+}) that could be converted into $VOPO_4$ (V^{5+}) was considered as the catalyst active phase. Therefore, the total theoretical concentration of active surface sites (C_{ST}) could be estimated by considering one mole of vanadium per each molecule of $VOPO_4$ with the molecular weight of 161.9 g/mol:

$$C_{ST} = \frac{1\ mole\ of\ V}{1\ mole\ of\ VOPO_4} = \frac{1\ mole}{161.9 \times 10^3 mg} = 6.18 \times 10^{-6}\ \frac{mol}{mg} \quad (5\text{-}27)$$

$$\theta_{O_2} = \frac{C_{SO_2}}{C_{ST}} \quad (5\text{-}28)$$

In Figure 5-5, the catalyst's initial oxygen coverage (θ_{0O_2}) values are plotted against the feed compositions at ambient and higher pressures. The initial oxidation state of the catalyst is increased when the oxygen concentration in the feed is increased. However, higher pressure shows an improving effect on the catalyst oxidation state only when there is adequate oxygen in the feed (O_2/C_4H_{10} > 1.1). It is interesting to note that the pressure has a negative effect on the catalyst oxidation state while operating at relatively high n-butane concentrations (O_2/C_4H_{10} = 1.1). Predicted data show that the catalyst is slightly reduced at higher pressure while working at fuel rich conditions. However; the observed changes are in the range of model parameters confidence intervals. These trends might indicate that while the feed is reducing, the pressure has a more pronounced effect on the catalyst reduction rate; under these conditions, the catalyst oxidation rate might be lower than its reduction rate. Wang and Barteau, (2002) observed similar higher catalyst reduction rates while simulating the CFB reactor operations in a microbalance reactor. They reported that the difference in redox rates is more sensible at higher temperatures.

5.6.2.3 Transient oxidation trends

Based on the estimated values for initial catalyst oxygen coverage (θ_{0O_2}), the kinetic model was able to predict the dynamic changes in the catalyst oxygen coverage (θ_{O_2}) during the reaction (Figure 5-6). These data provided more insight on the actual behaviour of the VPP catalyst during redox operations. The same trend as Figure 5-5 was observed: as the feed was more reducing (O_2/C_4H_{10} = 1.1), the catalyst oxygen coverage decreased by increasing pressure. Moreover, a slight decrease in catalyst oxidation state by time was observed only when the feed was more reducing (O_2/C_4H_{10} = 1.1 and 3.6). Similarly, when there is adequate oxygen in the gas phase, by increasing the pressure, the catalyst surface tends to be rather oxidized; however, at higher n-

butane concentrations in the feed, as the pressure increases, the catalyst loses its surface oxygen coverage due to excessive reduction rates.

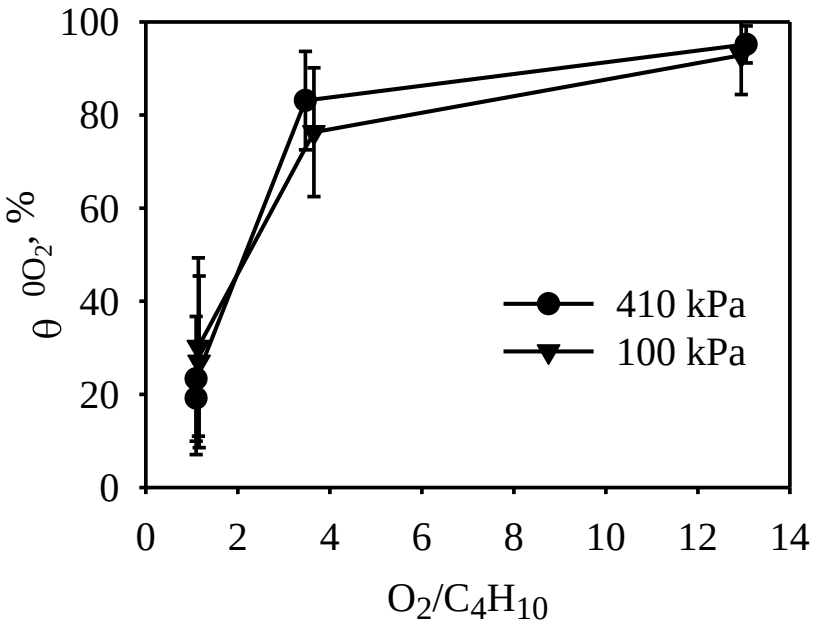

Figure 5-5: Estimated initial VPP oxygen coverage

(T = 380 °C, Flow rate = 40 mL/min (STP), Oxidation time = 1 and 10 min)

5.6.2.4 Activation energies

Table 5.3 summarizes the estimated activation energies for the redox reactions at ambient and high pressure. According to these data, higher pressure increased the activation energies for all reactions. However, this increase was more noticeable for the oxidation reaction: as the pressure increased, the activation energy (E_1) for the catalyst oxidation increased by about 20%. The observed increase in the activation energies could be related to the effect of pressure on the catalyst oxidation state. As the pressure increases, the catalyst oxidation state changes depending on the feed composition (Figures 5-5 and 5-6). The activation energies presented in Table 5.3 are obtained for the conditions where the feed composition falls in the fuel rich region (O_2/C_4H_{10} = 1.1). Therefore, according to the observed VPP behaviour at higher pressure, a decrease in the catalyst oxidation state would be expected. Based on these results, the increase observed in the activation energies could be associated with the decrease in catalyst oxidation state. Schuurman

and Gleaves (1997) reported the same observation while injecting consecutive pulses of n-butane over a pre-oxidized VPP catalyst. They observed that the activation energy for n-butane conversion increases from 50.2 to 96.2 kJ/mol as the catalyst moves from an oxidized ($V^{4.1+}$) to a reduced ($V^{4.0+}$) state. They related the observed increase in the activation energy to the accumulation of low energy sites (V^{4+}) versus the high energy sites (V^{5+}) over the catalyst surface as the catalyst was gradually reduced by n-butane pulses.

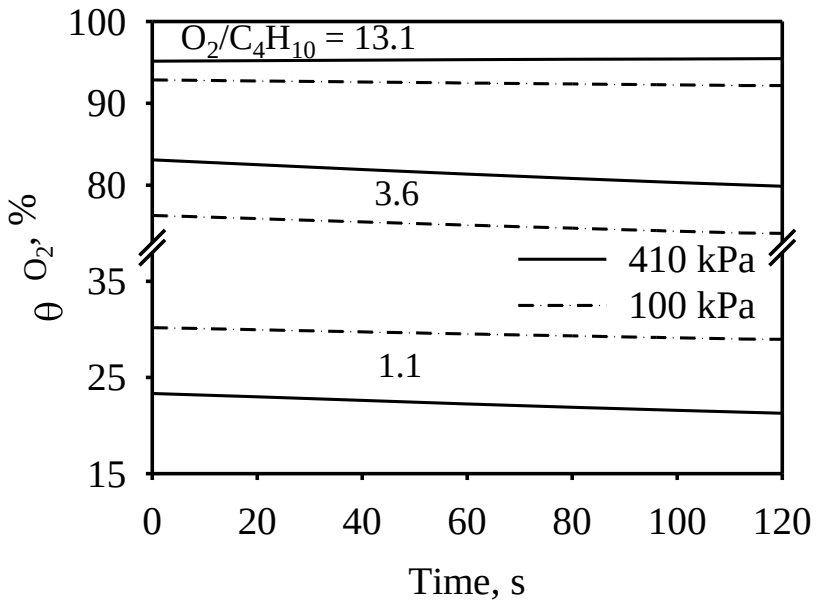

Figure 5-6: Transient VPP oxidation during reaction

(T = 380 °C, Flow rate = 40 mL/min (STP), Oxidation time = 10 min)

Table 5.3: Activation energies, kJ/mol

	100 kPa	**410 kPa**	**ΔE_i, %**
E_1	199.2	240.6	20.8
E_2	135.6	149.0	9.9
E_3	154.4	157.3	1.9

5.6.3 Model validation

5.6.3.1 Predictions vs. experimental data

Figures 5-7 to 5-10 demonstrate the model predictions versus experimental data for n-butane and oxygen conversions as well as the maleic anhydride and CO_x selectivity. Also, Figure 5-11 represents the parity graph of the same data. According to these data, there is a very good agreement between the model predictions and the experimental data. Considering the simplicity of the proposed kinetic model and the redox mechanism, the proposed kinetic model remarkably predicts the experimentally observed trends. The model prediction bands were estimated using the available statistical analysis tools in Matlab® program. The vertical bars on the experimental data represent the calculated standard error for at least 3-5 replicates for each measurement point. As a measure for goodness of fit, the root mean square error (RMSE) for the deviation of model predictions from experimental data was approximately 3.8 for both sets of ambient and high pressure data.

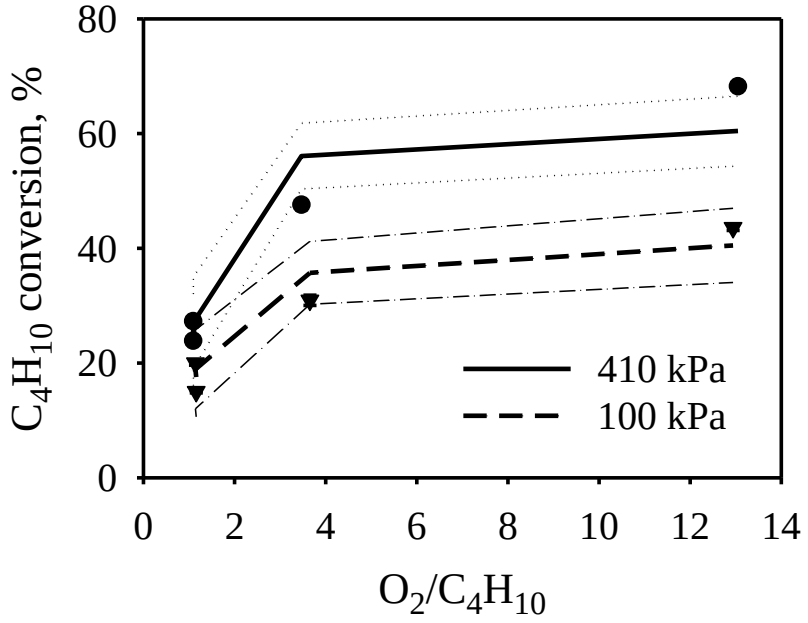

Figure 5-7: n-Butane conversion vs. model

(T = 380 °C, Flow rate = 40 mL/min (STP), Oxidation time = 1 and 10 min)

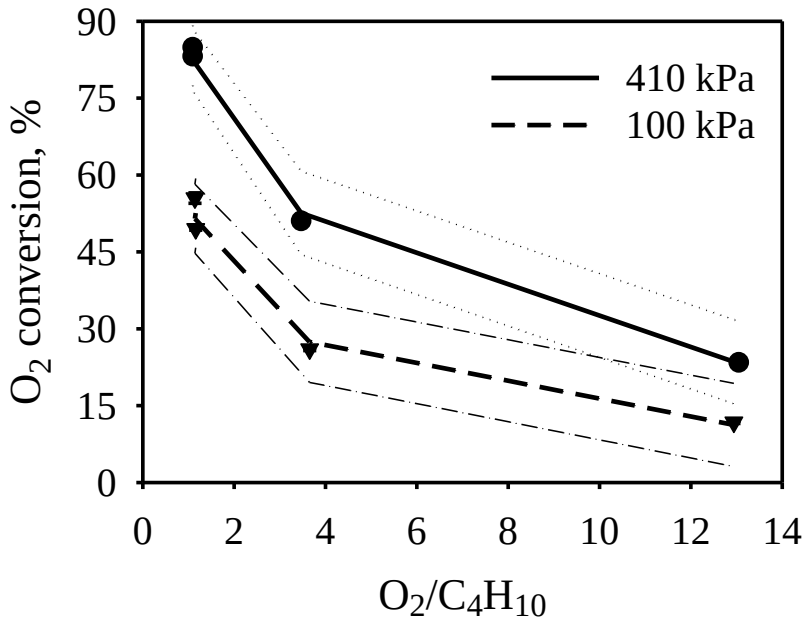

Figure 5-8: Oxygen conversion vs. model

(T = 380 °C, Flow rate = 40 mL/min (STP), Oxidation time = 1 and 10 min)

Data presented in Figures 5-7 and 5-8 show that the reactor pressure considerably affects the n-butane and oxygen conversions as well as the byproduct selectivity (Shekari and Patience, 2011). The effect of pressure was more noticeable while the oxygen concentration in the feed was higher (O_2/C_4H_{10} = 3.6 and 13.1). By increasing the pressure, n-butane conversion increased by about 40 to 60 % and an increase of about 50 to 100 % was observed for oxygen conversion. The byproduct carbon oxides (CO_x) selectivity was also increased by an average of about 35 %. However, the maleic anhydride selectivity dropped by around 18 % on average. Despite the observed drop in maleic anhydride selectivity, the overall MA yield was improved by about 10-30 %.

The increase in n-butane and oxygen conversions could be attributed to the effect of pressure on the catalyst surface oxygen coverage while the feed is oxidizing (O_2/C_4H_{10} > 1.1) or the higher predicted catalyst reduction rates at reducing feed conditions (Figure 5-6). Increase in redox rates due to higher reactants partial pressures or promotion of gas phase reactions at higher pressure

should also be taken into account. By increasing the pressure at oxidizing feed conditions, higher concentration of surface oxygen sites ($O_2 \cdot S$) would enhance the conversion of n-butane and accordingly more oxygen would be consumed to re-oxidize the surface. However, when the feed is reducing (O_2/C_4H_{10} = 1.1), higher population of surface reduced sites (S) would ensure a high oxygen conversion. The higher reduction rates under these conditions might be responsible for the higher n-butane conversion observed.

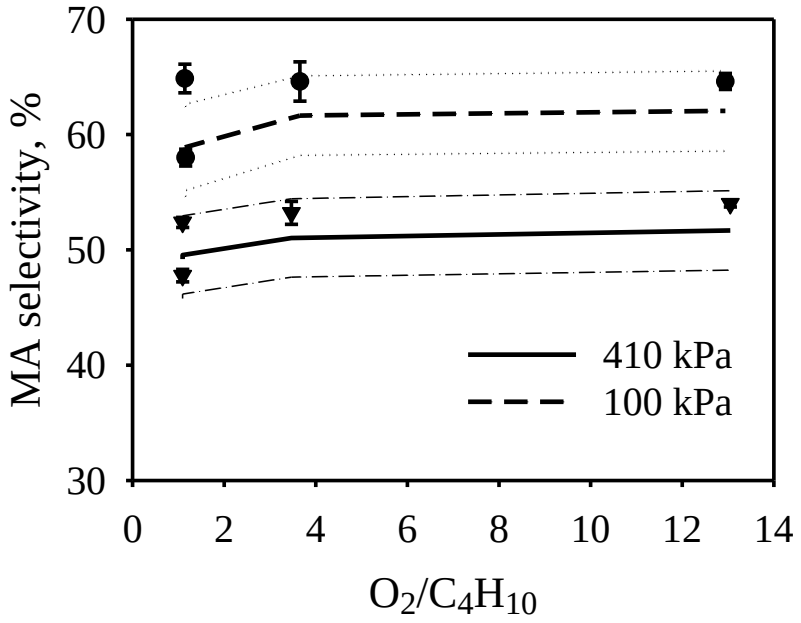

Figure 5-9: MA selectivity vs. model

(T = 380 °C, Flow rate = 40 mL/min (STP), Oxidation time = 1 and 10 min)

Regarding the MA and CO_x selectivity, as the surface oxygen species ($O_2 \cdot S$) are participating in both selective and non-selective reactions ((5-4) and (5-5)), the MA selectivity is not necessarily improved by increasing the pressure. Actually, the effect of pressure on the relative rates of these two reactions would determine the selectivity toward maleic anhydride or carbon oxide byproducts. This could be more clearly explained by looking at the activation energies of these two reactions presented in Table 5.3 or the corresponding predicted reaction rate constants in Figure 5-4. In Table 5.3, the activation energy of the selective Reaction (5-4) is estimated to be

more sensitive to the pressure than the non-selective Reaction (5-5) (9.9 % increase vs. 1.9 %). This could result in a higher chance for the non-selective reaction to proceed while increasing the pressure. Moreover, the reaction rate data presented in Figure 5-4 show that at ambient pressure, the rate constant k_2 for selective Reaction (5-4) is almost 2 times the rate constant k_3 for non-selective Reaction (5-5) (2.3 vs. 1.2 s^{-1}); while at elevated pressure, the two rate constants become almost identical (1.1 vs. 1.0 s^{-1}). This could be another reason for lower MA selectivity observed at higher pressure.

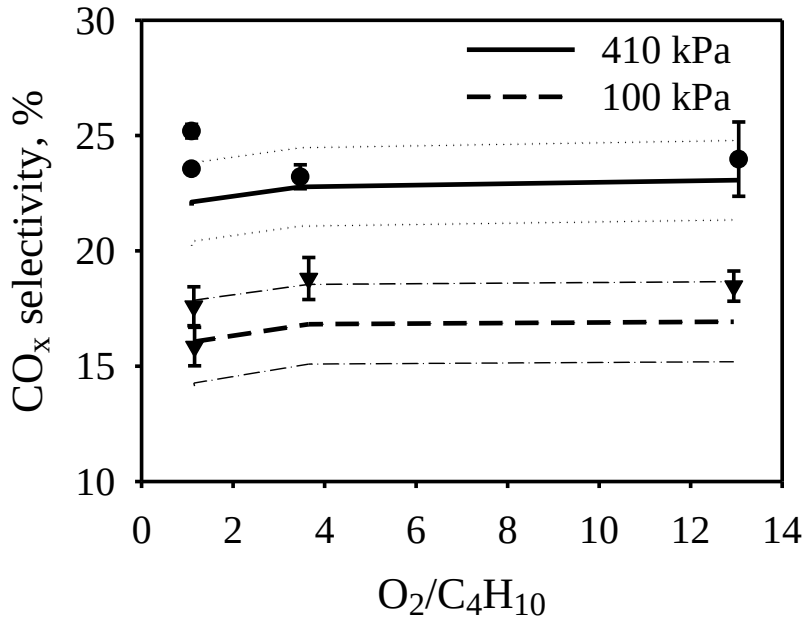

Figure 5-10: CO_x selectivity vs. model

(T = 380 °C, Flow rate = 40 mL/min (STP), Oxidation time = 1 and 10 min)

5.6.3.2 Adequacy check

Figure 5-12 demonstrates that the residuals of the proposed kinetic model are distributed in a fairly random and "structureless" pattern. Moreover, the probability plot in Figure 5-13 shows that the distribution of residuals and their underlying errors is reasonably normal. Therefore, the proposed kinetic model could be considered as "correct" since two adequacy check assumptions

which are the normality and interdependent distribution of the errors are satisfactorily met (Montgomery, 2008).

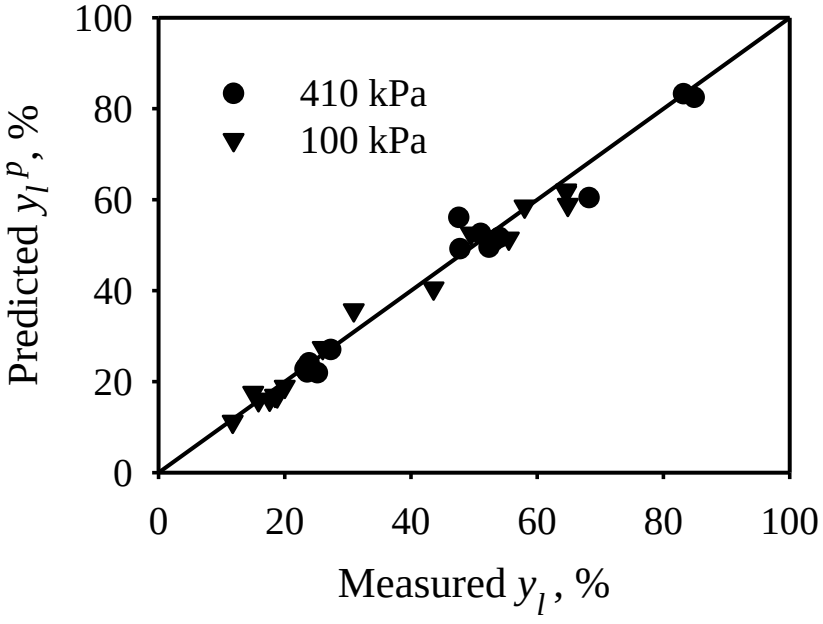

Figure 5-11: Model predictions vs. experimental data

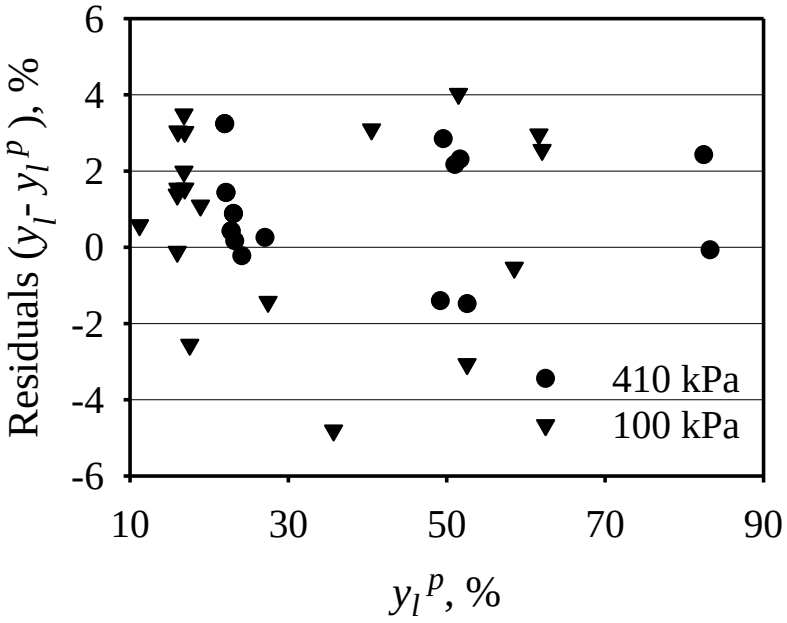

Figure 5-12: Residuals versus predicted values

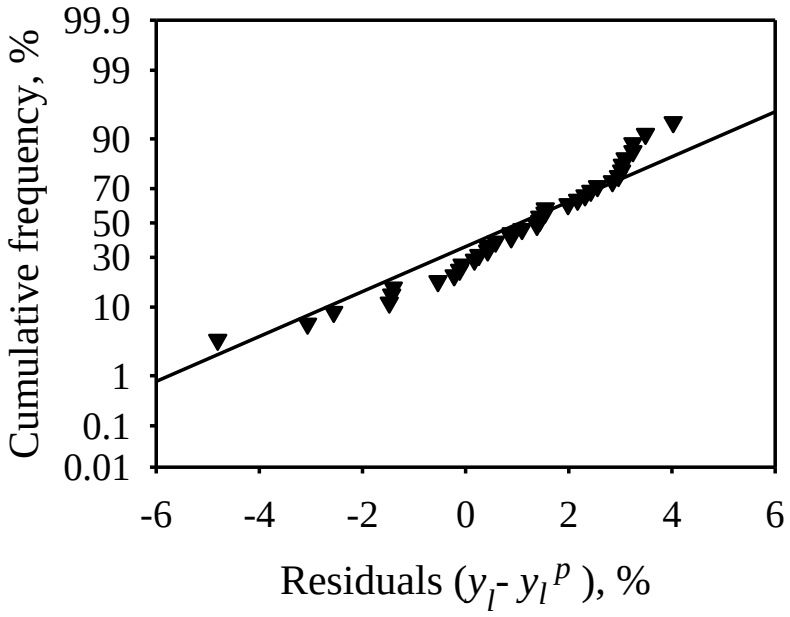

Figure 5-13: Normal probability plot of the residuals

5.7 Conclusions

The model predicted trends for catalyst oxidation state helped better understanding of the observed VPP redox behaviour under transient regimes and higher pressure. Despite its simple mechanism of three elementary reactions, the proposed kinetic model was found to successfully predict the observed experimental trends. The model adequacy was assessed by means of errors distribution pattern and residuals normality check. The predicted range of confidence for the model parameters (Figure 5-4) suggests that the same kinetic model could be applied for the ambient and high pressure conditions. Moreover, the model validity for a relatively wide range of redox feed compositions makes it applicable to predict catalytic performance in fixed bed, fluidized bed and CFB reactors.

The reactor pressure significantly affects the VPP catalytic activity. Up to 60 % increase in n-butane conversion, 100 % in oxygen conversion and 35 % in CO_x selectivity was observed by elevating the reactor pressure to 410 kPa. MA selectivity dropped by about 20 %. However, the

overall MA yield was improved by up to 30 %. According to the model predictions, the observed effect of pressure could be primarily attributed to the changes in catalyst oxidation state, reaction rates and the activation energies. As the pressure increases, the catalyst oxidation state is affected depending on the feed composition. The catalyst is more oxidized at higher pressures provided that there is adequate oxygen in the feed. It is important to note that while operating at fuel rich feed conditions (O_2/C_4H_{10} = 1.1), the catalyst surface tends to be more reduced at higher pressures. This observation highlights the critical need to compensate for catalyst surface oxygen loss to maintain the optimal MA yields and to prevent catalyst over-reduction. In addition to the observed oxidation state effects, an increase in the selective reaction's (5-4) activation energy and the corresponding decrease in its rate constant (k_2) was suggested to be among the identified reasons for the observed drop in MA selectivity. The increase in activation energies by pressure could be attributed to lower catalyst oxidation state at fuel rich conditions.

5.8 Acknowledgements

The authors gratefully appreciate funding of this research project by the Natural Sciences and Engineering Research Council of Canada (NSERC), Ministère du Développement Economique, de l'Innovation et de l'Exportation (MDEIE) of Quebec and the Canadian Foundation for Innovation (CFI) as well as the DuPont Company for providing the VPP catalyst samples.

5.9 Nomenclature

CO_x	Averaged property between CO and CO_2
C_{SO_2}	Surface oxygen concentration, mol/mg
C_{ST}	Total concentration of surface sites, mol/mg
CSTR	Continuously Stirred Tank Reactor
C_T	Total gas concentration, mol/mL
E_i	i^{th} reaction activation energy, kJ/mol
ΔE_i	i^{th} activation energy difference, %

$E(t)$	Residence time distribution, s^{-1}
$E(\theta)$	Normalized residence time distribution = $\bar{t}E(t)$
F_{0Ar}	Initial molar flow rate of argon, mol/s
F_j	Molar flow rate of component *j* in general form, mol/s
$F_{j1}(t)$	Inlet molar flow rate function for component *j*, mol/s
$F_{j,n}(t)$	Molar flow rate of component *j* entering n^{th} sub-section, mol/s
$F_j(t,n)$	Molar flow rate of component *j* at time *t* entering sub-section *n*, mol/s
$F_7(0,n)$	Molar flow rate of argon at time zero entering sub-section *n*, mol/s
F_T	Total molar flow rate, mol/s
$F_{T1}(t)$	Inlet total molar flow rate function, mol/s
$F_T(t,n)$	Total molar flow at time *t* entering sub-section *n*, mol/s
k_i	i^{th} reaction rate constant, s^{-1}
k_{r_i}	i^{th} reference reaction rate constant, s^{-1}
n	Index representing the n^{th} catalyst bed or blank sub-section
N	Total number of tanks in series
N_r	Number of tanks in series for catalyst bed
$O_2 \cdot S$	Catalyst's oxidized site
O_2/C_4H_{10}	Oxygen to n-butane molar ratio
Pe	Peclet number = $2(N\text{-}1)$
r_i	i^{th} transient reaction rate, mol/mg.s
R	Universal gas constant = 8.314 J/mol.K
R_l^2	R-square of fit for data point *l*, Equation (5-25)
$R_j(t,n)$	Global reaction rate of component *j* at time *t* and sub-section *n*, mol/mg.s
S	Catalyst's reduced site

S_{CO_x}	CO_x selectivity, %
S_{MA}	Maleic anhydride selectivity, %
STP	Standard Temperature and Pressure
t	Time, s
$\bar{t}$	Gas residence time, s
T	Reaction temperature, K
T_r	Reference reaction temperature = 653.15 K
u_g	Superficial gas velocity, cm/s
V^{4+}, V^{5+}	Vanadium oxidation states
$V(n)$	Gas phase volume at n^{th} sub-section, mL
$W(n)$	Catalyst weight at n^{th} bed sub-section, mg
$X_{C_4H_{10}}$	n-Butane conversion, %
X_{O_2}	Oxygen conversion, %
y_l	Experimental value for data point l, %
y_l^p	Predicted value for data point l, %
$\bar{y}_l$	Average value of all experimental values for data point l, %

Greek letters

θ	Normalized time, $t/\bar{t}$
θ_{O_2}	Oxygen surface coverage, %
θ_{0O_2}	Initial catalyst surface oxygen coverage, %
$\theta_{O_2}(t,n)$	Oxygen surface coverage at time t and bed sub-section n, %
v_{ij}	Stoichiometric coefficient for component j in i^{th} reaction

σ^2	Variance of *E(t)* curve, s^2
σ_θ^2	Variance of *E(θ)* curve
Φ_{fmin}	Objective function for minimization method
Φ_{lsq}	Objective function for least square method

Subscripts and superscripts

i	Number of reactions
j	Components: C_4H_{10}, O_2, MA, H_2O, CO, CO_2 and Ar
l	$X_{C_4H_{10}}, X_{O_2}, S_{MA}$ and S_{CO_x}
m	Number of experiments
p	Predicted values

5.10 References

Ballarini N., Cavani F., Cortelli C., Ligi S., Pierelli F., Trifirò F., Fumagalli C., Mazzoni G. and Monti T., "VPO catalyst for n-butane oxidation to maleic anhydride: A goal achieved, or a still open challenge?", Topics in Catalysis, 2006, 38, 1-3, 147-156.

Bej S. K., Rao M. S., "Selective Oxidation of n-Butane to Maleic Anhydride. 3. Modelling Studies", Ind. Eng. Chem. Res., 1991, 30, 1829-1832.

Brandstädter W. M., Kraushaar-Czarnetzki B., "Maleic Anhydride from Mixtures of n-Butenes and n-Butane: Simulation of a Production-Scale Nonisothermal Fixed-Bed Reactor", Ind. Eng. Chem. Res., 2007, 46, 1475-1484.

Buchanan J. S., Sundaresan S., “Kinetics and Redox Properties of Vanadium Phosphate Catalysts for Butane Oxidation”, Appl. Catal. 1986, 26, 211-226.

Cavani F., Ligi S., Monti T., Pierelli F., Trifirò F., Albonetti S. and Mazzoni G., “Relationship between structural/surface characteristics and reactivity in n-butane oxidation to maleic anhydride The role of V3+ species”, Catalysis Today, 2000, 61, 203-210.

Emig G., Uihlein K. and Hacker C.-J., “Separation of Catalyst Oxidation and Reduction - An Alternative to the Conventional Oxidation of n-Butane to Maleic Anhydride?” in “New Developments in Selective Oxidation II”, V. Cortés-Corberan and S. Vic Bellon Eds., Elsevier, Amsterdam, 1994, 243-251.

Fogler H. S., “Elements of Chemical Reaction Engineering, Fourth Edition”, Prentice Hall, Boston, MA (2006), pp. 871-885 and 948-955.

Gascón J., Valenciano R., Téllez C., Herguido J. and Menéndez M., “A generalized kinetic model for the partial oxidation of n-butane to maleic anhydride under aerobic and anaerobic conditions”, Chemical Engineering Science, 2006, 61, 6385-6394.

Gleaves J. T., Yablonsky G., Zheng X., Fushimi R., Mills P. L., “Temporal analysis of products (TAP)–Recent advances in technology for kinetic analysis of multi-component catalysts”, J. Mol. Catal., 2010, A 315 (2), 108-134.

Hakimelahi H. R., Sotudeh-Gharebagh R., Mostoufi N., “Cluster-Based Modeling of Fluidized Catalytic Oxidation of n-Butane to Maleic Anhydride”, Int. J. Chem. Reactor Eng., 2006, 4, Article A23.

Huang X.-F., Chen B.-H., Liu B.-J., Silveston P. L. and Li C.-Y., "Re-oxidation kinetics of a VPO catalyst", Catalysis Today, 2002a, 74, 121-130.

Huang X.-F., Li C.-Y., Chen B.-H. and Silveston P. L., "Transient Kinetics of n-Butane Oxidation to Maleic Anhydride over a VPO Catalyst", AIChE Journal, 2002b, 48, 4, 846-855.

Hutchings G. J., "Vanadium phosphate: a new look at the active components of catalysts for the oxidation of butane to maleic anhydride", J. Mater. Chem., 2004, 14, 3385-3395.

Lorences M. J., Patience G. S., Díez F. V. and Coca J., "Butane Oxidation to Maleic Anhydride: Kinetic Modeling and Byproducts", Ind. Eng. Chem. Res., 2003, 42, 6730-6742.

Lorences M. J., Patience G. S., Díez F. V. and Coca J., "Transient n-butane partial oxidation kinetics over VPO", Applied Catalysis A: General, 2004, 263, 193-202.

Lorences M. J., Patience G. S., Cenni R., Díez F. and Coca J., "VPO transient lattice oxygen contribution", Catalysis Today, 2006, 112, 45-48.

Marín P., Hamel C., Ordóñez S., Díez F. V., Tsotsas E., Seidel-Morgenstern A., "Analysis of a fluidized bed membrane reactor for butane partial oxidation to maleic anhydride: 2D modelling", Chemical Engineering Science, 2010, 65, 3538-3548.

Mills P. L., Randall H. T. and McCracken J. S., "Redox kinetics of VOPO4 with butane and oxygen using the TAP reactor system", Chemical Engineering Science, 1999, 54, 3709-3721.

Montgomery D. C., "Design and Analysis of Experiments, Seventh Edition", Wiley, New York, (2008), pp. 75-83.

Mota S., Abon M., Volta J. C. and Dalmon J. A., “Selective Oxidation of n Butane on a V-P-O Catalyst: Study under Fuel-Rich Conditions”, Journal of Catalysis, 2000, 193, 308-318.

Patience G. S. and Lorences M. J., “VPO Transient Oxidation Kinetics”, Int. J. Chem. Reactor Eng., 2006, 4, Article A22.

Patience G. S., Bockrath R. E., Sullivan J. D. and Horowitz H. S., “Pressure Calcination of VPO Catalyst”, Ind. Eng. Chem. Res., 2007, 46, 4374-4381.

Patience G. S. and Bockrath R. E., “Butane oxidation process development in a circulating fluidized bed”, Applied Catalysis A: General, 2010, 376, 4-12.

Rodemerck U., Kubias B., Zanthoff H.-W., Wolf G.-U. and Baerns M., “The reaction mechanism of the selective oxidation of butane on (VO)2P2O7 catalysts: The influence of the valence state of vanadium”, Applied Catalysis A: General, 1997, 153, 217-231.

Schuurman Y. and Gleaves J. T., “Activation of Vanadium Phosphorus Oxide Catalysts for Alkane Oxidation. The Influence of the Oxidation State on Catalyst Selectivity”, Ind. Eng. Chem. Res., 1994, 33, 2935-2941.

Schuurman Y. and Gleaves J. T., “A comparison of steady-state and unsteady-state reaction kinetics of n-butane oxidation over VPO catalysts using a TAP-2 reactor system”, Catalysis Today, 1997, 33, 25-37.

Shekari A. and Patience G. S., “Maleic anhydride yield during cyclic n-butane/oxygen operation”, Catalysis Today, 2010, 157, 334-338.

Shekari A. and Patience G. S., “Transient Redox Activity of Vanadyl Pyrophosphate at Ambient and Elevated Pressure”, Submitted to Int. J. Chem. Reactor Eng., February 2011.

Taufiq-Yap Y. H., Goh C. K., Hutchings G. J., Dummer N. and Bartley J., “Dependence of n-Butane Activation on Active Site of Vanadium Phosphate Catalysts”, Catal. Lett., 2009, 130, 327-334.

Volta J.-C., “Vanadium phosphorus oxides, a reference catalyst for mild oxidation of light alkanes: a review”, C. R. Acad. Sci. Paris, Série IIc, Chimie / Chemistry, 2000, 3, 717-723.

Wang D. and Barteau M. A., “Kinetics of Butane Oxidation by a Vanadyl Pyrophosphate Catalyst”, Journal of Catalysis, 2001, 197, 17-25.

Wang D. and Barteau M. A., “Oxidation kinetics of partially reduced vanadyl pyrophosphate catalyst”, Applied Catalysis A: General, 2002, 223, 205 214.

Wang D. and Barteau M. A., “Differentiation of active oxygen species for butane oxidation on vanadyl pyrophosphate”, Catalysis Letters, 2003, 90, 1-2, 7 11.

GENERAL DISCUSSION

As was discussed in Chapter 1, during the past four decades, there has been an enormous challenge to understand the complex catalytic behaviour of the VPO catalyst under redox conditions. Despite these efforts, considerable controversies remain and the research is still being actively pursued. The catalyst behaviour is even more complicated while operating under transient regimes. Under these conditions, the catalyst surface phases undergo dynamic transformations and the surface oxidation state becomes extremely sensitive to the feed composition. For these reasons, majority of the research studies are focused on the identification of catalyst's active phases and the role of adsorbed or lattice oxygen in surface reactions. It is generally agreed that vanadyl pyrophosphate – $(VO)_2P_2O_7$ – is the catalyst's active phase and presence of limited amounts of oxidized $VOPO_4$ phase (V^{5+}) is essential for optimal catalytic activity. Moreover, the lattice oxygen has been commonly regarded as the selective species with respect to surface adsorbed oxygen. However, its participation in surface reactions has been reported to be limited.

Among the major developments in this field, DuPont commercialized a circulating fluidized bed technology for maleic anhydride production, which primarily relied on catalyst's lattice oxygen as a source of selective oxygen. Findings proved that the VPO is not naturally an efficient oxygen carrier. This suggested that maintaining a high catalytic performance in CFB reactor would depend on providing adequate oxygen to the catalyst in the reaction zone. Other research motivation was to optimize the catalyst regeneration conditions in order to maximize catalyst oxygen transfer to the reaction zone. In this thesis, the findings in fluidized bed sparger experiments as well as the oxygen injection trials in commercial reactor confirmed that the presence and proper distribution of co-feed oxygen in the gas phase during reaction is an absolute requirement to maintain MA productivity. When the oxygen injection point was switched to a lower nozzle, the oxygen contact time with catalyst was longer and the catalyst oxidation state was maintained; as a result, the MA productivity increased by up to 15 %.

Generally, the most important challenge for a selective catalyst has been to keep the VPO surface in an oxidized state during reaction. The situation is more critical while operating at higher n-butane feed concentrations. Under these conditions, the catalyst surface might undergo extensive or sometimes irreversible reduction (V^{5+} to V^{4+} or V^{3+}) which would directly affect the MA selectivity and catalytic activity. In some extreme cases, carbon deposition might occur as a result of long contact times at high n-butane concentrations, which would require intensive treatment during catalyst regeneration. This ultimately affects the process economies by bringing down the production rates. Catalyst deactivation due to excessive catalyst oxidation or irreversible surface crystallization into V^{5+} phases was also mentioned in the literature. Moreover, keeping the surface P/V ratio at optimized values of slightly above 1.0 was emphasized for a selective catalyst.

As a general rule, the oxygen presence in the gas phase during fuel rich conditions has to be given an outmost importance. Oxygen prevents the catalyst from being excessively reduced and maintains the catalytic activity by regenerating the reduced active sites. Moreover, gas phase interaction with surface provides surface oxygen species, which have been identified as the principal source of n-butane activation, and in general sense, the catalyst activity. During the experimental course of this study, these facts were confirmed at several instances. Results indicated that at an equimolar ratio of oxygen to n-butane in the feed, MA production could be maximized. This was related to counteracting negative and positive effects while increasing n-butane concentration in the feed. A higher concentration of n-butane improved the MA productivity while increasing n-butane concentration beyond certain points was accompanied by catalyst reduction and consequently a decrease in MA selectivity. While, having adequate amounts of co-fed oxygen in the feed could compensate for catalyst reduction and therefore the yield could be maximized.

The experiments on the effect of oxidation time on catalytic performance emphasized the importance of adequate catalyst regeneration during redox operations. The effect of catalyst oxidation time was improving irrespective of reduction feed composition. The interesting observation was that even at highly oxidizing feed conditions, which are typical for fixed bed

reactor operations, the MA rate could still be enhanced by extending the catalyst oxidation time. These experiments also showed that the highest improvement in the production was achievable while the feed was purely reducing. Similar observations were reported in the literature (Emig, 1994; Patience and Lorences, 2006). Moreover, in the commercial CFB reactor, there were some speculations that the solids residence time was affected by flow distribution in the regenerator, which could have affected the catalyst regeneration and overall yield. In general, the improvement in MA rates was related to higher oxygen availability at longer oxidation times. A linear correlation was found to exist between MA production rate and the catalyst oxidation time. These experiments highlighted the importance of efficient catalyst regeneration in the CFB reactor where each redox zone could be optimized independently.

The redox experiments showed that n-butane conversion is generally the main contributor to MA yield improvement. The MA selectivity is significantly affected while operating at reducing feed conditions or shorter catalyst regeneration time. A considerable drop in n-butane conversion in the absence of gas phase oxygen might indicate that the surface adsorbed oxygen is mainly responsible for n-butane activation. It might also indicate that the participation of lattice oxygen is not adequate in surface reactions. These observations are in agreement with the literature. The drop in catalytic activity under extremely reducing conditions (pure redox mode) was not compensated even after extensive catalyst re-oxidation. This might show that the presence of oxygen during reaction is more critical than its re-oxidation while working at extremely reducing feed conditions. The catalyst activity loss is such that the MA production rates drop after a few redox cycles. The effect of surface adsorbed oxygen is believed to be significant in preserving the catalytic activity. Their concentration on the surface is directly connected to the presence of gas phase oxygen. These effect were reported by several authors (Wang and Barteau, 2003; Gascón et al., 2006).

The micro-reactor setup coupled to an online MS was shown to be a reliable approach to characterize catalytic redox activity while simulating transient regimes. The catalyst bed was fixed and the reactive streams could be alternated using a switching valve. The reactor flow model was found to be very close to plug flow. The simplicity in the flow model helped

characterize the intrinsic catalytic activity free from hydrodynamic complications. Moreover, due to the small particle size (100-200 µm) and high porosity, as well as the low rate of reactions, the mass transfer limitations could be neglected. The catalyst was shown to preserve its activity after hundreds of redox cycles. This was confirmed by activity measurements under base case conditions after few months of operation. The characteristics of the reactor system and the experimental conditions were such that no carbon deposition was observed during reduction even under the pure reduction mode (no oxygen in the feed) and the shortest re-oxidation time. This was attributed to relatively high superficial gas velocities and gas residence times in the order of a fraction of a second in the catalyst bed. The only major catalyst deactivation was observed during pure redox mode due to catalyst excessive reduction. The reason for using high gas flow rates was primarily a better temperature control and shorter delays in MS responses. Other reasons were around the water and MA delays due to their adsorption on internal tube walls. A higher flow rate helped a faster system purge and eliminated the inward leaks. The mass spectrometer analysis was satisfactory with regard to the frequency of data collection and convenience in operation. While major overlaps between detected mass signals made the data analysis and the calibrations challenging. HPLC was the most reliable instrument; the results helped cross check the conductivity acid measurements. However, only few byproduct acids were detectable at very low quantities. This could be related to the extremely short residence times in the catalyst bed (0.2-0.5 s).

With regard to the kinetic modeling, several mechanisms were found to only partially fit the experimental data. There has been a challenge in the literature to propose a comprehensive mechanism that could cover a wide range of feed compositions. The major complications might arise from dynamic transformations of the catalyst surface phases and unclear role of oxygen species while operating under transient regimes. Some authors such as Gascón et al. (2006) considered rather complicated mechanisms with several equilibrium reactions including adsorption terms as well as sub-surface oxygen diffusion. Including the adsorption terms in the mechanism was not desirable as there was uncertainty around assuming the existence of equilibrium states between gas phase and surface species or between surface adsorbed species under transient conditions. Moreover, it was preferable to avoid proposing a complicated kinetic model with several parameters. Therefore, based on a previous kinetic study (Lorences et al.,

2003, 2004), a single site mechanism of the type Mars-van Krevelen was proposed. The mechanism was found to adequately represent the catalyst redox behaviour by assuming a lumped behaviour for the surface oxidized or reduced sites. It was interesting to note that despite the known complexities in catalytic system, the VPP transient activity could be well represented by a single site redox mechanism.

The effect of pressure on VPP kinetics has been rarely considered in the literature. Since none of the industrial reactors operates at ambient pressure, one objective was to investigate the effect of reactor pressure on VPP redox activity and propose a kinetic model, which could be applicable to higher pressures. Pressure showed a significant effect on VPP activity. The effect was improving with respect to overall MA yield. The MA selectivity dropped by 20 % as the pressure increased to 4.1 bar. This was due to operation at fuel rich conditions, where the catalyst was reduced as the pressure increased. The positive effect of pressure should also be regarded as decreasing the reactor size and increasing the overall productivity by operating at higher n-butane concentrations. The proposed kinetic model successfully predicted the whole range of studied conditions. This range was from oxidizing to reducing feed conditions. The simplicity of the kinetic model was believed to make it conveniently applicable to reactor design of the transient catalytic systems involving redox mechanisms.

CONCLUSIONS AND RECOMMENDATIONS

Conclusions

The principal objective of this research thesis has been to characterize and optimize the redox activity of VPP catalyst under transient regimes as well as to propose a kinetic model, which could be applicable to the wide range of redox conditions inducing higher reactor pressure. To achieve this objective, the research study was conducted under four categories: 1) analysis of catalyst performance data in fluidized bed and commercial reactor, 2) optimization of MA rates in lab scale micro-reactor, 3) studying the effect of pressure on VPP transient activity and 4) developing a transient kinetic model.

The reactor performance data from fluidized bed sparger experiments showed that the VPP catalytic activity is extremely sensitive to reactor feed configuration. The MA production rate was improved as the n-butane and oxygen feed streams were closer to each other. The MA production was the highest when n-butane and oxygen were co-fed through the distributor under fuel rich conditions. The same effect was observed in the commercial reactor. As the oxygen injection point was switched from the middle to the lower nozzle (1.5 m below), about 15 % improvement in MA production rate was observed. These results show that keeping the catalyst at an oxidized state is essential to maintain high MA productivities. This could be achieved by supplying additional oxygen to the reaction zone especially at high n-butane concentrations and allowing for adequate contact time between catalyst and oxygen to prevent catalyst excessive reduction. These experiments showed that the operation of an industrial CFB reactor could be significantly improved only by adding more oxygen to the recycle stream entering the lower section of the fast bed reactor.

According to the micro-reactor experiments, the MA rates were found to primarily depend on feed composition and catalyst regeneration time. A linear correlation was observed between MA productivity and catalyst oxidation time. Irrespective of the feed composition, up to 50 % increase in MA yield was observed by increasing the oxidation time from 0.3 to 10 minutes. Even

at highly oxidizing feed compositions, typical of fixed bed operations, the MA yield could be enhanced by extending the catalyst oxidation time. The effect of catalyst oxidation time on MA production rate was more significant at higher n-butane concentrations in the feed. Under pure redox mode, the MA rate increased by a factor of 3.5 as the catalyst oxidation time was extended to 10 minute. These data highlighted the importance of efficient catalyst regeneration during industrial fuel rich operations. They also showed that even at highly oxidizing conditions, the catalytic activity could be improved by efficient catalyst regeneration. Feed composition data showed that there is an optimum equimolar concentration (~ 6 vol. %) for n-butane and oxygen at which the MA production could be maximized. A slight catalyst deactivation under fuel rich conditions was compensated by longer catalyst regeneration. However, at pure redox mode, the catalyst underwent a considerable and rapid deactivation. Even extensive catalyst regeneration could not recover the catalytic activity. These observations reconfirmed the critical role of gas phase oxygen during redox operations at highly reducing conditions.

The VPP catalytic activity was significantly affected by reactor pressure. Up to 60 % increase in n-butane conversion was observed. While, MA selectivity decreased by about 20 %. However, the increase in n-butane conversion improved the overall MA yield by up to 30 %. Data showed that the effect of temperature on catalytic performance is improving at higher pressure and when there was more oxygen in the feed. Therefore, the maximum productivity should be achievable at higher pressures and oxidizing feed conditions. However, the temperature increase has to be limited to some optimized values due to its negative effect on MA selectivity specially under reducing feed conditions.

Redox data at ambient pressure demonstrated that under oxidizing feed conditions, n-butane conversion is the major contributor to the improvement observed for MA yield. MA selectivity showed a strong dependency on catalyst oxidation time under reducing feed compositions and shorter oxidation times. Under these conditions, both n-butane conversion and MA selectivity contributed to any improvement observed in the MA yield. A considerable drop in n-butane conversion in the absence of gas phase oxygen might indicate that the adsorbed oxygen is the main responsible for n-butane activation. Even excessive catalyst regeneration could not

compensate for the observed drop in n-butane conversion. This might also indicate that under fuel rich conditions the participation of surface lattice oxygen in surface reactions is very limited. The presence of adsorbed oxygen originated from gas phase was shown to be critical to maintain adequate n-butane conversion and MA yield while operating at highly reducing feed conditions.

Data also showed that under transient regimes, the MA selectivity increases with n-butane conversion. This trend is opposite to conventional steady state operations where MA selectivity normally decreases by increasing n-butane conversion. The opposite behaviour is attributable to the transient operation in which the reduction and oxidation zones are separate. The data trends also showed that the effect of gas phase oxygen on improving MA selectivity is more noticeable as the catalyst oxidation time is in the range of industrial CFB operation (< 1 min). Under these conditions, a higher slope was observed for MA selectivity vs. n-butane conversion.

In the last part of the thesis, a transient kinetic model was proposed. A single site mechanism of the type Mars-van Krevelen was found to adequately represent the wide range of feed compositions as well as higher reactor pressure. These observations might indicate that despite its complex reactive system, only a single pair of surface active sites (V^{4+}/V^{5+}) could adequately represent the VPP catalytic activity. The predicted trends for transient catalyst oxidation state during reaction were helpful in describing the effect of pressure on catalytic activity. Data showed that the catalyst oxidation state is affected by pressure depending on the feed composition. The catalyst was oxidized at higher pressure while operating under oxidizing feed conditions. However, the catalyst surface was more reduced when n-butane concentration was higher. These findings showed that maintaining the catalyst oxidation state is more critical at higher pressure. The predicted increase in activation energies was attributed to higher concentration of surface reduced sites. This could be the reason for drop in MA selectivity as the pressure increased. Other reason might be the estimated decrease in selective reaction rate constant at higher pressure.

Recommendations

1- Dual site mechanism

Although the proposed kinetic model in this study adequately predicted the observed experimental trends, it could be interesting to investigate the applicability of other simple kinetic models with dual site mechanisms. One suggested mechanism could be described as considering a $VOPO_4$ site which is activated by molecular oxygen and then this activated site oxidizes the principal catalyst phase which is $(VO)_2P_2O_7$ into a selective intermediate phase. The "slightly" oxidized phase undergoes reaction to MA by sharing selective oxygen while the "non-oxidized" active phase participates in non-selective CO_x formation. At the same time, the reduced forms of both selective and non-selective sites are continually regenerated by the gas phase oxygen. The role of $VOPO_4$ phase would be to initialize the redox cycle and keep it running until the deactivation occurs. This mechanism resembles the current picture of VPP catalyst behaviour under redox conditions. The original idea was suggested by Professor Patricio Ruiz from Université Catholique de Louvain in Belgium.

2- Initial oxygen concentration

While studying the transient kinetics, it is extremely important to have a clear idea on initial oxygen concentration on the catalyst surface. This parameter is highly dependent on redox conditions and catalyst's redox history. Thermogravimetric analysis (TGA) is suggested to study the affecting parameters on VPP oxygen storage and surface oxygen concentration as well as to provide correct estimates for these values.

3- Activation energies

The kinetic model in this study predicted an increase in activation energies at higher pressure under reducing feed conditions. Similar effects have been reported in the literature (Schuurman and Gleaves, 1997); however, it seems that the reasons behind this variation are not clearly identified. Findings show that probably an opposite trend between the catalyst oxidation state and the redox activation energies exists. It could be interesting to study the effect of feed composition on activation energy at higher pressures.

4- Byproduct acid profile

A wide range of byproduct acid formation was reported in the literature (Lorences et al., 2003). In this study, the HPLC measurement detected only a number of byproduct acids at very low concentrations (mainly acetic and methacrylic acids as well as some unknown peaks). The reason for limited byproduct formation could be attributed to lower chance of surface adsorbed carbon intermediates to undergo parallel reaction pathways. Identifying the parameters that affect the byproduct acid profile seems to be interesting for further investigation.

5- Carbon formation

In this study, no instance of catalyst deactivation due to carbon deposition was detected. Short gas residence times in the catalyst bed could be the main reason. There are some indications on carbon formation under fuel rich conditions (Patience and Lorences, 2006). The affecting parameters have been identified as n-butane to oxygen ratio and probably higher reactor temperature. It would be interesting to characterize the carbon formation under reducing conditions in an attempt to minimize it during reduction.

6- MS instrument

Due to its high frequency data collection and convenient operation, online MS was proven an efficient instrument for transient redox studies. However, some inherent issues such as peak overlaps and sensitivity variations have to be taken into account while using MS for experiments. Some examples are: mass 28 of n-butane and CO_2 molecules, which overlap with CO main peak at 28. Moreover, MS sensitivity toward different components highly depends on their concentrations as well as the presence of other components in the gas mixture. It is recommended to clearly quantify the overlaps and relative sensitivity (RS) factors for reliable measurements. Other notes are that in transient measurements, water and CO_2 peaks are usually delayed compared to other components (CO, O_2, n-butane, etc.). Moreover, MA peak could never be detected with MS. Some reasons might be low MS sensitivity to MA or its deposition on the connecting lines (b.p. = 202 °C).

BIBLIOGRAPHY

AitLachgar, K., Abon, M., & Volta, J. C. (1997). Selective oxidation of n-butane to maleic anhydride on vanadyl pyrophosphate. 1. Influence of oxidation pretreatments on the catalytic performances. *Journal of Catalysis, 171*(2), 383-390.

Ait-Lachgar, K., Tuel, A., Brun, M., Herrmann, J. M., Krafft, J. M., Martin, J. R., et al. (1998). Selective oxidation of n-butane to maleic anhydride on vanadyl pyrophosphate - II. Characterization of the oxygen-treated catalyst by electrical conductivity, Raman, XPS, and NMR spectroscopic techniques. *Journal of Catalysis, 177*(2), 224-230.

Ballarini, N., Cavani, F., Cortelli, C., Gasparini, F., Mignani, A., Pierelli, F., et al. (2005). The contribution of homogeneous and non-oxidative side reactions in the performance of vanadyl pyrophosphate, catalyst for the oxidation of n-butane to maleic anhydride, under hydrocarbon-rich conditions. *Catalysis Today, 99*(1-2), 115-122.

Ballarini, N., Cavani, F., Cortelli, C., Ligi, S., Pierelli, F., Trifiro, F., et al. (2006a). VPO catalyst for n-butane oxidation to maleic anhydride: A goal achieved, or a still open challenge? *Topics in Catalysis, 38*(1-3), 147-156.

Ballarini, N., Cavani, F., Cortelli, C., Ricotta, M., Rodeghiero, F., Trifiro, F., et al. (2006b). Non-steady catalytic performance as a tool for the identification of the active surface in VPO, catalyst for n-butane oxidation to maleic anhydride. *Catalysis Today, 117*(1-3), 174-179.

Bej, S. K., & Rao, M. S. (1991). Selective Oxidation of Normal-Butane to Maleic-Anhydride. 1. Optimization Studies. *Industrial & Engineering Chemistry Research, 30*(8), 1819-1824.

Bej, S. K., & Rao, M. S. (1991). Selective Oxidation of Normal-Butane to Maleic-Anhydride. 2. Identification of Rate Expression for the Reaction. *Industrial & Engineering Chemistry Research, 30*(8), 1824-1828.

Bej, S. K., & Rao, M. S. (1991). Selective Oxidation of Normal-Butane to Maleic-Anhydride. 3. Modeling Studies. *Industrial & Engineering Chemistry Research, 30*(8), 1829-1832.

Brandstadter, W. M., & Kraushaar-Czarnetzki, B. (2007). Maleic anhydride from mixtures of n-butenes and n-butane: Simulation of a production-scale nonisothermal fixed-bed reactor. *Industrial & Engineering Chemistry Research, 46*(5), 1475-1484.

Buchanan, J. S., & Sundaresan, S. (1986). Kinetics and redox properties of vanadium phosphate catalysts for butane oxidation. *Applied Catalysis, 26*, 211-226.

Cavani, F., Ligi, S., Monti, T., Pierelli, F., Trifiro, F., Albonetti, S., et al. (2000). Relationship between structural/surface characteristics and reactivity in n-butane oxidation to maleic anhydride - The role of V3+ species. *Catalysis Today, 61*(1-4), 203-210.

Cavani, F., Luciani, S., Degli Esposti, E., Cortelli, C., & Leanza, R. (2010a). Surface Dynamics of A Vanadyl Pyrophosphate Catalyst for n-Butane Oxidation to Maleic Anhydride: An In Situ Raman and Reactivity Study of the Effect of the P/V Atomic Ratio. *Chemistry - A European Journal, 16*(5), 1646-1655.

Cavani, F., De Santi, D., Luciani, S., Lofberg, A., Bordes-Richard, E., Cortelli, C., et al. (2010b). Transient reactivity of vanadyl pyrophosphate, the catalyst for n-butane oxidation to maleic anhydride, in response to in-situ treatments. *Applied Catalysis A: General, 376*(1-2), 66-75.

Centi, G., & Trifiro, F. (1984). Some aspects of the control of selectivity in catalytic oxidation on mixed oxides:a review. *Applied Catalysis, 12*(1), 1-21.

Centi, G., Trifiro, F., Ebner, J. R., & Franchetti, V. M. (1988). Mechanistic aspects of maleic anhydride synthesis from C_4 hydrocarbons over phosphorus vanadium oxide. *Chemical Reviews, 88*(1), 55-80.

Chen, B., & Munson, E. J. (2002). Investigation of the mechanism of n-butane oxidation on vanadium phosphorus oxide catalysts: Evidence from isotopic labeling studies. *Journal of the American Chemical Society, 124*(8), 1638-1652.

Chen, D., Bjorgum, E., Christensen, K. O., Holmen, A., & Lodeng, R. (2007). Characterization of Catalysts under Working Conditions with an Oscillating Microbalance Reactor. *Advances in Catalysis, Vol 51, 51*, 351-382.

Contractor, R. M. (1986). EP189261-A1; EP189261-A; JP61191680-A; US4668802-A; CA1234129-A; EP189261-B; DE3665713-G; JP94039469-B2.

Contractor, R. M., Bergna, H. E., Horowitz, H. S., Blackstone, C. M., Malone, B., Torardi, C. C., et al. (1987). Butane oxidation to maleic anhydride over vanadium phosphate catalysts. *Catalysis Today, 1*(1-2), 49-58.

Contractor, R. M., Garnett, D. I., Horowitz, H. S., Bergna, H. E., Patience, G. S., Schwartz, J. T., et al. (1994). A New Commercial-Scale Process for n-Butane Oxidation to Maleic-Anhydride Using a Circulating Fluidized-Bed Reactor. *New Developments in Selective Oxidation II, 82*, 233-242.

Contractor, R. M. (1995). Duponts New Process for n-Butane to Tetrahydrofuran. *Applied Catalysis B: Environmental, 6*(1), N3-N4.

Contractor, R. M., Horowitz, H. S., Sisler, G. M., & Bordes, E. (1997). The effects of steam on n-butane oxidation over VPO as studied in a riser reactor. *Catalysis Today, 37*(1), 51-57.

Contractor, R. M. (1999). Dupont's CFB technology for maleic anhydride. *Chemical Engineering Science, 54*(22), 5627-5632.

Creaser, D., Andersson, B., Hudgins, R. R., & Silveston, P. L. (1999). Transient kinetic analysis of the oxidative dehydrogenation of propane. *Journal of Catalysis, 182*(1), 264-269.

Dowell, D., Gleaves, J. T., & Schuurman, Y. (1997). The nature of the active/selective phase in VPO catalysts and the kinetics of n-butane oxidation. *3rd World Congress on Oxidation Catalysis, 110*, 199-208.

Dubois, J. L., Garrait, D., Legall, A., Bazin, G., Serreau, S., Dubois, J., et al. (2006). FR2880346-A1; WO2006072682-A1; EP1833603-A1; IN200704214-P1; KR2007095899-A; CN101087648-A; US2008139844-A1; JP2008526718-W.

Dummer, N. F., Weng, W. H., Kiely, C., Carley, A. F., Bartley, J. K., Kiely, C. J., et al. (2010). Structural evolution and catalytic performance of DuPont V-P-O/SiO_2 materials designed for fluidized bed applications. *Applied Catalysis A: General, 376*(1-2), 47-55.

Emig, G., Uihlein, K., & Hacker, C. J. (1994). Separation of Catalyst Oxidation and Reduction - an Alternative to the Conventional Oxidation of n-Butane to Maleic-Anhydride. *New Developments in Selective Oxidation II, 82*, 243-251.

Fernandez, J. R., Vega, A., & Diez, F. V. (2010). Partial oxidation of n-butane to maleic anhydride over VPO in a simulated circulating fluidized bed reactor. *Applied Catalysis A: General, 376*(1-2), 76-82.

Fogler, H. S. (2006). Elements of chemical reaction engineering (4th ed., Ch. 13, 14, pp. 871-885, 948-955). Upper Saddle River, NJ: Prentice Hall PTR.

Gascon, J., Tellez, C., Herguido, J., & Menendez, A. (2005). A two-zone fluidized bed reactor for catalytic propane dehydrogenation. *Chemical Engineering Journal, 106*(2), 91-96.

Gascon, J., Tellez, C., Herguido, J., & Menendez, M. (2005). Fluidized bed reactors with two-zones for maleic anhydride production: Different configurations and effect of scale. *Industrial & Engineering Chemistry Research, 44*(24), 8945-8951.

Gascon, J., Valenciano, R., Tellez, C., Herguido, J., & Menendez, M. (2006). A generalized kinetic model for the partial oxidation of n-butane to maleic anhydride under aerobic and anaerobic conditions. *Chemical Engineering Science, 61*(19), 6385-6394.

Gleaves, J. T., Yablonskii, G. S., Phanawadee, P., & Schuurman, Y. (1997). TAP-2: An interrogative kinetics approach. *Applied Catalysis A: General, 160*(1), 55-88.

Gleaves, J. T., Yablonsky, G., Zheng, X. L., Fushimi, R., & Mills, P. L. (2010). Temporal analysis of products (TAP)-Recent advances in technology for kinetic analysis of multi-component catalysts. *Journal of Molecular Catalysis A: Chemical, 315*(2), 108-134.

Golbig, K. G., & Werther, J. (1997). Selective synthesis of maleic anhydride by spatial separation of n-butane oxidation and catalyst reoxidation. *Chemical Engineering Science, 52*(4), 583-595.

Hakimelahi, H. R., Sotudeh-Gharebagh, R., & Mostoufi, N. (2006). Cluster-based modeling of fluidized catalytic oxidation of n-butane to maleic anhydride. *International Journal of Chemical Reactor Engineering, 4*, Article A23.

Havecker, M., Mayer, R. W., Knop-Gericke, A., Bluhm, H., Kleimenov, E., Liskowski, A., et al. (2003). In situ investigation of the nature of the active surface of a vanadyl pyrophosphate catalyst during n-butane oxidation to maleic anhydride. *Journal of Physical Chemistry B, 107*(19), 4587-4596.

Havecker, M., Knop-Gericke, A., Bluhm, H., Kleimenov, E., Mayer, R. W., Fait, M., et al. (2004). Dynamic surface behaviour of VPO catalysts under reactive and non-reactive gas compositions: an in situ XAS study. *Applied Surface Science, 230*(1-4), 272-282.

Herguido, J., Menendez, M., & Santamaria, J. (2005). On the use of fluidized bed catalytic reactors where reduction and oxidation zones are present simultaneously. *Catalysis Today, 100*(1-2), 181-189.

Huang, X. F., Li, C. Y., Chen, B. H., Qiao, C. Z., & Yang, D. H. (2001). Investigation of the unsteady-state oxidation of n-butane to maleic anhydride in fixed-bed reactors. *Industrial & Engineering Chemistry Research, 40*(3), 768-773.

Huang, X. F., Chen, B. H., Liu, B. J., Silveston, P. L., & Li, C. Y. (2002a). Re-oxidation kinetics of a VPO catalyst. *Catalysis Today, 74*(1-2), 121-130.

Huang, X. F., Li, C. Y., & Chen, B. H. (2002b). Transient kinetics of n-butane oxidation to maleic anhydride over a VPO catalyst. *AIChE Journal, 48*(4), 846-855.

Hutchenson, K. W., La Marca, C., Patience, G. S., Laviolette, J. P., & Bockrath, R. E. (2010). Parametric study of n-butane oxidation in a circulating fluidized bed reactor. *Applied Catalysis A: General, 376*(1-2), 91-103.

Hutchings, G. J. (1991). Effect of Promoters and Reactant Concentration on the Selective Oxidation of n-Butane to Maleic-Anhydride Using Vanadium Phosphorus Oxide Catalysts. *Applied Catalysis, 72*(1), 1-32.

Hutchings, G. J. (2004). Vanadium phosphate: a new look at the active components of catalysts for the oxidation of butane to maleic anhydride. *Journal of Materials Chemistry, 14*(23), 3385-3395.

Johansson, E., Lyngfelt, A., Mattisson, T., & Johnsson, F. (2003). Gas leakage measurements in a cold model of an interconnected fluidized bed for chemical-looping combustion. *Powder Technology, 134*(3), 210-217.

Jordan, S. P., & Jordan, S. J. (1989). EP320904-A1; US4801731-A; EP320904-A; JP2000258-A; EP320904-B1; DE3877730-G.

Kamiya, Y., Nishikawa, E., Okuhara, T., & Hattori, T. (2001). Catalytic property of vanadyl pyrophosphates for selective oxidation of n-butane at high n-butane concentrations. *Applied Catalysis A: General, 206*(1), 103-112.

Keil, F. J. (1999). Methanol-to-hydrocarbons: process technology. [Review]. *Microporous and Mesoporous Materials, 29*(1-2), 49-66.

Kirk, R. E., & Othmer, D. F. (2001). Encyclopedia of chemical technology, *Maleic anhydride, maleic acid, and fumaric acid* (4th ed., Vol. 15, pp. 1-49). New York: Wiley InterScience.

Kleimenov, E., Bluhm, H., Havecker, M., Knop-Gericke, A., Pestryakov, A., Teschner, D., et al. (2005). XPS investigations of VPO catalysts under reaction conditions. *Surface Science, 575*(1-2), 181-188.

Kubias, B., Rodemerck, U., Zanthoff, H. W., & Meisel, M. (1996). The reaction network of the selective oxidation of n-butane on $(VO)_2P_2O_7$ catalysts: Nature of oxygen containing intermediates. *Catalysis Today, 32*(1-4), 243-253.

Liang, R. Z., Li, Y. X., Li, C. Y., Chen, B. H., & Hu, S. Y. (2003). On-line mass spectroscopic transient measurement of vanadium-phosphorous oxide re-oxidation. *Chinese Journal of Catalysis, 24*(11), 881-884.

Liu, H. C., & Zhang, S. H. (2010). Relationship between the Structures of Metal Oxide Catalysts and Their Properties in Selective Oxidation of Light Alkanes. *Acta Physico-Chimica Sinica, 26*(4), 895-907.

Lorences, M. J., Patience, G. S., Diez, F. V., & Coca, J. (2003). Butane oxidation to maleic anhydride: Kinetic modeling and byproducts. *Industrial & Engineering Chemistry Research, 42*(26), 6730-6742.

Lorences, M. J., Patience, G. S., Diez, F. V., & Coca, J. (2004). Transient n-butane partial oxidation kinetics over VPO. *Applied Catalysis A: General, 263*(2), 193-202.

Lorences, M. J., Patience, G. S., Cenni, R., Diez, F., & Coca, J. (2006). VPO transient lattice oxygen contribution. *Catalysis Today, 112*(1-4), 45-48.

Mallada, R., Sajip, S., Kiely, C. J., Menendez, M., & Santamaria, J. (2000). Influence of the reaction atmosphere on the characteristics and performance of VPO catalysts. *Journal of Catalysis, 196*(1), 1-7.

Marin, P., Hamel, C., Ordonez, S., Diez, F. V., Tsotsas, E., & Seidel-Morgenstern, A. (2010). Analysis of a fluidized bed membrane reactor for butane partial oxidation to maleic anhydride: 2D modelling. *Chemical Engineering Science, 65*(11), 3538-3548.

Miller, L. W. (2000). US6166282-B; US6166282-A; CA2316325-A1; AU200053491-A; NO200004156-A; NL1015957-C2; AU770811-B2; IN200000742-I1; CA2316325-C; IN210795-B; GC138-B.

Mills, P. L., Randall, H. T., & McCracken, J. S. (1999). Redox kinetics of $VOPO_4$ with butane and oxygen using the TAP reactor system. *Chemical Engineering Science, 54*(15-16), 3709-3721.

Montgomery, D. C. (2008). Design and analysis of experiments (7th ed., pp. 75-83). Hoboken, NJ: Wiley.

Mota, S., Abon, M., Volta, J. C., & Dalmon, J. A. (2000). Selective oxidation of n-butane on a V-P-O catalyst: Study under fuel-rich conditions. *Journal of Catalysis, 193*(2), 308-318.

Mota, S., Miachon, S., Volta, J. C., & Dalmon, J. A. (2001). Membrane reactor for selective oxidation of butane to maleic anhydride. *Catalysis Today, 67*(1-3), 169-176.

Patience, G. S., & Lorences, M. J. (2006). VPO transient oxidation kinetics. *International Journal of Chemical Reactor Engineering, 4*, Article A22.

Patience, G. S., Bockrath, R. E., Sullivan, J. D., & Horowitz, H. S. (2007). Pressure calcination of VPO catalyst. *Industrial & Engineering Chemistry Research, 46*(13), 4374-4381.

Patience, G. S., Godefroy, A., Tzakova, T., Garrait, D., & Dubois, J. L. (2009). Reactor Technologies for Propane Partial Oxidation to Acrylic Acid. *Chemical Engineering & Technology, 32*(3), 373-379.

Patience, G. S., & Bockrath, R. E. (2010). Butane oxidation process development in a circulating fluidized bed. *Applied Catalysis A: General, 376*(1-2), 4-12.

Perez-Moreno, L., Irusta, S., Soler, J., Herguido, J., & Menendez, M. (2009). Effect of the use in circulating fluidized bed on the performance of a VPO catalyst: Characterization and transient studies. *Chemical Engineering Journal, 147*(2-3), 330-335.

Rodemerck, U., Kubias, B., Zanthoff, H. W., & Baerns, M. (1997a). The reaction mechanism of the selective oxidation of butane on $(VO)_2P_2O_7$ catalysts: The role of oxygen in the reaction chain to maleic anhydride. *Applied Catalysis A: General, 153*(1-2), 203-216.

Rodemerck, U., Kubias, B., Zanthoff, H. W., Wolf, G. U., & Baerns, M. (1997b). The reaction mechanism of the selective oxidation butane on $(VO)_2P_2O_7$ catalysts: The influence of the valence state of vanadium. *Applied Catalysis A: General, 153*(1-2), 217-231.

Rownaghi, A. A., Taufiq-Yap, Y. H., & Rezaei, F. (2009). Influence of Rare-Earth and Bimetallic Promoters on Various VPO Catalysts for Partial Oxidation of n-Butane. *Catalysis Letters, 130*(3-4), 504-516.

Rubio, O., Mallada, R., Herguido, J., & Menendez, M. (2002). Experimental study on the oxidation of butane to maleic anhydride in a two-zone fluidized bed reactor. *Industrial & Engineering Chemistry Research, 41*(21), 5181-5186.

Ryden, M., Lyngfelt, A., & Mattisson, T. (2006). Synthesis gas generation by chemical-looping reforming in a continuously operating laboratory reactor. *Fuel, 85*(12-13), 1631-1641.

Sakakini, B. H., Taufiq-Yap, Y. H., & Waugh, K. C. (2000). A study of the kinetics and mechanism of the adsorption and anaerobic partial oxidation of n-butane over a vanadyl pyrophosphate catalyst. *Journal of Catalysis, 189*(2), 253-262.

Schuurman, Y., & Gleaves, J. T. (1994). Activation of Vanadium Phosphorus Oxide Catalysts for Alkane Oxidation - the Influence of the Oxidation-State on Catalyst Selectivity. *Industrial & Engineering Chemistry Research, 33*(12), 2935-2941.

Schuurman, Y., Gleaves, J. T., Jr, E., & Mummey, M. J. (1994). Activation of Vanadium Phosphorus Oxide Catalysts for Alkane Oxidation Oxygen Storage and Catalyst Performance. *New Developments in Selective Oxidation II, 82*, 203-212.

Schuurman, Y., & Gleaves, J. T. (1997). A comparison of steady-state and unsteady-state reaction kinetics of n-butane oxidation over VPO catalysts using a TAP-2 reactor system. *Catalysis Today, 33*(1-3), 25-37.

Shekari, A., Patience, G. S., & Bockrath, R. E. (2010). Effect of feed nozzle configuration on n-butane to maleic anhydride yield: From lab scale to commercial. *Applied Catalysis A: General*, *376*(1-2), 83-90.

Shekari, A., & Patience, G. S. (2010). Maleic anhydride yield during cyclic n-butane/oxygen operation. *Catalysis Today*, *157*(1-4), 334-338.

Shekari, A., & Patience, G. S. (February 2011). Transient Redox Activity of Vanadyl Pyrophosphate at Ambient and Elevated Pressure. *Submitted to: International Journal of Chemical Reactor Engineering*.

Song, N. X., Xuan, Z. Q., Bartley, J. K., Taylor, S. H., Chadwick, D., & Hutchings, G. J. (2006). Oxidation of butane to maleic anhydride using vanadium phosphate catalysts: comparison of operation in aerobic and anaerobic conditions using a gas-gas periodic flow reactor. *Catalysis Letters*, *106*(3-4), 127-131.

SRI Consulting. (January 2011). World Petrochemicals Program. Retrieved July 27, 2011, from http://www.sriconsulting.com/WP/Public/Reports/ma/

TaufiqYap, Y. H., Sakakini, B. H., & Waugh, K. C. (1997). Investigation of the nature of the oxidant (selective and unselective) in/on a vanadyl pyrophosphate catalyst. *Catalysis Letters*, *48*(1-2), 105-110.

Taufiq-Yap, Y. H., Goh, C. K., Hutchings, G. J., Dummer, N., & Bartley, J. (2009). Dependence of n-Butane Activation on Active Site of Vanadium Phosphate Catalysts. *Catalysis Letters*, *130*(3-4), 327-334.

Turk, B., & Schlather, J. (2006). Paper presented at the Gasification Technologies Conference. Retrieved July 27, 2011, from http://www.gasification.org/uploads/downloads/Conferences/2006/53SCHL.pdf

Volta, J. C. (2000). Vanadium phosphorus oxides, a reference catalyst for mild oxidation of light alkanes: a review. *Comptes Rendus De L Academie Des Sciences Serie II Fascicule C-Chimie*, *3*(9), 717-723.

Wang, D. X., Kung, H. H., & Barteau, M. A. (2000). Identification of vanadium species involved in sequential redox operation of VPO catalysts. *Applied Catalysis A: General*, *201*(2), 203-213.

Wang, D. X., & Barteau, M. A. (2001). Kinetics of butane oxidation by a vanadyl pyrophosphate catalyst. *Journal of Catalysis*, *197*(1), 17-25.

Wang, D. X., & Barteau, M. A. (2002). Oxidation kinetics of partially reduced vanadyl pyrophosphate catalyst. *Applied Catalysis A: General*, *223*(1-2), 205-214.

Wang, D. X., & Barteau, M. A. (2003). Differentiation of active oxygen species for butane oxidation on vanadyl pyrophosphate. *Catalysis Letters*, *90*(1-2), 7-11.

Xue, Z. Y., & Schrader, G. L. (1999). Transient FTIR studies of the reaction pathway for n-butane selective oxidiation over vanadyl pyrophosphate. *Journal of Catalysis*, *184*(1), 87-104.

APPENDIX A – EFFECT OF FEED NOZZLE CONFIGURATION ON N-BUTANE TO MALEIC ANHYDRIDE YIELD: FROM LAB SCALE TO COMMERCIAL

This article was published in Applied Catalysis A: General, Volume: 376, Year: 2010, Pages: 83-90, the Special Issue on "International VPO Workshop".

A.1 Presentation of the article

This article presents the analysis on the experimental data collected in a 9 cm fluidized bed reactor as well as the MA production rates in DuPont's commercial scale CFB reactor. The objective was to demonstrate the effect of feed configuration and providing additional oxygen to the reaction zone on the reactor performance. The fluidized bed reactor was equipped with a feed sparger adjustable at different bed heights. The commercial reactor had the provisions to inject oxygen through side nozzles. The results showed that a higher MA yield could be achieved when the sparger was closer to the distributor or when oxygen was co-fed with n-butane through distributor. The industrial data confirmed that the MA productivity could be improved by 15 % only by injecting additional oxygen in the lower section of the reaction zone.

These data showed that the VPP catalyst is extremely sensitive to the feed composition. Keeping the VPP surface in an oxidized state was found to be the key factor in maintaining high MA production rates. The entire experimental work presented in this paper was conducted in DuPont's experimental and commercial facilities by the co-authors. The literature study, data analysis, discussions and conclusions were performed by the first author. The motivation was the significant relevancy of these data to the research scope of this thesis. The analyses helped better understanding of VPP redox behaviour in response to redox conditions at different reactor scales.

Effect of Feed Nozzle Configuration on n-Butane to Maleic Anhydride Yield: From Lab Scale to Commercial

Ali Shekari, Gregory S. Patience, Richard E. Bockrath

A.2 Abstract

In the process to produce maleic anhydride via the partial oxidation of n-butane, selectivity is sensitive to feed gas configuration of both oxygen and n-butane. Based on laboratory scale fluidized bed experiments, selectivity was superior when the n-butane was co-fed together with oxygen. When the oxygen and n-butane were fed separately through a distributor and a sparger, selectivity was highest when the sparger was closest to the distributor (independent of whether the n-butane was fed through the sparger and the oxygen through the distributor or vice-versa). Various feed gas configurations were tested in a 4.2 m diameter commercial circulating fluidized bed reactor equipped with 926 spargers at three different levels. Maleic acid production rate increased by about 15 % when oxygen was fed to a lower sparger 0.45 m above the distributor compared to when it was fed at a height of 1.9 m. These observations indicate that maintaining the catalyst in an atmosphere containing oxygen is important for overall n-butane conversion and maleic anhydride selectivity.

Keywords: maleic anhydride, n-butane partial oxidation, vanadyl pyrophosphate, VPO, fluidized bed, circulating fluidized bed, oxygen sparger

A.3 Introduction

Maleic anhydride is commercially produced by the partial oxidation of n-butane over Vanadyl Pyrophosphate (VPP) catalyst in both fixed bed and fluidized bed reactors. DuPont commercialized a Circulating Fluidized Bed (CFB) process whereby the catalyst active phase, $(VO)_2P_2O_7$ (V^{4+}), was partly oxidized by air in a fluidized bed regenerator to $VOPO_4$ (V^{5+}). The partly oxidized catalyst was then transferred to a transport bed reactor where it was reduced in an

n-butane rich feed stream. This configuration could achieve higher yields (defined as the product of conversion and selectivity or equivalently the maleic production rate divided by the feed rate of n-butane), conversion and superior economies of scale due to the higher n-butane concentrations and recycle of unreacted n-butane [1-3].

One key features of the CFB technology is the ability of the VPP catalyst to transfer oxygen from the oxidation zone to the reduction zone. The amount of oxygen that can be incorporated into the catalyst lattice determines the maximum production rate possible in a pure redox mode (The pure redox mode refers to operation when molecular oxygen is absent in the reduction step). However, since the oxygen transfer capability of the VPP catalyst is limited [3-5], the overall process yield of the redox mode is low. As a consequence of limited oxygen transfer by the catalyst, extremely high solids recirculation rate in the reactor would be required to ensure economic production rates. Emig et al. [6] reported that solid recirculation rate of 650 kg/s would be required to ensure supplying sufficient oxygen for a production rate of 20,000 tons/year of maleic anhydride; this corresponds approximately to the production of one gram maleic anhydride per kilogram of the catalyst. Wang et al. [4] also predicted that the maximum possible oxygen that could be stored in the VPP catalyst was 990 μg O_2/mg and the available catalyst oxygen for the reaction could be increased by increasing n-butane concentrations in the feed. However in practice, the oxygen transfer ability of the catalyst is mostly limited by oxidation kinetics and depends on the operating conditions.

Improving the reactor performance for the production of maleic anhydride has been the subject of several research studies. Different reactor configurations and catalyst modifications have been proposed. The catalyst modifications include improving the catalyst oxygen storage capacity by adding suitable doping elements to the catalyst structure or improvement of the physico-chemical properties by using a support [7]. Modifications in the reactor design include using alternative reactor types such as membrane reactors [8] or provisions to maintain the catalyst in an oxidized state in fluidized bed reactors. Controlling the oxygen availability inside the reactor is achievable by distributed feeding or separation of oxidation and reduction zones [9-11]. Different feed sparger configurations have also been proposed in the patent literature that ensures uniform

distribution of the oxygen in the bed [12]. As a practical solution, in large scale reactors, gas phase oxygen is preferably co-fed with n-butane feed to maintain high catalyst oxidation states and prevent the catalyst from becoming overly reduced. As a result, higher production rates may be achievable and the catalyst inventory or the catalyst recirculation rate could be reduced. The primary objective in all studies has been to improve the process economics by decreasing the operational costs and increasing maleic anhydride production rates.

Oxygen treatment of VPP catalyst has been reported to improve maleic anhydride yield. In a recent study, we observed that even under oxidizing reaction conditions (1.4 vol. % n-butane in air), soaking catalyst in air for 10 minutes increases maleic anhydride production rate to greater than 50 % [13]. Schuurman and Gleaves [14] also reported higher production rates and maleic anhydride selectivity when the catalyst was maintained in a highly oxidized state. Emig et al. [6] observed that under cyclic redox operating conditions, maleic anhydride production rate increased by a factor of three when the regeneration duration was increased from 30 minutes to 18 hours. During their transient kinetics experiments, Patience et al. [2] observed a high level of n-butane conversion and maleic anhydride selectivity during the first few minutes after exposing the catalyst to reducing conditions. These observations show that the maleic anhydride selectivity is directly affected by the oxygen availability in the reactor. The literature clearly demonstrates that maintaining high yields depends on the catalyst oxygen treatment history or the oxygen availability during reaction.

Studies show that maleic anhydride selectivity decreases by increasing n-butane concentrations in the feed [2, 15]. Furthermore, at higher n-butane concentrations (5-10 %), incremental increases in hydrocarbon in the feed may lead to a decrease in maleic anhydride production due to a greater than proportionate drop in selectivity. Selectivity decrease is probably due to lower catalyst oxidation state. Direct injection of gas phase oxygen into the reaction bed through additional feed spargers might be a solution to maintain the catalyst oxidation state at a higher level and to prevent excessive catalyst reduction in the reactor. However, to achieve design production rates in an industrial scale reactor, increasing the oxygen concentration in the feed is reported to be practically limited by gas phase combustion and thermal runaways at the exit of the reactor [16].

Therefore, a proper configuration of the oxygen and hydrocarbon feeds in the reaction bed might be helpful to minimize such effects by uniformly distributing the reactants in the bed.

Feed sparger configuration has shown to have a significant impact on the reactor performance and some work has been described in the patent literature. In particular, Jordan [12] modified the fuel sparger geometry of an acrylonitrile fluidized bed reactor. The oxidant – air – was fed through the distributor and both ammonia and propylene were introduced to the reactor through a sparger with multiple downward facing nozzles. Feeding the oxidant and hydrocarbon separately in the bed permits higher concentrations since the reactants contact the solid catalyst that acts as a diluent as well as a free radical trap. When the two streams are poorly mixed, combustion may take place resulting in lower yields. The optimum configuration described in the patent involved placing a downward facing fuel nozzle above every orifice in the distributor plate. The acrylonitrile yield improved by as much as 1 % compared to a random configuration where the nozzles were evenly distributed throughout the bed. The opposing jet feed configuration presumably maintained the gas stream in the optimal stoichiometric ratio for the reaction. Thus, gas phase combustion is limited and the oxidation state of the catalyst may be at the most favourable condition.

In the current work, we have studied the effect of several feed stream configurations on the maleic anhydride production rate in a laboratory scale fluidized bed. We have also reported the effect of oxygen distribution on the performance of DuPont commercial CFB. The objective was to maximize the maleic anhydride production by distributing additional oxygen together with n-butane to minimize catalyst over reduction.

A.4 Experimental

A.4.1 Lab scale fluidized bed

Experimental data were collected in an 89 mm fluidized bed in which n-butane and oxygen were either co-fed through the distributor or sparger or separately into the bed, as shown in Figure A-1.

The sparger was placed at four different heights with four feed configurations: n-butane/nitrogen, air, n-butane/air and n-butane/nitrogen/air mixture.

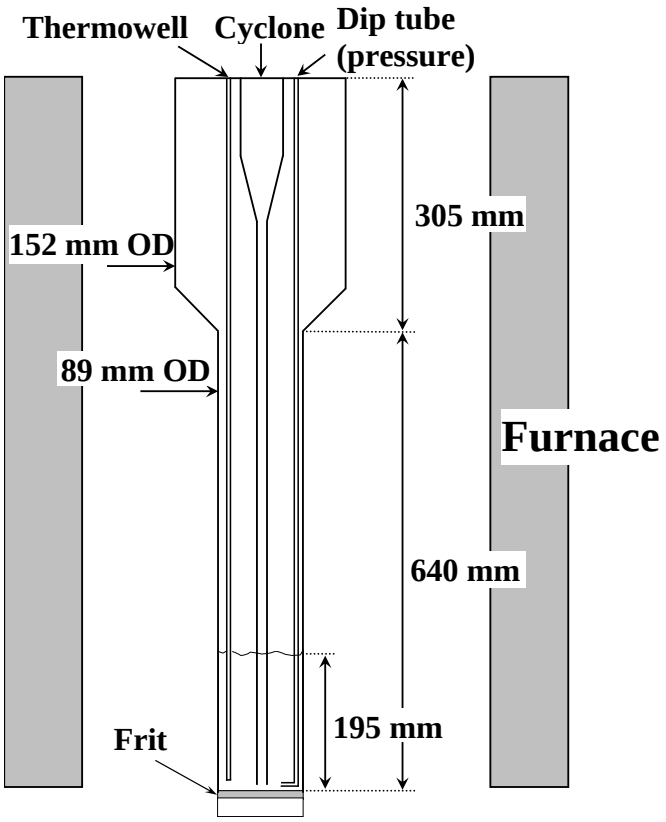

Figure A-1: 89 mm OD fluidized bed reactor

The fluidized bed was made of quartz and had a sintered glass frit as a distributor. The lower section was 89 mm in diameter and 640 mm long. The catalyst disengagement section was 150 mm in diameter and 300 mm long. The attrited catalyst that elutriated out of the bed was accumulated in a glass flask downstream of the internal cyclone. The reactor was placed in an electric furnace and the heat input was controlled based on a thermocouple 150 mm above the catalyst bed. The catalyst bed was 195 mm deep at the operating gas velocity. Three thermocouples measured the bed temperature at heights of 20, 80 and 120 mm and a fifth thermocouple measured the temperature in the annular region between the reactor and furnace

wall (not shown). Brooks mass flow controllers metered the n-butane, air and nitrogen flows. Process gas, fed through the distributor, first passed through a shallow plenum 30 mm deep. A 6.4 mm tube located off center in the reactor was used as a sparger. Glass wool insulations at the top and bottom of the reactor reduced heat losses and helped to maintain isothermal conditions.

The experiments were conducted with DuPont's industrially calcined catalyst that mainly consisted of vanadyl pyrophosphate (VPP). The catalyst precursor (vanadyl hydrogen phosphate hemihydrate – $VOHPO_4 \cdot ½H_2O$) was synthesized in an organic solvent, and then micronized to less than 2 μm after drying. The micronized powder was slurried and spray dried with polysilicic acid to form a protective attrition resistant shell. The average particle size was approximately 70 μm and the catalyst BET surface area ranged from 28 to 35 m^2/g.

A.4.2 Pilot plant reactor

The purpose of the pilot plant reactor (Figure A-2) was basically to verify the attrition resistance of the catalyst and to demonstrate catalytic performance and operability of the commercial plant. The design basis for the pilot plant was a scaled version of the projected commercial plant geometry. These included solids circulation rate, gas phase composition, gas and solids residence times in the separate vessels. In the pilot plant reactor, we fed oxygen and recycle gas separately. The recycle gas contained as much as 12 % n-butane and 4 % oxygen. To better distribute the reactor feeds in the bed, we tested three different recycle gas spargers and designed various oxygen spargers.

Additional oxygen was injected into the reaction bed to improve the reactor performance. For this purpose, we originally fed as much as 45 kg/h oxygen through a single nozzle 0.9 m above the recycle gas sparger, Figure A-2. After this point we began to detect "temperature excursions" – a sudden increase of temperature as little as 1 °C – that was accompanied by a measurable increase in CO_2 and decrease in oxygen. To deal with these excursions, we increased the number of oxygen spargers to try to distribute the oxygen more uniformly. We eventually, installed three

multi-nozzle spargers with 6.4 kg/h oxygen through each nozzle. The fast bed of the pilot plant was 6.1 m tall and the spargers were located 0.9, 2.1 and 3.7 m above the recycle gas.

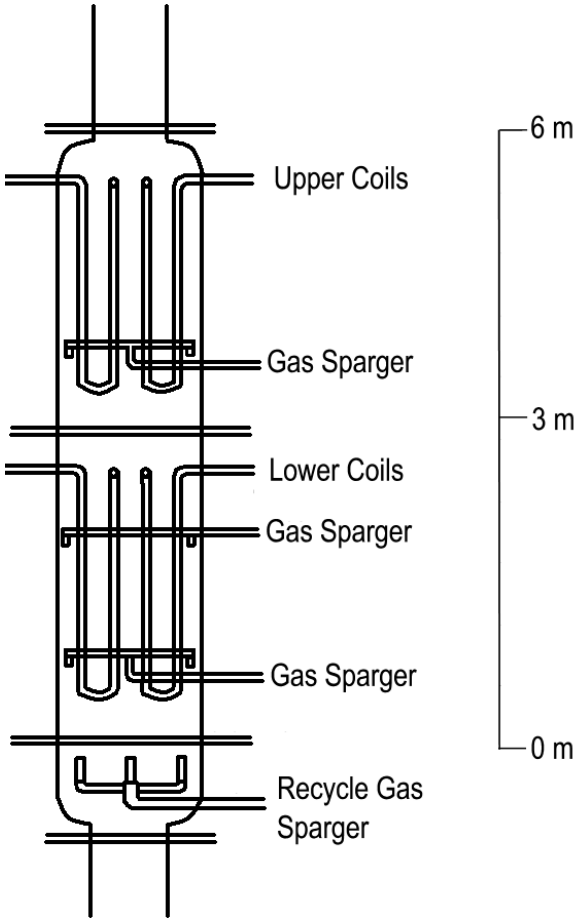

Figure A-2: Pilot plant reactor

A.4.3 Commercial CFB reactor

In the commercial plant, to reduce the risk of catalyst over reduction, we attempted to minimize total catalyst inventory and the residence time between the recycle gas and oxygen spargers, Figure A-3. The catalyst inventory in the entire reactor loop was approximately 170 t with 60 t in the fast bed/riser. In the pilot plant, solids and gas entered the fast bed co-currently form the bottom. However, at the commercial scale, it appeared that this configuration would lead to a

long catalyst residence time in a reducing environment (between the lower oxygen sparger and the distributor). For this reason, we adopted a solids side entry configuration, as shown in Figure A-3. This configuration minimized the solids residence time between the lower oxygen sparger and the distributor. We maintained the same nozzle dimensions and oxygen feed rate per nozzle (6.4 kg/h), as demonstrated in the pilot plant. However, the plant was originally built with only two oxygen spargers: one at 1.9 meter above the distributor and the upper sparger at 5.5 m.

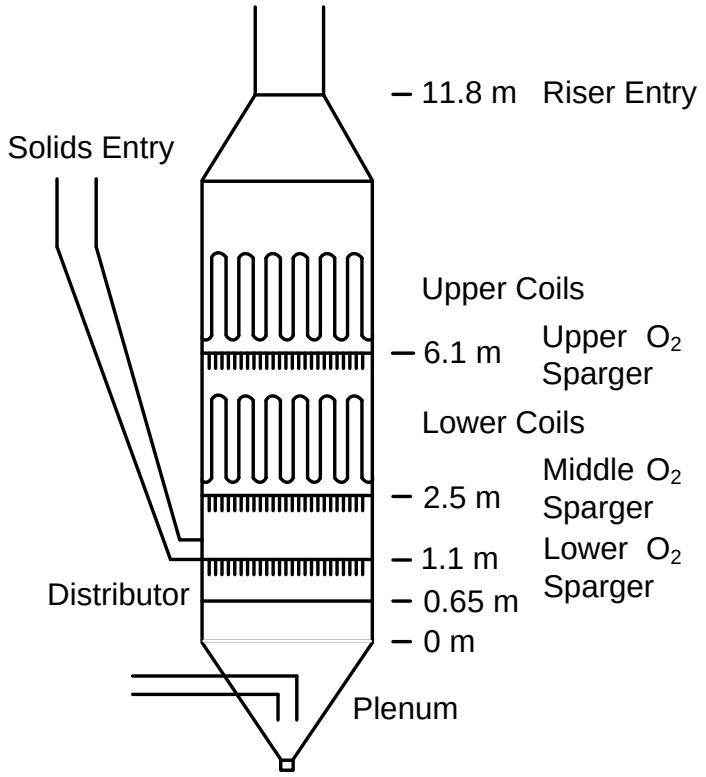

Figure A-3: Commercial CFB reactor

We feared that long catalyst residence time in a reducing atmosphere would reduce selectivity and conversion. However, in the final commercial design, catalyst residence time in the reducing zone was twice as long as it was in the pilot plant. One hope was that the region below the lower coils might act like a completely backmixed reactor as far as the oxygen fed to the sparger was concerned. In that way, oxygen concentrations would be sufficiently high such that the catalyst would not become over-reduced. The reason we did not consider placing the oxygen sparger

closer to the distributor may have been related to the uncertainty around the interaction between the oxygen from the sparger and recycle gas from the distributor as well as the hydrodynamics of solids entering from the side. We injected a radioactive isotope in the riser of the commercial reactor and measured the residence time distribution with NaI scintillator detectors positioned at sixteen points in the reactor loop. Based on the responses at the entrance and exit of the fast bed, the hydrodynamics could be best characterized as three continuous stirred tanks in series.

A.5 Results and discussion

A.5.1 Lab scale fluidized bed

In the 89 mm laboratory scale fluidized bed, we conducted experiments in which we only varied the n-butane and oxygen feed configurations. We ran all experiments at the same gas velocity, temperature, n-butane and oxygen concentrations. We calcined the catalyst precursor ($VOHPO_4 \cdot ½H_2O$) according to the commercial protocol in a 41 mm pressure fluidized bed and activated it in a 6.4 mm riser for 100 h with a stream of 10 % n-butane and 6 % oxygen at 380 °C. We loaded 1000 g of catalyst into the fluidized bed and ran it for 450 h at standard – base case – conditions: 380 °C, 1.5 % n-butane, 20 % oxygen, and a flow rate of 6.6 l/min (STP). Initially, the maleic anhydride yield was 4.8 gC/h, which is equivalent to 11.6 gMAC/h. After 1200 h on stream, the yield was 4.3 gC/h and it appeared steady [17]. The decline in yield and conversion was, in part, due to the drop in catalyst inventory (120 g less) and because we ran the reactor at a 20 °C lower temperature. The major part of the 120 g drop in catalyst inventory was due to catalyst withdrawals for characterisation.

The gas contact times in the fluidized bed were calculated for both bed sections: from distributor to the sparger and from the sparger to the top of the bed. The gas contact times calculated for the lower section of the fluidized bed were in accordance with the actual gas residence times in the commercial reactor (0.6 - 6.9 s).

A.5.1.1 n-Butane/N_2 to the sparger

In the first series of experiments, we fed n-butane and nitrogen to the sparger and air through the distributor. We positioned the sparger at a height of 20, 50, 80 and 180 mm above the distributor. The mass of catalyst during this experiment was 873 g. Maleic anhydride production rate was 4.2 gC/h when we co-fed all the gases to the distributor: conversion was 60 % and selectivity was 58 %. Table A.1 shows the trends of conversion and selectivity as we began moving the sparger higher up the bed. n-Butane conversion dropped as expected. However, selectivity also dropped. When we co-fed all the gases, selectivity was 58 % and it was 44 % when we were feeding n-butane through the sparger 180 mm above the distributor, which was about 15 mm below the surface of the bed. It is surprising that we got much conversion (19 %) at all with such a short contact time (0.3 s – defined as the bed height above the sparger divided by the superficial gas velocity). In this experiment, a reduction in contact time of a factor 12.7 (3.8 s/0.3 s) resulted in a maleic anhydride yield loss of a factor 4.3 (from 34 % to 8 %).

Table A.1: Air to distributor and n-butane/N_2 to sparger (5.0 /0.1/1.6 l/min (STP))

Sparger height, mm	**Contact time, s (above/below sparger)**	**MAC rate, gC/h**	**Conversion, % n-butane**	**Selectivity, % MAC**	**Freeboard temperature, °C**
0[1]	3.8/0.0	4.2	60	58	407
20	3.2/0.5	3.7	50	57	436
50	2.7/1.2	3.4	47	53	441
80	2.2/2.0	2.4	36	53	415
180	0.3/4.5	1.0	19	44	428

[1]Air/n-butane co-fed through the distributor

In fixed bed reactors, selectivity normally increases with decreasing conversion, whereas for the experimental data shown in Table A.1, selectivity decreased with a decrease in conversion. This trend was observed in the Asturias commercial plant data but it was attributable to the fact that

we increased n-butane concentration – in this case, the lower conversion resulted in lower maleic anhydride selectivity but a higher production rate.

A decrease in the concentration of surface lattice oxygen could account for the drop in selectivity shown in Table A.1. The oxidation state might decrease by extended exposure of the catalyst to a reducing environment due to limited mass transfer of species between bubbles and emulsion phases in the bed. From a molecular point of view, in the absence of sufficient oxygen in the upper section of the bed, the adsorbed n-butane species on the surface may stay for a longer time compared to when there is sufficient surface oxygen for a selective reaction. Therefore, these species have more chance of being oxidized to CO and CO_2.

Figure A-4 shows the conversion and selectivity of several experiments performed in a Multiple Automated Reactor System (MARS) [18] at six different n-butane and oxygen concentrations. We ran n-butane lean and oxygen rich conditions as well as n-butane rich and oxygen lean conditions at five gas flow rates each – 15, 24, 39, 62 and 100 ml/min (STP) with 0.7 g of catalyst – and at 350, 380 and 410 °C. Under n-butane lean conditions (i.e. 2 % n-butane), oxygen concentration had little effect on maleic anhydride selectivity. At a given level of conversion, the selectivity was almost the same for 20 %, 10 % and 4 % oxygen. However, as we raised n-butane concentration, at a constant inlet oxygen concentration, selectivity decreased. We ran experiments with 2 %, 5 % and 9 % n-butane and 10 % oxygen in the feed. At 22 % n-butane conversion, maleic anhydride selectivity was about 78 % with 2 % n-butane, 74 % with 5 % n-butane and only 68 % with 9 % n-butane.

In the fluidized bed sparger studies, the average n-butane concentration exiting the sparger was about 6 vol. % and bubbles formed at the tip of the sparger dispersed mostly at the upper portion of the bed. Therefore, the bulk feed composition in the upper portion of the bed could be considered to be in net reducing environment. The data presented in Figure A-4 at high n-butane concentrations correspond with the results observed for fluidized bed sparger study: as the catalyst is exposed more to a rich n-butane environment the selectivity tends to decrease. In both cases the reason for the drop in selectivity could be due to a decrease in the oxidation state of the

catalyst. However, for fixed bed experiments in Figure A-4, the lower catalyst oxidation state is due to a higher n-butane concentration in the feed. While, for the sparger studies in the fluidized bed the lower catalyst oxidation state could probably be related to the feed configuration in the bed.

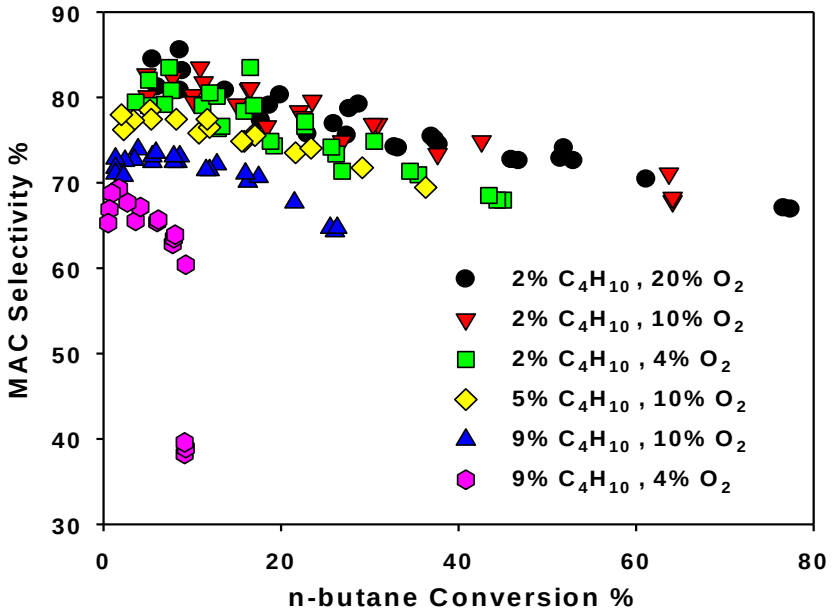

Figure A-4: Fixed bed experiments: selectivity vs. conversion

(Feed flow rates: 15, 24, 39, 62 and 100 ml/min (STP), Temperatures: 350, 380 and 410 °C, Catalyst weight: 0.7 g)

A.5.1.2 Air to the sparger

In the second series of experiments, we simply reversed the feed locations of the first series and fed n-butane and nitrogen to the distributor and air to the sparger. This test more closely approximates the commercial plant operation. However, comparing the plant data directly with these experimental data is unrealistic because the scales of the two reactors are so different as well as the fluidization regimes. Therefore, we should only expect to recognize similar trends in

the data which is that maleic anhydride selectivity and n-butane conversion drop with separation distance between the feeds. These data are presented in Table A.2.

Compared to the first sparger experiment, in the second series of experiments the n-butane conversion was generally lower. Maleic anhydride selectivity was more or less constant up to a sparger height of 50 mm but it began to drop at the height of 80 mm. It was only 37 % at a height of 180 mm, which was lower than the first experiment. Here, a reduction in contact time of the order 12.7 (3.8 s/0.3 s) resulted in a maleic anhydride yield drop of a factor 5.7 (from 34 % to 6 %).

Table A.2: Air to sparger and n-butane/N_2 to distributor (5.0 /0.1/1.6 l/min (STP))

Sparger height, mm	**Contact time, s (above/below sparger)**	**MAC rate, gC/h**	**Conversion, % n-butane**	**Selectivity, % MAC**	**Freeboard temperature, °C**
0[1]	3.8/0.0	4.2	60	58	407
20	3.2/1.4	2.9	38	61	446
50	2.7/3.6	2.6	35	58	439
80	2.1/5.7	2.1	30	53	452
180	0.3/13.2	0.8	17	37	435

[1]Air/n-butane co-fed through the distributor

When n-butane is fed through the distributor, the major portion of the catalyst bed below the sparger is bathed in a rich n-butane environment (~ 6 vol. %) with little oxygen. From the results observed in the two sparger experiments, we may conclude that the bulk concentration of n-butane in the fluidized bed has a detrimental effect on conversion. In other words, when the n-butane and the oxygen streams are fed separately to the bed, to maximize productivity, the distance between the two feed streams should be minimized. This observation suggests that to improve conversion at high n-butane concentrations, oxygen must always be present and mixed properly with n-butane in the bed [2, 19]. In this regard, proper backmixing and degree of

turbulency in the fluidized bed seem to play important roles in reactor performance at relatively high n-butane concentrations. Limited mass transfer from bubbles to the emulsion phase or vice versa could also promote catalyst over reduction when operating at high n-butane concentrations.

A.5.1.3 Air/n-butane to the sparger

In the third series of experiments, we fed both air and n-butane to the sparger and nitrogen through the distributor. In agreement with the first two experiments, both conversion and selectivity dropped with increasing sparger height, Table A.3. The values of conversion agree reasonably well with the second experiment (air to the sparger). However, the values of selectivities were the lowest among all four sparger experiments which resulted in the lowest yield. In fact, maleic anhydride yield dropped by a factor of 10.3 (from 41 % to 4 %) when the gas residence time in the bed above the sparger varied from 3.8 to 0.3 seconds.

Table A.3: Air/n-butane to sparger and N_2 to distributor (5.0/0.1/1.6 l/min (STP))

Sparger height, mm	**Contact time, s (above/below sparger)**	**MAC rate, gC/h**	**Conversion, % n-butane**	**Selectivity, % MAC**	**Freeboard temperature, °C**
0[1]	3.8/0.0	4.6	69	59	397
20	3.4/1.6	2.6	39	55	407
50	2.8/4.1	2.0	34	49	409
80	2.2/6.4	1.4	27	43	421
180	0.3/14.6	0.5	15	29	415
220	0.0/0.0	0.16	6	26	420

[1]Air/n-butane co-fed through the distributor

From a hydrodynamic point of view, compared to the first two series of experiments, the bulk phase of the catalyst bed in the third experiment was soaked in an inert nitrogen phase. Therefore, the reaction may have occurred predominantly in the bubble phase. In this case, the effect of

mass transfer and backmixing of bubbles in the emulsion phase was more pronounced especially because we observed the lowest overall selectivities for this experiment. Actually, the sparger bubbles travelled up in the bed and exited from the bed surface rapidly. Therefore there should have been little chance for reactive species to diffuse out and react in the larger portion of the bed.

As shown in Table A.3, an additional experiment was conducted in which the sparger was positioned just above the top of the catalyst bed at a height of 220 mm. Maleic acid selectivity was 26 % with 6 % n-butane conversion. The temperature in the freeboard (high above the fluidized bed) during this test was 420 °C, which would contribute to the lower selectivity but would not account for such a low value.

A.5.1.4 Oxygen co-feed with n-butane

In the fourth series of experiments, 20 % of the main air stream entered together with n-butane and nitrogen through the distributor. The balance of the air entered through the sparger. Maleic anhydride yield was even higher compared to the conditions where both feeds entered through the distributor (5.2 vs. 4.6 gC/h). Although n-butane conversion was slightly higher (70 vs. 69 %), the main difference was in the selectivity, It increased by 10 % (from 59 to 65 %), Table A.4. Raising the height of the sparger to 50 mm did not seem to affect the overall yield – conversion increased a bit and selectivity dropped, but the difference was within experimental error. These results suggest that having oxygen co-fed with n-butane in the emulsion phase in the fluidized bed could considerably improve the reactor performance at high n-butane concentrations. Comparing this feed configuration with the second sparger experiment (air to the sparger) shows that the major improvement observed for the yield comes from the oxygen being partly fed thorough the distributor. Due to the presence of oxygen in the bed, no drop in selectivity or conversion was observed by increasing the sparger height. This may indicate that by setting a feed arrangement similar to this experiment, the catalyst bed would remain in an oxidized state even at high n-butane concentrations.

Figure A-5 shows a plot of selectivity against conversion for the sparger data (circles) versus standard fluidized bed operation with all gases co-fed to the plenum below the distributor (squares). The data were collected in the same fluidized bed reactor described in section A.4.1 but the all gas was fed together below the distributor. The amount of catalyst was the same as sparger experiments – 870 g. The experiments were conducted at 355, 380 and 405 °C. The total feed flow rate was 3.3, 6.6 and 9.4 l/min (STP). The feed composition to the reactor was a mixture of 1-2 vol. % n-butane in air with a water content including 0, 5 and 10 vol. %. In the standard fluidized bed configuration, maleic anhydride selectivity decreased as n-butane conversion increased, which agrees with the fixed bed reactor data presented in Figure A-4. However, the data show that the yields in a fluidized bed are generally lower than the fixed bed reactor and the selectivity drops off at a lower conversion. This might be due to lower oxidation state of the catalyst in a fluidized bed reactor while operating at higher n-butane concentrations (up to 4 vol. %) compared to a fixed bed reactor (around 1.8 vol. %).

Table A.4: Air to sparger air/n-butane/N_2 to distributor (4.1 and 0.9/0.1/1.6 l/min (STP))

Sparger height, mm	**Contact time, s (above/below sparger)**	**MAC rate, gC/h**	**Conversion, % n-butane**	**Selectivity, % MAC**	**Freeboard temperature, °C**
0[1]	3.8/0.0	4.6	69	59	397
20	3.4/1.0	5.2	69	65	398
50	2.9/2.5	5.2	70	64	387

[1]Air/n-butane co-fed through the distributor

Contrary to the fluidized bed co-feed data, the sparger data presented in Figure A-5 showed the opposite trend: as the conversion increased, the maleic anhydride selectivity also increased. The reason for an increase in selectivity with conversion could be attributed to the effect of feed configuration. In a typical fluidized bed reactor, when both feeds enter through the distributor, an increase in the conversion is usually achievable by increasing n-butane concentration in the feed. Therefore, higher conversion is always accompanied by a lower catalyst oxidation state and hence a lower selectivity. While, in the sparger experiments, where one feed enters the reactor

through a sparger, an increase in the conversion at certain n-butane concentration is only possible when the sparger is close to the distributor. A lower sparger height translates to a higher exposure of the catalyst to oxygen and thus perhaps to a higher surface lattice concentration of V^{5+} species. Therefore, achieving higher maleic anhydride selectivity would be possible even at a higher conversion.

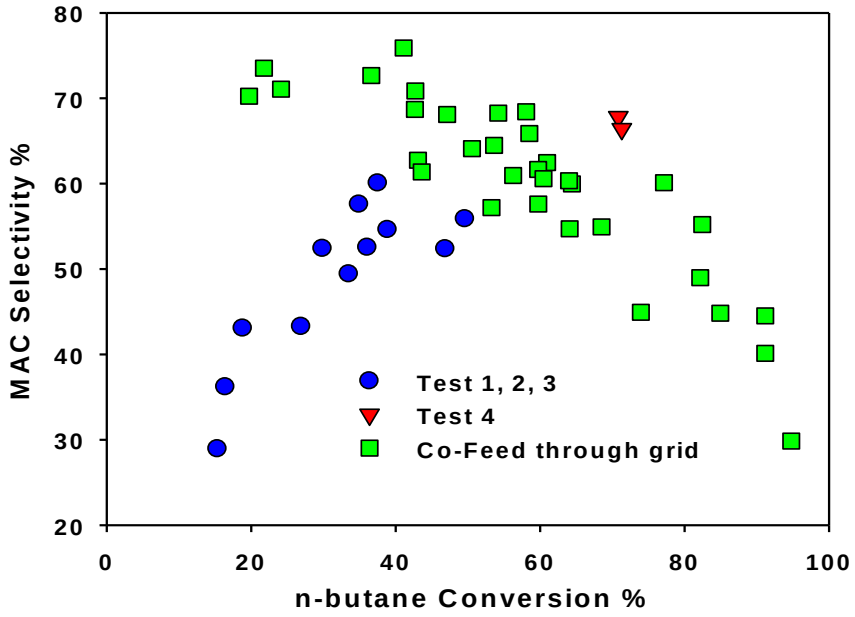

Figure A-5: Sparger experimental data compared to operation when all gases are co-fed through the distributor

(Feed flow rates: 3.3, 6.6, 9.4 l/min (STP), Feed composition: 1-2 % n-butane in air (0-10 % water), Temperatures: 355, 380 and 405 °C, Catalyst weight: ~ 870 g)

Among the four sparger configurations, the last sparger configuration (triangles in Figure A-5), where some oxygen entered with n-butane thorough the distributor, showed the highest maleic anhydride yield. For this experiment, the n-butane concentration was about 4 % and for the oxygen it was 8 %. However, the mixed-cup concentration of n-butane was only 1.5 % and for the oxygen it was 16 %. These data suggest that in the commercial plant, increasing the oxygen concentration in the recycle gas would result in higher conversion and selectivity. In the

commercial plant, selectivity declined when we increased the n-butane feed rate. If we could maintain high partial pressures of oxygen in the bed, the catalyst might not have overly reduced and, selectivity might have remained high.

The first two sparger experiments clearly demonstrate that by separating feed streams in a fluidized bed, selectivity and conversion decline. Furthermore, as the distance between the oxygen and n-butane feeds increases, the selectivity gets worse. These data suggest that optimizing the gas injection configuration is critical for plant performance and provide an experimental basis justifying the installation of a third oxygen sparger in the commercial plant. The data also suggest that both conversion and selectivity would increase with an increase in oxygen concentration in the recycle gas.

A.5.2 Effect of freeboard temperature

In the lab scale fluidized bed reactor, we measured the temperature at different heights in the bed as well as in the furnace and in the freeboard above the bed. The bed temperature was controlled at 380 °C. However, temperatures in the freeboard of as much as 450 °C were recorded (Tables A.1-A.4). We attempted to correlate these high temperatures with n-butane combustion in the disengagement section. Figure A-6 shows the relationship between freeboard temperature and n-butane conversion and maleic acid selectivity. In fact, the opposite trend of that we were expecting is evident. The lowest conversion corresponded to the highest temperature in the freeboard. There seems to be a slight trend with higher temperature and lower selectivity but the effect is slight. Clearly, freeboard conversion of n-butane is not the principal cause of the high temperature in the freeboard. Rather, it might be related to the temperature control of the reactor. More heat is generated under conditions of high n-butane conversion and requires less energy from the heater to maintain the overall temperature. More radiant heat is supplied to the reactor under low n-butane conversion, which results in a higher temperature in the freeboard.

Figure A-7 demonstrates the relationship between maleic anhydride selectivity and the separation distance between the distributor and sparger tip. Regardless of the feed configuration, the selectivity drops as the separation distance increases.

A.5.3 Commercial reactor – oxygen sparger studies

There were originally two oxygen spargers installed in the fast bed of the commercial CFB reactor. These spargers were located at the heights of 1.9 and 5.5 meter above the distributor (at 0.65 m). Based in part on the fluidized bed experimental program, a third oxygen sparger was installed later to enable injecting additional oxygen into the reaction bed to improve the reactor performance. The shroud tips of the third oxygen sparger were only 0.45 m above the distributor, which was just below the solids entry.

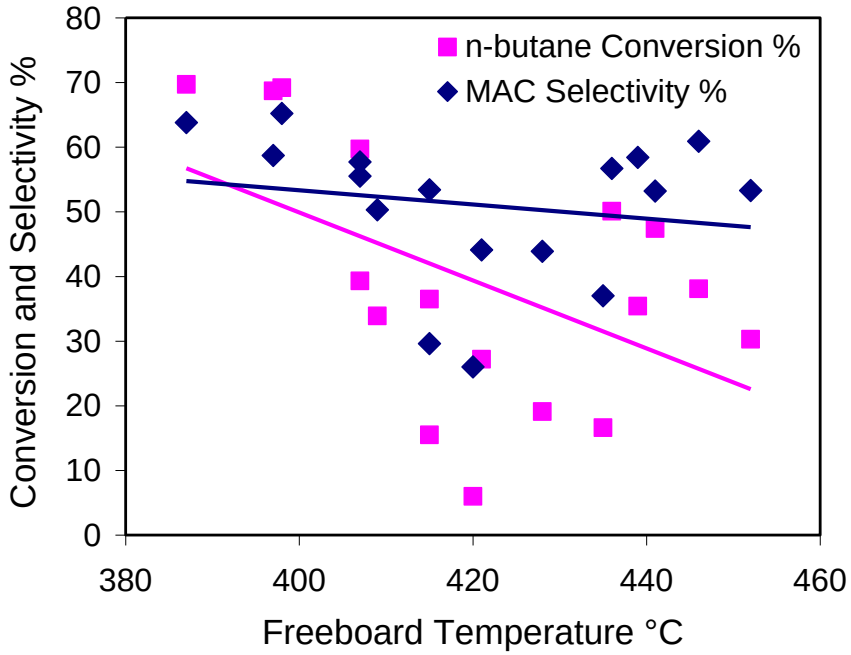

Figure A-6: n-Butane conversion and maleic acid selectivity versus freeboard temperature

(Feed flow rates: 5.0, 4.1 and 0.9 (air), 0.1 (n-butane) and 1.6 (N_2) l/min (STP), Temperature: 380 °C, Sparger heights: 0, 20, 50, 80, 180 and 220 mm, Catalyst weight: 873 g)

Table A.5 shows the initial operating conditions of the commercial reactor before starting to switch the oxygen feed locations. Initially, all the supplemental molecular oxygen (in addition to oxygen that comes from the standpipe and in the recycle gas) entered through the middle sparger. Under these conditions, the selectivity was 55.8 %. However, as we raised the n-butane and the oxygen feed rates, the maleic acid (MAC) production rate increased to 3500 kg/h but the selectivity dropped by about 0.5 % absolute. The rows 3 and 4 in Table A.5 (at 9.1 and 11.3 days of operation) contain four days of steady state data immediately before switching the oxygen feeds. The feed configuration in this case corresponds best to the conditions in the fourth sparger experiment (section A.5.1.4) where the oxygen sparger was located at 50 mm above the distributor (contact time = 2.5 s in Table A.4)

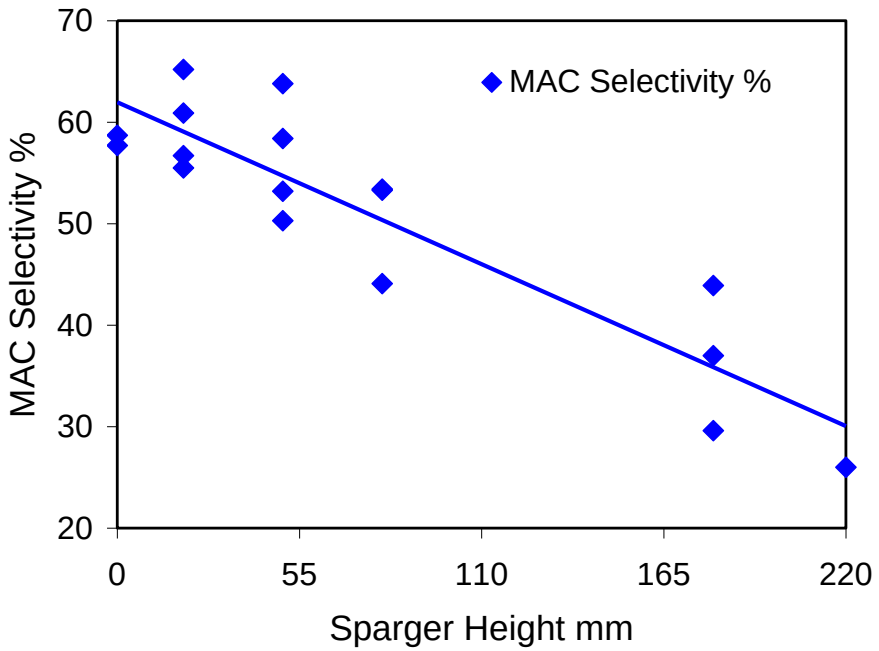

Figure A-7: Effect of sparger height on maleic acid selectivity

(Feed flow rates: 5.0, 4.1 and 0.9 (air), 0.1 (n-butane) and 1.6 (N_2) l/min (STP), Temperature: 380 °C, Catalyst weight: 873 g)

Table A.5: Initial reactor conditions before switching the oxygen feed (Temperature ≈ 380 °C)

Time, days	MAC, kg/h	%C_4 in	%O_2 out	MAC Sel., %	n-butane Conv., %	Yield, %	O_2 Middle Sparger, kg/h	Contact time[1], s
0.8	2990	3.0	3.3	55.8	52.5	29.3	4413	2.4
4.9	3530	4.0	3.1	55	45.5	25.0	5780	2.4
9.1	3500	4.1	2.9	55.3	44.6	24.7	5785	2.4
11.3	3560	4.1	3.0	55.5	44.6	24.8	5784	2.4

[1]Gas residence time from distributor to the middle oxygen sparger (at 1.9 m)

A.5.3.1 Oxygen switch to the upper sparger

At first, we studied the effect of switching oxygen feed from the middle sparger (at 1.9 m) to the upper sparger (at 5.5 m). In this experiment, the catalyst was poorly active and contained approximately 5 % fines (particles with a diameter less than 44 μm). For this reason, we were unable to feed n-butane and oxygen at high rates, and thus, maleic acid production rates were low. The experimental conditions are summarized in Table A.6. We ran three main conditions: (1) high oxygen feed to the middle sparger with 2.3 % oxygen at the exit; (2) low oxygen feed to the middle sparger with 2.0 % oxygen at the exit; and, (3) low oxygen feed to the upper sparger with 2.4 % oxygen at the exit. At Conditions 2 and 3 the maleic acid production was about 1500 kg/h. At Condition 1 a higher production rate of 1740 kg/h was achieved. The Condition 4 (similar to Condition 3) had the highest oxygen feed rate and thus exit oxygen, which increased the production rate to 1810 kg/h.

These data are consistent with the results obtaiend in the lab scale fluidized bed sparger experiments: selectivity increases as the oxygen sparger height decreases. The gas residence times for these conditions could be compared to the contact times in the sparger experiments where the sparger was located at 50 mm or 80 mm above the distributor (2.5 s and 5.7 s in Tables A.4 and A.2). For the commercial reactor, Table A.6 shows that the selectivity increased going from the upper sparger (Condition 3) to the middle sparger (Condition 2) – from 46 to 51 %. In

this experiment, maleic acid production rate was 1740 kg/h in Condition 1 compared to 1500 kg/h in Condition 3 with almost the same exit oxygen concentrations. In Condition 4 (upper sparger), we increased both n-butane and oxygen feed rates and we were able to produce as much maleic acid as in Condition 1 (middle sparger). However, if we would have fed as much n-butane and oxygen in Condition 1, we would probably have made more maleic acid at a lower exit oxygen concentration. The importance of exit oxygen concentration is to do with avoiding thermal excursions at the reactor exit. This means that the exit oxygen concentration is limiting for the plant production and it could not go beyond a certain value.

Table A.6: Switching oxygen to the upper oxygen sparger (Temperature ≈ 380 °C)

Condition	**MAC, kg/h**	**%O_2 out**	**MAC Sel., %**	**Oxygen, kg/h**	**n-butane, kg/h**	**Sparger Location**	**Contact time[1], s**
1	1740	2.3	48	3550	2350	Middle	2.4
2	1530	2.0	51	2970	1950	Middle	2.4
3	1500	2.4	46	3050	2170	Upper	6.9
4	1810	2.4	48	3780	2460	Upper	6.9

[1]Gas residence times from distributor to the middle and upper oxygen spargers (at 1.9 and 5.5 m)

A.5.3.2 Oxygen switch to the lower sparger

Figure A-8 shows the effect of switching oxygen from the middle to the lower sparger on maleic acid production rate. During the switch, we first reduced oxygen feed to the middle sparger then began to add it to the lower sparger. So, as we were switching, the total oxygen feed flow rate was lower than it was at the start. When we reached a 50/50 split between lower and middle spargers (time = 13 days), we held the condition for 14 h. Production was up to almost 3700 kg/h and both conversion and selectivity increased somewhat. During the switch, exit oxygen concentration dropped by an order of 10 % relative difference. At this condition, we fed the same amount as oxygen as we did before we started switching – 5784 kg/h.

As we continued switching oxygen to the lower sparger, selectivity was still over 56 % and conversion rose slightly and the production rate increased to almost 3800 kg/h. Exit oxygen concentration continued to decline and by the time we had switched all the oxygen to the lower sparger, the exit oxygen concentration had dropped to 2.5 %. The next step in the test was to bring both exit oxygen and n-butane concentrations to their original values. We fed additional oxygen through the middle sparger – about 900 kg/h; production rose from almost 3800 to over 4000 kg/h. The production rate before switching oxygen was about 3500 kg/h and it increased to more than 4000 kg/h after switching oxygen feed to the lower sparger, this corresponds to almost 15 % increase in the plant production rate.

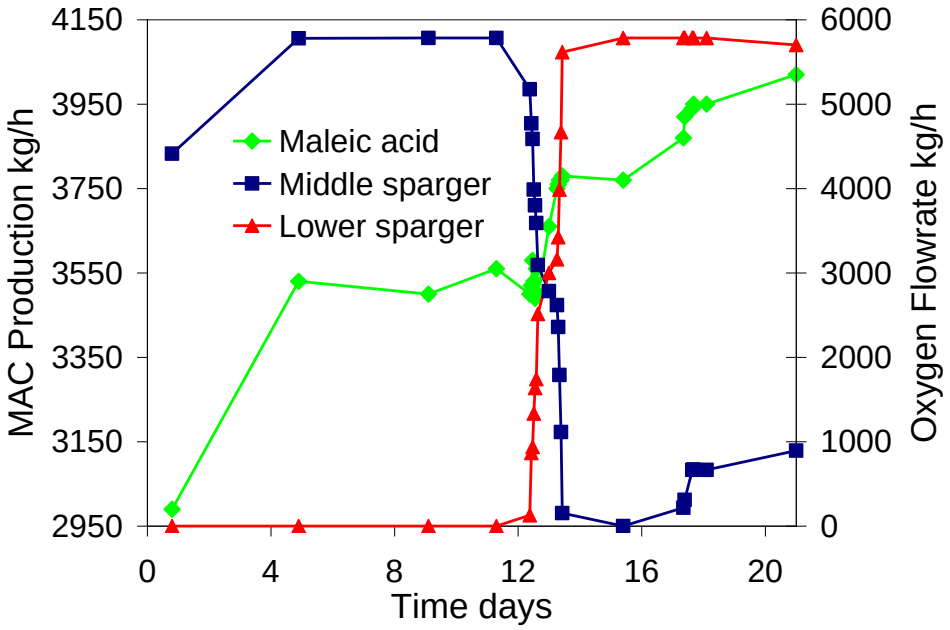

Figure A-8: Maleic acid productivity versus feed rates to the oxygen spargers

(Average inlet n-butane: 4.1 %, exit oxygen: 2.5-3.2 %, Temperature: ~ 380 °C, catalyst inventory: ~ 170 t (reactor loop), ~ 60 t (fast bed/riser))

In summary, as we switched the oxygen from the middle to lower sparger, exit oxygen concentration dropped but the yield increased. As we began increasing oxygen feed rates and thus exit oxygen concentrations, maleic acid yield began to climb again. These data show how

important it is to be able to feed extra oxygen to the reactor. This observation is also in agreement with previous oxygen sparger experiment where the production rate increased as we switched the oxygen from the upper sparger to the middle sparger. Also in the lab scale fluidized bed experiments, decreasing the oxygen sparger level closer to the distributor was similarly accompanied by an increase in the maleic acid production rate. The gas residence times are comparable to the experiments where the sparger was located at only 20 mm above the distributor (contact times of 0.5-1.6 s in Tables A.1-A.4). These data show that there is an optimum feeding configuration at which the concentration of the reactants in the catalyst bed is such that the catalyst remains at its highest oxidation state without being over reduced. In our experiments, this optimum concentration was achievable only by feeding extra oxygen to a lower section of the fluidized bed right above the distributor.

A.6 Conclusions

Our studies on the lab scale fluidized bed showed that maleic anhydride yield is sensitive to the gas feed configuration. We observed that maleic anhydride selectivity and n-butane conversion increase as the distance between n-butane and oxygen feed in the bed decreases. The highest yield was achieved by co-feeding n-butane with oxygen at high n-butane concentrations. The main reason for higher yields under these conditions is presumably maintaining the catalyst at an oxidized state and minimizing the chance of catalyst over reduction in the reactor.

In the commercial plant, the production rate was increased by about 15 % only by feeding the oxygen to a lower sparger 1.5 m below. Both maleic acid selectivity and n-butane conversion increased. The same oxygen concentration at the reactor exit was maintained to prevent thermal excursions. Our observations suggest that a higher maleic acid yield was obtainable only by increasing the co-fed oxygen in the recycle gas to the reactor.

A.7 References

[1] R.M. Contractor, D.I. Garnett, H.S. Horowitz, H.E. Bergna, G.S. Patience, J.T. Schwartz, G.M. Sisler, Stud. Surf. Sci. Catal. 82 (1994) 233-242.

[2] G.S. Patience, M.J. Lorences, Int. J. Chem. Reactor Eng. 4 (2006) 1-18.

[3] X.-F. Huang, C.-Y. Li, and B.-H. Chen, P.L. Silveston, AIChE J. 48 (2002) 846-855.

[4] D.X. Wang, M.A. Barteau, J. Catal. 197 (2001) 17-25.

[5] J. Gascón, R. Valenciano, C. Téllez, J. Herguido, M. Menéndez, Chem. Eng. Sci. 61 (2006) 6385-6394.

[6] G. Emig, K. Uihlein, C.-J. Hacker, in: V.C. Corberan, S.V. Bellon (Eds.), New Developments in Selective Oxidation, Elsevier, Amsterdam, 1994, pp. 243-251.

[7] A.A. Rownaghi, Y.H. Taufiq-Yap, F. Rezaei, Catal. Lett. 130 (2009) 504-516.

[8] S. Mota, S. Miachon, J.-C. Volta, J.-A. Dalmon, Catal. Today 67 (2001) 169–176.

[9] O. Rubio, R. Mallada, J. Herguido, M. Menéndez, Ind. Eng. Chem. Res. 41 (2002) 5181-5186.

[10] J. Gascón, C. Téllez, J. Herguido, M. Menéndez, Ind. Eng. Chem. Res. 44 (2005) 8945-8951.

[11] J. Herguido, M. Menéndez, J. Santamaría, Catal. Today 100 (2005) 181-189.

[12] S.P. Jordan, E.I. Du Pont de Nemours and Company, US Patent 4,801,731 (1989).

[13] A. Shekari, G.S. Patience, Catal. Today 157 (2010) 334-338.

[14] Y. Schuurman, J.T. Gleaves, Ind. Eng. Chem. Res. 33 (1994) 2935-2941.

[15] N. Ballarini, F. Cavani, C. Cortelli, F. Gasparini, A. Mignani, F. Pierelli, F. Trifiro, C. Fumagalli, G. Mazzoni, Catal. Today 99 (2005) 115-122.

[16] K.W. Hutchenson, C. La Marca, G.S. Patience, J.-P. Laviolette, R.E. Bockrath, Appl. Catal. A: Gen. 376 (2010) 91-103.

[17] G.S. Patience, R.E. Bockrath, Appl. Catal. A: Gen. 376 (2010) 4-12.

[18] G.S. Patience, R.E. Bockrath, J.D. Sullivan, H.S. Horowitz, Ind. Eng. Chem. Res. 46 (2007) 4374-4381.

[19] N. Ballarini, F. Cavani, C. Cortelli, S. Ligi, F. Pierelli, F. Trifiro, C. Fumagalli, G. Mazzoni, T. Monti, Top. Catal. 38 (2006) 147-156.

APPENDIX B – DATA ANALYSIS

MATLAB® program for MS data calculations

```
clear
clc

global data_r data_c

%-------------------------------------------------------------------------------
% This program calculates the "reduction" MS results for all components
% (y, C, F, v etc). The X, S and Y is calculated for all components in transient
% and total values. Also C, H, O and Ar balances are calculated in transient or
% total. MA data are taken from conductivity. Since the conductivity MA rate is
% slower, the MS data are corrected based on an average MA rate. The m/e overlap
% factors have to be taken from feed/mixed feed profiles. HPLC result
% for total MA production per cycle is used to calculate the total molar
% balances and total MA selectivity/yield. The MA rates from conductivity are
% corrected based on the ratio of MA from HPLC to COND There is a baseline
% correction for O2, CO, CO2 and H2O pp values. The time steps of all data are now
% equalized.
%-------------------------------------------------------------------------------
[data_r] = xlsread('1-1-1-r7.xls'); % reduction data from MS (10 minutes)
[data_c] = xlsread('1-1-1-c7.xls'); % MA flow rate data from absorber (10 minutes)

TIME_R(:,1) = (data_r(:,2)-data_r(1,2))/1000/60; % zeroed MS time for reduction, minutes
TIME_C(:,1) = data_c(:,1); % conductivity time, minutes
F_MA_c(:,1) = data_c(:,2); % instant MA exit flow rate from conductivity, gmole/min
%-------------------------------------------------------------------------------
% MS data - subtracting m/e overlaps (confirm the factors by looking at feed profiles)
%-------------------------------------------------------------------------------
ppC4H10_r(:,1) = data_r(:,7);
ppAR_r(:,1) = data_r(:,3)-0.02*ppC4H10_r(:,1); % subtraction based on NIST data
ppCO2_r(:,1) = data_r(:,6)-0.03*ppC4H10_r(:,1); % according to mixed feed or n-butane gas
alone cracking patterns
ppCO_r(:,1) = data_r(:,4)-0.35*ppC4H10_r(:,1)-0.15*ppCO2_r(:,1); % according to mixed feed
or n-butane gas alone and CO2 cracking patterns
ppO2_r(:,1) = data_r(:,5);
ppH2O_r(:,1) = data_r(:,8)-0.01*ppC4H10_r(:,1); % correction for mixed feed or n-butane gas
water content


%-------------------------------------------------------------
```

```
% Spline cubic interpolation to equalize time steps of MS data
%-------------------------------------------------------------
TIME_Rs(:,1) = linspace(0,max(TIME_R(:,1)),length(TIME_R(:,1)));
ppC4H10_r(:,1) = spline(TIME_R(:,1),ppC4H10_r(:,1),TIME_Rs(:,1));
ppAR_r(:,1)= spline(TIME_R(:,1),ppAR_r(:,1),TIME_Rs(:,1));
ppCO2_r(:,1)= spline(TIME_R(:,1),ppCO2_r(:,1),TIME_Rs(:,1));
ppCO_r(:,1)= spline(TIME_R(:,1),ppCO_r(:,1),TIME_Rs(:,1));
ppO2_r(:,1)= spline(TIME_R(:,1),ppO2_r(:,1),TIME_Rs(:,1));
ppH2O_r(:,1)= spline(TIME_R(:,1),ppH2O_r(:,1),TIME_Rs(:,1));
TIME_R(:,1) = TIME_Rs(:,1);
%-----------------------------------------------------------------------------------------
% Spline cubic interpolation to synchronize the time steps of conductivity with MS data
%-----------------------------------------------------------------------------------------
F_MA_r = zeros(length(data_r),2);
F_MA_r(:,2) = spline(TIME_C(:,1),F_MA_c(:,1),TIME_R(:,1));
%---------------------------
% Smoothing - Savitzky Golay
%---------------------------
ppARs_r(:,1) = smooth(TIME_R(:,1),ppAR_r(:,1),30,'sgolay',1);
ppCOs_r(:,1) = smooth(TIME_R(:,1),ppCO_r(:,1),30,'sgolay',1);
ppO2s_r(:,1) = smooth(TIME_R(:,1),ppO2_r(:,1),30,'sgolay',1);
ppCO2s_r(:,1) = smooth(TIME_R(:,1),ppCO2_r(:,1),30,'sgolay',1);
ppC4H10s_r(:,1) = smooth(TIME_R(:,1),ppC4H10_r(:,1),30,'sgolay',1);
ppH2Os_r(:,1) = smooth(TIME_R(:,1),ppH2O_r(:,1),30,'sgolay',1);
%-------------------------------------
% Correcting the baseline of pp values
%-------------------------------------
% For amb P tests
ppO2s_r(:,1) = ppO2s_r(:,1)-mean(ppO2s_r(10:20,1));
ppCOs_r(:,1) = ppCOs_r(:,1)-mean(ppCOs_r(10:20,1));
ppCO2s_r(:,1) = ppCO2s_r(:,1)-mean(ppCO2s_r(10:20,1));
ppH2Os_r(:,1) = ppH2Os_r(:,1)-mean(ppH2Os_r(10:20,1));
%---------------------------------
% Zeroing small/negative pp values
%---------------------------------
for i = 1:length(data_r)
if (ppARs_r(i,1) < 1e-12)
ppARs_r(i,1) = 0.0;
end
if (ppCOs_r(i,1) < 1e-12)
ppCOs_r(i,1) = 0.0;
end
if (ppO2s_r(i,1) < 1e-12)
ppO2s_r(i,1) = 0.0;
end
if (ppCO2s_r(i,1) < 1e-12)
ppCO2s_r(i,1) = 0.0;
```

```
end
if (ppC4H10s_r(i,1) < 1e-12)
ppC4H10s_r(i,1) = 0.0;
end
if (ppH2Os_r(i,1) < 1e-12)
ppH2Os_r(i,1) = 0.0;
end
end
%---------------------------------
% Zeroing negative MA rate values
%---------------------------------
for i = 1:length(data_r)
if (F_MA_r(i,2) < 0.0)
F_MA_r(i,2) = 0.0;
end
end
%-------------------------------------------------
% Calculating ideal molar fractions (1/RSi = 1.0)
%-------------------------------------------------
yAR_r = zeros(length(data_r),20);
yCO_r = zeros(length(data_r),20);
yO2_r = zeros(length(data_r),20);
yCO2_r = zeros(length(data_r),20);
yC4H10_r = zeros(length(data_r),20);
yH2O_r = zeros(length(data_r),20);
%-------------------------------------------------
yAR_r(:,1) =
ppARs_r(:,1)./(ppARs_r(:,1)+ppCOs_r(:,1)+ppO2s_r(:,1)+ppCO2s_r(:,1)+ppC4H10s_r(:,1)+ppH
2Os_r(:,1));
yCO_r(:,1) =
ppCOs_r(:,1)./(ppARs_r(:,1)+ppCOs_r(:,1)+ppO2s_r(:,1)+ppCO2s_r(:,1)+ppC4H10s_r(:,1)+ppH
2Os_r(:,1));
yO2_r(:,1) =
ppO2s_r(:,1)./(ppARs_r(:,1)+ppCOs_r(:,1)+ppO2s_r(:,1)+ppCO2s_r(:,1)+ppC4H10s_r(:,1)+ppH
2Os_r(:,1));
yCO2_r(:,1) =
ppCO2s_r(:,1)./(ppARs_r(:,1)+ppCOs_r(:,1)+ppO2s_r(:,1)+ppCO2s_r(:,1)+ppC4H10s_r(:,1)+pp
H2Os_r(:,1));
yC4H10_r(:,1) =
ppC4H10s_r(:,1)./(ppARs_r(:,1)+ppCOs_r(:,1)+ppO2s_r(:,1)+ppCO2s_r(:,1)+ppC4H10s_r(:,1)+
ppH2Os_r(:,1));
yH2O_r(:,1) =
ppH2Os_r(:,1)./(ppARs_r(:,1)+ppCOs_r(:,1)+ppO2s_r(:,1)+ppCO2s_r(:,1)+ppC4H10s_r(:,1)+pp
H2Os_r(:,1));


%---------------------------------
```

```
% Calculating initial 1/RS values
%---------------------------------
RS_AR_r = ones(length(data_r),20);
RS_CO_r = zeros(length(data_r),20);
RS_O2_r = zeros(length(data_r),20);
RS_CO2_r = zeros(length(data_r),20);
RS_C4H10_r = zeros(length(data_r),20);
RS_H2O_r = zeros(length(data_r),20);
%-----------------------------------
for i = 1:20
RS_CO_r(:,i) = (0.708*(1-exp(-5.2512*yCO_r(:,i)*100))+0.7007*(1-exp(-
0.1213*yCO_r(:,i)*100))); % upper fit
% RS_CO_r(:,i) = 0.74*(1-exp(-5.4355*yCO_r(:,i)*100)); %lower fit (does not make a large
difference)
RS_O2_r(:,i) = (0.9502+0.3343*exp(-0.4196*yO2_r(:,i)*100)); % lower fit
% RS_O2_r(:,i) = 1.0886+0.2884*exp(-0.8991*yO2_r(:,i)*100); % upper fit (does not make a
large difference)
RS_CO2_r(:,i) = (0.8314*(1-exp(-8.2868*yCO2_r(:,i)*100))+235.0045*(1-exp(-
0.000080174*yCO2_r(:,i)*100)));
RS_C4H10_r(:,i) = (0.8648+0.1608*exp(-
1.6851*yC4H10_r(:,i)*100)+0.0069778*yC4H10_r(:,i)*100);
RS_H2O_r(:,i) = (0.7941*(1-exp(-2.4685*yH2O_r(:,i)*100)));
%---------------------------------
% Calculating real molar fractions
%---------------------------------
yAR_r(:,i+1) =
RS_AR_r(:,i).*ppARs_r(:,1)./(RS_AR_r(:,i).*ppARs_r(:,1)+RS_CO_r(:,i).*ppCOs_r(:,1)+RS_O
2_r(:,i).*ppO2s_r(:,1)+ ...
RS_CO2_r(:,i).*ppCO2s_r(:,1)+RS_C4H10_r(:,i).*ppC4H10s_r(:,1)+RS_H2O_r(:,i).*ppH2Os_r
(:,1));
yCO_r(:,i+1) =
RS_CO_r(:,i).*ppCOs_r(:,1)./(RS_AR_r(:,i).*ppARs_r(:,1)+RS_CO_r(:,i).*ppCOs_r(:,1)+RS_O
2_r(:,i).*ppO2s_r(:,1)+ ...
RS_CO2_r(:,i).*ppCO2s_r(:,1)+RS_C4H10_r(:,i).*ppC4H10s_r(:,1)+RS_H2O_r(:,i).*ppH2Os_r
(:,1));
yO2_r(:,i+1) =
RS_O2_r(:,i).*ppO2s_r(:,1)./(RS_AR_r(:,i).*ppARs_r(:,1)+RS_CO_r(:,i).*ppCOs_r(:,1)+RS_O2
_r(:,i).*ppO2s_r(:,1)+ ...
RS_CO2_r(:,i).*ppCO2s_r(:,1)+RS_C4H10_r(:,i).*ppC4H10s_r(:,1)+RS_H2O_r(:,i).*ppH2Os_r
(:,1));
yCO2_r(:,i+1) =
RS_CO2_r(:,i).*ppCO2s_r(:,1)./(RS_AR_r(:,i).*ppARs_r(:,1)+RS_CO_r(:,i).*ppCOs_r(:,1)+RS_
O2_r(:,i).*ppO2s_r(:,1)+ ...
RS_CO2_r(:,i).*ppCO2s_r(:,1)+RS_C4H10_r(:,i).*ppC4H10s_r(:,1)+RS_H2O_r(:,i).*ppH2Os_r
(:,1));
```

```
yC4H10_r(:,i+1) =
RS_C4H10_r(:,i).*ppC4H10s_r(:,1)./(RS_AR_r(:,i).*ppARs_r(:,1)+RS_CO_r(:,i).*ppCOs_r(:,1)
+ ...
RS_O2_r(:,i).*ppO2s_r(:,1)+RS_CO2_r(:,i).*ppCO2s_r(:,1)+RS_C4H10_r(:,i).*ppC4H10s_r(:,1
)+RS_H2O_r(:,i).*ppH2Os_r(:,1));
yH2O_r(:,i+1) =
RS_H2O_r(:,i).*ppH2Os_r(:,1)./(RS_AR_r(:,i).*ppARs_r(:,1)+RS_CO_r(:,i).*ppCOs_r(:,1)+RS
_O2_r(:,i).*ppO2s_r(:,1)+ ...
RS_CO2_r(:,i).*ppCO2s_r(:,1)+RS_C4H10_r(:,i).*ppC4H10s_r(:,1)+RS_H2O_r(:,i).*ppH2Os_r
(:,1));
if ((abs(yAR_r(:,i+1)-yAR_r(:,i)) <= 0.0001) & (abs(yCO_r(:,i+1)-yCO_r(:,i)) <= 0.0001) & ...
(abs(yO2_r(:,i+1)-yO2_r(:,i)) <= 0.0001) & (abs(yCO2_r(:,i+1)-yCO2_r(:,i)) <= 0.0001) & ...
(abs(yC4H10_r(:,i+1)-yC4H10_r(:,i)) <= 0.0001) & (abs(yH2O_r(:,i+1)-yH2O_r(:,i)) <=
0.0001))
N_r = i+1;
break
end
end
%-----------------------------------------------------
% Defining matrices of all parameters (y, v, C and F)
%-----------------------------------------------------
%---------------------------------------
% Vectors of components molar fractions
%---------------------------------------
y_AR_r = zeros(length(data_r),2);
y_CO_r = zeros(length(data_r),2);
y_O2_r = zeros(length(data_r),2);
y_CO2_r = zeros(length(data_r),2);
y_C4H10_r = zeros(length(data_r),2);
y_H2O_r = zeros(length(data_r),2);
y_MA_r = zeros(length(data_r),2);
%-------------------------------------------
% Vectors of components volumetric flowrates
%-------------------------------------------
v_AR_r = zeros(length(data_r),2);
v_CO_r = zeros(length(data_r),2);
v_O2_r = zeros(length(data_r),2);
v_CO2_r = zeros(length(data_r),2);
v_C4H10_r = zeros(length(data_r),2);
v_H2O_r = zeros(length(data_r),2);
v_MA_r = zeros(length(data_r),2);
v_T_r = zeros(length(data_r),2); % vectors of total volumetric flowrates in reduction, mL/min
%-------------------------------------
% Vectors of components concentrations
%-------------------------------------
C_AR_r = zeros(length(data_r),2);
C_CO_r = zeros(length(data_r),2);
```

```
C_O2_r = zeros(length(data_r),2);
C_CO2_r = zeros(length(data_r),2);
C_C4H10_r = zeros(length(data_r),2);
C_H2O_r = zeros(length(data_r),2);
C_MA_r = zeros(length(data_r),2);
C_T_r = zeros(length(data_r),2); % vectors of total concentrations in reduction, gmole/mL
%---------------------------------------
% Vectors of components molar flowrates
%---------------------------------------
F_AR_r = zeros(length(data_r),2);
F_CO_r = zeros(length(data_r),2);
F_O2_r = zeros(length(data_r),2);
F_CO2_r = zeros(length(data_r),2);
F_C4H10_r = zeros(length(data_r),2);
F_H2O_r = zeros(length(data_r),2);
F_T_r = zeros(length(data_r),2); % vectors of total molar flowrates in reduction, gmole/min
%-------------------------------------------------------------
% Calculating inlet values of all parameters (v, y, C and F)
%-------------------------------------------------------------
%-----------------
% Input parameters
%-----------------
R = 760*22400/273.15; % universal gas constant, mmHg.mL/K.gmole
W_CAT = 472.7; % mg for amb P tests
% W_CAT = 459.0; % mg for P tests
%-------------------------------
P0 = 750.8; % mmHg for 1-1-1
T0 = 23.4; % °C for 1-1-1
%---------------------------------------
v_B_r = 0.0; % mL/min for 1-1-1
v_C_r = 41.9; % mL/min for 1-1-1
%-----------------------------------------
N_MA_HPLC = 11.06; % mmol/kgcat/cycle for 1-1-1, ave
%-------------------------------------------------------------------------
% Correcting instant exit MA values from HPLC and conductivity total values
%-------------------------------------------------------------------------
N_MA_COND = trapz(TIME_R(:,1),F_MA_r(:,2)); % total moles of exit MA in reduction (from
conductivity data), gmole
N_MA_HPLC = N_MA_HPLC/1000*(W_CAT/1000000); % total moles of MA produced in a
redox cycle (from HPLC, ave), gmole
RATIO = N_MA_HPLC/N_MA_COND; % ratio of total MA produced from HPLC to MA
calcualted from conductivity
F_MA_r(:,2) = RATIO*F_MA_r(:,2); % correcting MA rates from conductivity to give total
values equal to HPLC results
```

```
%---------------------------------------
% Calculating inlet volumetric flowrates
%---------------------------------------
v_CO_r(:,1)= 0.0;
v_CO2_r(:,1) = 0.0;
v_H2O_r(:,1) = 0.0;
v_MA_r(:,1) = 0.0;
v_C4H10_r(:,1) = 0.0994*v_C_r;
v_O2_r(:,1) = 0.211*v_B_r;
v_AR_r(:,1) = (1-0.0994)*v_C_r+(1-0.211)*v_B_r;
v_T_r(:,1) = v_C_r+v_B_r; % total inlet volumetric flowrate in reduction, mL/min
%----------------------------------
% Calculating inlet molar fractions
%----------------------------------
y_CO_r(:,1) = 0.0;
y_CO2_r(:,1) = 0.0;
y_H2O_r(:,1) = 0.0;
y_MA_r(:,1) = 0.0;
y_C4H10_r(:,1) = v_C4H10_r(:,1)./v_T_r(:,1);
y_O2_r(:,1) = v_O2_r(:,1)./v_T_r(:,1);
y_AR_r(:,1) = v_AR_r(:,1)./v_T_r(:,1);
%----------------------------------
% Calculating inlet concentrations
%----------------------------------
C_T_r(:,1) = P0/(R*(T0+273.15)); % total inlet concentration, gmol/mL
C_CO_r(:,1) = 0.0;
C_CO2_r(:,1) = 0.0;
C_H2O_r(:,1) = 0.0;
C_MA_r(:,1) = 0.0;
C_C4H10_r(:,1) = y_C4H10_r(:,1).*C_T_r(:,1);
C_O2_r(:,1) = y_O2_r(:,1).*C_T_r(:,1);
C_AR_r(:,1) = y_AR_r(:,1).*C_T_r(:,1);
%----------------------------------
% Calculating inlet molar flowrates
%----------------------------------
F_CO_r(:,1) = 0.0;
F_CO2_r(:,1) = 0.0;
F_H2O_r(:,1) = 0.0;
F_MA_r(:,1) = 0.0;
F_C4H10_r(:,1) = C_C4H10_r(:,1).*v_T_r(:,1);
F_O2_r(:,1) = C_O2_r(:,1).*v_T_r(:,1);
F_AR_r(:,1) = C_AR_r(:,1).*v_T_r(:,1);
F_T_r(:,1) = C_T_r(:,1).*v_T_r(:,1); % total inlet molar flowrate in reduction, gmol/min
```

```
%-------------------------------------------------------------------
% Calculating exit parameters
%-------------------------------------------------------------------
%-----------------------------------
% Assumption for exit total flowrates
%-----------------------------------
C_T_r(:,2) = C_T_r(:,1);
v_T_r(:,2) = v_T_r(:,1);
F_T_r(:,2) = C_T_r(:,2).*v_T_r(:,2); % total exit molar flowrate in reduction, gmol/min
%-----------------------------------------------------------------------
% Putting calculated exit molar fractions in a new vector (not final values
% (over estimated) due to non accounted presence of MA in products)
%-----------------------------------------------------------------------
y_CO_r(:,2) = yCO_r(:,N_r);
y_CO2_r(:,2) = yCO2_r(:,N_r);
y_H2O_r(:,2) = yH2O_r(:,N_r);
y_C4H10_r(:,2) = yC4H10_r(:,N_r);
y_O2_r(:,2) = yO2_r(:,N_r);
y_AR_r(:,2) = yAR_r(:,N_r);
%-------------------------------------------------------------------------------------------
% Calculating exit molar flowrates (considering average MA exit molar flowrate in addition)
%-------------------------------------------------------------------------------------------
F_MA_ave = mean(F_MA_r(:,2));
F_CO_r(:,2) = y_CO_r(:,2).*(F_T_r(:,2)-F_MA_ave);
F_CO2_r(:,2) = y_CO2_r(:,2).*(F_T_r(:,2)-F_MA_ave);
F_H2O_r(:,2) = y_H2O_r(:,2).*(F_T_r(:,2)-F_MA_ave);
F_C4H10_r(:,2) = y_C4H10_r(:,2).*(F_T_r(:,2)-F_MA_ave);
F_O2_r(:,2) = y_O2_r(:,2).*(F_T_r(:,2)-F_MA_ave);
F_AR_r(:,2) = y_AR_r(:,2).*(F_T_r(:,2)-F_MA_ave);
%-------------------------------------------------------------------
% Correcting exit molar fractions (to account for MA molar fraction)
%-------------------------------------------------------------------
y_CO_r(:,2) = F_CO_r(:,2)./F_T_r(:,2);
y_CO2_r(:,2) = F_CO2_r(:,2)./F_T_r(:,2);
y_H2O_r(:,2) = F_H2O_r(:,2)./F_T_r(:,2);
y_C4H10_r(:,2) = F_C4H10_r(:,2)./F_T_r(:,2);
y_O2_r(:,2) = F_O2_r(:,2)./F_T_r(:,2);
y_AR_r(:,2) = F_AR_r(:,2)./F_T_r(:,2);
y_MA_r(:,2) = F_MA_r(:,2)./F_T_r(:,2);
%---------------------------------------
% Calculating exit volumetric flowrates
%---------------------------------------
v_CO_r(:,2) = y_CO_r(:,2).*v_T_r(:,2);
v_CO2_r(:,2) = y_CO2_r(:,2).*v_T_r(:,2);
v_H2O_r(:,2) = y_H2O_r(:,2).*v_T_r(:,2);
v_C4H10_r(:,2) = y_C4H10_r(:,2).*v_T_r(:,2);
v_O2_r(:,2) = y_O2_r(:,2).*v_T_r(:,2);
```

```
v_AR_r(:,2) = y_AR_r(:,2).*v_T_r(:,2);
v_MA_r(:,2) = y_MA_r(:,2).*v_T_r(:,2);
%--------------------------------
% Calculating exit concentrations
%--------------------------------
C_CO_r(:,2) = y_CO_r(:,2).*C_T_r(:,2);
C_CO2_r(:,2) = y_CO2_r(:,2).*C_T_r(:,2);
C_H2O_r(:,2) = y_H2O_r(:,2).*C_T_r(:,2);
C_C4H10_r(:,2) = y_C4H10_r(:,2).*C_T_r(:,2);
C_O2_r(:,2) = y_O2_r(:,2).*C_T_r(:,2);
C_AR_r(:,2) = y_AR_r(:,2).*C_T_r(:,2);
C_MA_r(:,2) = y_MA_r(:,2).*C_T_r(:,2);
%-------------------------------------------------------------
% Calculating instant values of conversions and selectivities
%-------------------------------------------------------------
%---------------------------------------
% Calculating instant n-butane conversion
%---------------------------------------
X_C4H10i = zeros(length(data_r),1); % instant n-butane conversion
X_C4H10i(:,1) = (F_C4H10_r(:,1)-F_C4H10_r(:,2))./F_C4H10_r(:,1)*100;
%-----------------------------------------------
% Calculating instant oxygen conversion in reduction
%-----------------------------------------------
X_O2i_r = zeros(length(data_r),1); % instant oxygen conversion in reduction
X_O2i_r(:,1) = (F_O2_r(:,1)-F_O2_r(:,2))./F_O2_r(:,1)*100;
%-----------------------------------------------------
% Calculating instant product selectivities in reduction
%-----------------------------------------------------
S_COi_r = zeros(length(data_r),1); % instant CO selectivity in reduction
S_CO2i_r = zeros(length(data_r),1); % instant CO2 selectivity in reduction
S_H2Oi_r = zeros(length(data_r),1); % instant H2O selectivity in reduction
S_MAi_r = zeros(length(data_r),1); % instant MA selectivity in reduction
%-------------------------------------------------------------
S_COi_r(:,1) = F_CO_r(:,2)./(4*(F_C4H10_r(:,1)-F_C4H10_r(:,2)))*100;
S_CO2i_r(:,1) = F_CO2_r(:,2)./(4*(F_C4H10_r(:,1)-F_C4H10_r(:,2)))*100;
S_H2Oi_r(:,1) = F_H2O_r(:,2)./(5*(F_C4H10_r(:,1)-F_C4H10_r(:,2)))*100;
S_MAi_r(:,1) = F_MA_r(:,2)./(F_C4H10_r(:,1)-F_C4H10_r(:,2))*100;
%-----------------------------------------------------
% Calculating total values of conversions and selectivities
%-----------------------------------------------------
%---------------------------------
% Total moles of feeds and products
%---------------------------------
N_CO_r = zeros(1,2);
N_CO2_r = zeros(1,2);
N_H2O_r = zeros(1,2);
N_C4H10_r = zeros(1,2);
```

```
N_O2_r = zeros(1,2);
N_AR_r = zeros(1,2);
N_AR_rs = zeros(1,2); % shifted values only for argon balance calculation
N_MA_r = zeros(1,2);
%-----------------------------------------------
N_C4H10_r(1,1) = F_C4H10_r(1,1)*2.0; % total moles of inlet n-butane in TIME_R = 2.0
minutes reduction, gmole
N_C4H10_r(1,2) = trapz(TIME_R(:,1),F_C4H10_r(:,2)); % total moles of exit n-butane in
reduction, gmole
%-----------------------------------------------
N_O2_r(1,1) = F_O2_r(1,1)*2.0; % total moles of inlet oxygen in TIME_R = 2.0 minutes
reduction, gmole
N_O2_r(1,2) = trapz(TIME_R(:,1),F_O2_r(:,2)); % total moles of exit oxygen in reduction,
gmole
%-----------------------------------------------
N_CO_r(1,2) = trapz(TIME_R(:,1),F_CO_r(:,2)); % total moles of exit CO in reduction, gmole
N_CO2_r(1,2) = trapz(TIME_R(:,1),F_CO2_r(:,2)); % total moles of exit CO2 in reduction,
gmole
N_H2O_r(1,2) = trapz(TIME_R(:,1),F_H2O_r(:,2)); % total moles of exit H2O in reduction,
gmole
%-----------------------------------------------
% N_MA_r(1,2) = N_MA_COND; % to calculate the total MA selectivity or
% total molar balances based on conductivity results (no difference with HPLC now)
% N_MA_r(1,2) = N_MA_HPLC; % to calculate the total MA selectivity or total molar balances
based on HPLC results
N_MA_r(1,2) = trapz(TIME_R(:,1),F_MA_r(:,2)); % total moles of exit MA in reduction, gmole
%-----------------------------------------------
N_AR_r(1,1) = F_AR_r(1,1)*2.0; % total moles of inlet argon in TIME_R = 2.0 minutes
reduction, gmole
N_AR_r(1,2) = trapz(TIME_R(:,1),F_AR_r(:,2)); %  total moles of exit argon in reduction,
gmole; not a correct value look at the
% graph of F_AR_r(:,2), but not used anywhere
%-----------------------------------------------
N_AR_rs(1,1) = (mean(F_AR_r(1:30,2))-F_AR_r(1,1))*2.0; % shifted inlet value only for argon
balance calculation, gmole
N_AR_rs(1,2) = trapz(TIME_R(:,1),(mean(F_AR_r(1:30,2))-F_AR_r(:,2))); % shifted exit value
only for argon balance calculation, gmole
%---------------------------
% Total n-butane conversion
%---------------------------
X_C4H10t = zeros(1,1); % total n-butane conversion
X_C4H10t(1,1) = (N_C4H10_r(1,1)-N_C4H10_r(1,2))/N_C4H10_r(1,1)*100;
%-------------------------------------
% Total oxygen conversion in reduction
%-------------------------------------
X_O2t_r = zeros(1,1); % total oxygen conversion in reduction
X_O2t_r(1,1) = (N_O2_r(1,1)-N_O2_r(1,2))/N_O2_r(1,1)*100;
```

```
%-----------------------------------------
% Total products selectivities in reduction
%-----------------------------------------
S_COt_r = zeros(1,1); % total CO selectivity in reduction
S_CO2t_r = zeros(1,1); % total CO2 selectivity in reduction
S_H2Ot_r = zeros(1,1); % total H2O selectivity in reduction
S_MAt_r = zeros(1,1); % total MA selectivity in reduction
%-------------------------------------------------
S_COt_r(1,1) = N_CO_r(1,2)/(4*(N_C4H10_r(1,1)-N_C4H10_r(1,2)))*100;
S_CO2t_r(1,1) = N_CO2_r(1,2)/(4*(N_C4H10_r(1,1)-N_C4H10_r(1,2)))*100;
S_H2Ot_r(1,1) = N_H2O_r(1,2)/(5*(N_C4H10_r(1,1)-N_C4H10_r(1,2)))*100;
S_MAt_r(1,1) = N_MA_r(1,2)/(N_C4H10_r(1,1)-N_C4H10_r(1,2))*100; %  total MA
selectivity
%-----------------------------------------------------------
% Calculating instant and total product yields in reduction
%-----------------------------------------------------------
%-------------------------------------------------
% Calculating instant product yields in reduction
%-------------------------------------------------
Y_COi_r = zeros(length(data_r),1); % instant CO yield in reduction
Y_CO2i_r = zeros(length(data_r),1); % instant CO2 yield in reduction
Y_H2Oi_r = zeros(length(data_r),1); % instant H2O yield in reduction
Y_MAi_r = zeros(length(data_r),1); % instant MA yield in reduction
%-----------------------------------------------------------
Y_COi_r(:,1) = F_CO_r(:,2)./(4*F_C4H10_r(:,1))*100;
Y_CO2i_r(:,1) = F_CO2_r(:,2)./(4*F_C4H10_r(:,1))*100;
Y_H2Oi_r(:,1) = F_H2O_r(:,2)./(5*F_C4H10_r(:,1))*100;
Y_MAi_r(:,1) = F_MA_r(:,2)./F_C4H10_r(:,1)*100;
%-----------------------------------------------
% Calculating total product yields in reduction
%-----------------------------------------------
Y_COt_r = zeros(1,1); % total CO yield in reduction
Y_CO2t_r = zeros(1,1); % total CO2 yield in reduction
Y_H2Ot_r = zeros(1,1); % total H2O yield in reduction
Y_MAt_r = zeros(1,1); % total MA yield in reduction
%-----------------------------------------------------------
Y_COt_r(1,1) = N_CO_r(1,2)/(4*N_C4H10_r(1,1))*100;
Y_CO2t_r(1,1) = N_CO2_r(1,2)/(4*N_C4H10_r(1,1))*100;
Y_H2Ot_r(1,1) = N_H2O_r(1,2)/(5*N_C4H10_r(1,1))*100;
Y_MAt_r(1,1) = N_MA_r(1,2)/N_C4H10_r(1,1)*100; % total MA yield
%-----------------------------------------------------------
% Calculating instant and total molar balances in reduction
%-----------------------------------------------------------
%-------------------------------------------------
% Calculating instant molar balaces in reduction
%-------------------------------------------------
C_BALi_r = zeros(length(data_r),1); % instant carbon balance
```

```
O_BALi_r = zeros(length(data_r),1); % instant oxygen balance
H_BALi_r = zeros(length(data_r),1); % instant hydrogen balance
AR_BALi_r = zeros(length(data_r),1); % instant argon balance
%-----------------------------------------------------------
C_BALi_r(:,1) = (1-(4*F_C4H10_r(:,1)-4*F_C4H10_r(:,2)-F_CO_r(:,2)-F_CO2_r(:,2)-
4*F_MA_r(:,2))./(4*F_C4H10_r(:,1)))*100;
O_BALi_r(:,1) = (1-(2*F_O2_r(:,1)-2*F_O2_r(:,2)-F_CO_r(:,2)-2*F_CO2_r(:,2)-F_H2O_r(:,2)-
3*F_MA_r(:,2))./(2*F_O2_r(:,1)))*100;
H_BALi_r(:,1) = (1-(10*F_C4H10_r(:,1)-10*F_C4H10_r(:,2)-2*F_H2O_r(:,2)-
2*F_MA_r(:,2))./(10*F_C4H10_r(:,1)))*100;
AR_BALi_r(:,1) = (1-(F_AR_r(:,1)-F_AR_r(:,2))./F_AR_r(:,1))*100;
%-----------------------------------------------------
% Calculating total molar balances in reduction
%-----------------------------------------------------
C_BALt_r = zeros(1,1); % total carbon balance
O_BALt_r = zeros(1,1); % total oxygen balance
H_BALt_r = zeros(1,1); % total hydrogen balance
AR_BALt_r = zeros(1,1); % total argon balance
%-----------------------------------------------------
C_BALt_r(1,1) = (1-(4*N_C4H10_r(1,1)-4*N_C4H10_r(1,2)-N_CO_r(1,2)-N_CO2_r(1,2)-
4*N_MA_r(1,2))/(4*N_C4H10_r(1,1)))*100;
O_BALt_r(1,1) = (1-(2*N_O2_r(1,1)-2*N_O2_r(1,2)-N_CO_r(1,2)-2*N_CO2_r(1,2)-
N_H2O_r(1,2)-3*N_MA_r(1,2))/(2*N_O2_r(1,1)))*100;
H_BALt_r(1,1) = (1-(10*N_C4H10_r(1,1)-10*N_C4H10_r(1,2)-2*N_H2O_r(1,2)-
2*N_MA_r(1,2))/(10*N_C4H10_r(1,1)))*100;
AR_BALt_r(1,1) = (1+(N_AR_rs(1,1)-N_AR_rs(1,2))/N_AR_rs(1,1))*100; % 1+... because the
values of F_AR_r(:,1) and F_AR_r(:,2) were shifted like a mirror
```

APPENDIX C – KINETIC MODELING PROGRAM

MATLAB® programs for fitting, model, kinetics and blank calculations

```
clear
clc

global time   DT     N      Nr     V      W      C_T    C_VT...
      F_11   F_21   F_31   F_41   F_51   F_61   F_71   F_T1...
      F_12   F_22   F_32   F_42   F_52   F_62   F_72   F_T2...
      F_13   F_23   F_33   F_43   F_53   F_63   F_73   F_T3...
      F_14   F_24   F_34   F_44   F_54   F_64   F_74   F_T4...
      y_V41  y_V51  M1     X_C41  X_O21  S1...
      y_V42  y_V52  M2     X_C42  X_O22  S2...
      y_V43  y_V53  M3     X_C43  X_O23  S3...
      y_V44  y_V54  M4     X_C44  X_O24  S4...
      R2_XC4 R2_XO2 R2_SMA R2_SCOx ypred ypredd
%-----------------------------------------------------------
Nr = 40;
Nb = 40;
N = Nr+Nb;                                  % Number of CSTR in series
tmax = 150;                                 % Maximum simulation time, second
DT = 0.1;                                   % Solver time steps, second
time = linspace(0,tmax,tmax/DT+1);          % Time vector, second
time = time';
%-----------------------------------------------------------
xdata = zeros(4,5);
ydata = zeros(4,5);

xdataa = zeros(20,1);
ydataa = zeros(20,1);

ypred = zeros(4,5);
ypredd = zeros(20,1);

v1 = zeros(length(time),N+1);               % Total volumetric flowrate, mL/s
v2 = zeros(length(time),N+1);
v3 = zeros(length(time),N+1);
v4 = zeros(length(time),N+1);

V = zeros(N,1);
W = zeros(Nr,1);
```

```
y_11 = zeros(length(time),N+1);                % C4H10
y_21 = zeros(length(time),N+1);                % MA
y_31 = zeros(length(time),N+1);                % O2
y_41 = zeros(length(time),N+1);                % H2O
y_51 = zeros(length(time),N+1);                % CO
y_61 = zeros(length(time),N+1);                % CO2
y_71 = ones(length(time),N+1);                 % Ar
y_12 = zeros(length(time),N+1);
y_22 = zeros(length(time),N+1);
y_32 = zeros(length(time),N+1);
y_42 = zeros(length(time),N+1);
y_52 = zeros(length(time),N+1);
y_62 = zeros(length(time),N+1);
y_72 = ones(length(time),N+1);

y_13 = zeros(length(time),N+1);
y_23 = zeros(length(time),N+1);
y_33 = zeros(length(time),N+1);
y_43 = zeros(length(time),N+1);
y_53 = zeros(length(time),N+1);
y_63 = zeros(length(time),N+1);
y_73 = ones(length(time),N+1);

y_14 = zeros(length(time),N+1);
y_24 = zeros(length(time),N+1);
y_34 = zeros(length(time),N+1);
y_44 = zeros(length(time),N+1);
y_54 = zeros(length(time),N+1);
y_64 = zeros(length(time),N+1);
y_74 = ones(length(time),N+1);

y_V41 = zeros(length(time),Nr);
y_V51 = zeros(length(time),Nr);

y_V42 = zeros(length(time),Nr);
y_V52 = zeros(length(time),Nr);

y_V43 = zeros(length(time),Nr);
y_V53 = zeros(length(time),Nr);

y_V44 = zeros(length(time),Nr);
y_V54 = zeros(length(time),Nr);

F_11 = zeros(length(time),N+1);
F_21 = zeros(length(time),N+1);
F_31 = zeros(length(time),N+1);
F_41 = zeros(length(time),N+1);
```

```
F_51 = zeros(length(time),N+1);
F_61 = zeros(length(time),N+1);
F_71 = zeros(length(time),N+1);
F_T1 = zeros(length(time),N+1);

F_12 = zeros(length(time),N+1);
F_22 = zeros(length(time),N+1);
F_32 = zeros(length(time),N+1);
F_42 = zeros(length(time),N+1);
F_52 = zeros(length(time),N+1);
F_62 = zeros(length(time),N+1);
F_72 = zeros(length(time),N+1);
F_T2 = zeros(length(time),N+1);

F_13 = zeros(length(time),N+1);
F_23 = zeros(length(time),N+1);
F_33 = zeros(length(time),N+1);
F_43 = zeros(length(time),N+1);
F_53 = zeros(length(time),N+1);
F_63 = zeros(length(time),N+1);
F_73 = zeros(length(time),N+1);
F_T3 = zeros(length(time),N+1);

F_14 = zeros(length(time),N+1);
F_24 = zeros(length(time),N+1);
F_34 = zeros(length(time),N+1);
F_44 = zeros(length(time),N+1);
F_54 = zeros(length(time),N+1);
F_64 = zeros(length(time),N+1);
F_74 = zeros(length(time),N+1);
F_T4 = zeros(length(time),N+1);

M1 = zeros(6,2);
X_C41 = zeros(1,2);
X_O21 = zeros(1,2);
S1 = zeros(3,2);

M2 = zeros(6,2);
X_C42 = zeros(1,2);
X_O22 = zeros(1,2);
S2 = zeros(3,2);

M3 = zeros(6,2);
X_C43 = zeros(1,2);
X_O23 = zeros(1,2);
S3 = zeros(3,2);
```

```
M4 = zeros(6,2);
X_C44 = zeros(1,2);
X_O24 = zeros(1,2);
S4 = zeros(3,2);

O2_C4 = zeros(4,1);
X_C4O2 = zeros(4,4);
S_MACOx = zeros(4,6);
%-----------------------------------------------------------
R = 760*22400/273.15;              % Universal gas constant, mmHg.mL/K.gmol
W_T = 472.7;                       % Catalyst weight, ambient pressure, mg
rhoB = 780;                        % Bulk density of VPO, mg/mL (measured)
rhoP = 1700;                       % Particle density of VPO, mg/mL
epsilon = (1-rhoB/rhoP);           % VPO catalyst voidage
Vr = W_T/rhoB;                     % Total bed volume, mL
Vg = epsilon*Vr;                   % Total gas volume in bed, mL
Vb = 175;                          % Blank space volume, mL
%-----------------------------------------------------------
for ii = 1:Nr

   W(ii,1) = (ii/Nr)*W_T;          % Sectional mass of catalyst, mg
   V(ii,1) = (ii/Nr)*Vg;           % Sectional volume of gas at reaction section, mL

end

for jj = Nr+1:N

   V(jj,1) = Vg+(jj-Nr/Nb)*Vb;     % Sectional volume of gas at blank space, mL

end
%-----------------------------------------------------------
P = (0.5+14.7)/14.7*760;           % Reactor pressure, mmHg
T = 380;                           % Reactor temperature, °C

P01 = 738.8;         % For 4-3-1   % Lab pressure, mmHg
T01 = 24.7;                        % Lab temperature, °C

P02 = 735.0;         % For 4-1-1R
T02 = 26.2;

P03 = 745.2;         % For 5-1-1
T03 = 23.2;

P04 = 742.9;         % For 6-1-1
T04 = 23.3;
```

```
%-----------------------------------------------------------
v_A1 = 47.2/60;        % For 4-3-1   % Argon gas flow rate, mL/s: to purge
v_B1 = 16.2/60;                     % Oxygen gas flow rate, mL/s
v_C1 = 29.7/60;                     % n-butane gas flow rate, mL/s

v_A2 = 48.0/60;        % For 4-1-1R
v_B2 = 16.2/60;
v_C2 = 30.1/60;

v_A3 = 45.9/60;        % For 5-1-1
v_B3 = 28.9/60;
v_C3 = 16.8/60;

v_A4 = 46.4/60;        % For 6-1-1
v_B4 = 40.1/60;
v_C4 = 6.6/60;
%-----------------------------------------------------------
v_BC1  = v_B1+v_C1;                 % Total inlet volumetric flowrate - lab conditions, mL/s
v_BC2  = v_B2+v_C2;
v_BC3  = v_B3+v_C3;
v_BC4  = v_B4+v_C4;

C_T = P/(R*(T+273.15));             % Total concentration, gmol/mL
C_VT = (1/162)/1000;                % Total V in VPP: VOPO4 as basis, gmol/mg
%-----------------------------------------------------------
y0_C4H101 = 0.0643;    % For 4-3-1          % n-butane inlet molar fraction
y0_O21 = 0.0745;                          % Oxygen inlet molar fraction
y0_Ar1 = 0.8612;                          % Argon inlet molar fraction

y0_C4H102 = 0.0646;    % For 4-1-1R
y0_O22 = 0.0738;
y0_Ar2 = 0.8616;

y0_C4H103 = 0.0365;    % For 5-1-1
y0_O23 = 0.1334;
y0_Ar3 = 0.8301;

y0_C4H104 = 0.0140;    % For 6-1-1
y0_O24 = 0.1812;
y0_Ar4 = 0.8048;
%-----------------------------------------------------------
X_C41(1,1) = 15.0;     % For 4-3-1
X_O21(1,1) = 49.5;
S1(1,1) = 58.0;        % MA
S1(2,1) = 18.7;        % CO
S1(3,1) = 16.0;        % CO2
```

```
X_C42(1,1) = 20.0;      % For 4-1-1R
X_O22(1,1) = 55.5;
S2(1,1) = 64.9;         % MA
S2(2,1) = 19.7;         % CO
S2(3,1) = 18.5;         % CO2

X_C43(1,1) = 30.9;      % For 5-1-1
X_O23(1,1) = 26.0;
S3(1,1) = 64.6;         % MA
S3(2,1) = 20.0;         % CO
S3(3,1) = 20.6;         % CO2

X_C44(1,1) = 43.6;      % For 6-1-1
X_O24(1,1) = 11.8;
S4(1,1) = 64.6;         % MA
S4(2,1) = 19.1;         % CO
S4(3,1) = 20.8;         % CO2

COx1 = (S1(2,1)+S1(3,1))/2;
COx2 = (S2(2,1)+S2(3,1))/2;
COx3 = (S3(2,1)+S3(3,1))/2;
COx4 = (S4(2,1)+S4(3,1))/2;

S1(2,1) = COx1;
S1(3,1) = COx1;

S2(2,1) = COx2;
S2(3,1) = COx2;

S3(2,1) = COx3;
S3(3,1) = COx3;

S4(2,1) = COx4;
S4(3,1) = COx4;
%-----------------------------------------------------------
for h = 1:length(time)

   if (time(h,1) < 120)

      v1(h,1)   =  v_BC1* (P01/P)*(T+273.15)/(T01+273.15);
% Total mixed gas volumetric flowrate - bed conditions, mL/s
      v2(h,1)   =  v_BC2* (P02/P)*(T+273.15)/(T02+273.15);
      v3(h,1)   =  v_BC3* (P03/P)*(T+273.15)/(T03+273.15);
      v4(h,1)   =  v_BC4* (P04/P)*(T+273.15)/(T04+273.15);

   else
```

```
      v1(h,1)   = v_A1* (P01/P)*(T+273.15)/(T01+273.15);
% Total purge stream volumetric flowrate - bed conditions, mL/s
      v2(h,1)   = v_A2* (P02/P)*(T+273.15)/(T02+273.15);
      v3(h,1)   = v_A3* (P03/P)*(T+273.15)/(T03+273.15);
      v4(h,1)   = v_A4* (P04/P)*(T+273.15)/(T04+273.15);

   end

end

v1(1,:)  =  v1(tmax/DT+1,1);
v2(1,:)  =  v2(tmax/DT+1,1);
v3(1,:)  =  v3(tmax/DT+1,1);
v4(1,:)  =  v4(tmax/DT+1,1);
%-----------------------------------------------------------
for z = 1:length(time)                          % Inlet molar fractions

   if (time(z,1) < 120)

      y_11(z,1) = y0_C4H101;
      y_31(z,1) = y0_O21;
      y_71(z,1) = y0_Ar1;

      y_12(z,1) = y0_C4H102;
      y_32(z,1) = y0_O22;
      y_72(z,1) = y0_Ar2;

      y_13(z,1) = y0_C4H103;
      y_33(z,1) = y0_O23;
      y_73(z,1) = y0_Ar3;

      y_14(z,1) = y0_C4H104;
      y_34(z,1) = y0_O24;
      y_74(z,1) = y0_Ar4;

   end

end

y_11(1,:) = 0.0;
y_31(1,:) = 0.0;
y_71(1,:) = 1.0;

y_12(1,:) = 0.0;
y_32(1,:) = 0.0;
y_72(1,:) = 1.0;
```

```
y_13(1,:) = 0.0;
y_33(1,:) = 0.0;
y_73(1,:) = 1.0;
y_14(1,:) = 0.0;
y_34(1,:) = 0.0;
y_74(1,:) = 1.0;
%-----------------------------------------------------------
F_T1(:,1) =  v1(:,1)*C_T;                    % Total inlet molar flow rate, gmol/s
F_T2(:,1) =  v2(:,1)*C_T;
F_T3(:,1) =  v3(:,1)*C_T;
F_T4(:,1) =  v4(:,1)*C_T;
%-----------------------------------------------------------
F_11(:,1) = y_11(:,1).*F_T1(:,1);            % Inlet molar flow rates, gmol/s
F_21(:,1) = 0.0;
F_31(:,1) = y_31(:,1).*F_T1(:,1);
F_41(:,1) = 0.0;
F_51(:,1) = 0.0;
F_61(:,1) = 0.0;
F_71(:,1) = y_71(:,1).*F_T1(:,1);

F_12(:,1) = y_12(:,1).*F_T2(:,1);
F_22(:,1) = 0.0;
F_32(:,1) = y_32(:,1).*F_T2(:,1);
F_42(:,1) = 0.0;
F_52(:,1) = 0.0;
F_62(:,1) = 0.0;
F_72(:,1) = y_72(:,1).*F_T2(:,1);

F_13(:,1) = y_13(:,1).*F_T3(:,1);
F_23(:,1) = 0.0;
F_33(:,1) = y_33(:,1).*F_T3(:,1);
F_43(:,1) = 0.0;
F_53(:,1) = 0.0;
F_63(:,1) = 0.0;
F_73(:,1) = y_73(:,1).*F_T3(:,1);

F_14(:,1) = y_14(:,1).*F_T4(:,1);
F_24(:,1) = 0.0;
F_34(:,1) = y_34(:,1).*F_T4(:,1);
F_44(:,1) = 0.0;
F_54(:,1) = 0.0;
F_64(:,1) = 0.0;
F_74(:,1) = y_74(:,1).*F_T4(:,1);
%-----------------------------------------------------------
F_71(1,:) = F_71(tmax/DT+1,1);               % Initial Ar flow rate, gmol/s
F_T1(1,:) = F_T1(tmax/DT+1,1);               % Initial total flow rate, gmol/s
```

```
F_72(1,:) = F_72(tmax/DT+1,1);
F_T2(1,:) = F_T2(tmax/DT+1,1);
F_73(1,:) = F_73(tmax/DT+1,1);
F_T3(1,:) = F_T3(tmax/DT+1,1);

F_74(1,:) = F_74(tmax/DT+1,1);
F_T4(1,:) = F_T4(tmax/DT+1,1);
%-------------------------------------------------------
O2_C4(1,1) = y0_O21/y0_C4H101;
O2_C4(2,1) = y0_O22/y0_C4H102;
O2_C4(3,1) = y0_O23/y0_C4H103;
O2_C4(4,1) = y0_O24/y0_C4H104;

X_C4O2(1,1) = X_C41(1,1);
X_C4O2(2,1) = X_C42(1,1);
X_C4O2(3,1) = X_C43(1,1);
X_C4O2(4,1) = X_C44(1,1);
X_C4O2(1,3) = X_O21(1,1);
X_C4O2(2,3) = X_O22(1,1);
X_C4O2(3,3) = X_O23(1,1);
X_C4O2(4,3) = X_O24(1,1);

S_MACOx(1,1) = S1(1,1);
S_MACOx(2,1) = S2(1,1);
S_MACOx(3,1) = S3(1,1);
S_MACOx(4,1) = S4(1,1);
S_MACOx(1,3) = S1(2,1);
S_MACOx(2,3) = S2(2,1);
S_MACOx(3,3) = S3(2,1);
S_MACOx(4,3) = S4(2,1);
S_MACOx(1,5) = S1(3,1);
S_MACOx(2,5) = S2(3,1);
S_MACOx(3,5) = S3(3,1);
S_MACOx(4,5) = S4(3,1);
%-------------------------------------------------------
xdata(:,1) = O2_C4(:,1);
xdata(:,2) = O2_C4(:,1);
xdata(:,3) = O2_C4(:,1);
xdata(:,4) = O2_C4(:,1);
xdata(:,5) = O2_C4(:,1);

ydata(:,1) = X_C4O2(:,1);
ydata(:,2) = X_C4O2(:,3);
ydata(:,3) = S_MACOx(:,1);
ydata(:,4) = S_MACOx(:,3);
ydata(:,5) = S_MACOx(:,5);
```

```
%-----------------------------------------------------------
ydataa(1:4,1) = ydata(:,1);
ydataa(5:8,1) = ydata(:,2);
ydataa(9:12,1) = ydata(:,3);
ydataa(13:16,1) = ydata(:,4);
ydataa(17:20,1) = ydata(:,5);

xdataa(1:4,1) = xdata(:,1);
xdataa(5:8,1) = xdata(:,2);
xdataa(9:12,1) = xdata(:,3);
xdataa(13:16,1) = xdata(:,4);
xdataa(17:20,1) = xdata(:,5);
%-----------------------------------------------------------
% LB = zeros(7,1);
% UB = [inf; inf; inf; 1; 1; 1; 1];
% options = optimset('MaxFunEvals',1000,'MaxIter',1000,'PlotFcns',@optimplotx,...
%     'Algorithm',{'levenberg-marquardt',0.01},'TolFun',1E-10,'TolX',1E-10);
% [k,resnorm,residual,exitflag,output,lambda,J] = ...
% lsqcurvefit(@modelLlsq,k,xdataa,ydataa,[],[],options);
% CIK = nlparci(k,residual,'jacobian',J,'alpha',0.05);
% [ypred2,CIP] = nlpredci(@modelLlsq,xdataa,k,residual,'jacobian',J,'alpha',0.05);
%-----------------------------------------------------------
load k;                                                 % Reaction rate constants, mg/gmol.s

options = statset('Display','iter','TolFun',1E-10,'TolX',1E-
10,'MaxIter',1000,'Robust','on','WgtFun','bisquare');
% options = statset('Display','iter','TolFun',1E-10,'TolX',1E-10,'MaxIter',1000);

% [...] = statset(...,'Tune',scalar positive value,...) lower tune makes higher weights

[k,residual,J,CVR,MSE] = nlinfit(xdataa,ydataa,@modelLlsq,k,options);

CIK = nlparci(k,residual,'covar',CVR,'alpha',0.05);
[ypred2,CIP] = nlpredci(@modelLlsq,xdataa,k,residual,'covar',CVR,'alpha',0.05,'mse',MSE);
% [...] = nlpredci(...,'simopt','on','predopt','observation')
%-----------------------------------------------------------
% load CIK;
%
% k = CIK(:,2);
% opts = optimset('fminsearch');
% opts.Display = 'iter';
%
% LB = k;
% UB = k;
%
% [k, fval] = fminsearchbnd(@modelLlsq,k,LB,UB,opts);
```

```
%-----------------------------------------------------------
v1(:,:)  =  F_T1(:,:)/C_T;
v2(:,:)  =  F_T2(:,:)/C_T;
v3(:,:)  =  F_T3(:,:)/C_T;
v4(:,:)  =  F_T4(:,:)/C_T;
%-----------------------------------------------------------
y_11(:,:) = F_11(:,:)./F_T1(:,:);
y_21(:,:) = F_21(:,:)./F_T1(:,:);
y_31(:,:) = F_31(:,:)./F_T1(:,:);
y_41(:,:) = F_41(:,:)./F_T1(:,:);
y_51(:,:) = F_51(:,:)./F_T1(:,:);
y_61(:,:) = F_61(:,:)./F_T1(:,:);
y_71(:,:) = F_71(:,:)./F_T1(:,:);

y_12(:,:) = F_12(:,:)./F_T2(:,:);
y_22(:,:) = F_22(:,:)./F_T2(:,:);
y_32(:,:) = F_32(:,:)./F_T2(:,:);
y_42(:,:) = F_42(:,:)./F_T2(:,:);
y_52(:,:) = F_52(:,:)./F_T2(:,:);
y_62(:,:) = F_62(:,:)./F_T2(:,:);
y_72(:,:) = F_72(:,:)./F_T2(:,:);

y_13(:,:) = F_13(:,:)./F_T3(:,:);
y_23(:,:) = F_23(:,:)./F_T3(:,:);
y_33(:,:) = F_33(:,:)./F_T3(:,:);
y_43(:,:) = F_43(:,:)./F_T3(:,:);
y_53(:,:) = F_53(:,:)./F_T3(:,:);
y_63(:,:) = F_63(:,:)./F_T3(:,:);
y_73(:,:) = F_73(:,:)./F_T3(:,:);

y_14(:,:) = F_14(:,:)./F_T4(:,:);
y_24(:,:) = F_24(:,:)./F_T4(:,:);
y_34(:,:) = F_34(:,:)./F_T4(:,:);
y_44(:,:) = F_44(:,:)./F_T4(:,:);
y_54(:,:) = F_54(:,:)./F_T4(:,:);
y_64(:,:) = F_64(:,:)./F_T4(:,:);
y_74(:,:) = F_74(:,:)./F_T4(:,:);
%-----------------------------------------------------------
X_C4O2(1,2) = X_C41(1,2);
X_C4O2(2,2) = X_C42(1,2);
X_C4O2(3,2) = X_C43(1,2);
X_C4O2(4,2) = X_C44(1,2);
X_C4O2(1,4) = X_O21(1,2);
X_C4O2(2,4) = X_O22(1,2);
X_C4O2(3,4) = X_O23(1,2);
X_C4O2(4,4) = X_O24(1,2);
```

```
S_MACOx(1,2) = S1(1,2);
S_MACOx(2,2) = S2(1,2);
S_MACOx(3,2) = S3(1,2);
S_MACOx(4,2) = S4(1,2);
S_MACOx(1,4) = S1(2,2);
S_MACOx(2,4) = S2(2,2);
S_MACOx(3,4) = S3(2,2);
S_MACOx(4,4) = S4(2,2);
S_MACOx(1,6) = S1(3,2);
S_MACOx(2,6) = S2(3,2);
S_MACOx(3,6) = S3(3,2);
S_MACOx(4,6) = S4(3,2);
%-------------------------------------------------------
X_C4(X_C41,X_C42,X_C43,X_C44);
X_O2(X_O21,X_O22,X_O23,X_O24);
S_MA(S1,S2,S3,S4);
S_COx(S1,S2,S3,S4);

XC4O2(O2_C4,X_C4O2);
SMACOx(O2_C4,S_MACOx);

R2_XC4;
R2_XO2;
R2_SMA;
R2_SCOx;

save('k','k');
save('CIK','CIK');
```

```
function f = modelLlsq(k,xdataa)

global time   DT     N      Nr      n      m...
      F_11   F_21   F_31   F_41    F_51   F_61   F_71   F_T1...
      F_12   F_22   F_32   F_42    F_52   F_62   F_72   F_T2...
      F_13   F_23   F_33   F_43    F_53   F_63   F_73   F_T3...
      F_14   F_24   F_34   F_44    F_54   F_64   F_74   F_T4...
      y_V41  y_V51  M1     X_C41   X_O21  S1...
      y_V42  y_V52  M2     X_C42   X_O22  S2...
      y_V43  y_V53  M3     X_C43   X_O23  S3...
      y_V44  y_V54  M4     X_C44   X_O24  S4...
      R2_XC4 R2_XO2 R2_SMA R2_SCOx ypred  ypredd
%-----------------------------------------------------------
y_V51(1,:) = k(4);                                          % Initial V5 coverages
y_V41(1,:) = 1-y_V51(1,:);

y_V52(1,:) = k(5);
y_V42(1,:) = 1-y_V52(1,:);

y_V53(1,:) = k(6);
y_V43(1,:) = 1-y_V53(1,:);

y_V54(1,:) = k(7);
y_V44(1,:) = 1-y_V54(1,:);
%-----------------------------------------------------------
options1 = odeset('NonNegative',1:10,'MaxStep',DT);
options2 = odeset('NonNegative',1:8,'MaxStep',DT);

% options1 = odeset('MaxStep',DT);
% options2 = odeset('MaxStep',DT);
%-----------------------------------------------------------
for n = 1:Nr

   I01 = [F_11(1,n) F_21(1,n) F_31(1,n) F_41(1,n) F_51(1,n) F_61(1,n)...
% Initial molar flow rates and V coverages, gmol/mL
      F_71(1,n) F_T1(1,n) y_V41(1,n) y_V51(1,n)];
   I02 = [F_12(1,n) F_22(1,n) F_32(1,n) F_42(1,n) F_52(1,n) F_62(1,n)...
      F_72(1,n) F_T2(1,n) y_V42(1,n) y_V52(1,n)];
   I03 = [F_13(1,n) F_23(1,n) F_33(1,n) F_43(1,n) F_53(1,n) F_63(1,n)...
      F_73(1,n) F_T3(1,n) y_V43(1,n) y_V53(1,n)];
   I04 = [F_14(1,n) F_24(1,n) F_34(1,n) F_44(1,n) F_54(1,n) F_64(1,n)...
      F_74(1,n) F_T4(1,n) y_V44(1,n) y_V54(1,n)];

   [t,F1]  =  ode15s(@(t,F)kineticsL1lsq(t,F,k),  time, I01, options1);
   [t,F2]  =  ode15s(@(t,F)kineticsL2lsq(t,F,k),  time, I02, options1);
   [t,F3]  =  ode15s(@(t,F)kineticsL3lsq(t,F,k),  time, I03, options1);
   [t,F4]  =  ode15s(@(t,F)kineticsL4lsq(t,F,k),  time, I04, options1);
```

```
    F_11(:,n+1) = F1(:,1);
    F_21(:,n+1) = F1(:,2);
    F_31(:,n+1) = F1(:,3);
    F_41(:,n+1) = F1(:,4);
    F_51(:,n+1) = F1(:,5);
    F_61(:,n+1) = F1(:,6);
    F_71(:,n+1) = F1(:,7);
    F_T1(:,n+1) = F1(:,8);
    y_V41(:,n)  = F1(:,9);
    y_V51(:,n)  = F1(:,10);

    F_12(:,n+1) = F2(:,1);
    F_22(:,n+1) = F2(:,2);
    F_32(:,n+1) = F2(:,3);
    F_42(:,n+1) = F2(:,4);
    F_52(:,n+1) = F2(:,5);
    F_62(:,n+1) = F2(:,6);
    F_72(:,n+1) = F2(:,7);
    F_T2(:,n+1) = F2(:,8);
    y_V42(:,n)  = F2(:,9);
    y_V52(:,n)  = F2(:,10);

    F_13(:,n+1) = F3(:,1);
    F_23(:,n+1) = F3(:,2);
    F_33(:,n+1) = F3(:,3);
    F_43(:,n+1) = F3(:,4);
    F_53(:,n+1) = F3(:,5);
    F_63(:,n+1) = F3(:,6);
    F_73(:,n+1) = F3(:,7);
    F_T3(:,n+1) = F3(:,8);
    y_V43(:,n)  = F3(:,9);
    y_V53(:,n)  = F3(:,10);

    F_14(:,n+1) = F4(:,1);
    F_24(:,n+1) = F4(:,2);
    F_34(:,n+1) = F4(:,3);
    F_44(:,n+1) = F4(:,4);
    F_54(:,n+1) = F4(:,5);
    F_64(:,n+1) = F4(:,6);
    F_74(:,n+1) = F4(:,7);
    F_T4(:,n+1) = F4(:,8);
    y_V44(:,n)  = F4(:,9);
    y_V54(:,n)  = F4(:,10);

end
```

```
for m = Nr+1:N

    J01 = [F_11(1,m) F_21(1,m) F_31(1,m) F_41(1,m) F_51(1,m) F_61(1,m)...
       F_71(1,m) F_T1(1,m)];
    J02 = [F_12(1,m) F_22(1,m) F_32(1,m) F_42(1,m) F_52(1,m) F_62(1,m)...
       F_72(1,m) F_T2(1,m)];
    J03 = [F_13(1,m) F_23(1,m) F_33(1,m) F_43(1,m) F_53(1,m) F_63(1,m)...
       F_73(1,m) F_T3(1,m)];
    J04 = [F_14(1,m) F_24(1,m) F_34(1,m) F_44(1,m) F_54(1,m) F_64(1,m)...
       F_74(1,m) F_T4(1,m)];

    [t,F1]  =  ode15s(@(t,F)blank1(t,F),  time, J01, options2);
    [t,F2]  =  ode15s(@(t,F)blank2(t,F),  time, J02, options2);
    [t,F3]  =  ode15s(@(t,F)blank3(t,F),  time, J03, options2);
    [t,F4]  =  ode15s(@(t,F)blank4(t,F),  time, J04, options2);

    F_11(:,m+1) = F1(:,1);
    F_21(:,m+1) = F1(:,2);
    F_31(:,m+1) = F1(:,3);
    F_41(:,m+1) = F1(:,4);
    F_51(:,m+1) = F1(:,5);
    F_61(:,m+1) = F1(:,6);
    F_71(:,m+1) = F1(:,7);
    F_T1(:,m+1) = F1(:,8);

    F_12(:,m+1) = F2(:,1);
    F_22(:,m+1) = F2(:,2);
    F_32(:,m+1) = F2(:,3);
    F_42(:,m+1) = F2(:,4);
    F_52(:,m+1) = F2(:,5);
    F_62(:,m+1) = F2(:,6);
    F_72(:,m+1) = F2(:,7);
    F_T2(:,m+1) = F2(:,8);

    F_13(:,m+1) = F3(:,1);
    F_23(:,m+1) = F3(:,2);
    F_33(:,m+1) = F3(:,3);
    F_43(:,m+1) = F3(:,4);
    F_53(:,m+1) = F3(:,5);
    F_63(:,m+1) = F3(:,6);
    F_73(:,m+1) = F3(:,7);
    F_T3(:,m+1) = F3(:,8);

    F_14(:,m+1) = F4(:,1);
    F_24(:,m+1) = F4(:,2);
    F_34(:,m+1) = F4(:,3);
    F_44(:,m+1) = F4(:,4);
```

```
    F_54(:,m+1) = F4(:,5);
    F_64(:,m+1) = F4(:,6);
    F_74(:,m+1) = F4(:,7);
    F_T4(:,m+1) = F4(:,8);

end
%-----------------------------------------------------------
M1(1,1) = F_11(2,1)*120;
M1(3,1) = F_31(2,1)*120;
M1(1,2) = trapz(time,F_11(:,N+1));
M1(2,2) = trapz(time,F_21(:,N+1));
M1(3,2) = trapz(time,F_31(:,N+1));
M1(4,2) = trapz(time,F_41(:,N+1));
M1(5,2) = trapz(time,F_51(:,N+1));
M1(6,2) = trapz(time,F_61(:,N+1));

M2(1,1) = F_12(2,1)*120;
M2(3,1) = F_32(2,1)*120;
M2(1,2) = trapz(time,F_12(:,N+1));
M2(2,2) = trapz(time,F_22(:,N+1));
M2(3,2) = trapz(time,F_32(:,N+1));
M2(4,2) = trapz(time,F_42(:,N+1));
M2(5,2) = trapz(time,F_52(:,N+1));
M2(6,2) = trapz(time,F_62(:,N+1));

M3(1,1) = F_13(2,1)*120;
M3(3,1) = F_33(2,1)*120;
M3(1,2) = trapz(time,F_13(:,N+1));
M3(2,2) = trapz(time,F_23(:,N+1));
M3(3,2) = trapz(time,F_33(:,N+1));
M3(4,2) = trapz(time,F_43(:,N+1));
M3(5,2) = trapz(time,F_53(:,N+1));
M3(6,2) = trapz(time,F_63(:,N+1));

M4(1,1) = F_14(2,1)*120;
M4(3,1) = F_34(2,1)*120;
M4(1,2) = trapz(time,F_14(:,N+1));
M4(2,2) = trapz(time,F_24(:,N+1));
M4(3,2) = trapz(time,F_34(:,N+1));
M4(4,2) = trapz(time,F_44(:,N+1));
M4(5,2) = trapz(time,F_54(:,N+1));
M4(6,2) = trapz(time,F_64(:,N+1));
%-----------------------------------------------------------
X_C41(1,2) = (M1(1,1)-M1(1,2))/M1(1,1)*100;
X_O21(1,2) = (M1(3,1)-M1(3,2))/M1(3,1)*100;
S1(1,2) = M1(2,2)/(M1(1,1)-M1(1,2))*100;
S1(2,2) = M1(5,2)/(4*(M1(1,1)-M1(1,2)))*100;
```

```
S1(3,2) = M1(6,2)/(4*(M1(1,1)-M1(1,2)))*100;

X_C42(1,2) = (M2(1,1)-M2(1,2))/M2(1,1)*100;
X_O22(1,2) = (M2(3,1)-M2(3,2))/M2(3,1)*100;
S2(1,2) = M2(2,2)/(M2(1,1)-M2(1,2))*100;
S2(2,2) = M2(5,2)/(4*(M2(1,1)-M2(1,2)))*100;
S2(3,2) = M2(6,2)/(4*(M2(1,1)-M2(1,2)))*100;

X_C43(1,2) = (M3(1,1)-M3(1,2))/M3(1,1)*100;
X_O23(1,2) = (M3(3,1)-M3(3,2))/M3(3,1)*100;
S3(1,2) = M3(2,2)/(M3(1,1)-M3(1,2))*100;
S3(2,2) = M3(5,2)/(4*(M3(1,1)-M3(1,2)))*100;
S3(3,2) = M3(6,2)/(4*(M3(1,1)-M3(1,2)))*100;

X_C44(1,2) = (M4(1,1)-M4(1,2))/M4(1,1)*100;
X_O24(1,2) = (M4(3,1)-M4(3,2))/M4(3,1)*100;
S4(1,2) = M4(2,2)/(M4(1,1)-M4(1,2))*100;
S4(2,2) = M4(5,2)/(4*(M4(1,1)-M4(1,2)))*100;
S4(3,2) = M4(6,2)/(4*(M4(1,1)-M4(1,2)))*100;
%-----------------------------------------------------------
mean_XC4  = (X_C41(1,1)+X_C42(1,1)+X_C43(1,1)+X_C44(1,1))/4;
mean_XO2  = (X_O21(1,1)+X_O22(1,1)+X_O23(1,1)+X_O24(1,1))/4;
mean_SMA  = (S1(1,1)+S2(1,1)+S3(1,1)+S4(1,1))/4;
mean_SCO  = (S1(2,1)+S2(2,1)+S3(2,1)+S4(2,1))/4;
mean_SCO2 = (S1(3,1)+S2(3,1)+S3(3,1)+S4(3,1))/4;
%-----------------------------------------------------------
R2_XC4 = 1-((X_C41(1,1)-X_C41(1,2))^2+(X_C42(1,1)-X_C42(1,2))^2+(X_C43(1,1)-
X_C43(1,2))^2+...
   (X_C44(1,1)-X_C44(1,2))^2)/((X_C41(1,1)-mean_XC4)^2+(X_C42(1,1)-
mean_XC4)^2+(X_C43(1,1)-mean_XC4)^2+...
   (X_C44(1,1)-mean_XC4)^2);

R2_XO2 = 1-((X_O21(1,1)-X_O21(1,2))^2+(X_O22(1,1)-X_O22(1,2))^2+(X_O23(1,1)-
X_O23(1,2))^2+...
   (X_O24(1,1)-X_O24(1,2))^2)/((X_O21(1,1)-mean_XO2)^2+(X_O22(1,1)-
mean_XO2)^2+(X_O23(1,1)-mean_XO2)^2+...
   (X_O24(1,1)-mean_XO2)^2);

R2_SMA = 1-((S1(1,1)-S1(1,2))^2+(S2(1,1)-S2(1,2))^2+(S3(1,1)-S3(1,2))^2+...
   (S4(1,1)-S4(1,2))^2)/((S1(1,1)-mean_SMA)^2+(S2(1,1)-mean_SMA)^2+(S3(1,1)-
mean_SMA)^2+...
   (S4(1,1)-mean_SMA)^2);

R2_SCO = 1-((S1(2,1)-S1(2,2))^2+(S2(2,1)-S2(2,2))^2+(S3(2,1)-S3(2,2))^2+...
   (S4(2,1)-S4(2,2))^2)/((S1(2,1)-mean_SCO)^2+(S2(2,1)-mean_SCO)^2+(S3(2,1)-
mean_SCO)^2+...
   (S4(2,1)-mean_SCO)^2);
```

```
R2_SCO2 = 1-((S1(3,1)-S1(3,2))^2+(S2(3,1)-S2(3,2))^2+(S3(3,1)-S3(3,2))^2+...
   (S4(3,1)-S4(3,2))^2)/((S1(3,1)-mean_SCO2)^2+(S2(3,1)-mean_SCO2)^2+(S3(3,1)-
mean_SCO2)^2+...
   (S4(3,1)-mean_SCO2)^2);

R2_SCOx = (R2_SCO+R2_SCO2)/2;
%-------------------------------------------------------
ypred(1,1) = X_C41(1,2);
ypred(2,1) = X_C42(1,2);
ypred(3,1) = X_C43(1,2);
ypred(4,1) = X_C44(1,2);
ypred(1,2) = X_O21(1,2);
ypred(2,2) = X_O22(1,2);
ypred(3,2) = X_O23(1,2);
ypred(4,2) = X_O24(1,2);

ypred(1,3) = S1(1,2);
ypred(2,3) = S2(1,2);
ypred(3,3) = S3(1,2);
ypred(4,3) = S4(1,2);
ypred(1,4) = S1(2,2);
ypred(2,4) = S2(2,2);
ypred(3,4) = S3(2,2);
ypred(4,4) = S4(2,2);
ypred(1,5) = S1(3,2);
ypred(2,5) = S2(3,2);
ypred(3,5) = S3(3,2);
ypred(4,5) = S4(3,2);
%-------------------------------------------------------
ypredd(1:4,1) = ypred(:,1);
ypredd(5:8,1) = ypred(:,2);
ypredd(9:12,1) = ypred(:,3);
ypredd(13:16,1) = ypred(:,4);
ypredd(17:20,1) = ypred(:,5);
% -------------------------------------------------------
f = ypredd;
```

```
function dF = kineticsL1lsq(t,F,k)

global time DT n V W C_T C_VT...
   F_11 F_21 F_31 F_41 F_51 F_61 F_71

%-----------------------------------------------------------
% 1- O2 + V4 --> V5
% 2- C4H10 + 3.5V5 --> C4H2O3 + 4H2O + 3.5V4
% 3- C4H10 + 5.5V5 --> 2CO + 2CO2 + 5H2O + 5.5V4
% -----------------------------------------------------------
r(1) = -k(1)*C_T*(F(3)/F(8))*F(9)*(V(n)/W(n));
r(2) = -k(2)*C_T*(F(1)/F(8))*F(10)*(V(n)/W(n));
r(3) = -k(3)*C_T*(F(1)/F(8))*F(10)*(V(n)/W(n));

R(1) = r(2)+r(3);
R(2) = -r(2);
R(3) = r(1);
R(4) = -4*r(2)-5*r(3);
R(5) = -2*r(3);
R(6) = -2*r(3);
R(7) = 0.0;
R(8) = 0.0;
R(9) = r(1)-3.5*r(2)-5.5*r(3);
R(10) = -r(1)+3.5*r(2)+5.5*r(3);
% -----------------------------------------------------------
dF = zeros(10,1);

DT_inv = 1/DT;
t_rnd = round(t*DT_inv)/DT_inv;
t_ind = find(time == t_rnd);

dF(1) = (F(8)/(C_T*V(n)))*(F_11(t_ind,n)-F(1)+(W(n)*R(1)))+(F(1)/F(8))*dF(8);
dF(2) = (F(8)/(C_T*V(n)))*(F_21(t_ind,n)-F(2)+(W(n)*R(2)))+(F(2)/F(8))*dF(8);
dF(3) = (F(8)/(C_T*V(n)))*(F_31(t_ind,n)-F(3)+(W(n)*R(3)))+(F(3)/F(8))*dF(8);
dF(4) = (F(8)/(C_T*V(n)))*(F_41(t_ind,n)-F(4)+(W(n)*R(4)))+(F(4)/F(8))*dF(8);
dF(5) = (F(8)/(C_T*V(n)))*(F_51(t_ind,n)-F(5)+(W(n)*R(5)))+(F(5)/F(8))*dF(8);
dF(6) = (F(8)/(C_T*V(n)))*(F_61(t_ind,n)-F(6)+(W(n)*R(6)))+(F(6)/F(8))*dF(8);
dF(7) = (F(8)/(C_T*V(n)))*(F_71(t_ind,n)-F(7)+(W(n)*R(7)))+(F(7)/F(8))*dF(8);

dF(8) = dF(1)+dF(2)+dF(3)+dF(4)+dF(5)+dF(6)+dF(7);

dF(9) = R(9)/C_VT;
dF(10) = R(10)/C_VT;
```

```
function dF = blank1(t,F)

global time DT m V C_T...
    F_11 F_21 F_31 F_41 F_51 F_61 F_71

%-------------------------------------------------------
dF = zeros(8,1);

DT_inv = 1/DT;
t_rnd = round(t*DT_inv)/DT_inv;
t_ind = find(time == t_rnd);

dF(1) = (F(8)/(C_T*V(m)))*(F_11(t_ind,m)-F(1));
dF(2) = (F(8)/(C_T*V(m)))*(F_21(t_ind,m)-F(2));
dF(3) = (F(8)/(C_T*V(m)))*(F_31(t_ind,m)-F(3));
dF(4) = (F(8)/(C_T*V(m)))*(F_41(t_ind,m)-F(4));
dF(5) = (F(8)/(C_T*V(m)))*(F_51(t_ind,m)-F(5));
dF(6) = (F(8)/(C_T*V(m)))*(F_61(t_ind,m)-F(6));
dF(7) = (F(8)/(C_T*V(m)))*(F_71(t_ind,m)-F(7));

dF(8) = dF(1)+dF(2)+dF(3)+dF(4)+dF(5)+dF(6)+dF(7);
```